HEI energy

NUMBER 240
MARCH 2026

RESEARCH REPORT

Predictive, Source-Oriented Modeling and Measurements to Evaluate Community Exposures to Air Pollutants and Noise from Unconventional Oil and Gas Development

Lea Hildebrandt Ruiz, David Allen, Pawel Misztal, Elizabeth Matsui, Roger Peng, Yosuke Kimura, David Sullivan, Shannon Stokes, Elena McDonald-Buller, Leif Jahn, Mrinali Modi, Joel Graves, Kat Konon, Lea El Khoury, Pearl Abue, Shihao Zhai, Austin Turner, Sewar Almasalha, Chou-Hsien Lin, Evelyn Deveraux, Daniel Blomdahl, Daniel Sung, Qining Chen, Lucas Henneman, Munshi Md Rasel, and Mohammadreza Bohloul

INCLUDES A COMMENTARY BY THE HEI ENERGY REVIEW COMMITTEE

www.healtheffects.org
www.HEIenergy.org

Predictive, Source-Oriented Modeling and Measurements to Evaluate Community Exposures to Air Pollutants and Noise from Unconventional Oil and Gas Development

Lea Hildebrandt Ruiz, David Allen, Pawel Misztal, Elizabeth Matsui, Roger Peng, Yosuke Kimura, David Sullivan, Shannon Stokes, Elena McDonald-Buller, Leif Jahn, Mrinali Modi, Joel Graves, Kat Konon, Lea El Khoury, Pearl Abue, Shihao Zhai, Austin Turner, Sewar Almasalha, Chou-Hsien Lin, Evelyn Deveraux, Daniel Blomdahl, Daniel Sung, Qining Chen, Lucas Henneman, Munshi Md Rasel, and Mohammadreza Bohloul

with a Commentary by the HEI Energy Review Committee

Research Report 240
Health Effects Institute
Boston, Massachusetts

Trusted Science · Cleaner Air · Better Health

Publishing history: This report was posted at *www.healtheffects.org* in March 2026.

Citation for report:

Hildebrandt Ruiz L, Allen D, Misztal P, Matsui E, Peng R, Kimura Y, et al. 2026. Predictive, Source-Oriented Modeling and Measurements to Evaluate Community Exposures to Air Pollutants and Noise from Unconventional Oil and Gas Development. Research Report 240. Boston, MA: Health Effects Institute.

ISSN 2688-6855 (online)

CONTENTS

ABOUT HEI ENERGY

The Health Effects Institute's Energy Research program (HEI Energy) was formed to identify and conduct high-priority research on potential population exposures and health effects from the development of oil and natural gas in the United States. Since 2022, HEI Energy has supported population-level exposure research in multiple oil and gas regions. This research followed an extensive planning process that included preparing reviews of the scientific literature, hosting multisector workshops to learn about research priorities, and developing an online curated database and spatial bibliography to advance both public and scientific understanding. The research scope of HEI Energy is expanding beyond oil and gas to other forms of energy development, with an overarching goal of providing impartial knowledge about the benefits and drawbacks associated with various technologies.

The scientific review and research provided by HEI Energy contribute high-quality and credible science to the public debate about unconventional oil and natural gas development and provide needed support for decisions about how best to protect public health. To achieve this goal, HEI Energy has put into place a governance structure that mirrors the one successfully employed for nearly 40 years by its parent organization, the Health Effects Institute (HEI), with several critical features:

- Balanced funding from the US Environmental Protection Agency under a contract that funds HEI Energy exclusively and from the oil and natural gas industry, with other public and private organizations periodically providing support
- An independent Board of Directors consisting of leaders in science and policy who are committed to fostering the public–private partnership that is central to the organization
- A research program governed independently by individuals having no direct ties to or interests in sponsor organizations
- The HEI Energy Research Committee, whose members are internationally recognized experts in one or more subject areas relevant to the Committee's work, have demonstrated their ability to conduct and review scientific research impartially and have been vetted to avoid conflicts of interest
- Research that undergoes rigorous peer review by HEI Energy's Review Committee, which is not involved in the selection and oversight of HEI Energy studies
- Staff and committees that participate in open and extensive stakeholder engagement before, during, and after research and communicate all results in the context of other relevant research

In addition, HEI Energy publicly shares all literature reviews and original research that it funds, along with summaries written for a general audience. Without advocating policy positions, it provides impartial science targeted to make better-informed decisions.

HEI Energy is funded separately from the Health Effects Institute's other research programs (*www.healtheffects.org*), with financial support from the US Environmental Protection Agency, the oil and gas industry, and private foundations.

ABOUT THIS REPORT

HEI Energy Research Report 240, *Predictive, Source-Oriented Modeling and Measurements to Evaluate Community Exposures to Air Pollutants and Noise from Unconventional Oil and Gas Development*, presents a research project funded by HEI Energy and conducted by Lea Hildebrandt Ruiz at The University of Texas at Austin and her colleagues. The report contains three main sections:

The **HEI Statement**, prepared by staff at HEI Energy, is a brief, nontechnical summary of the study and its findings; it also briefly describes the HEI Energy Review Committee's comments on the study.

The **Investigators' Report**, prepared by Hildebrandt Ruiz and colleagues, describes the scientific background, aims, methods, results, and conclusions of the study.

The **Commentary**, prepared by members of the HEI Energy Review Committee with the assistance of HEI staff, places the study in a broader scientific context, points out its strengths and limitations, and discusses the remaining uncertainties and implications of the study's findings for public health and future research.

This report has gone through HEI Energy's rigorous review process. When an HEI Energy-funded study is completed, the investigators submit a draft final report presenting the background and results of the study. Outside technical reviewers first examine this draft report. The report and the reviewers' comments are then evaluated by members of the Review Committee, an independent panel of distinguished scientists who are not involved in selecting or overseeing HEI Energy studies. During the review process, the investigators have an opportunity to exchange comments with the Review Committee and, as necessary, to revise their report. The Commentary reflects the information provided in the final version of the report.

Although this report was produced with partial funding by the United States Environmental Protection Agency under Contract No. 68HERC19D0010 to the Health Effects Institute, it has not been subjected to the Agency's peer and administrative review and may not reflect the views of the Agency; thus, no official endorsement by the Agency should be inferred. This report also has not been reviewed by private party institutions, including those that support HEI Energy, and may not reflect the views or policies of these parties; thus, no endorsement by them should be inferred.

PREFACE

HEI's Research to Assess Community Exposures Associated with Unconventional Oil and Gas Development

INTRODUCTION

The scale and rate of onshore oil and natural gas development since the early 2000s differ markedly from earlier development, stemming from technological changes involving the increased use of hydraulic fracturing combined with horizontal drilling. While hydraulic fracturing has captured much public attention, this process alone is not new. Neither is horizontal drilling or the extraction of oil and gas from unconventional formations, such as tight (i.e., low permeability) sandstone and shale. What is new is the use of high-volume (millions of gallons of water per well), multistage hydraulic fracturing combined with horizontal drilling (thousands of feet in length).

This combination of technological innovations has influenced the scale of development and where development is feasible. With their extensive number of fracture stages along lengthy horizontal wells, today's unconventional oil and gas wells intersect more of the targeted oil- or gas-bearing rock than earlier vertical wells, which involves the following:

- Larger well pads with extensive amounts of equipment that are transported to and from the pad
- More raw materials that must be transported to the well pad for drilling, cementing, and hydraulically fracturing the target hydrocarbon-bearing formation to produce the oil or gas
- More liquid and solid waste from multiple wells drilled on one well pad that must be captured, transported, and treated, for reuse or ultimate disposal
- A longer period of industrial activity is required at a single well pad when multiple wells are developed on it and
- Increased truck traffic, changing demands on community infrastructure, and other possible community effects associated with population mobility.

Consequently, unconventional oil and gas development (UOGD) can be associated with a wide range of potential exposures to chemical and nonchemical agents. The rapid expansion of this development has given rise to concerns about potential effects on human health.

Current evidence indicates that people can be exposed to chemical agents (e.g., criteria and hazardous air pollutants, radioactive material, indicators of produced water, and odorous compounds) and nonchemical agents (e.g., noise, light, and vibration) released from UOGD processes. HEI Energy compiled this evidence in two extensive literature reviews (HEI Energy Research Committee 2019, 2020). But despite this literature and considering the recommendations of a wide variety of government, industry, and academic stakeholders at three HEI-hosted research planning workshops, HEI Energy concluded that important gaps remain in our understanding of who might be exposed, the full range of exposures, which processes lead to exposures, and how exposures vary over time and across regions. Specifically, few studies to date provide the information necessary for linking chemical or nonchemical agents from UOGD processes with exposed communities. In addition, the applicability of study results to UOGD operations, geographic areas, and populations beyond those investigated in the studies is not clear. Given the current state of knowledge, HEI issued complementary requests for applications in 2020 (*RFAs E20-1 and E20-2*) to improve the understanding of human exposure to UOGD.

OBJECTIVES OF THE RFAs

HEI solicited studies that can document one or more complete exposure pathway(s), should one exist, between UOGD process(es) and a population(s) potentially exposed to UOGD chemical emissions to air, chemical releases to water, or noise. The research should inform future health studies and be designed in an efficient way to maximize understanding of the variability in potential human exposures under routine operating conditions, while also being capable of capturing exposures associated with accidental scenarios.

OBJECTIVES OF RFA E20-1

RFA E20-1: Community Exposures Associated with Unconventional Oil and Natural Gas Development solicited studies that apply a combination of approaches

to quantify the spatial and temporal variability in human exposures to UOGD-generated atmospheric chemical concentrations and noise. To maximize the generalizability of the research, HEI encouraged research that couples established rigorous methods to measure air and noise exposure at multiple spatial scales with equally rigorous fate and transport modeling. The RFA had five major objectives:

1. Identify the UOGD processes that have resulted or might result in releases of chemicals or noise to outdoor air and the potential for human exposure resulting from such releases.
2. Quantify the magnitude, frequency, and duration of potential exposures to chemicals in outdoor air and to noise released from specific UOGD processes at multiple spatial and temporal scales.
3. Quantify the influence of various factors (e.g., varying meteorology, topography, operational characteristics, proximity to populations, and population behavior) on potential UOGD-related human exposures to characterize variability in exposures and enable the results of the research to be generalized to other conditions.
4. Estimate community exposures from UOGD sources across spatial and temporal scales relevant to a current or future assessment of potential health effects.
5. Distinguish potential UOGD exposures from other conventional oil and gas development and any other background source to the extent practicable.

OBJECTIVES OF RFA E20-2

RFA E20-2: Community Exposures Associated with Unconventional Oil and Natural Gas Development solicited studies that involve the synthesis and modeling of existing data and original research to better understand the nature, extent, and frequency of potential exposures related to UOGD impacts on water quality. The RFA had four major objectives:

1. Determine the UOGD processes that have resulted or might result in releases to groundwater or surface water and potential for leading to human exposure.
2. Quantify the magnitude, frequency, and duration of potential exposures to chemicals in surface water or groundwater released from specific UOGD processes.
3. Quantify the influence of various factors (e.g., varying geology) on potential human exposures to maximize the generalizability of the research and inform decision-making.
4. Distinguish potential UOGD exposures from conventional oil and gas development and any other background sources to the extent practicable.

STUDIES FUNDED UNDER RFA E20-1

HEI Energy funded three research teams to collaborate on improving our understanding of community exposures associated with air quality and noise from UOGD. The collaboration, "TRAcking Community Exposures and Releases (TRACER) from UOGD" (1) quantified acute and chronic human exposures in three regions of the United States, and (2) developed a model that captures our collective understanding of UOGD emission sources, estimates their impacts on local and regional air quality, and can be updated as UOGD operations and UOGD governance change over time.

"Measuring and Modeling Air Pollution and Noise Exposure Near Unconventional Oil and Gas Development in Colorado," Jeffrey L. Collett Jr., Colorado State University, USA The research team assessed population exposures to chemicals and noise in air associated with specific UOGD processes over the UOGD life cycle at four well pads in the Colorado North Front Range, located within the Denver-Julesburg Basin. With the cooperation of well pad operators, the team conducted fixed-site air and noise monitoring and mobile air monitoring at multiple locations surrounding multiwell pads to connect specific UOGD processes with air monitoring results. These processes included well drilling, hydraulic fracturing, coiled tubing/millout operations, flowback, and early production. The team obtained samples of drilling mud and compared emissions from different formulations. In addition to the monitoring program, they collaborated with Dr. Lea Hildebrandt Ruiz to provide preproduction input data to the TRACER model, developed a preproduction emissions model designed for use by a variety of stakeholders to forecast HAPs and other VOC emissions from planned drilling and well completion operations and to assess whether efforts to reduce emissions achieve the desired goals. The team applied the model to simulate emissions and dispersion around specific well pads and estimate effects on local air quality, interpreting findings in the context of Colorado's regulatory setback distances separating UOGD from residences, schools, and other forms of development.

"Assessing Source Contributions to Air Quality and Noise in Unconventional Oil Shale Plays," Meredith Franklin, University of Toronto, Canada The research team assessed population exposures to ambient air pollution, radioactivity, and noise associated with UOGD. The team has coupled air, noise, and radioactivity measurements with meteorology and land use data to characterize UOGD sources of human exposure in the study regions: Permian Basin, Texas, and Eagle Ford Shale, Texas. To understand temporal variability in chemical concentrations in air, radioactivity, and noise levels, they conducted time-resolved fixed-site monitoring in the Permian Basin and leveraged ongoing fixed-site monitoring in the Denver-Julesburg basin. To understand spatial variability, they deployed passive samplers in both study regions. They linked monitoring data with satellite observations to characterize the location and magnitude of flaring.

"Predictive, Source-Oriented Modeling and Measurements to Evaluate Community Exposures to Air Pollutants and Noise from Unconventional Oil and Gas Development," Lea Hildebrandt Ruiz, University of Texas at Austin, USA The research team utilized a combination of measurement and modeling approaches in diverse study sites to assess the quality of an emission and dispersion modeling tool (TRACER model), which was advanced and refined from an existing model for methane emissions. The capabilities of the pre-existing model were expanded from modeling emission and dispersion of methane from single UOGD well pads to assessing community exposures from multiple well pads. The expanded model included additional sources of emissions, regional-scale modeling, a broad suite of pollutants of concern to human health, including secondary pollutants, and evaluation of the model for the purpose of exposure assessment in future health studies. The original scope of work focused on the Eagle Ford Shale region in Texas. The project was later expanded to also include monitoring in the Permian Basin in New Mexico and modeling in the Marcellus Shale Region in the Northeastern United States, in close collaboration with the other two studies funded under this RFA.

DESCRIPTION OF THE RESEARCH PROGRAM

Three studies were funded under RFA E20-1, and two studies were funded under RFA E20-2 to cover the various RFA objectives; they are summarized below (**Preface Table**). The study locations stretch across several major oil and gas producing regions of the United States (**Preface Figure**).

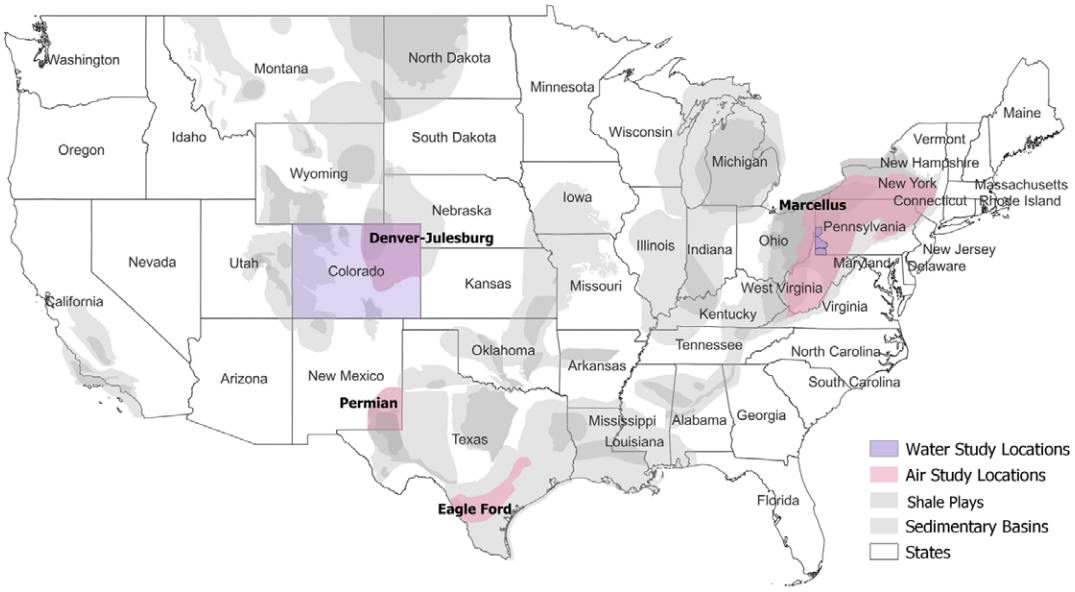

Preface Figure. Map of RFA E20-1 and E20-2 study locations and associated plays and basins across the United States.

STUDIES FUNDED UNDER RFA E20-2

HEI funded two studies in Colorado and Pennsylvania to combine existing water quality data and modeling to assess community exposures associated with UOGD releases to water. Both studies provide frameworks for identifying areas of potential water contamination, apportioning the sources of contamination, and identifying exposure pathways that connect UOGD to community water sources.

"Using Geoscientific Analysis and Community Engagement to Analyze Exposures to Potential Groundwater Contamination Related to Hydrocarbon Extraction in Southwestern Pennsylvania," Jennifer Baka, Susan L. Brantley, and Lingzhou Xue,* The Pennsylvania State University, USA The research team assessed linkages between UOGD and potential water contamination in a tri-county region of Southwestern Pennsylvania with a long history of industrial activity. Using an existing database of greater than 28,000 groundwater samples, the team investigated whether they could distinguish constituents associated with UOGD from other regional sources of similar contaminants (e.g., conventional oil and gas development and coal mining). The research team used statistical analysis and a machine learning tool (nonnegative matrix factorization, NMF) to isolate the influences of natural and anthropogenic processes on groundwater chemistry and identify potential linkages between UOGD and water contamination. The team hosted focus groups to elicit community concerns regarding UOGD, water contamination, and public health, and they considered what they learned in completing their assessment of potential community exposures associated with UOGD.

"Assessing the Effects of Unconventional Oil and Gas Development on Community Water Sources," Joseph Ryan, University of Colorado, USA The research team used existing data to assess the potential for community exposure to releases attributable to UOGD in ground and surface waters used as community water supplies. The team used monitoring data for water quality near oil and gas development, records of community water supplies, and records related to oil and gas operations in the Denver-Julesburg, Piceance, San Juan, and Raton Basins (e.g., well construction and integrity) to assess temporal and spatial correlations with water quality issues affecting communities. They identified chemicals of possible concern detected in the water quality dataset and coupled those with multiphase subsurface fluid flow and transport models to predict the likelihood of complete transport pathways in the Denver-Julesburg Basin.

*Co-principal investigators.

REFERENCES

HEI-Energy Research Committee. 2019. Potential Human Health Effects Associated with Unconventional Oil and Gas Development: A Systematic Review of the Epidemiology Literature. Special Report 1. Boston, MA: Health Effects Institute.

HEI-Energy Research Committee. 2020. Human Exposure to Unconventional Oil and Gas Development: A Literature Survey for Research Planning. Communication 1. Boston, MA: Health Effects Institute.

Preface Table. Key Characteristics of HEI's Research to Assess Community Exposures Associated with Unconventional Oil and Gas Development

Principal Investigator	Location	Study Period	Study Population	Main Pollutants in Air or Water	Monitoring Data	Exposure Assessment
RFA E20-1: Community Exposures Associated with Unconventional Oil and Gas Development — Air Quality and Noise						
Collett	Northern Front Range, Colorado (part of the Denver-Julesburg basin)	2022–2024	All subpopulations in the study location	VOCs, methane, $PM_{2.5}$, NO_x, A- and C-weighted noise	Fenceline fixed-site and mobile	TRACER emissions model and local air quality modeling
Franklin	Carlsbad-Loving, New Mexico (part of the Permian basin), Eagle Ford Shale region, Texas	2022–2024	All subpopulations in the study location	VOCs, methane, $PM_{2.5}$, NO_x, A- and C-weighted noise, ozone, H2S, radioactivity (alpha)	Regional fixed-site (NM) and passive (TX)	Non-negative matrix factorization for source apportionment
Hildebrandt Ruiz	Eagle Ford Shale region, Texas, Permian Basin, New Mexico, and Marcellus Shale Region	2022–2024	All subpopulations in the study location	VOCs, methane, PM_1, NO_x, A- and C-weighted noise, ozone, H2S, black carbon	Fixed-site (TX) and mobile (TX and NM)	TRACER emissions model and local and regional air quality modeling
RFA E20-2: Community Exposures Associated with Unconventional Oil and Gas Development — Water Quality						
Baka, Brantley, and Xue	Beaver, Greene, and Washington Counties in Southwestern Pennsylvania	2022–2024	All subpopulations in the study location	VOCs, metals	Existing state-level data	Machine learning and statistical modeling
Ryan	State of Colorado	2022–2024	All subpopulations in the study location	VOCs, metals	Existing state-level data	Chemical transport model and statistical tests

HEI STATEMENT

Synopsis of Research Report 240

Monitoring and Modeling to Evaluate Community Exposures to Air Pollutants from Unconventional Oil and Gas Development

BACKGROUND

The rapid expansion of unconventional oil and natural gas development (UOGD) has given rise to concerns about potential effects on human health from a wide range of potential exposures to chemical and nonchemical agents, but knowledge gaps about these exposures remain. HEI Energy, therefore, issued *Request for Applications E20-1* in August 2020 to better understand the nature, extent, and frequency of potential exposures related to UOGD on air quality and noise.

Dr. Lea Hildebrandt Ruiz, University of Texas at Austin, was one of three investigators funded under this Request for Application. Hildebrandt Ruiz and colleagues developed a TRAcking Community Exposures and Releases (TRACER) model to assess exposures to air pollution from UOGD and to inform future health studies. The original scope of work focused on the Eagle Ford Shale region in Texas. The project was later expanded to the Permian Basin in New Mexico and the Marcellus Shale region in Ohio, Pennsylvania, and West Virginia.

APPROACH

The investigators used a combination of monitoring and modeling approaches at various study sites to assess the quality of the TRACER model, which they advanced and refined from an existing model for methane emissions. The TRACER model combined emissions modeling with dispersion modeling to assess exposure to various air pollutants from UOGD. The capabilities of the preexisting model were expanded from modeling emission and dispersion of methane from single UOGD well pads to assessing population exposures from multiple well pads.

The study team conducted detailed mobile and fixed-site monitoring campaigns over 3 months across two seasons in the Eagle Ford Shale in 2023 and over 2 weeks in the Permian Basin in the spring of 2024. They used advanced instrumentation, such as mass spectrometry, which provided high-resolution data, including measurements of real-time volatile organic compounds. A suite of air pollutants was examined, including particulate matter, nitrogen oxides, and numerous air toxics. Noise was measured as well.

The investigators conducted extensive modeling in the Eagle Ford and Marcellus Shale regions, which included developing improved UOGD emissions estimates, dispersion modeling for primary pollutants, and chemical transport modeling for secondary pollutants. The investigators expanded the Methane Emission Estima-

What This Study Adds

- The study includes extensive monitoring and modeling across three oil and gas regions in the United States: Eagle Ford Shale, Permian Basin, and Marcellus Shale.
- The investigators developed a model (the TRACER model) to assess exposures to air pollution from oil and gas development and inform future health studies. The model included additional sources of emissions, regional-scale modeling, a broad suite of pollutants, and evaluation for the purpose of exposure assessment in future health studies.
- Ethane concentrations were affected by oil and gas development emission sources up to 50 km away in modeling. The study reported typically high correlations between ethane and other volatile organic compounds from different exposure models and with direct observations. CALPUFF appeared to be the best-performing model in reducing bias for ethane.

This Statement, prepared by HEI Energy, summarizes a research project funded by HEI Energy and conducted by Dr. Lea Hildebrant Ruiz at The University of Texas at Austin and her colleagues. Research Report 240 contains the detailed Investigators' Report and a Commentary on the study prepared by the HEI Energy Review Committee.

tion Tool to create the TRACER model. The expanded model included updated emissions from additional UOGD sources, improved the spatial and temporal resolution of UOGD emissions, and broadened to a suite of nonmethane pollutants of concern for human health. The investigators applied the TRACER model to estimate emissions from individual wells and coupled the emissions with an air pollution dispersion model (CALPUFF) to estimate air pollution concentrations of ethane at receptor sites in the Eagle Ford Shale. For the modeling, they used an approximate 200 km × 200 km domain centered on the Karnes City monitoring site — located in the center of the Eagle Ford Shale — using data on more than 20,000 oil and gas wells. They focused on ethane in these analyses, which, in the Eagle Ford Shale region, is emitted almost entirely by oil and gas operations.

A similar type of TRACER modeling was also conducted in the Marcellus Shale region, although the UOGD emissions estimates were aggregated over 4 km × 4 km grid cells. Further, the investigators used a chemical transport model (CAMx) to examine the importance of detailed spatial and temporal allocation of nitrogen oxides emissions from hydraulic fracturing on predicted ozone formation in the Eagle Ford Shale. They developed various scenarios that differed in the number of wells being fractured and the duration of the fracturing process.

Lastly, the investigators compared various approaches with increasing levels of complexity to estimate exposure to UOGD in Karnes County in the Eagle Ford Shale, including various air pollution dispersion models (e.g., CALPUFF and AERMOD) and inverse distance weighting. They assessed model performance by comparing model predictions with Karnes City monitoring site data, with a focus on ethane. Many features of the modeling were further explored, such as the influence of meteorology and emissions variability.

KEY RESULTS

The investigators found that ambient concentrations of air pollutants in UOGD regions showed strong diurnal variation, with (short-term) peak concentrations occurring during late night and early morning hours. However, mean concentrations of various air pollutants and noise from the entire UOGD measurement campaigns in Eagle Ford Shale and Permian Basin were generally low and did not exceed the National Ambient Air Quality Standards concentrations (and other health-related guidelines). Caution is warranted because the measurements and the short-term health standards and guidelines have different averaging times.

With extensive modeling of the Eagle Ford Shale, the study team found that mean and peak ethane concentrations were affected by UOGD emission sources up to 50 km away. This influence was highly variable and depended on whether the nearest UOGD sources were upwind from the site and whether stable atmospheric conditions with low wind speeds occurred, which may facilitate peak concentrations.

Further, the study team found high variability in emission factors of volatile organic compounds across UOGD locations. Similarly, the study team reported nitrogen oxide emission rates from hydraulic fracturing from specific wells at specific times varied by two to three orders of magnitude across the scenarios. The improved emissions estimates might have led to increased estimated ozone formation in the Eagle Ford Shale region — a region with abundant biogenic volatile organic compounds.

Hildebrandt Ruiz and colleagues reported high correlations (>0.7) across different exposure models for ethane and five other volatile organic compounds, except for the inverse weighting model without meteorological data. Regarding ethane, CALPUFF appeared to be the best-performing model for reducing bias between model predictions and observational data, but it is also the most computationally intensive model. Of the less computational-demanding models, AERMOD was the best performing.

INTERPRETATION AND CONCLUSIONS

In its independent review of the study, the HEI Energy Review Committee thought the study presented a comprehensive approach to evaluating air pollution from UOGD. The broad scope of the study, detailed monitoring campaigns, and use of state-of-the-art instrumentation that provided high-resolution data were its strengths. Other strengths were the extensive modeling efforts, including the development of improved UOGD emissions estimates, dispersion modeling, and chemical transport modeling.

Although the Review Committee broadly agreed with the investigators' conclusions, the report had some limitations that should be considered when interpreting the results. The Committee thought the lack of discussion, integration, and synthesis across the many parts of the study was a missed opportunity to maximize the study's impact and limited the generalizability of the findings. The lack of integration might stem partly from the study's history because mobile monitoring in the Permian Basin and modeling in the Marcellus Shale region began after other aspects of the research had already started. The Review Committee recommends three areas of future work: application of the TRACER model in the Permian Basin, one of the most productive UOGD regions in the United States; a more thorough evaluation of the TRACER model beyond mainly ethane; and expansion of research

efforts to other potential chemical and nonchemical exposures related to UOGD, in addition to air pollution.

Overall, the Review Committee thought the study findings and the TRACER model would be of broad interest and value to a wide audience, such as resource managers, state and federal policymakers, UOGD industry practitioners, research scientists, and local communities.

Predictive, Source-Oriented Modeling and Measurements to Evaluate Community Exposures to Air Pollutants and Noise from Unconventional Oil and Gas Development

Lea Hildebrandt Ruiz[1], David Allen[1], Pawel Misztal[1], Elizabeth Matsui[1], Roger Peng[1], Yosuke Kimura[1], David Sullivan[1], Shannon Stokes[1], Elena McDonald-Buller[1], Leif Jahn[1], Mrinali Modi[1], Joel Graves[1], Kat Konon[1], Lea El Khoury[1], Pearl Abue[1], Shihao Zhai[1], Austin Turner[1], Sewar Almasalha[1], Chou-Hsien Lin[1], Evelyn Deveraux[1], Daniel Blomdahl[1], Daniel Sung[1], Qining Chen[1], Lucas Henneman[2], Munshi Md Rasel[2], and Mohammadreza Bohloul[2]

[1]*The University of Texas at Austin, USA;* [2]*George Mason University, Fairfax, Virginia, USA*

ABSTRACT

Introduction The main goal of this project was to develop the TRACER (TRAcking Community Exposures and Releases) model to assess exposures to air pollutants from unconventional oil and gas development (UOGD*) and to inform future health studies. The project's main focus was on the Eagle Ford Shale in south-central Texas, a large oil and gas production region that includes the production of dry gas, wet gas, and oil. This heterogeneity of production types makes the Eagle Ford Shale a microcosm of UOGD sites throughout the United States. The project was later expanded to also include mobile measurements in the Permian Basin and modeling in the Marcellus Shale.

Methods We expanded a model originally designed to predict emissions of methane to pollutants of concern to human health. We coupled the expanded emissions model with dispersion models to evaluate impacts of UOGD emissions on concentrations of pollutants at a receptor site and regionally, and we compared the performance of different dispersion models. We also coupled the emissions model with a chemical transport model to evaluate the impacts of UOGD emissions on ozone, a secondary pollutant. We conducted targeted stationary and mobile measurements to evaluate emissions from flaring, which were then included as inputs to the TRACER model, and to provide a comprehensive dataset for model evaluation. Finally, we evaluated community exposures in Karnes County, Texas, to pollutants of concern to human health emitted by UOGD, and differences in exposure by income and ethnicity/race.

Results We found that destruction efficiencies and emission ratios from flares are highly variable. Ambient concentrations at receptor sites, and therefore population exposures, have high diurnal variability, with the highest concentrations and exposures observed at night. Elevated concentrations observed at night can be due to both large nonroutine emissions events and routine emissions, coupled with wind speeds and atmospheric stability conditions that are conducive to producing high concentrations. Ambient concentrations are affected by thousands of UOGD sources that are tens of kilometers from receptor sites, and thus, predicting concentrations at these sites requires high computational intensity. We evaluated and compared different dispersion models and found that the CALPUFF dispersion model (using stability classification to predict dispersion parameters) generally performs best but is also the most computationally expensive. Coupling the emissions model with the chemical transport model (Comprehensive Air Quality Model with extensions) revealed that realistic temporal and spatial allocation of nitrogen oxides emissions can result in higher predicted ozone concentrations. Reduced-complexity exposure approaches that include meteorology generally capture salient features (e.g., spatial-temporal variability) found in observations and in more complex models, but concentrations from these approaches have higher bias than CALPUFF.

Conclusions We show strengths and limitations of multiple methods to assess UOGD source-specific concentration enhancements and spatial-temporal exposure patterns. Combined with spatial differences among population group residences, spatial variability in emissions and dominant wind patterns leads to differences in exposure between racial or ethnic and income groups. All groups experience higher exposure at night than during the day.

This Investigators' Report is one part of Health Effects Institute Research Report 240, which also includes a Commentary by the HEI Energy Review Committee and an HEI Statement about the research project. Correspondence concerning the Investigators' Report may be addressed to Dr. Lea Hildebrandt Ruiz, The University of Texas at Austin, 200 E. Dean Keeton St, Austin, TX 78712; email: *lhr@che.utexas.edu*. Principal investigator Lea Hildebrant Ruiz served on the US EPA Scientific Advisory Board from October 2024 to January 2025 but did not serve on any committees. Co-author Leif Jahn has not contributed to this report since starting his position at the US EPA's Office of Research and Development. No other potential conflicts of interest were reported by the authors.

Although this report was produced with partial funding by the United States Environmental Protection Agency under Contract No. 68HERC19D0010 to the Health Effects Institute, it has not been subjected to the Agency's peer and administrative review and may not reflect the views of the Agency; thus, no official endorsement by the Agency should be inferred. This report also has not been reviewed by private party institutions, including those that support HEI Energy, and may not reflect the views or policies of these parties; thus, no endorsement by them should be inferred.

*A list of abbreviations and other terms appears at the end of this report.

CHAPTER 1: INTRODUCTION

Horizontal drilling and hydraulic fracturing have greatly increased the scale and rate of unconventional oil and gas development (UOGD) in the United States. Scientific evidence suggests that communities are exposed to air pollutants and noise from UOGD (Allshouse et al. 2019; Brown et al. 2014; Czolowski et al. 2017; Kroepsch et al. 2019; McCawley 2013; Slonecker and Milheim 2015), and that these exposures adversely affect human health (Casey et al. 2016; McKenzie et al. 2014, 2017; Rabinowitz et al. 2015; Rasmussen et al. 2016; Stacy et al. 2015; Steinzor et al. 2013; Tustin et al. 2017). There is a critical need for better characterization and understanding of these exposures.

UOGD operations are complex and heterogeneous, with equipment, operations, and emissions varying significantly from site to site. These source differences, the multiple pollutants emitted from UOGD, and the atmospheric reactions that transform the emissions make it challenging to characterize air pollutant exposures resulting from UOGD. Predictive tools are needed to appropriately focus and place in context measurement campaigns to assess exposures. The main goal of this project was to generate a broadly applicable community model to assess exposures to air pollutants from UOGD and to inform future health studies.

The project's main focus was on the Eagle Ford Shale in south-central Texas, a large oil and gas production region that includes the production of dry gas, wet gas, and oil. This heterogeneity of production types makes the Eagle Ford Shale a microcosm of UOGD sites throughout the United States. The project was extended in 2024 to also include modeling activities in the Marcellus Shale region and measurements from the Permian Basin. The final model (named TRAcking Community Exposures and Releases or TRACER model) can be used in other regions with appropriate input data.

REFERENCES

Allshouse WB, McKenzie LM, Barton K, Brindley S, Adgate JL. 2019. Community noise and air pollution exposure during the development of a multi-well oil and gas pad. Environ Sci Technol 53: 7126–7135; *https://doi.org/10.1021/acs.est.9b00052*.

Brown D, Weinberger B, Lewis C, Bonaparte H. 2014. Understanding exposure from natural gas drilling puts current air standards to the test. Rev Environ Health 29:277–292; *https://doi.org/10.1515/reveh-2014-0002*.

Casey JA, Savitz DA, Rasmussen SG, Ogburn EL, Pollak J, Mercer DG, Schwartz BS. 2016. Unconventional natural gas development and birth outcomes in Pennsylvania, USA. Epidemiology 27: 163–172; *https://doi.org/10.1097/ede.0000000000000387*.

Czolowski E D, Santoro RL, Srebotnjak T, Shonkoff SBC. 2017. Toward consistent methodology to quantify populations in proximity to oil and gas development: a national spatial analysis and review. Environ Health Perspect 125:086004; *https://doi.org/10.1289/ehp1535*.

Kroepsch A C, Maniloff P T, Adgate JL, McKenzie LM, Dickinson KL. 2019. Environmental justice in unconventional oil and natural gas drilling and production: a critical review and research agenda. Environ Sci Technol 53:6601–6615; *https://doi.org/10.1021/acs.est.9b00209*.

McKenzie LM, Guo R, Witter RZ, Savitz DA, Newman LS, Adgate JL. 2014. Birth outcomes and maternal residential proximity to natural gas development in rural Colorado. Environ Health Perspect 122:412–417; *https://doi.org/10.1289/ehp.1306722*.

McKenzie LM, Allshouse WB, Byers TE, Bedrick EJ, Serdar B, Adgate JL. 2017. Childhood hematologic cancer and residential proximity to oil and gas development. PLoS One 12: e0170423; *https://doi.org/10.1371/journal.pone.0170423*.

McCawley M. 2013. Air, Noise, and Light Monitoring Results for Assessing Environmental Impacts of Horizontal Gas Well Drilling Operations (ETD-10 Project). Available: *https://dep.wv.gov/oil-and-gas/Horizontal-Permits/legislativestudies/Documents/WVU%20Final%20Air%20Noise%20Light%20Report.pdf*.

Rabinowitz PM, Slizovskiy IB, Lamers V, Trufan SJ, Holford TR, Dziura JD, et al. 2015. Proximity to natural gas wells and reported health status: results of a household survey in Washington County, Pennsylvania. Environ Health Perspect 123:21–26; *https://doi.org/10.1289/ehp.1307732*.

Rasmussen SG, Ogburn EL, McCormack M, Casey JA, Bandeen-Roche K, Mercer DG, et al. 2016. Association between unconventional natural gas development in the Marcellus shale and asthma exacerbations. JAMA Intern Med 176:1334–1343; *https://doi.org/10.1001/jamainternmed.2016.2436*.

Slonecker TE, Milheim LE. 2015. Landscape disturbance from unconventional and conventional oil and gas development in the Marcellus Shale region of Pennsylvania, USA. Environments 2:200–220; *https://doi.org/10.3390/environments2020200*.

Stacy SL, Brink LAL, Larkin JC, Sadovsky Y, Goldstein BD, Pitt BR, et al. 2015. Perinatal outcomes and unconventional natural gas operations in Southwest Pennsylvania. PLoS One 10:e0126425; *https://doi.org/10.1371/journal.pone.0126425*.

Steinzor N, Subra W, Sumi L. 2013. Investigating links between shale gas development and health impacts through a community survey project in Pennsylvania. New Solut 23:55–83; *https://doi.org/10.2190/ns.23.1.e*.

Tustin AW, Hirsch AG, Rasmussen SG, Casey JA, Bandeen-Roche K, Schwartz BS. 2017. Associations between unconventional natural gas development and nasal and sinus, migraine headache, and fatigue symptoms in Pennsylvania. Environ Health Perspect 125:189–197; *https://doi.org/10.1289/ehp281*.

CHAPTER 2: SPECIFIC AIMS AND OVERARCHING APPROACH

We developed the TRACER model to assess exposures to air pollutants from UOGD and to inform future health studies. The model combines detailed emissions modeling with dispersion modeling to predict concentrations for various pollutants at receptor sites. The work described here builds on modeling capabilities developed at The University of Texas at Austin that predict the magnitude and intermittency of emissions at individual sources on UOGD sites and, when coupled with dispersion modeling, generate concentration fields of pollutants that can be used to assess community exposures. The original model was developed to predict methane emissions from UOGD. As part of this work, we further expanded that model by adding sources of emissions that were not previously included and by incorporating a broader suite of pollutants. We conducted targeted field measurements to evaluate and refine the original model and used the updated model to assess community exposure. We also conducted modeling with the Comprehensive Air Quality Model with extensions (CAMx) to estimate exposures to secondary pollutants from UOGD emissions on a regional scale.

We intended to accomplish the following aims, which are described in the following chapters:

1. **Conduct field measurements in the Eagle Ford Shale.** These measurements included stationary measurements colocated with the Texas Commission on Environmental Quality (TCEQ) monitoring station in Karnes City, as well as mobile measurements in the surrounding areas. Mobile measurements focused on characterizing emissions from flares in the area. Measured emission ratios from flares were used in the emissions modeling. Measurements at the stationary location (especially of ethane) were used in model evaluations. Some stationary measurements (e.g., of particulate matter, PM) provided additional insights into air quality in the region but were not directly used in modeling.
2. **Conduct field measurements in the Permian Basin.** These measurements were primarily conducted to build on previous HEI-funded work by Professor Meredith Franklin's team in the area (Franklin et al. 2025), offering insights into the spatial distribution of pollutants and enabling a comparison with measurements conducted in the Eagle Ford Shale. Because this project does not include modeling conducted in the Permian Basin, results from these measurements were not used in the modeling or in subsequent chapters of this report.
3. **Estimate emissions from UOGD.** We developed various spatial and temporal allocation methods and new emission factors, and we assembled emission composition data. In Chapter 5, we describe the application of these emissions estimates in the Marcellus oil and gas production region. The remaining chapters for this report (6, 7, 8, and 9) utilized those same emission estimation methods. An expanded version of Chapter 5 has been published (Chen et al. 2025).
4. **Couple emission estimation with dispersion modeling for primary pollutants**. In Chapter 6, we couple the emissions estimation model (described in Chapter 5) with dispersion modeling to predict concentrations at a receptor site in the Eagle Ford Shale. This work has been published (Graves et al. 2025).
5. **Couple emissions with chemical transport models for secondary pollutants**. In Chapter 7, we couple the emissions model described in Chapter 5 with chemical transport modeling to evaluate the impacts of nitrogen oxides emissions from UOGD on regional concentrations of ozone, a secondary pollutant. Chapter 7 summarizes the work, and the full published manuscript is included in additional materials (Modi et al. 2025).

RESEARCH ROADMAP

Aims and Research Conducted	Methods Description
Aim 1 (Chapter 3)	
Conduct field measurements in the Eagle Ford Shale	Chapter 3 and Additional Materials A
Aim 2 (Chapter 4)	
Conduct field measurements in the Permian Basin	Chapter 4 and Additional Materials B
Aim 3 (Chapter 5)	
Estimate emissions from UOGD	Chapter 5 and Additional Materials C
Aim 4 (Chapter 6)	
Couple emissions with dispersion models	Chapter 6 and Additional Materials D
Aim 5 (Chapter 7)	
Couple emissions with chemical transport models	Chapter 7 and Additional Materials E
Aim 6 (Chapter 8)	
Assess the performance of dispersion models	Chapter 8
Aim 7 (Chapter 9)	
Analyze exposure from UOGD and consider implications for future health studies	Chapter 9 and Additional Materials F

6. **Assess the performance of dispersion models**. In Chapter 8, we assess the performance of three different dispersion models applied to the Eagle Ford Shale. The work described in this chapter has been submitted for publication to ACS Environmental Au (Graves et al. 2026) and is available in preprint on ChemRxiv (10.26434/chemrxiv-2025-xkhh9).

7. **Analyze exposure from UOGD and consider implications for future health studies**. In Chapter 9, we combine emissions modeling (described in Chapter 5) with dispersion modeling to estimate exposures in Karnes County, Texas. We evaluate different dispersion models, including reduced-complexity models, for use in exposure estimates.

REFERENCES

Chen Q, Raksi N, Niewenhous L, Almasalha SJ, Graves JD, Brown VJ, et al. 2025. Spatial and temporal variability in atmospheric emissions from oil and gas sector sources in the Marcellus production region. Atmosphere 16:1048; *https://doi.org/10.3390/atmos16091048*.

Franklin M, Schade G, Helmig D, Cushing L, Johnston J. 2025. Assessing Source Contributions to Air Quality and Noise in Unconventional Oil Shale Plays. Research Report 229. Boston, MA: Health Effects Institute.

Graves J, Kimura Y, Modi M, Stokes S, Meyer M, Hildebrandt Ruiz L, et al. 2025. Source attribution of elevated ethane concentrations detected by regional monitors in oil and gas production regions. ACS ES&T Air 2:2038–2046; *https://doi. org/10.1021/acsestair.5c00235*.

Graves J, Kimura Y, Modi M, Stokes S, Meyer N, Hildebrandt Ruiz L, et al. 2026. Performance of dispersion models in predicting ambient ethane concentrations at a regional air quality monitor in an oil and gas producing region. ACS Environ Au [preprint]; *https://chemrxiv.org/doi/full/10.26434/chemrxiv-2025-xkhh9*

Modi M, Kimura Y, Hildebrandt Ruiz L, Allen DT. 2025. Fine-scale spatial and temporal allocation of NO_x emissions from unconventional oil and gas development can result in increased predicted regional ozone formation. ACS ES&T Air 2:130–140, *https://doi.org/10.1021/acsestair.4c00077*.

CHAPTER 3: FIELD MEASUREMENTS IN THE EAGLE FORD SHALE

INTRODUCTION

In the last several decades, UOGD has grown significantly in the United States. UOGD emissions depend on the oil and gas composition, which depends on the well location. The Eagle Ford Shale, an active oil and gas shale play, has experienced significant production growth over the past two decades. This growth has elevated human health concerns, as some volatile organic compounds (VOCs) detected in these areas can be potentially harmful or carcinogenic (Benedict et al. 2020; Edwards et al. 2014; Gilman et al. 2013; Koss et al. 2017). Previous studies confirmed the presence of oxidized hydrocarbons in UOGD regions, including in the Eagle Ford Shale (McPherson et al. 2024), which can lead to the formation of PM and ozone, a reactive gas that can harm human respiratory health.

In this work, we report in situ mobile and stationary observations to characterize the sources and concentrations of PM_1 (particulate matter <1 µm in aerodynamic diameter) and gas-phase pollutants to understand the influence of UOGD on air quality in the Eagle Ford Shale area, specifically in the region of Karnes City, Texas — a small town in the center of the Eagle Ford Shale. Karnes City is in the wet gas zone, surrounded by oil wells to the north and gas wells to the south. It stretches 50 miles southeast (and is often upwind) of San Antonio, Texas — the third-largest metropolitan area in Texas. The stationary measurement site in Karnes City is colocated with a continuous ambient monitoring station (CAMS) run by the TCEQ and was an anchor point for mobile measurements. We used advanced mass spectrometry in an electric mobile lab, which helped us to analyze different compositions over time and space in the region. It also allowed us to understand the variability of flaring emission ratios and how evaporative and flaring contributors can be fingerprinted and evaluated for their effects on regional air quality.

STUDY DESIGN AND METHODS

We conducted two field campaigns in Karnes City, Texas: an 8-week spring campaign from March 28 to May 14, 2023, and a 4-week fall campaign from October 20 to November 15, 2023. Karnes City — denoted by the yellow star in Additional Materials A, Figure A-1 — is located in Karnes County (Note: Additional Materials are located on the *HEI website*). Karnes County has one of the highest oil and gas well densities of the counties in the Eagle Ford Shale, with up to seven wells per square kilometer. Both campaigns included stationary and mobile measurements. Stationary measurements of PM_1 were collected with instruments housed in a 21 × 8 ft air-conditioned trailer, whereas VOCs real-time measurements were conducted from an electric van (**Figure 3-1**). The fixed-site monitoring location was 0.83 miles north of the nearest well site. In addition to continuous stationary measurements, mobile measurements were conducted to observe UOGD contributions to the spatiotemporal variability of air composition as well as to fingerprint near-source plumes and to estimate emission ratios from observed concentrations. The measured markers included VOCs, methane, carbon dioxide, black carbon, and other markers. Eleven drives were conducted during the spring campaign, and eight drives were conducted during the fall campaign, amounting to 2,279 km, 5,607 minutes, and 0.24 terabytes of data. The mobile campaign included public roads — both exploratory survey routes and focused tracks. Route planning was guided by meteorological forecasts and site accessibility. On survey days, field teams targeted areas downwind of active flares as they became visible from the road; these flares were added to the observational database and documented. For focused measurements, routes were preselected based on Visible Infrared Imaging Radiometer Suite (VIIRS)-detected flare activity and prior field observations, ensuring coverage of representative flare sites. These drives followed survey and focused tracks designed to characterize the areas close to UOGD sites and, in particular, flaring sites in the Karnes City area, informed by GIS observations, field observations, well density, and VIIRS satellite imagery.

INSTRUMENTATION

We used a wide suite of instrumentation to study particle and gas-phase species at the stationary site, and gas-phase constituents were measured in mobile measurements. For the particle phase, a Scanning Electrical Mobility Spectrometer (SEMS; Brechtel Manufacturing Incorporated Model 2002), an Aerosol Chemical Speciation Monitor (ACSM; Aerodyne Research Inc.), and an aethalometer (Magee Scientific AE33) were used. The ACSM operated with a leak in the spring (discovered post-campaign), which rendered the spring campaign data unreliable. Therefore, we are reporting ACSM data from the fall campaign only.

Gas-phase data were collected using a Vocus 2R proton-transfer-reaction time-of-flight mass spectrometer (Vocus PTR-TOF-MS) (Krechmer et al. 2018) a high-resolution time-of-flight chemical ionization mass spectrometer operated in iodide mode (CIMS; Aerodyne Research Inc.), a cavity attenuated phase shift nitrogen dioxide analyzer (CAPS-NO_2, Environment S.A AS32M) (Kebabian et al. 2008), a chemiluminescence NO/nitrogen oxides analyzer (Teledyne Model 200E), a photometric ozone analyzer (Teledyne Model 400E), a pulsed fluorescence sulfur dioxide/hydrogen sulfide analyzer (Thermo Scientific 450iQ), and a methane/formaldehyde/water gas analyzer (Picarro G2307). An automated gas chromatograph (auto-GC) operated by the TCEQ measured nonmethane organic carbons. These VOCs retrieved at hourly concentrations from the Texas Air Monitoring Information System (TAMIS) portion of the TCEQ website further complement the real-time (1-second) data measured by the Vocus.

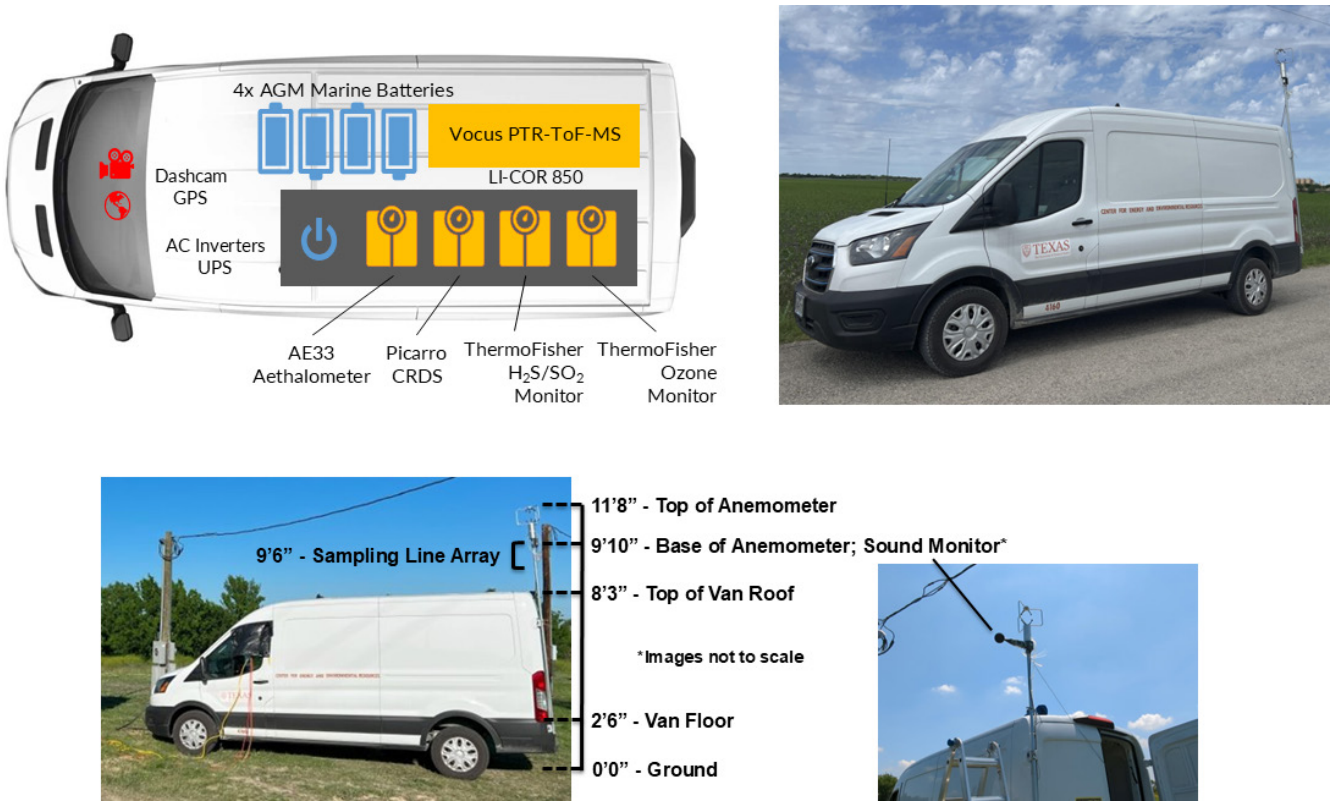

Figure 3-1. Configuration of The University of Texas electric mobile laboratory.

The mobile measurement van was outfitted with a sampling mast on its driver's side rear door, on which the sampling lines for the instruments within were secured. The mast also held several instruments: a Davis Sonic Anemometer (Davis Instruments) to measure wind direction and wind speed; a Brüel & Kjær 2245 Sound Level Meter mounted below the anemometer to measure ambient sound levels and frequencies; and a QuantAQ Modulair-Gas affixed farther down the mast to measure binned PM, carbon monoxide, nitrogen oxides, and nitrogen dioxide. GPS measurements and dashcam video were collected using a VAVA 2K dashcam. Equipment on the mobile van is summarized in Additional Materials A, Table A-1.

DATA ANALYSIS OF STATIONARY MEASUREMENTS

The data from time-of-flight mass spectrometers were analyzed using Igor Pro 8.04 (WaveMetrics), a postprocessing software for data visualization and interpretation. Igor incorporates data analysis packages for the ACSM, CIMS, and Vocus, which are provided by the instrument manufacturers. ACSM data were processed in "ACSM local" (Aerodyne Research), whereas CIMS and Vocus analyses were in Tofware V3.2.3–V4.0.1 (Tofwerk). Further processing and quality control, including calibration and background subtraction, were performed in MATLAB following standardized routines (e.g., Brodfuehrer et al. 2024; de Gouw and Warneke 2006; Werner et al. 2021). Vocus data points were corrected for reduced transmission efficiency in the lower mass range following the approach described in Li and colleagues (2024). All Vocus data points that were below the detection limit were replaced with 0.5 × detection limit (Helsel 1990). Detection limits were calculated for each reported compound after every calibration following Taipale and colleagues (2008).

ACSM and SEMS recorded measurements every minute, but hourly post-averaging was applied. All ACSM data points that were below the detection limit were replaced with 0.5 × detection limit. Finally, to account for the particle losses at the vaporizer, a composition-dependent collection efficiency was applied (Middlebrook et al. 2012). Wind roses were created from the TCEQ meteorological data using R (R Studio), a tool for data analysis and statistical computing.

The stationary trailer was colocated with a TCEQ CAMS (CAMS 1070, US EPA Site 482551070, coordinates: 28.8804400, –97.8880650). Auto-GC data from this station were retrieved on the TAMIS portion of the TCEQ website (TCEQ 2024). The auto-GC collects samples for 40 minutes and then analyzes them for a suite of nonmethane organic compounds. The result is reported as an hourly concentration. Calibrations were conducted daily for all reported spe-

cies (TCEQ 2025b). Compounds reported from the auto-GC data for this project are as follows: ethane, propane, n-butane, n-pentane, n-hexane, n-heptane, n-octane, n-nonane, n-decane, propylene, isobutane, 1,3-butadiene, cyclopentane, cyclohexane, methylcyclohexane, benzene, toluene, m/p-xylene, o-xylene, ethylbenzene, styrene, and isoprene. The methane/formaldehyde/water gas analyzer (Picarro G2307) acquired data at a rate of 1 Hz. Data were averaged to 1-hour intervals during processing to be consistent with auto-GC data.

The Vocus acquired data at a rate of 1 Hz. Data were averaged over 1-minute intervals during processing for the stationary period from April 3 to 27, and over 10-second intervals for the mobile periods from March 24 to April 2 and November 8 to November 16. The ion-molecule reactor pressure was 2.3 millibar, the reactor temperature was set to 65°C, and the front and back voltages were set to 645 V and 15 V, respectively. The electric field strength divided by the concentration of neutral gas ratio was calculated to be 134 Trolands. Calibrations were conducted generally before and after each mobile measurement period. Reaction rate constants were retrieved for compounds that were explicitly calibrated using an Apel-Reimer gas standard described in Additional Materials A, Table A-2. Sensitivities obtained from each of the calibrant analytes were plotted to obtain a correlation plot relating sensitivity to respective proton-transfer-reaction rate coefficients obtained from Pagonis and colleagues (2019). This relationship was used to quantify compounds that were not included in the calibration standard. During the stationary period, a calibration was conducted every one to two days, with 18 in total. Compounds reported from the Vocus data for this project are as follows: $C_6H_6OH^+$ (phenol), $C_{10}H_8OH+$ (total naphthols), $C_2H_4OH^+$ (acetaldehyde), $C_7H_6OH^+$ (benzaldehyde), $C_{10}H_8H^+$ (naphthalene), $C_6H_6^+$ (benzene), $C_7H_8H^+$ (toluene), $C_8H_{10}H^+$ (total C8-aromatics), $C_8H_8H^+$ (styrene), $C_2H_6SH^+$ (dimethylsulfide+ethanethiol), $C_{10}H_{16}H^+$ (total monoterpenes), and $C_8H_8OH^+$ (acetophenone). Vocus data were processed using Tofware V3.2.3–V4.0.1 (Tofwerk). An initial peak list comprising 1,311 protonated ions was used from the NOAA FIREX 2016 laboratory experiment (Koss et al. 2018). Additional peaks were added manually to include calibrant ions and the benzene charge transfer $C_6H_6^+$ ion (Coggon et al. 2024). Raw counts per second data were then exported to a custom MATLAB program for further analysis.

DATA ANALYSIS OF MOBILE MEASUREMENTS

Data analysis of mobile measurements was generally consistent with that described above for stationary data. The datasets were synchronized with the coordinate data recorded by GPS, and the time shifts of different instruments have been evaluated and corrected as needed. The major shift was observed in the Picarro methane/formaldehyde instrument, which was measured on a separate PC aligned using the plume data from other instruments. The mobile Vocus data were averaged over 10-second intervals to maintain high spatiotemporal resolution for capturing short-lived plumes near UOGD sources. Averaged data were integrated with GPS and other monitor data for flare plume analysis.

Black carbon was measured with the Magee Scientific AE33 Aethalometer at 1 Hz. The AE33 uses Teflon-coated glass fiber filter tape to collect aerosol from the sample stream, then measures the attenuation of light transmitted through the filter at seven wavelengths simultaneously: 370 nm, 470 nm, 520 nm, 590 nm, 660 nm, 880 nm, and 950 nm. Black carbon concentration is associated with the light attenuation at 880 nm. The Neutral Density Optical Filters Kit was used to verify the response of the optical detectors on the AE33. This tool comprises a series of optical filters with known, stable optical absorption values, which are consecutively placed before the optical detectors in the aethalometer to test their performance and consistency. The relationship between the output signals from the optical detectors and the known filter densities provides a measure of the detectors' performance, and the stability of that relationship across multiple tests — and compared with the original factory values — indicates their consistency over time.

Sound levels and frequencies were measured with the Brüel & Kjær 2245 Sound Level Meter, affixed below the sonic anemometer on the sampling mast approximately 9'10" above the ground and 1'7" above the roof of the van. The sound meter was set to log measured noise levels and frequency spectra at 1 Hz, and the sound level measurements include both A-frequency-weighted (notional human hearing response, conforming to IEC 61672 and ANSI S1.4) and C-frequency-weighted (lower frequency sounds; used for peak sound pressure measurements) data. The data were exported using the HBK Enviro Noise Partner software, with the following sound level metrics: LAFmax (maximum time-weighted sound level, with A-frequency and fast time weighting), LAFmin (minimum time-weighted sound level, with A-frequency and fast time weighting), LCpeak (peak sound level, with C-frequency weighting), and LAeq (equivalent continuous sound level, with A-frequency weighting). The frequency spectra used the following intervals: LBeq (equivalent continuous sound level, with B-frequency weighting) 12.5 Hz, 16 Hz, 20 Hz, 25 Hz, 31.5 Hz, 40 Hz, 50 Hz, 63 Hz, 80 Hz, 100 Hz, 125 Hz, 160 Hz, 200 Hz, 250 Hz, 315 Hz, 400 Hz, 500 Hz, 630 Hz, 800 Hz, 1 kHz, 1.25 kHz, 1.6 kHz, 2 kHz, 2.5 kHz, 3.15 kHz, 4 kHz, 5 kHz, 6.3 kHz, 8 kHz, 10 kHz, 12.5 kHz, 16 kHz, and 20 kHz. The sound meter was calibrated with the Brüel & Kjær 4231 Calibrator immediately before the start of each mobile measurement drive during the fall 2023 campaign. The 4231 calibrator uses a calibration frequency of 1 kHz ±0.1% and calibration pressures of 94.0 decibels (dB) ±0.2 dB (principal sound pressure level) and 114.0 dB ±0.2 dB (for environments with higher background noise and to check linearity with the +20 dB step); the reference level is 20 microPascals. The calibrator reports deviations from the most recent check and the initial factory calibration and will flag any deviations greater than 0.05 dB from either of those references. All calibration checks during the fall 2023 campaign passed.

RESULTS

Data from mobile and stationary measurements are available at *https://utexas.app.box.com/s/sgo6nnoaaf646a2y3oqhfpy60mr7yd3k*.

SPATIOTEMPORAL DISTRIBUTION OF SOURCES

While the stationary trailer monitored pollutant concentrations at the TCEQ background location in Kanes City, the mobile van was able to conduct more spatially extensive surveys and get close to specific UOGD sources. The van drove routes on public roads throughout Karnes City and neighboring towns, as shown in **Figures 3-2** and **3-3**. Colocated stationary overnight measurements were conducted using the mobile platform at the background location. Colocated measurements were also conducted at a second TCEQ background location for a single day (US EPA Site 484931038, CAMS 1038, Floresville Hospital Boulevard).

FINGERPRINTING AND PLUME ANALYSIS FROM UOGD SITES

Thirty-five active oil and gas sources were selected either beforehand or in exploratory drives and visited numerous times to transect source plumes during favorable meteorological conditions and wind direction, allowing for measurements from public roads. When plumes were observed during real-time measurements, the mobile platform remained stationary to better characterize the plume downwind of sources. An example of real-time plume measurement is shown in **Figure 3-4**.

Following quality control and investigation of plume types and strengths, 17 plume sources from 12 separate flares were selected for deeper analysis based on observations of flares at individual sites. A summary of flare analysis is summarized in Additional Materials A, Table A-4, and can be accessed at *https://utexas.app.box.com/s/sgo6nnoaaf646a2y3oqhfpy60mr7yd3k*.

For a given source plume, 10-second average periods during the highest carbon dioxide concentration enhancement were selected for analysis; 10-second measurement periods distant from the plume were subtracted from the plume measurements to calculate the concentration enhancement at a given site. Emission ratios were calculated as the ΔVOC-to-ΔCO_2 ratio (in ppt/ppm), and methane destruction removal efficiencies were calculated using **Equation 3-1** below, following the methodology of Caulton and colleagues (2014).

$$\text{Destruction removal efficiencies (\%)} = \left(1 - \left(\frac{\mu CH_4}{(x \times \mu CO_2) + \mu CH_4}\right)\right) \times 100 \qquad \textit{(3-1)}$$

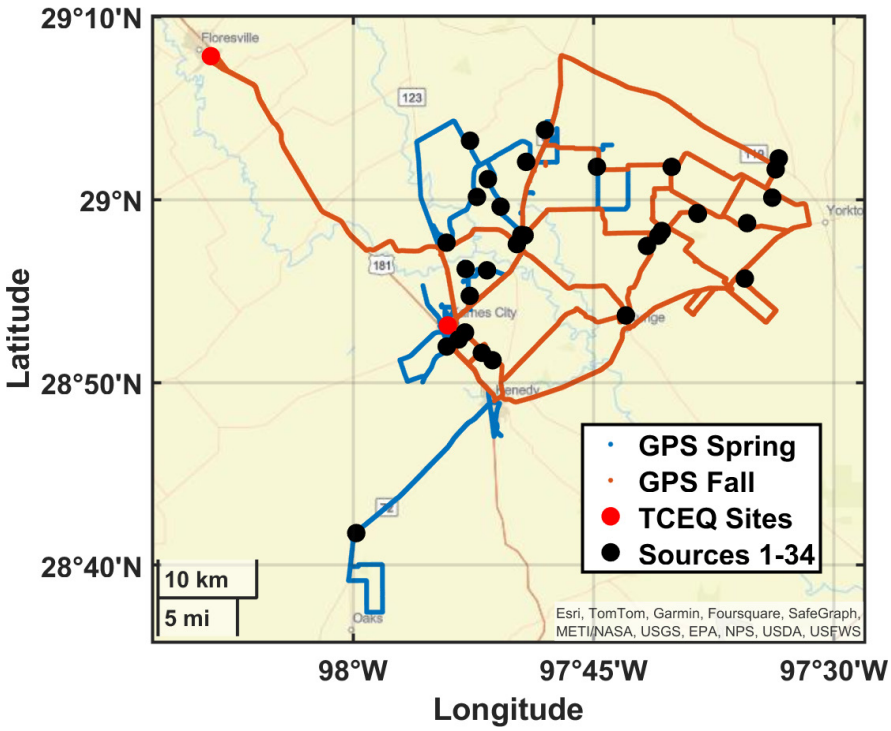

Figure 3-2. Mobile measurement overview of the intensive campaigns in spring and fall 2023.

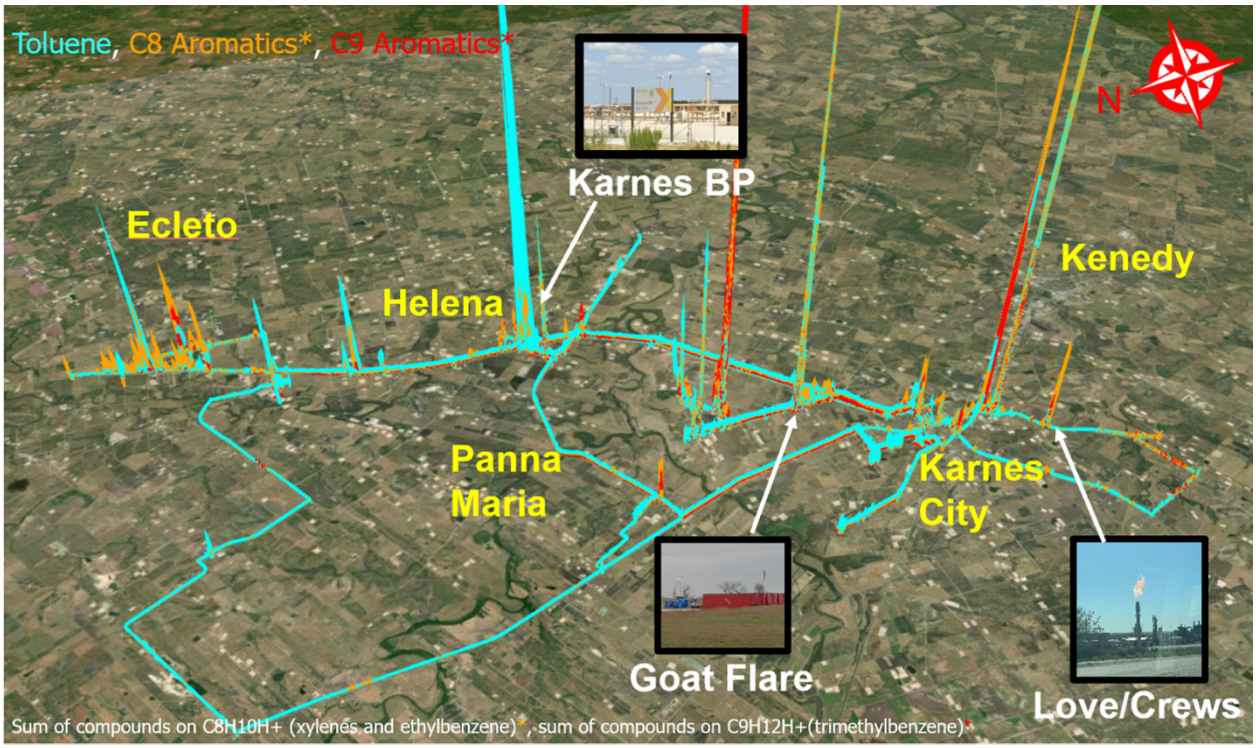

Figure 3-3. Mobile measurements of benzene, toluene, and total C8-aromatic compounds in spring 2023.

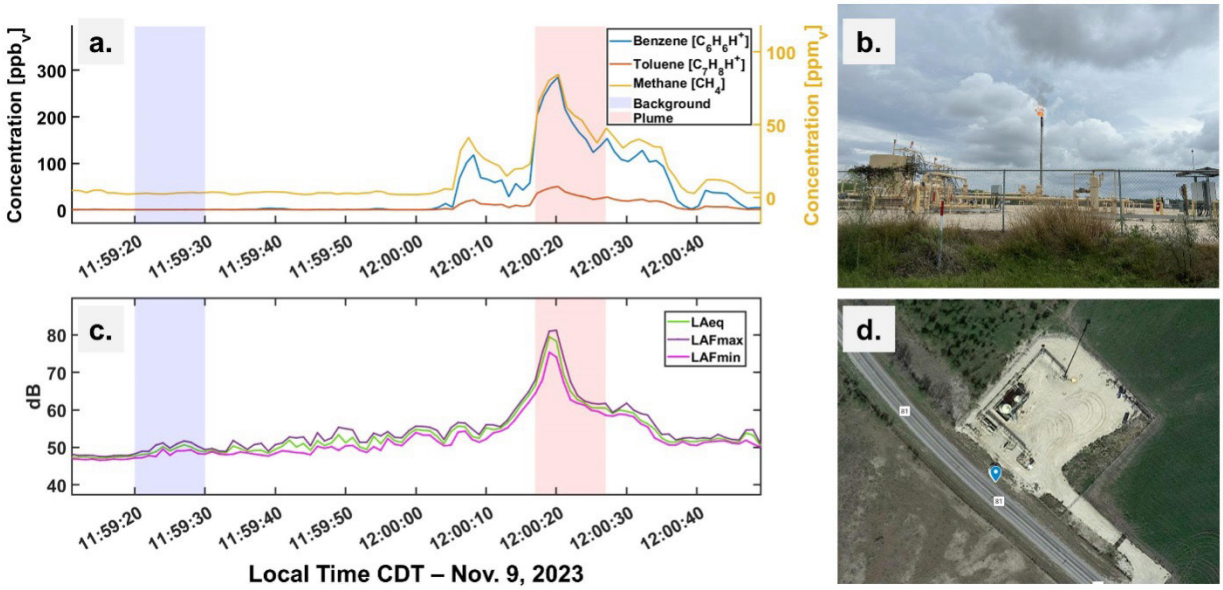

Figure 3-4. Concentrations of toluene, benzene, and methane (A) and sound levels (C) measured in a plume observed near a flaring site; a photograph (B) and satellite image (D) of the flaring site.

X is the average mole fraction of methane in natural gas received (~0.74) taken from the EPA Facility Level Information on GreenHouse Gases Tool for two facilities near Karnes City (EOG Resources, Milton Hub, and Area 71B CGP Facility) for the 2023 reporting year. To constrain a potential interference of nonflaring contributions, destruction removal efficiencies were not calculated if the carbon dioxide/methane enhancement ratio was below 10.

Each source was characterized by different source strengths and showed compositional similarities as well as differences. The destruction removal efficiencies spanned from 76.46% to 99.16%, with a mean of 94.46% and a median of 96.644%, which is in a range similar to that observed in the aircraft campaign by Lavoie and colleagues (2017) in the Eagle Ford Shale flares, indicating that methane destruction is not always complete in this region. Emission ratios for methane were generally higher than the estimates reported by Caulton and colleagues (2014), with mean values of 0.046 ppm methane/ppm carbon dioxide in our study compared with 0.0011 ppm methane/ppm carbon dioxide reported by Caulton and colleagues.

In addition to visual inspection of plumes, multivariate factor analysis (Worton et al. 2011) was applied to individual flare plumes to investigate potential contributions from multiple sources at a given site (i.e., flare emissions versus nonflaring evaporative emissions, such as from storage tanks or unintended leaks). Specifically, factor analysis was used to remove plumes that did not have a dominant "flaring factor" associated with carbon dioxide, and plume averages reported in Table A-4 were averaged over periods during which the carbon dioxide factor was most enhanced and to avoid influence from other factors.

The MATLAB *factoran* function was run with 13 VOC species and carbon dioxide, and increasing factor numbers from 3 to 6. Two dominant factors emerged in most cases: (1) one most closely associated with carbon dioxide, which was assigned to flaring combustion, and (2) one most closely associated with UOGD-related VOCs, which was assigned to emissions from storage tanks or unintended leaks. Within these two common factors, individual sites showed source differences and varied factor loadings for each reported compound. A previous study from Schade and Roest also identified two dominant factors upwind of the Eagle Ford Shale using a similar factor analysis approach (Schade and Roest 2016). These near-source profiles provide unique loadings previously unobserved far downwind at the stationary site in Floresville. An example factor analysis for one of the sites is shown in **Figure 3-5**. Filtered tables of factor loadings (>0.4) and figures illustrating all other flare plumes can be found in Additional Materials A, Tables A-10 through A-18, and Figures A-12 through A-20.

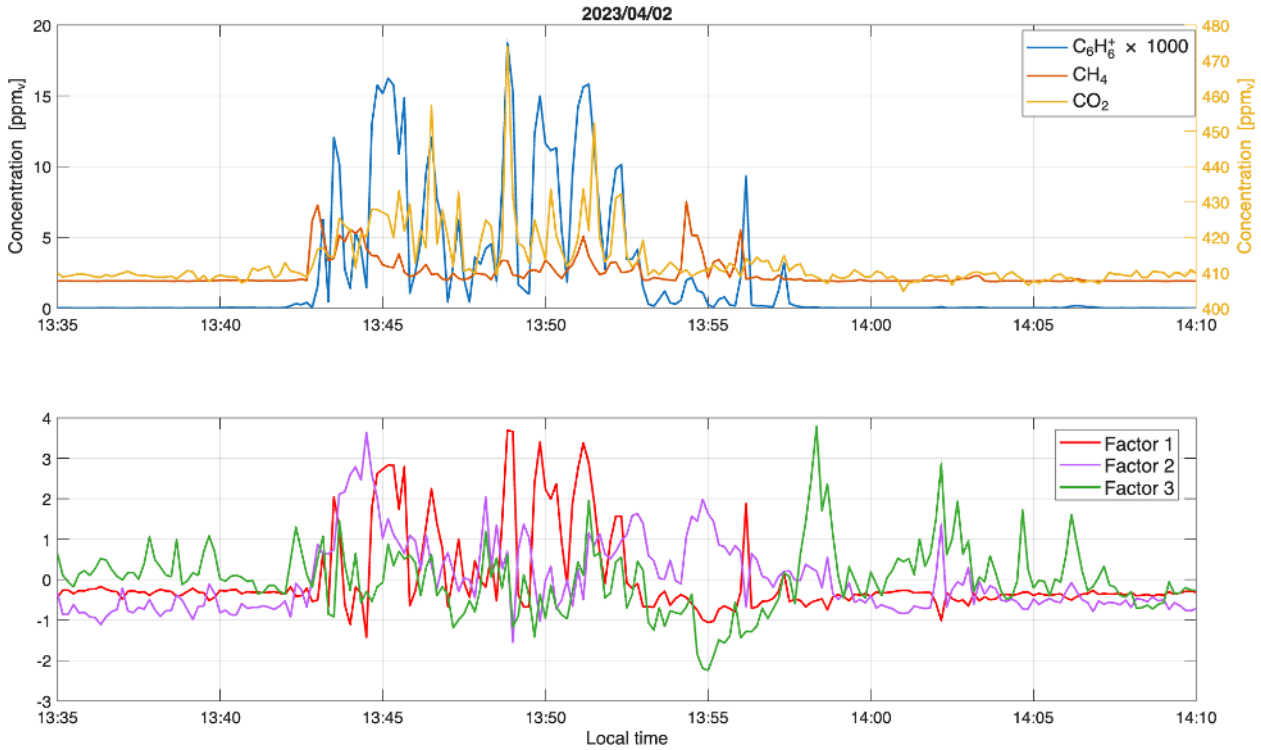

Figure 3-5. Plume variability of benzene ($C_6H_6^+$), methane (CH_4), and carbon dioxide (CO_2) concentrations (top panel); multivariate factor analysis, three-factor solution (bottom panel).

The value of this analysis is clear; without it, the proportion of sources in the mixed plumes would not be visually discernible. In the example given above, the flaring contributions were grouped in Factor 1, which is enhanced during the period when carbon dioxide, benzene, and methane are all correlated (13:45–13:50). The evaporative (nonflaring) contributions are well represented by Factor 2, which was not associated with carbon dioxide in the loading. Starting at 13:43 local time, the plume appears to be mostly evaporative, mixing and becoming pure flaring as the van gets positioned in the center of the plume. After exiting the flaring plume at 13:53, the van encounters an evaporative nonflaring plume again. While in this example the plumes can be distinctly separated, at a certain angle and wind direction, it is possible to receive both plumes simultaneously when the factor loadings can quantify the proportion of each plume. Factor 3 was likely not directly associated with UOGD, representing other source types such as agricultural or diffuse oxidative sources. In other words, the analysis can point to where flare source contribution is pure (~100%), mixed, or nonflaring.

VOC EMISSION RATIOS FROM FLARING SITES

The flaring plume enhancement data served to estimate the emission ratios with respect to carbon dioxide. The emission ratios are shown in Table A-5.

Overall, we observed high variability in these emission ratios across the sites, reflecting differences in the burned mixtures as well as burning conditions. The replicated plumes from the same site at different times showed similar emission ratios within the same order of magnitude. Across all the sites, the emission ratios of benzene spanned from 1.8 to 688 ppt/ppm carbon dioxide, with a mean of 89 ppt/ppm carbon dioxide and a median of 8 ppt/ppm carbon dioxide. The high mean-to-median ratio points to the presence of super-emitters (e.g., caused by incomplete combustion) or could potentially come from mixed evaporative and flaring plumes. While the mean-to-median ratio was very high for benzene and other aromatics (>10), it was lower for benzaldehyde (less than a factor of 2). The formation of this toxic air pollutant seems more uniform across the sources and less sensitive to flaring conditions. Benzaldehyde is believed to be a styrene oxidation product, but styrene variability seems much larger than that of benzaldehyde, consistent with noncombustive oxidation as one source of this hazardous air pollutant. The emission ratios of methane spanned from 0.006 to 0.228 ppm/ppm carbon dioxide, with a mean of 0.046 ppm/ppm carbon dioxide and a median of 0.026 ppm/ppm carbon dioxide. These methane emission ratios are overall higher than the estimates reported by Caulton and colleagues (2014), with the mean exceeding their reported maximum value of 0.035 ppm/ppm carbon dioxide.

ASSOCIATING SOUND AND CHEMISTRY

Although the sound meter logged data continuously during the mobile measurement drives, the time periods when the van was moving were excluded from the sound analysis to minimize the effects of motion-induced wind noises. We primarily examined the periods when the van was stationary and near an active flare, called the "stationary near-site" period. Using 10-second averages, the sound level time series is plotted alongside the measured concentrations of targeted compounds, which are typical in flaring plumes, to identify the times and locations at which noise and chemical exposures could potentially coincide (**Figure 3-6**). The stationary period is highlighted in green in the bottom panel of Figure 3-6. During this time, wind-related sound interference was minimal because the van was not in motion. The frequency spectrum averaged over the stationary period provides insight into the signal strength of different frequency ranges over the entire stationary near-site period (**Figure 3-7**).

Patterns in detected sound levels during stationary near-site monitoring may point to certain sources or activities. For instance, the sound measurement on November 15, 2023, starting at 14:34, showed a series of distinct and periodic spikes in sound level, rising from a baseline of approximately 58 dB to around 72 dB, with some reaching as high as 89 dB. There were, on average, five such spikes per minute during this measurement segment, with ~8 seconds between each spike.

This pattern did not appear when the measurement vehicle was away from the flaring site, so it was likely related to the equipment that was in use at the site. The measurement team observed active flaring at the site and no personnel or other vehicles. The mobile measurement van was ~9 m from the nearest facility fence line and 75 m from the base of the active flare. The measurement team noted that the noise was perceivably louder at this site, but could not identify the specific source or machinery producing the sound. The maximum sound levels detected at the flaring sites are shown in Table A-4.

Frequency spectra differed in distribution and magnitude. At the stationary site, the average frequency spectra tended to skew to the right, showing a more gradual decrease in magnitude in the higher frequency bands. The average LAeq sound level was ~50 dB, consistent across different days and different times of day when the van was parked at the stationary site. More detailed insight into frequency distributions near sites can be found in Additional Materials A.

The frequency spectrum changed when the van approached a flaring site. Figure A-2 in Additional Materials A shows the average spectrum of the stationary near-site period starting on November 15, 2023, at 14:34, the same source as in **Figure 3-8**. All the frequency bands have a higher sound level than at the stationary site, with the 315 Hz band reaching a maximum LBeq of 63 dB. The average LAeq sound level was much louder as well, at 69.8 dB.

STATIONARY MEASUREMENTS

During stationary periods, we conducted measurements at the Karnes City site to observe the arrival of fresh and aged-diluted plumes during the day and night.

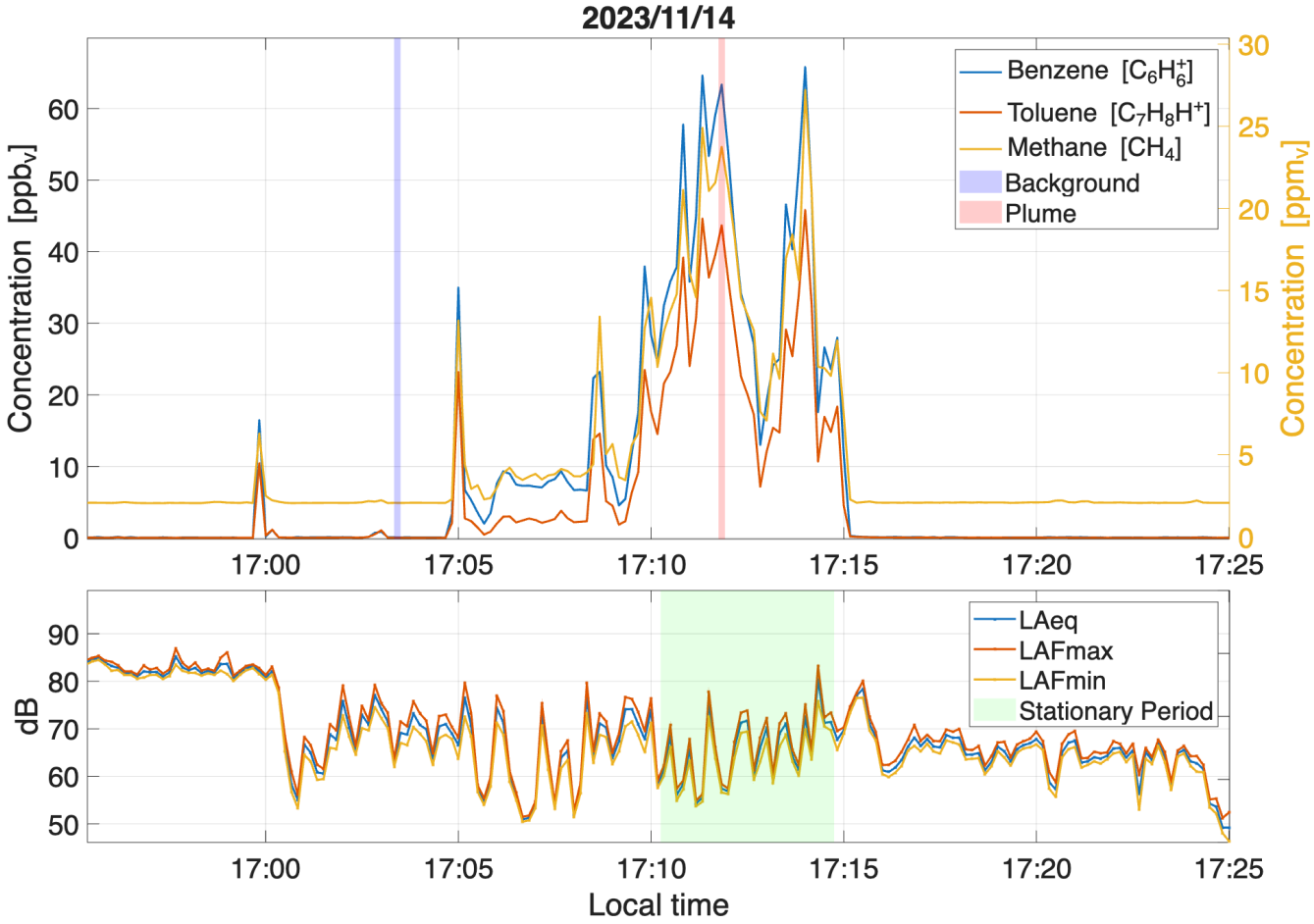

Figure 3-6. Corresponding time series of select compounds of interest and sound levels.

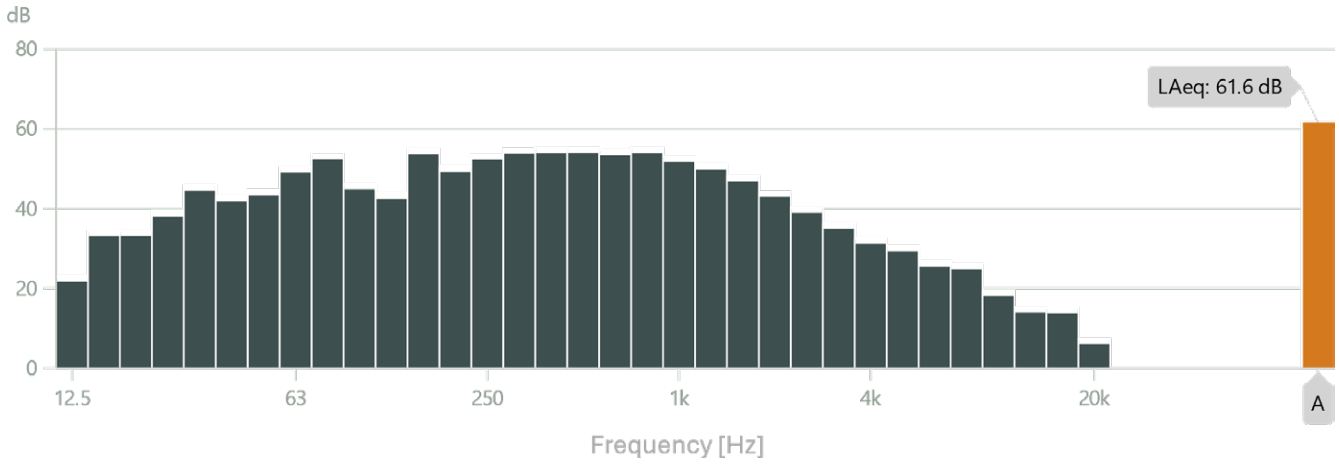

Figure 3-7. Average frequency spectrum and average sound level during stationary near-site period.

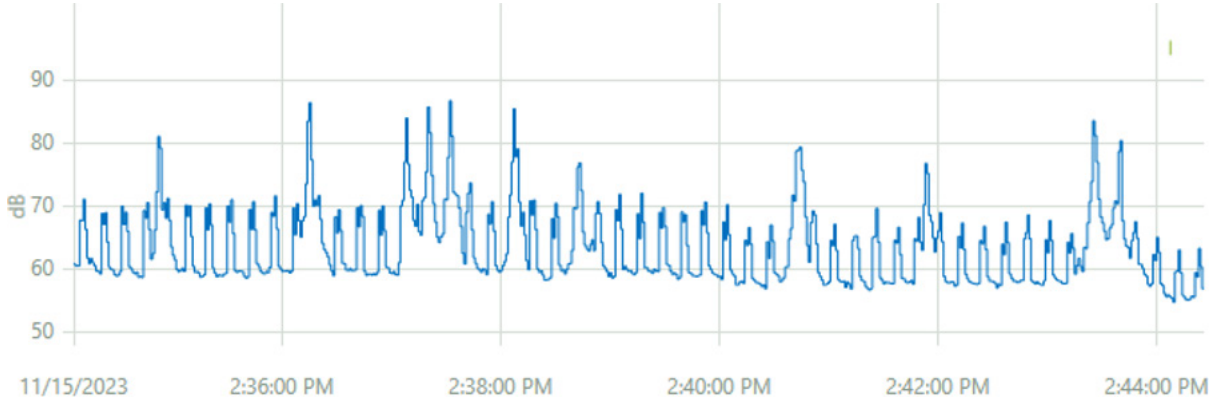

Figure 3-8. LAeq sound level during stationary near-site period on November 15, 2023, 14:34–14:44.

PARTICLE-PHASE DATA

In spring 2023, we measured particle-phase data using the SEMS. **Figure 3-9** shows a time series of total PM_1 concentrations from April 18 to May 14, 2023. Particle size distributions were measured by the SEMS, and PM_1 mass concentrations were calculated from particle volume by multiplying by an estimated density of 1.7 g/cm^3.

The maximum PM_1 concentration was 39.2 µg/m^3, with an average PM_1 concentration throughout the campaign of 6.7 µg/m^3. The average concentration was similar to that in spring 2021 (McPherson et al. 2024). Some periods were measured with PM_1 concentrations over four times the campaign average, especially in May 2023. The highest PM_1 concentrations were measured when the wind originated from the southeast and south-southeast directions.

Figure 3-10 shows the time series of nonrefractory PM_1 (NR-PM_1) mass concentrations and composition during the fall 2023 campaign. Nonrefractory is defined as a species that flash-vaporizes at the instrument's vaporizer temperature of 600ºC. The ACMS does not detect refractory species, including black carbon, ash, mineral dust, and most metals. On average, the NR-PM_1 comprised 64% organic aerosol, 18% sulfate, 10% ammonium, 7% nitrate, and 1% chloride. PM_1 consisted mainly of organic aerosol and sulfate. The maximum NR-PM_1 concentration was 12 µg/m^3, with an average NR-PM_1 concentration of 3.5 µg/m^3. Figure A-3 in Additional Materials A shows a time series of the organic components estimated from organic aerosol mass spectra (Ng et al. 2011). This analysis suggests that the organic aerosol measured at the Karnes City site was primarily oxygenated organic aerosol, consistent with secondary organic aerosol formed from oxidation of gas-phase compounds.

Even though nitrate and chloride constituted the smallest amount of the NR-PM_1, the highest concentrations of these components were observed when the wind was coming from the northeast. This scenario was also observed in a previous campaign conducted during the spring of 2021 in

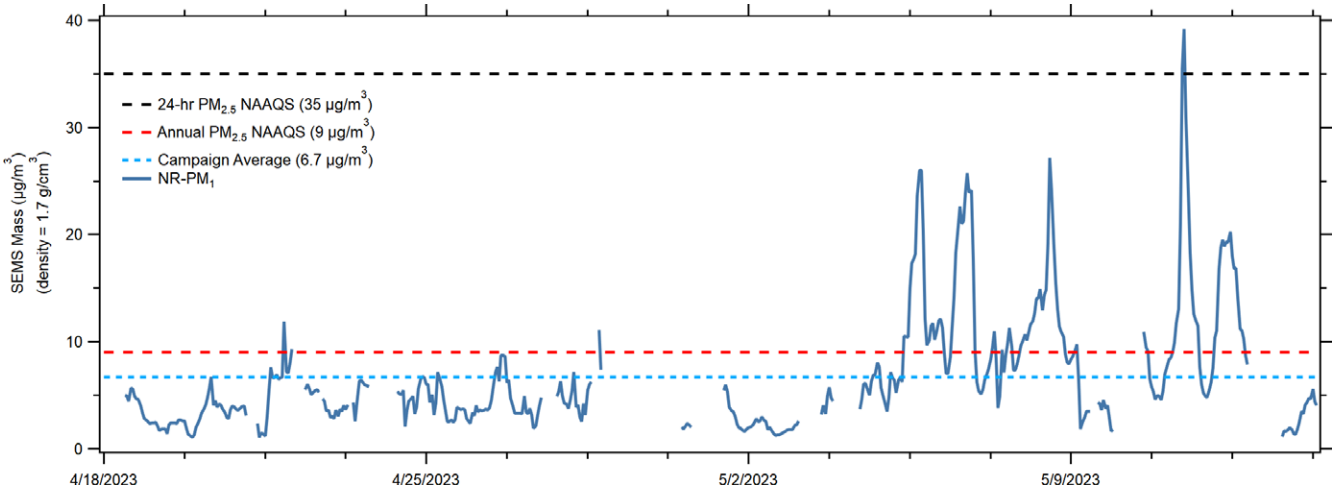

Figure 3-9. PM_1 mass concentrations time series from the SEMS in spring 2023. NAAQS = National Ambient Air Quality Standards; NR-PM_1 = nonrefractory PM_1; $PM_{2.5}$ = particulate matter ≤2.5 µm in aerodynamic diameter.

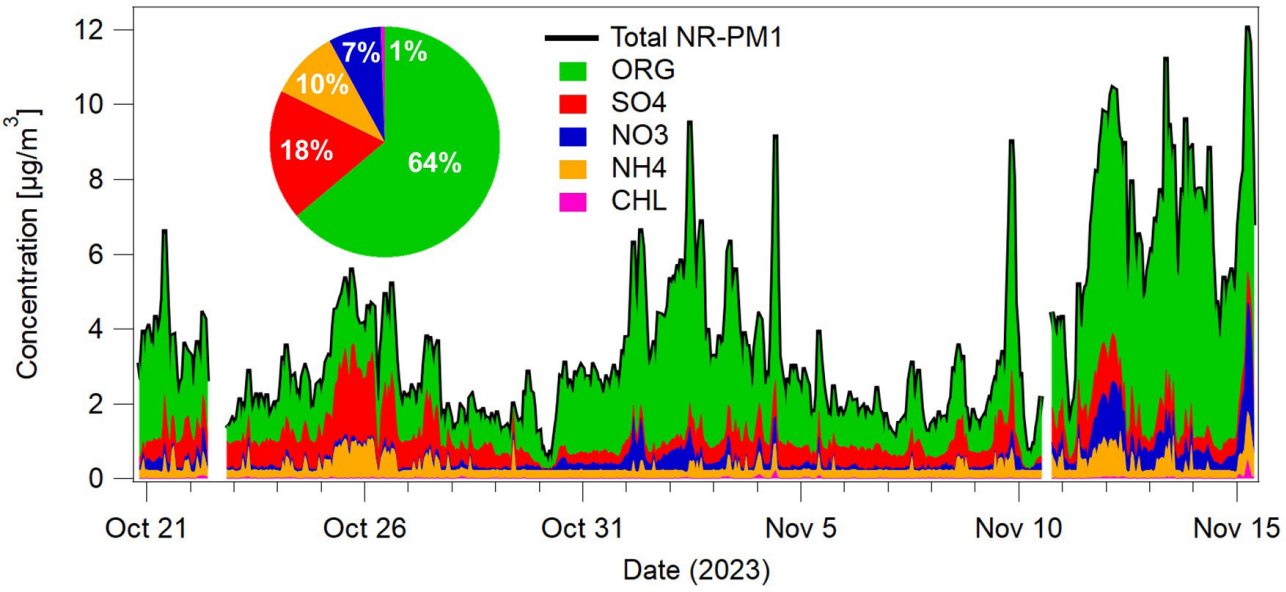

Figure 3-10. Time series of NR-PM_1 mass concentrations (µg/m³) and composition from the ACSM. Chl = chloride; NH_4 = ammonium; NO_3 = nitrate; NR-PM_1 = nonrefractory PM_1; Org = organic aerosol; PM = particulate matter; SO_4 = sulfate.

Karnes City (Masoud et al. 2023; McPherson et al. 2024). Concentrations of organic aerosol were also higher when the wind was coming from the northeast, where oil well density is higher. Overall, concentrations were lower in the fall than in the spring, and spring 2023 concentrations were similar to those observed in spring 2021 (McPherson et al. 2024). The average NR-PM_1 concentrations we measured in spring and fall 2023 were below the US EPA National Ambient Air Quality Standards (NAAQS) for particulate matter ≤2.5 µm in aerodynamic diameter ($PM_{2.5}$) (US EPA 2024) of 9 µg/m³ annual average and 35 µg/m³ daily average concentrations.

PARTICLE-PHASE DATA

Figure 3-11 shows the diurnal cycles of nitrogen oxide, ozone, sulfur dioxide, and hydrogen sulfide concentrations. The diurnal variations of NO_x and O_3 were similar to those from the 2021 measurements (McPherson et al. 2024). Nitrogen oxides concentrations peak in the morning and are lowest in the afternoon due to photochemistry and higher boundary layer heights in the afternoon. Concentrations of nitrogen oxides varied between 0 and 26 ppb, and the campaign average was 2 ppb, lower than the average from the spring 2021 campaign (McPherson et al. 2024). Ozone concentrations ranged from 3 to 65 ppb. Nitrogen oxides and ozone concentrations are consistent with typical ambient trends.

Hourly averaged hydrogen sulfide concentrations ranged from 0 to 22 ppb. Hourly averaged sulfur dioxide concentrations varied between 0 and 13 ppb with an average of 0.4 ppb, below the 75 ppb NAAQS 1-hour daily maximum concentrations (US EPA 2014). Hydrogen sulfide concentrations were consistently higher than sulfur dioxide concentrations during this campaign, and several distinct spikes in hydrogen sulfide occurred when methane and nonmethane organic compounds were also elevated. Overall, concentrations of hydrogen sulfide and methane over the entire campaign correlated only weakly (R^2 = 0.29), suggesting that UOGD activities that result in methane emissions sometimes also emit hydrogen sulfide. Sulfur dioxide, on the other hand, does not correlate with methane, as expected, as it is photochemically produced from hydrogen sulfide.

Figure 3-12 shows the diurnal cycles of methane and formaldehyde. Like many other VOCs, as well as nitrogen oxide, nitrogen dioxide, and hydrogen sulfide, shown in Figure 3-11, methane concentrations decrease throughout the day because of photolysis and a higher boundary layer. However, formaldehyde shows a daytime increase after sunrise and peaks in the afternoon, suggesting that the formaldehyde measured during these campaigns was generally a by-product of VOC oxidation. However, some periods of elevated formaldehyde concentrations (Figure A-4) may have been due to emissions from a primary source.

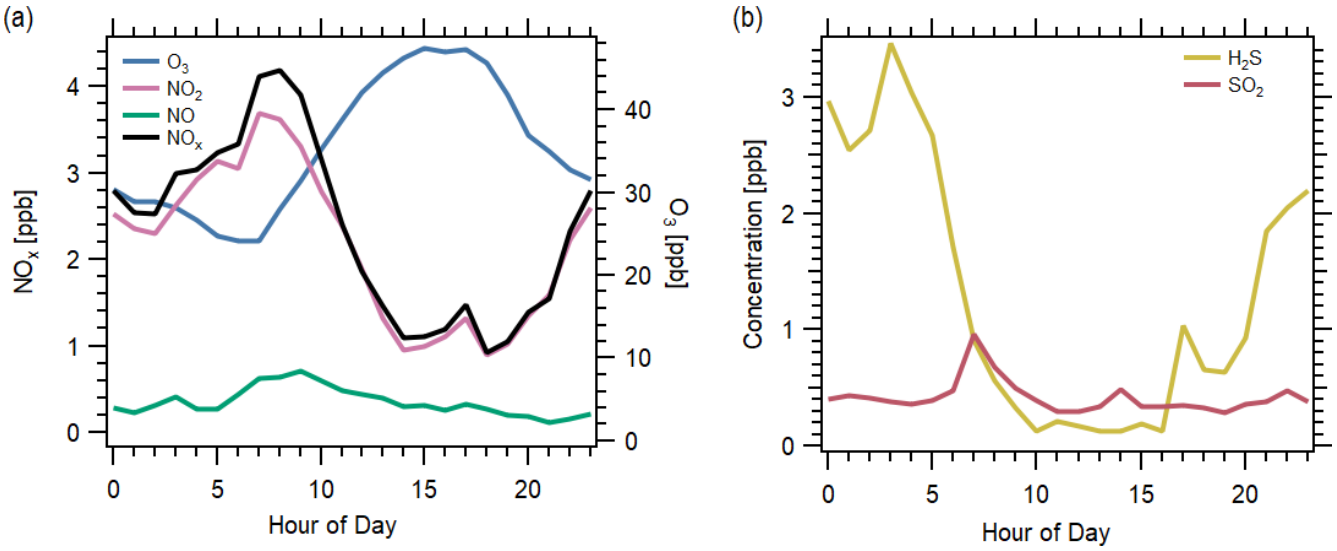

Figure 3-11. Diurnal cycles of nitrogen oxides (NO_x) and ozone (O_3) (A) and hydrogen sulfide (H_2S) and sulfur dioxide (SO_2) (B).

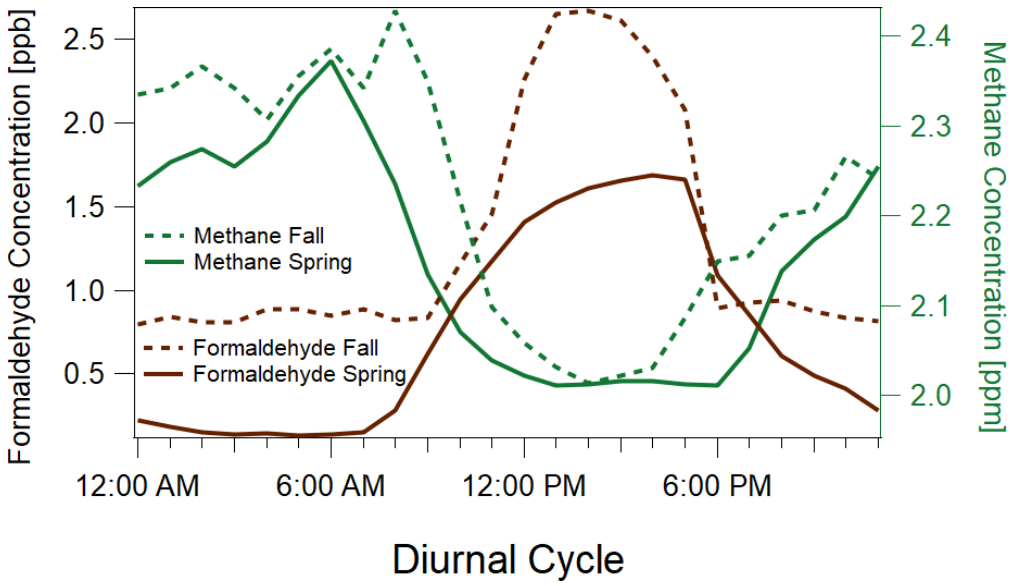

Figure 3-12. Diurnal cycles of methane and formaldehyde during the spring and fall campaigns.

Tables A-6 to A-8 in Additional Materials A show the limit of detection, mean, maximum, and minimum concentrations of VOCs of interest measured by the auto-GC, Vocus, and methane/formaldehyde/water gas analyzer, respectively. As shown in Table A-6, light alkanes had the highest concentrations of all VOCs measured during the campaign's stationary periods. Ethane, propane, and n-butane are plotted along with methane in **Figure 3-13**. These light alkane emissions often correlated with elevated concentrations of benzene and toluene, also shown in Figure 3-13.

Figure 3-13 shows intermittent, elevated concentrations of light alkanes, benzene, and toluene, suggesting that emissions from oil and gas production in the Eagle Ford Shale substantially influence air quality at this stationary background location. These plumes often occur at night and can be a result of routine emissions and favorable meteorological conditions or nonroutine emission events, as described in more detail in Chapter 6.

Additionally, Figure A-5 shows the ratio of ethane to methane during periods of elevated light alkane levels. The

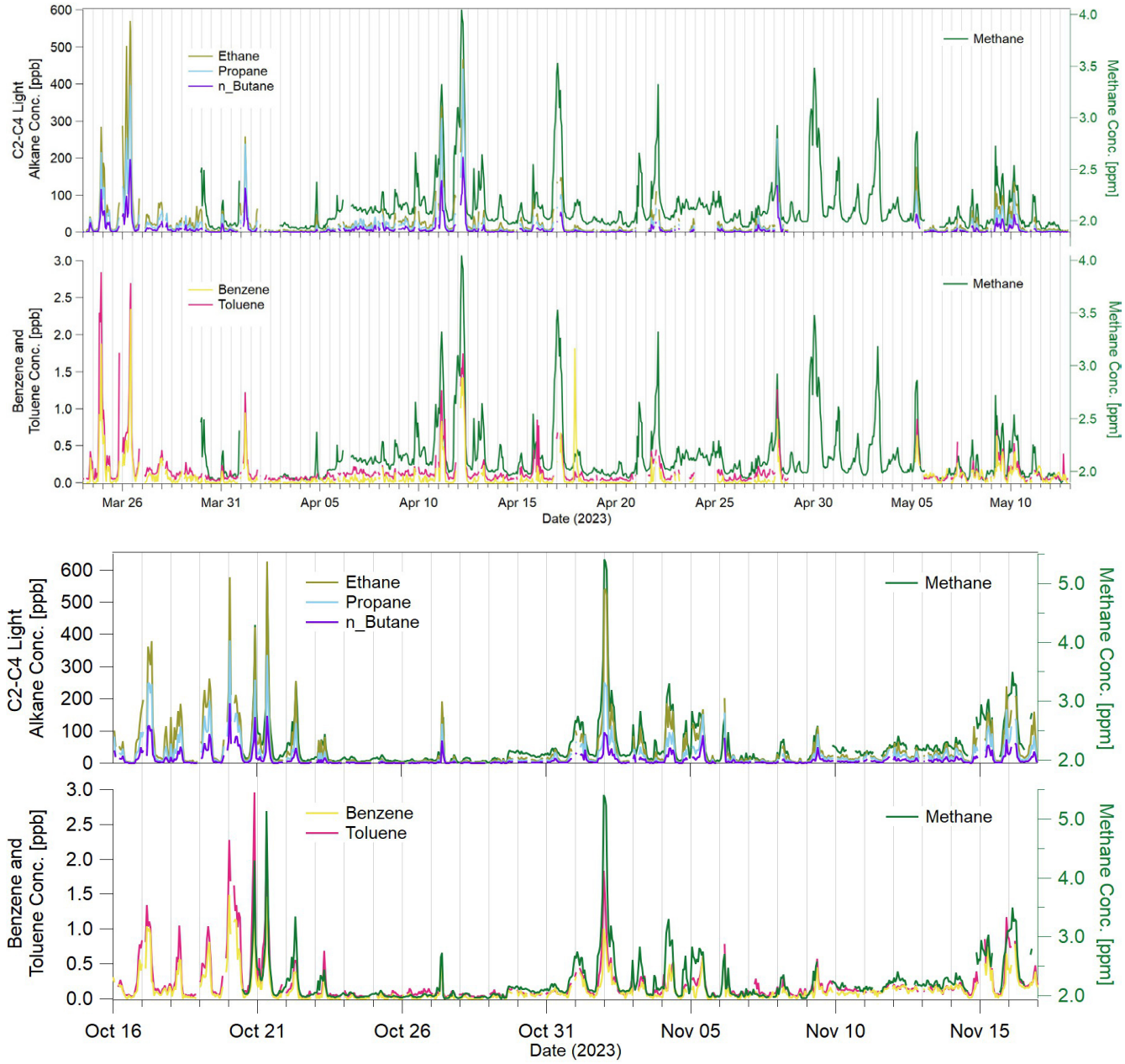

Figure 3-13. Time series of methane, ethane, propane, n-butane, benzene, and toluene from the spring (top: March 24–May 12) and fall (bottom: October 16–November 16) 2023 campaigns.

slope of the line is 0.182, which is consistent with characteristics of Eagle Ford Shale gas reported in the literature (see George and Bowles 2011). Other compounds that traveled to this stationary background location, likely originating from oil and gas activities, include benzene, toluene, ethylbenzene, and xylenes. The Vocus can detect compounds at lower concentrations and higher time resolution than an auto-GC. **Figure 3-14** shows a time series of benzene, toluene, and total C8-aromatic compounds during the stationary Vocus period from April 3 to 27. Each point represents a 1-minute average. Note that total C8-aromatic compounds contain ethylbenzene plus xylenes because the instrument cannot distinguish between compounds with the same molecular formula. Although distinct plume periods are shown, none of these compounds exceeded their respective short-term air monitoring comparison value (180 ppb for benzene, 4,000 ppb for toluene, and 1,700 ppb for xylenes, which is stricter than 20,000 ppb for ethylbenzene) for this time period.

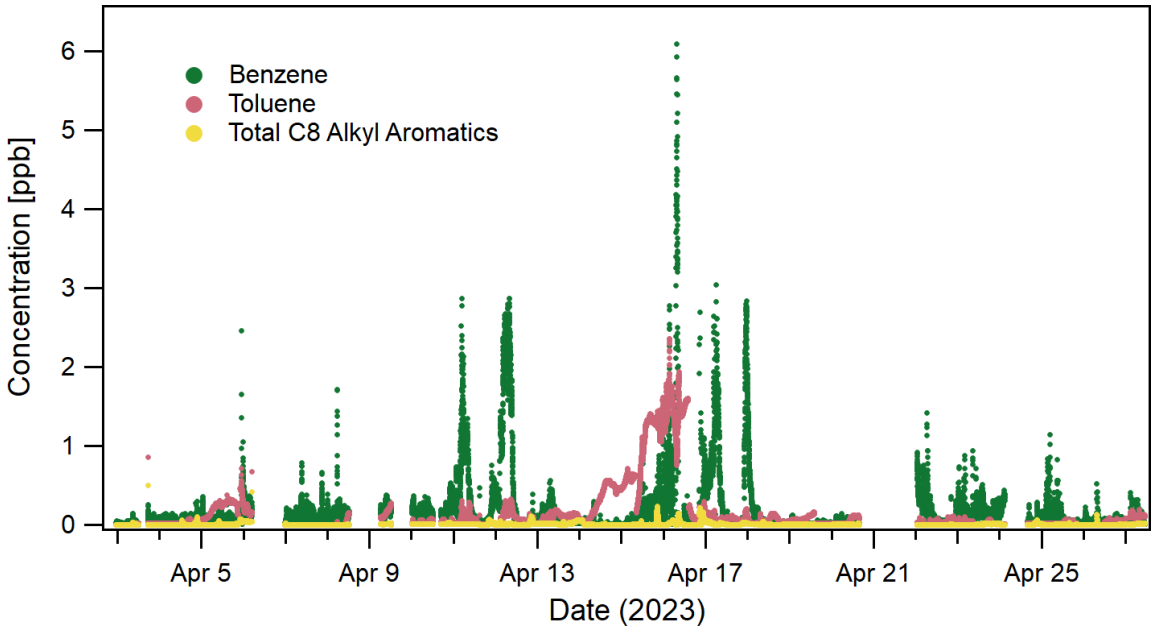

Figure 3-14. Time series of benzene, toluene, and total C8-aromatic compounds during the stationary Vocus period, April 3–27, 2023.

Additionally, the campaign average for each compound stayed well below its respective long-term air monitoring comparison value (1.4 ppb for benzene, 1,100 ppb for toluene, and 140 ppb for xylenes, which is stricter than 440 ppb for ethylbenzene). Air monitoring comparison values are screening levels used by the TCEQ to assess the potential for measured concentrations of specific chemicals to cause health or welfare effects. Health-based air monitoring comparison values are safe levels at which exposure is unlikely to result in adverse health effects (TCEQ 2025a). Figures for compounds measured by the Vocus during its stationary period, not included in Figure 3-14, are shown in Additional Materials A (Figures A-6 and A-7).

DISCUSSION AND CONCLUSIONS

This work measured the air pollutant mix in and around Karnes City, Texas, within the Eagle Ford Shale wet gas region. Criteria pollutants, ozone and nitrogen oxides, were below the NAAQS. The PM_1 concentrations for both campaigns were below the $PM_{2.5}$ NAAQS; however, the high-concentration periods may cause health concerns to the local population and downwind populations in Austin and San Antonio, Texas. Additional Materials A, Figure A-10 shows that some VOC peaks were followed by PM_1 peaks, suggestive of the formation of secondary organic aerosol from the photooxidation of emitted VOCs. Overall, UOGD emissions have a substantial effect on the pollutant mix, resulting in primary pollutants that can react to form secondary pollutants, both of which can pose human health risks. It is worth noting, however, that the measurements and the short-term and long-term health standards or guidelines have different averaging times.

Mobile measurements fingerprinted plumes and provided unprecedented data on the variabilities of individual VOCs, destruction removal efficiencies, and flaring emission ratios reported for this region. Flares can differ in emission ratios as a function of location, season, and conditions. The factor analysis emphasized its ability to separate subsources within the oil and gas facility, and in particular, evaporative emissions and emissions from flaring.

Even within the Eagle Ford Shale, emissions caused by UOGD are highly variable. To further characterize and quantify emissions, the team conducted another mobile measurement campaign in the Permian Basin, which is discussed in Chapter 4.

REFERENCES

Benedict KB, Prenni AJ, El-Sayed MMH, Hecobian A, Zhou Y, Gebhart KA, et al. 2020. Volatile organic compounds and ozone at four national parks in the southwestern United States. Atmos Environ 239:117783; *https://doi.org/10.1016/j.atmosenv.2020.117783*.

Brodfuehrer SH, Blomdahl DC, Wahman DG, Speitel GE, Misztal PK, Katz LE. 2024. Simultaneous time-resolved inorganic haloamine measurements enable analysis of disinfectant degradation kinetics and by-product formation. Nature Water 2:434–442; *https://doi.org/10.1038/s44221-024-00227-4*.

Caulton DR, Shepson PB, Cambaliza MOL, McCabe D, Baum E, Stirm BH. 2014. Methane destruction efficiency of natural gas flares associated with shale formation wells. Environ Sci Technol 4816:9548–9554; *https://doi.org/10.1021/es500511w*.

Coggon MM, Stockwell CE, Claflin MS, Pfannerstill EY, Xu L, Gilman JB, et al. 2024. Identifying and correcting interferences to PTR-ToF-MS measurements of isoprene and other urban volatile organic compounds. Atmos Meas Tech 172:801–825; *https://doi.org/10.5194/amt-17-801-2024*.

de Gouw J, Warneke C. 2006. Measurements of volatile organic compounds in the Earth's atmosphere using proton-transfer-reaction mass spectrometry. Mass Spectrom Rev 26:223–257; *https://doi.org/10.1002/mas.20119*.

Edwards PM, Brown SS, Roberts JM, Ahmadov R, Banta RM, DeGouw JA, et al. 2014. High winter ozone pollution from carbonyl photolysis in an oil and gas basin. Nature 514:351–354; *https://doi.org/10.1038/nature13767*.

George DL, Bowles EB. 2011. Shale gas measurement and associated issues. Pipeline Gas J 238:38–41.

Gilman JB, Lerner BM, Kuster WC, De Gouw JA. 2013. Source signature of volatile organic compounds from oil and natural gas operations in northeastern Colorado. Environ Sci Technol 473:1297–1305; *https://doi.org/10.1021/es304119a*.

Helsel, DR 1990. Less than obvious - statistical treatment of data below the detection limit. Environ Sci Technol 24:1766–1774; *https://doi.org/10.1021/es00082a001*.

Koss A, Yuan B, Warneke C, Gilman JB, Lerner BM, Veres PR, et al. 2017. Observations of VOC emissions and photochemical products over US oil- and gas-producing regions using high-resolution H3O+ CIMS PTR-ToF-MS. Atmos Meas Tech 108:2941–2968; *https://doi.org/10.5194/amt-10-2941-2017*.

Koss AR, Sekimoto K, Gilman JB, Selimovic V, Coggon MM, Zarzana KJ, et al. 2018. Non-methane organic gas emissions from biomass burning: identification, quantification, and emission factors from PTR-ToF during the FIREX 2016 laboratory experiment. Atmos Chem Phys 18:3299–3319; *https://doi.org/10.5194/acp-18-3299-2018*.

Kebabian PL, Wood EC, Herndon SC, Freedman A. 2008. A practical alternative to chemiluminescence-based detection of nitrogen dioxide: cavity attenuated phase shift spectroscopy. Environ Sci Technol 4216:6040–6045; *https://doi.org/10.1021/es703204j*.

Krechmer J, Lopez-Hilfiker F, Koss A, Hutterli M, Stoermer C, Deming B, et al. 2018. Evaluation of a new reagent-ion source and focusing ion-molecule reactor for use in proton-transfer-reaction mass spectrometry. Anal Chem 9020:12011–12018; *https://doi.org/10.1021/acs.analchem.8b02641*.

Lavoie TN, Shepson PB, Cambaliza MO, Stirm BH, Conley S, Mehrotra S, et al. 2017. Spatiotemporal variability of methane emissions at oil and natural gas operations in the Eagle Ford Basin. Environ Sci Technol 5114:8001–8009; *https://doi.org/10.1021/acs.est.7b00814*.

Li F, Huang DD, Tian L, Yuan B, Tan W, Zhu L, et al. 2024. Response of protonated, adduct, and fragmented ions in Vocus proton-transfer-reaction time-of-flight mass spectrometer (PTR-ToF-MS). Atmos Meas Techn 17:2415–2427; *https://doi.org/10.5194/amt-17-2415-2024*.

Masoud CG, Modi M, Bhattacharyya N, Jahn LG, McPherson KN, Abue P, et al. 2023. High chlorine concentrations in an unconventional oil and gas development region and impacts on atmospheric chemistry. Environ Sci Technol 5741:15454–15464; *https://doi.org/10.1021/acs.est.3c04005*.

McPherson KN, Jahn LG, Masoud CG, Bhattacharyya N, Modi M, Patel K, et al. 2024. Air pollution from unconventional oil and gas development in the Eagle Ford Shale. Atmos Environ 338:120812; *https://doi.org/10.1016/j.atmosenv.2024.120812*.

Middlebrook AM, Bahreini R, Jimenez JL, Canagaratna MR. 2012. Evaluation of composition-dependent collection efficiencies for the Aerodyne aerosol mass spectrometer using field data. Aerosol Sci Technol 463:258–271; *https://doi.org/10.1080/02786826.2011.620041*.

Ng NL, Canagaratna MR, Jimenez JL, Zhang Q, Ulbrich IM, Worsnop DR. 2011. Real-time methods for estimating organic component mass concentrations from aerosol mass spectrometer data. Environ Sci Technol 453:910–916; *https://doi.org/10.1021/es102951k*.

Pagonis D, Sekimoto K, de Gouw J. 2019. A library of proton-transfer reactions of H3O+ ions used for trace gas detection. J Am Soc Mass Spectrom 30:1330–1335; *https://doi.org/10.1007/s13361-019-02209-3*.

Schade GW, Roest G. 2016. Analysis of non-methane hydrocarbon data from a monitoring station affected by oil and gas development in the Eagle Ford shale, Texas. Elementa (Wash DC) 4:1–17; *https://doi.org/10.12952/journal.elementa.000096*.

Taipale R, Ruuskanen TM, Rinne J, Kajos MK, Hakola H. Pohja T, et al. 2008. Technical Note: Quantitative long-term measurements of VOC concentrations by PTR-MS – measurement, calibration, and volume mixing ratio calculation methods. Atmos Chem Phys 8:6681–6698; *https://doi.org/10.5194/acp-8-6681-2008*.

Texas Commission on Environmental Quality (TCEQ). 2024. TAMISWeb v5.2.3 — Report Selection. Available: *https://www17.tceq.texas.gov/tamis/index.cfm?fuseaction=report.main* [accessed 20 November 2024].

Texas Commission on Environmental Quality (TCEQ). 2025a. About Air Monitoring Comparison Values (AMCVs). Available: *https://www.tceq.texas.gov/toxicology/amcv* [accessed 22 January 2025].

Texas Commission on Environmental Quality (TCEQ). 2025b. Timeline for Near Real-time Ambient Air Quality Data Flows. Available: *https://www.tceq.texas.gov/airquality/monops/near-real-time-data-flows* [accessed 22 January 2025].

US Environmental Protection Agency (US EPA). 2014. NAAQS Table. Available: *https://www.epa.gov/criteria-air-pollutants/naaqs-table* [accessed 15 January 2025].

US Environmental Protection Agency (US EPA). 2024. National Ambient Air Quality Standards (NAAQS) for PM. Available: *https://www.epa.gov/pm-pollution/national-ambient-air-quality-standards-naaqs-pm* [accessed 15 January 2025].

US Environmental Protection Agency (US EPA). 2025. Facility Level Information on Greenhouse Gases Tool FLIGHT — 2023 Greenhouse Gas Emissions from Large Facilities. Available: *https://ghgdata.epa.gov/ghgp/main.do* [accessed 15 January 2025].

Werner C, Meredith LK, Ladd SN, Ingrisch J, Kübert A, Van Hare J, et al. 2021. Ecosystem fluxes during drought and recovery in an experimental forest. Science 374:1514–1518, *https://doi.org/10.1126/science.abj6789*.

Worton DR, Goldstein AH, Farmer DK, Docherty KS, Jimenez JL, Gilman JB, et al. 2011. Origins and composition of fine atmospheric carbonaceous aerosol in the Sierra Nevada Mountains, California. Atmos Chem Phys 11:10219–10241; *https://doi.org/10.5194/acp-11-10219-2011*.

CHAPTER 4: FIELD MEASUREMENTS IN THE PERMIAN BASIN

INTRODUCTION

The Permian Basin, spanning western Texas and southeastern New Mexico, is one of the most productive oil and gas regions in the United States (Francoeur et al. 2021). The largest methane emissions ever recorded were in this area, with 2.7 ± 0.5 teragrams emitted annually (Zhang et al. 2020). The region plays a pivotal role in the nation's energy landscape, but also contributes significantly to VOC emissions and other pollutants from UOGD, which have not been extensively quantified. Recent research has underscored the substantial influence of oil and gas emissions on regional air quality, particularly in the formation of ozone, as observed in southeastern New Mexico at Carlsbad Caverns National Park (Pollack et al. 2023). VOCs and nitrogen oxides from oil and gas activities are key contributors to both local and transported ozone production, frequently driving ozone concentrations beyond regulatory standards. Building on these findings, our 2-week field campaign, from April 29 to May 12, 2024, was designed to comprehensively characterize pollutant dynamics in the Permian Basin through mobile and stationary air quality measurements. Using an electric van equipped with advanced instrumentation, we monitored VOCs, methane, ozone, and PM, capturing both spatial and temporal gradients. This campaign provides valuable insights into the air quality impacts of UOGD, supporting efforts to mitigate air pollution in the region.

STUDY DESIGN AND METHODS

The mobile measurements on public roads in this study were conducted using the same Ford Transit electric van (equipped with similar instruments) described in Chapter 3. A QuantAQ Modulair-Gas, mounted at the back of the van, provided PM_1, $PM_{2.5}$, and particulate matter <10 µm in aerodynamic diameter (PM_{10}) measurements. In addition to the mobile measurements, stationary monitoring was conducted at two primary sites. The first of these was located at a KOA campground (32.586°N, −104.413°W), where measurements were taken over several nights from May 3 to May 10, 2024. This site provided continuous monitoring of pollutant concentrations, allowing us to identify plume events and study pollutant fluctuations in a controlled, stationary environment representative of a receptor site.

The second site involved a colocation study at a continuous monitoring station in Loving, New Mexico. This 2-day effort allowed us to compare the Vocus data collected by the University of Texas instruments with measurements taken by the custom-made GC system operated by Professor Franklin's project team, funded under the same HEI Request for Applications as the current study. The colocation effort provided valuable insights into the agreement between these different measurement systems, allowing for cross-validation of the results (for benzene and toluene).

The stationary time series analysis aimed to characterize air pollutant concentrations and detect plume events at the site near the Carlsbad KOA campground. Overnight time series plots were generated for a range of pollutants, including hydrogen sulfide, sulfur dioxide, black carbon, methane, carbon dioxide, PM, benzene, toluene, and C8 aromatic compounds. These time series plots were created for each night of data collection, helping to distinguish between sudden pollutant spikes, which were indicative of plume events, and periods of stable background concentrations, which represented nonplume conditions.

Wind roses were created using data on hydrogen sulfide concentrations, wind speed, and wind direction (a wind rose is a graphical tool used in meteorology to depict the frequency and direction of winds at a particular location over a specific timeframe). Hydrogen sulfide was chosen for these plots because it is strongly associated with the characteristic "rotten egg" odor, making it a clear marker for community odor complaints and pollutant impacts. Additionally, hydrogen sulfide emissions often originate from oil and gas extraction activities, serving as a practical indicator of potential downwind impacts from these operations. These wind "rose" plots were particularly useful for examining whether high concentrations of hydrogen sulfide were associated with specific wind conditions and whether such concentrations occurred predominantly during plume or nonplume periods. This analysis provided valuable insights into the movement of pollutant plumes in relation to prevailing wind patterns.

The mobile measurement time series analysis provided high spatial resolution, allowing us to detect localized variations in pollutant emissions. Before each mobile measurement drive, the team reviewed Google Maps to strategically plan the preliminary routes for the day. The team also monitored Vocus data in real time while driving the electric van, and when significant changes in pollutant concentrations (such as a rapid increase in benzene levels) were observed, the van was repositioned downwind of the suspected source to identify potential emission hotspots. Similar to the stationary time series analysis, time series plots of pollutant concentrations were generated as the van approached emission sources, which allowed for a detailed spatial understanding of pollutant distribution. Additionally, average VOC fingerprints were created to characterize the chemical composition of pollutant plumes, further aiding in the identification of emission sources.

Maps were generated to visualize pollutant concentrations across the Permian Basin region using the 2-week mobile dataset, thereby capturing the full range of spatial variability observed during the field campaign. These maps, which overlaid measured pollutant levels onto street base maps, highlighted areas with elevated emissions and offered a visual representation of spatial trends. This approach provided a comprehensive overview of emission patterns throughout the region.

The diurnal variation of ozone concentrations was also analyzed, with data collected from southeastern New Mexico (latitude 32.0°N–33.0°N, longitude –104.75°W–103.0°W) using a sonic anemometer on the mobile van. Hourly averages of ozone concentrations were computed to explore the day-night cycles and variations in ozone levels, which are crucial for understanding local air quality and atmospheric conditions.

DATA ANALYSIS

The data processing procedures, including the preprocessing, analysis, calibration, and zero-air subtraction of Vocus data, followed the detailed methodology described in Chapter 3. This approach ensured that all data were handled in a consistent and standardized manner, allowing for reliable interpretation and analysis.

To address the varying sampling rates of different instruments, we applied a uniform 1-minute averaging scheme to synchronize the data. Initially, pollutant concentrations were recorded at different time intervals, depending on the instrument. To harmonize these data, we established a uniform time vector with 1-minute intervals. For each pollutant's raw time-stamped measurements, we identified all data points that fell within a ±30-second window around each uniform minute. The average of these raw values was then calculated to represent the concentration for that specific minute. In instances when no data points fell within the designated time window, the value for that minute was set to "NaN." This approach effectively aligned the measurements from all instruments into a cohesive 1-minute uniform timeline, ensuring that subsequent analyses would be based on consistent time intervals.

For the wind-rose analysis, we binned hydrogen sulfide concentrations by both wind speed and direction (ranging from 0° to 360°) during each stationary period or manual subinterval. To highlight the most significant pollutant levels, we used the maximum statistic within each bin, identifying peak hydrogen sulfide concentrations for each combination of wind speed and direction. This allowed us to create detailed wind-rose plots, distinguishing between "plume" and "non-plume" periods, and thereby providing insights into how the spatial distribution of pollutants varied with changing wind conditions.

In analyzing ozone levels, we aggregated the data either on an hourly or daily basis to explore the diurnal patterns typical of the southeastern New Mexico region. By computing daily and hourly mean concentrations, we were able to assess differences in pollutant levels between day and night, revealing key insights into the temporal variability of ozone concentrations in the region.

To understand the spatial distribution of pollutants, we created spatial maps by overlaying pollutant concentrations onto a geographic base map. These concentrations were represented with color-coded percentile bins, allowing for a visual representation of pollutant hotspots. Particularly high concentrations — those exceeding the 99.5th percentile — were highlighted in black, drawing attention to the most significant areas of concern.

In addition to these analyses, we generated mobile time series plots to investigate how pollutant levels varied as the mobile platform approached different emission sources. These plots provided a detailed view of how pollutant concentrations changed over both space and time, offering valuable insights into the spatial variability of pollutant levels during mobile measurements.

For sound measurements, we applied a threshold of 10 mph to exclude data captured when the vehicle was traveling at higher speeds. This limit was necessary to eliminate noise that could be introduced by the motion of the vehicle, ensuring that the sound measurements reflected environmental conditions more accurately.

The analysis of black carbon data involved applying a 60-second moving average filter to smooth out short-term fluctuations and better capture underlying trends.

To assess the accuracy and consistency of measurements from different instruments, we conducted a colocation study between the Franklin group's readings and the nearest-in-time data from The University of Texas sensors. We compared the two datasets by performing linear regression and Pearson correlation analysis (R^2). This comparison allowed us to generate 1:1 scatter plots and time series overlays, providing a clear picture of the relationship between the two sets of measurements.

The data analysis was conducted using Igor Pro 8.04 (WaveMetrics), with instrument-specific analysis packages provided by the manufacturers. The data were processed using Tofware V3.2.3–V4.0.1 (Tofwerk), followed by further processing, including calibration and background subtraction, in MATLAB R2024. These steps adhered to standardized routines, as outlined in previous studies (e.g., Brodfuehrer et al. 2024; Werner et al. 2021) and consistent with the work in the Eagle Ford Shale (Chapter 3). Wind-rose plots were generated using the openair package in R. To ensure the reliability of the results, we verified the software versions and tested each analysis subroutine on sample data before proceeding with the full dataset.

RESULTS

The team conducted both mobile and stationary measurements in the Permian Basin. The observations are presented and discussed in this section. **Figures 4-1** and **4-2** below show an overview of the sampling results.

Table 4-1 shows the campaign average and standard deviations of different pollutants measured in the Permian Basin, along with short-term health standards or guidelines.

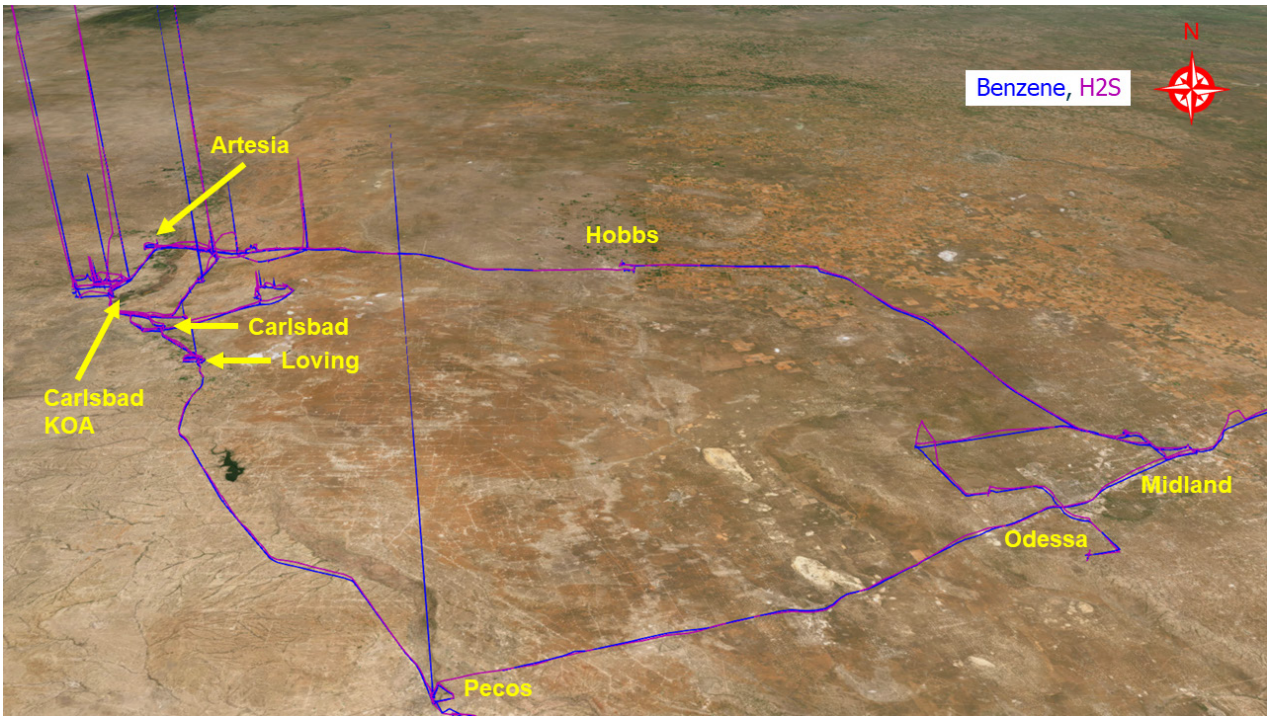

Figure 4-1. Overview of benzene and hydrogen sulfide (H_2S) levels measured in the Permian Basin.

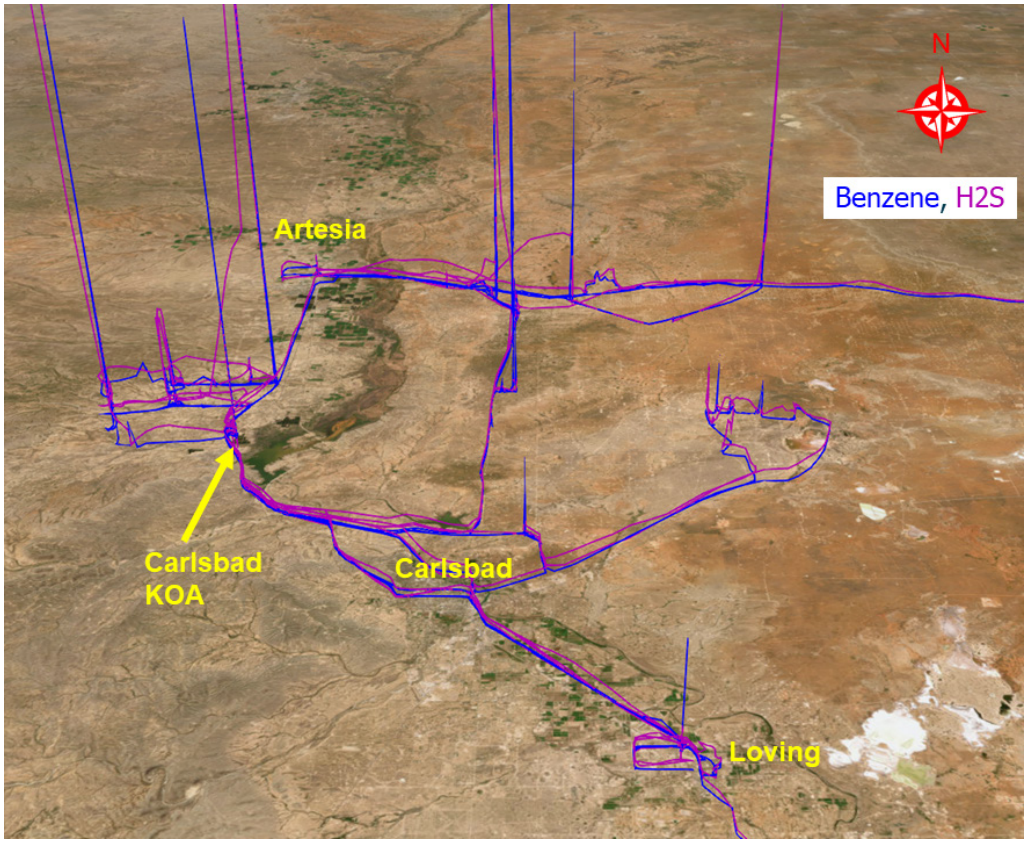

Figure 4-2. Overview of benzene and hydrogen sulfide (H_2S) levels measured in the Permian Basin, with a detailed view of the New Mexico area.

Table 4-1. Mean Concentrations and Standard Deviation of Various Air Pollutants from UOGD Measurement Campaign in the Permian Basin, with Short-term Health Standards or Guidelines

Name	Mean	Standard Deviation	Short-Term Health Standards or Guidelines
Hydrogen sulfide	2.3 ppb	13.3 ppb	70 ppb (acute-duration inhalation from ATSDR)
Sulfur dioxide	1.0 ppb	0.66 ppb	75 ppb (1 hr NAAQS)
Methane	2.2 ppm	0.76 ppm	–
Formaldehyde	0.96 ppb	0.97 ppb	40 ppb (acute-duration inhalation from ATSDR)
Carbon dioxide	423 ppm	6.5 ppm	–
Benzene	0.54 ppb	4.8 ppb	9 ppb (acute-duration inhalation from ATSDR)
Toluene	0.42 ppb	3.14 ppb	2,000 ppb (acute-duration inhalation from ATSDR)
C8 aromatics	0.22 ppb	1.0 ppb	–
Ozone	48 ppb	13.4 ppb	70 ppb (8 hr NAAQS)
PM_1	5.76 μg/m^3	7.65 μg/m^3	–
$PM_{2.5}$	8.78 μg/m^3	19.6 μg/m^3	35 μg/m^3 (24 hr NAAQS)
Black carbon	0.55 μg/m^3	1.48 μg/m^3	–

ATSDR = Agency for Toxic Substances and Disease Registry; NAAQS = National Ambient Air Quality Standards; PM_1 = particulate matter <1 μm in aerodynamic diameter; $PM_{2.5}$ = particulate matter ≤2.5 μm in aerodynamic diameter.

STATIONARY MEASUREMENTS AT SOURCE AND RECEPTOR LOCATIONS

Plume Analysis Points to Oil and Gas Sources in the Region Over multiple nights of stationary measurement at the KOA site, hydrogen sulfide, benzene, toluene, and C8 aromatics exhibited a recurring pattern of sharp increases typically centered between 22:00 and midnight. In each figure's time series, *hydrogen sulfide* appears to track these nighttime spikes in benzene, toluene, and C8 aromatics to within about 30 minutes, suggesting that the same local meteorological conditions or emission sources (likely oil and gas operations west or southwest of the campground) were driving these multipollutant plumes. The disconnected segments in these time series arise from periods when the instruments were undergoing calibration or experiencing temporary power outages; during these times, no valid measurements were recorded. The Carlsbad KOA site was considered a "polluted background site," with oil and gas developments located approximately 3 miles in the northwestern, western, and southwestern direction (refer to Additional Materials B, Figure B-1**5**).

More specifically, as shown in **Figure 4-3** (period 1: May 3–4, 2024), two distinct surges in hydrogen sulfide (reaching 15–20 ppb) coincide with elevated benzene (exceeding 2 ppb) and methane (~3 ppm). The first surge appears shortly before midnight, while a second event unfolds in the morning. This temporal overlap implies that emissions could be strongly modulated by the stable nocturnal boundary layer, allowing plumes to accumulate and drift toward the KOA site before sunrise.

In addition to the noticeable increase in gas-phase pollutants, we also observed an accompanying increase in particle concentrations. **Figure 4-4** shows the same overnight period as shown in Figure 4-3. We see a sharp increase in particle concentration just after midnight, with $PM_{2.5}$ concentration reaching about 10 μg/m^3. This elevated PM concentration increased again around 7 a.m. on May 4th, the same time as the beginning of the second spike in gas-phase pollutant concentrations shown in Figure 4-3.

Another example of higher gas-phase pollutant concentrations is demonstrated in **Figure 4-5** (period 5: May 8–9, 2024). We can see a pronounced nighttime surge in pollutant levels with hydrogen sulfide peaks above 25 ppb, closely mirroring the spikes in benzene, toluene, and C8 aromatics. Benzene reaches a maximum concentration of ~4 ppb, while toluene peaks at around 1.5 ppb. Methane also exhibits a significant rise, with levels reaching ~3.5 ppm. By morning, pollutant concentrations return to regional background levels, highlighting the transient nature of these nighttime events.

Similarly, **Figure 4-6** (period 6: May 9–10, 2024) shows more modest nighttime enhancements, although the pattern remains consistent. Hydrogen sulfide begins to climb sharply around 22:30, followed by a rise in toluene from the regional background level to ~0.3–0.4 ppb. Benzene shows a corre-

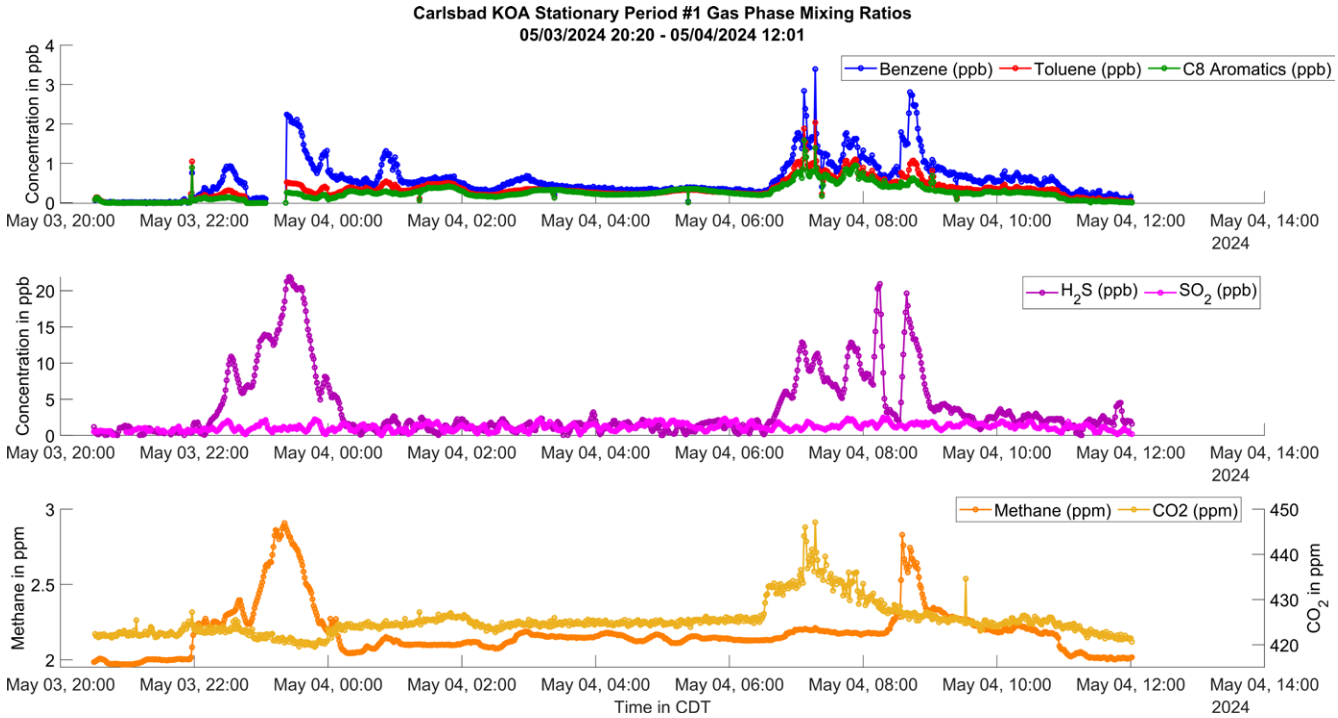

Figure 4-3. Time series plot of hydrogen sulfide (H_2S), sulfur dioxide (SO_2), methane, carbon dioxide (CO_2), benzene, toluene, and C8 aromatics during period 1 (May 3–4, 2024).

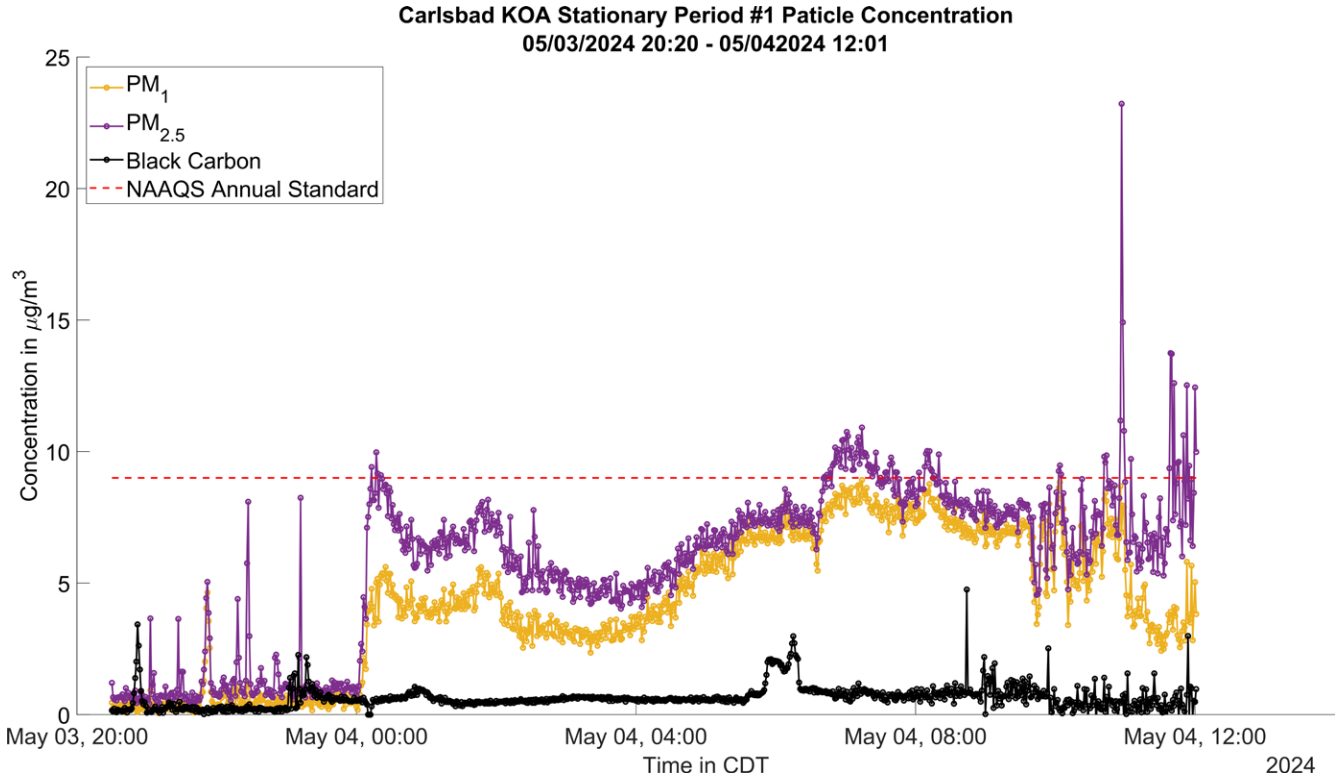

Figure 4-4. Time series plot of black carbon, PM_1, and $PM_{2.5}$ during period 1 (May 3–4, 2024).

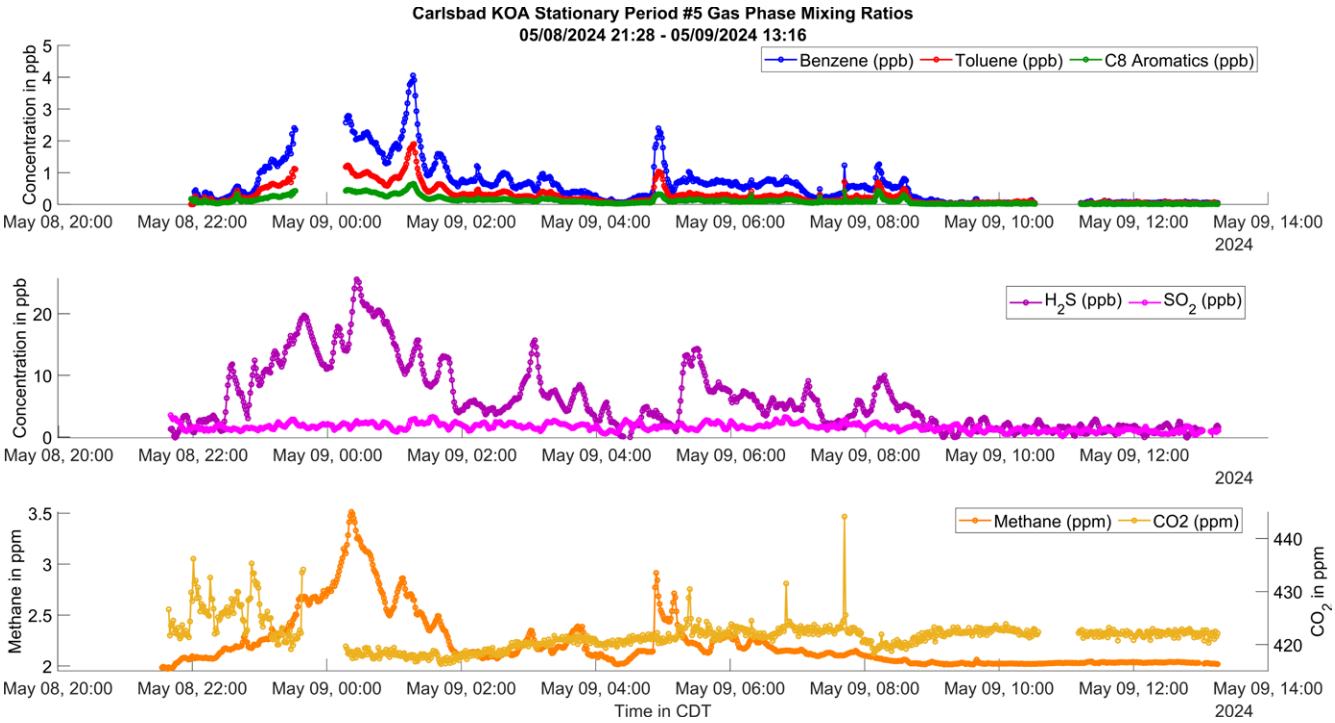

Figure 4-5. Time series plot of hydrogen sulfide (H_2S), sulfur dioxide (SO_2), methane, carbon dioxide (CO_2), benzene, toluene, and C8 aromatics during period 5 (May 8–9, 2024).

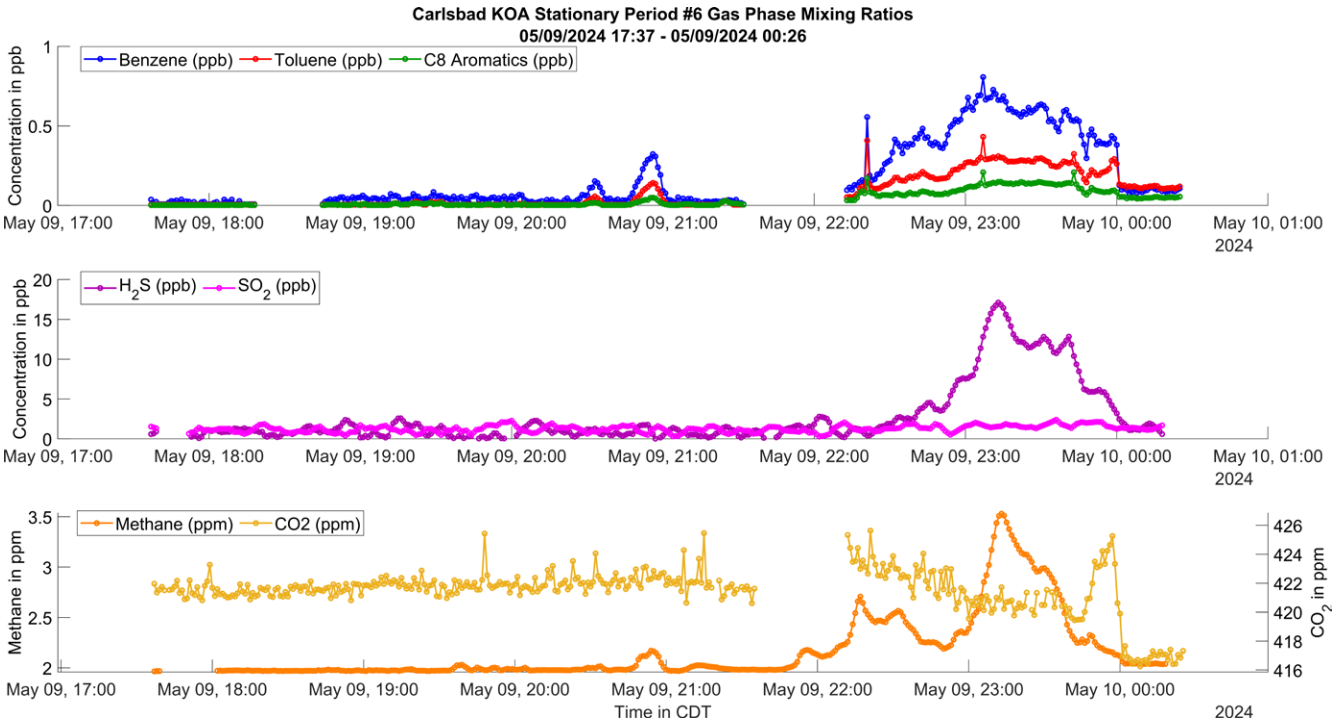

Figure 4-6. Time series plot of hydrogen sulfide (H_2S), sulfur dioxide (SO_2), methane, carbon dioxide (CO_2), benzene, toluene, and C8 aromatics during period 6 (May 9–10, 2024).

sponding increase, peaking at ~0.5 ppb. Methane also experiences a noticeable enhancement during the same period, peaking at around 3.5 ppm.

According to the Agency for Toxic Substances and Disease Registry (ATSDR), the minimal risk level for benzene, toluene, and hydrogen sulfide for acute inhalation duration is 9 ppb, 2,000 ppb, and 70 ppb, respectively (ATSDR 2025). Our stationary measurement at the Carlsbad KOA suggested that, even during high-concentration periods, benzene, toluene, and hydrogen sulfide levels did not exceed these levels, indicating that the risk of negative health effects from acute inhalation of these air pollutants in this area is low. However, Figures 4-3, 4-5, and 4-6 show clear enhancements from typical ambient conditions in the area. The effect of prolonged exposure to these enhanced pollutant levels should be further investigated, because there are no current NAAQS for benzene, toluene, and hydrogen sulfide.

In Figure 4-4, we see that the $PM_{2.5}$ level exceeded the annual average NAAQS for $PM_{2.5}$ of 9 $\mu g/m^3$ during this high-concentration period multiple times. However, long-term PM measurement with a research-grade monitor at this site could help us better assess the exposure level and health impacts because only short-term sampling was currently conducted.

Large Hydrogen Sulfide Plumes Are Associated with Westerly Wind Directions and Downwind Oil and Gas Extraction Activities Rose (wind) plots were generated for plume intervals and nonplume periods, and the plume analyses are presented on rose plots in **Figures 4-7** and **4-8**. Across the four wind-rose plots for period 1, which include two labeled "plume" intervals and two labeled "nonplume" intervals, it is evident that higher hydrogen sulfide concentrations (represented by red and orange regions on the color scale) are generally associated with winds originating from the west and southwest at low speeds, typically ranging from 2 to 4 mph. During the plume intervals, the western-sector dominance of red shading shows that maximum hydrogen sulfide levels (above 10 ppb) occur disproportionately when wind direction is confined to west-southwest flow. Conversely, during the nonplume intervals (bottom row), wind directions are more variable and lack any pronounced sector driving elevated hydrogen sulfide. Instead, these roses are largely blue (under ~2 ppb) and extend over broader directions, indicating lower and more diffuse pollutant transport.

Similarly, peak hydrogen sulfide concentrations for periods 5 and 6 are associated with westerly flow, consistent with the observations in period 1, as shown in Figure 4-6. However, during period 5, plume 1, the plume coincides with higher wind speeds compared with the plume intervals in periods 1 and 6.

Diurnal Ozone Variability Is Driven by Reactive Ozone Precursors and Photochemistry The diurnal cycle of ozone in southeastern New Mexico exhibits a distinct daily pattern. Individual daily profiles reveal that ozone levels can reach up to 80 ppb on certain days, as shown in **Figure 4-9**. However, when averaged across all days, the maximum ozone concentration is ~60 ppb, which underrepresents the peaks observed on high ozone days (**Figure 4-10**). Average ozone levels begin around 40–45 ppb during the early morning and progressively increase throughout the day, peaking at 55–60 ppb in the late afternoon. This rise aligns with photochemical reactions driven by sunlight, as ozone production intensifies during daylight hours.

MOBILE MEASUREMENT RESULTS IN THE PERMIAN BASIN

During the Permian Basin measurement period, The University of Texas mobile van collected more than 2,915 km of data, equivalent to 18,720 minutes and 0.3 terabytes. We were able to fingerprint several near-source and distant diluted plumes from various sources such as active flares, drill sites, storage tanks, and process facilities. We have organized the plumes by numbers chronologically, and their locations are available on this *Google Earth map*.

The spatial distribution of various pollutants, including methane, hydrogen sulfide, sulfur dioxide, benzene, toluene, C8 aromatics, and PM_1, $PM_{2.5}$, and PM_{10}, is illustrated across the measurement region. Here, we highlight the spatial distribution of benzene (**Figure 4-11**) and H_2S (**Figure 4-12**), with additional maps available in Additional Materials B. Each map employs a percentile-based color scheme to highlight concentration hotspots and trends, with higher concentrations marked by darker colors (e.g., purple and black). Three key points of interest — the hotspot for plume fingerprints, the KOA stationary site, and the Franklin collocation site — along with major cities, are labeled on the maps. The maps reveal clear spatial patterns with elevated levels of pollutants concentrated around specific areas, likely corresponding to industrial activity, oil and gas operations, or other emission sources.

Consistent with the Eagle Ford Shale, we observed a significant increase in VOC concentrations as the mobile van approached a source. **Figure 4-13** shows the time series of various gas-phase compounds as the van approached an active flare (plume 9).

As the van approached the flare, benzene, toluene, and C8 aromatics concentrations were elevated from ambient conditions. Benzene increased to as high as 126 ppb, toluene peaked at 37 ppb, and C8 aromatics reached 11 ppb. We also observed an increase in methane concentration, from the typical ambient concentration of around 2 ppm to as high as 20 ppm. Moreover, the Permian Basin UOGD also regularly releases hydrogen sulfide, a compound associated with the strong odor of rotten eggs. Figure 4-12 shows that the hydrogen sulfide concentration in plume 9 is as high as 481 ppb from its typical background concentration of less than 0.3 ppb in the atmosphere. Despite the example noted above that only displayed the data of one plume, we observed this trend of VOC increase accompanied by hydrogen sulfide increase in nearly all the plumes (both flare and nonflare) in this region. Additional figures similar to those discussed above for other plumes can be found in Additional Materials B.

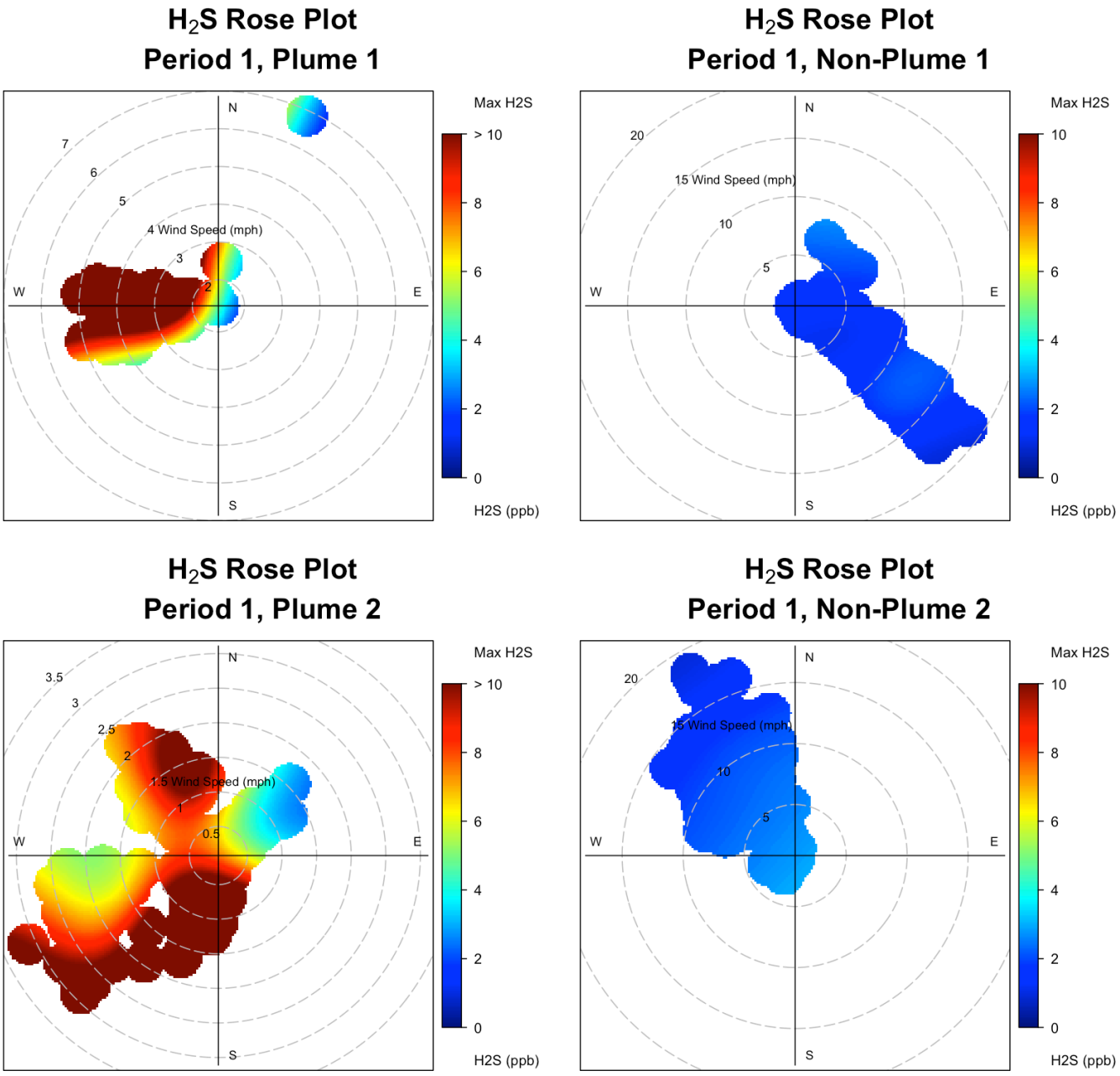

Figure 4-7. Hydrogen sulfide (H_2S) wind plots for period 1. The top left plot represents period 1, plume 1; the top right plot represents period 1, nonplume 1; the bottom left plot represents period 1, plume 2; and the bottom right plot represents period 1, nonplume 2.

In addition to gas-phase pollutants, we also observed particle-phase pollutant concentrations increase as a result of this active flare site. **Figure 4-14** shows the elevation of PM_1, $PM_{2.5}$, and black carbon as the van approaches the flare site. The black carbon concentration shows a significant increase to as high as 19 µg/m^3. Associated with the black carbon increase is the $PM_{2.5}$ increase, reaching a max of 35 µg/m^3.

Lastly, we detected a significant sound increase caused by the flare. Note that when we sampled this flare, it was very late at night, so the background noise was minimal. In addition, we filtered the sound data so that we only considered the sound recorded when the van was moving less than 10 mph. Because our van was electric, there was also no sound interference from the internal combustion engine. **Figure 4-15** shows the sound level as the van slowly approached the flare.

In addition to flaring sites, the mobile measurement in the Permian Basin also fingerprinted various other emission sources related to oil and gas development in the region. **Fig-**

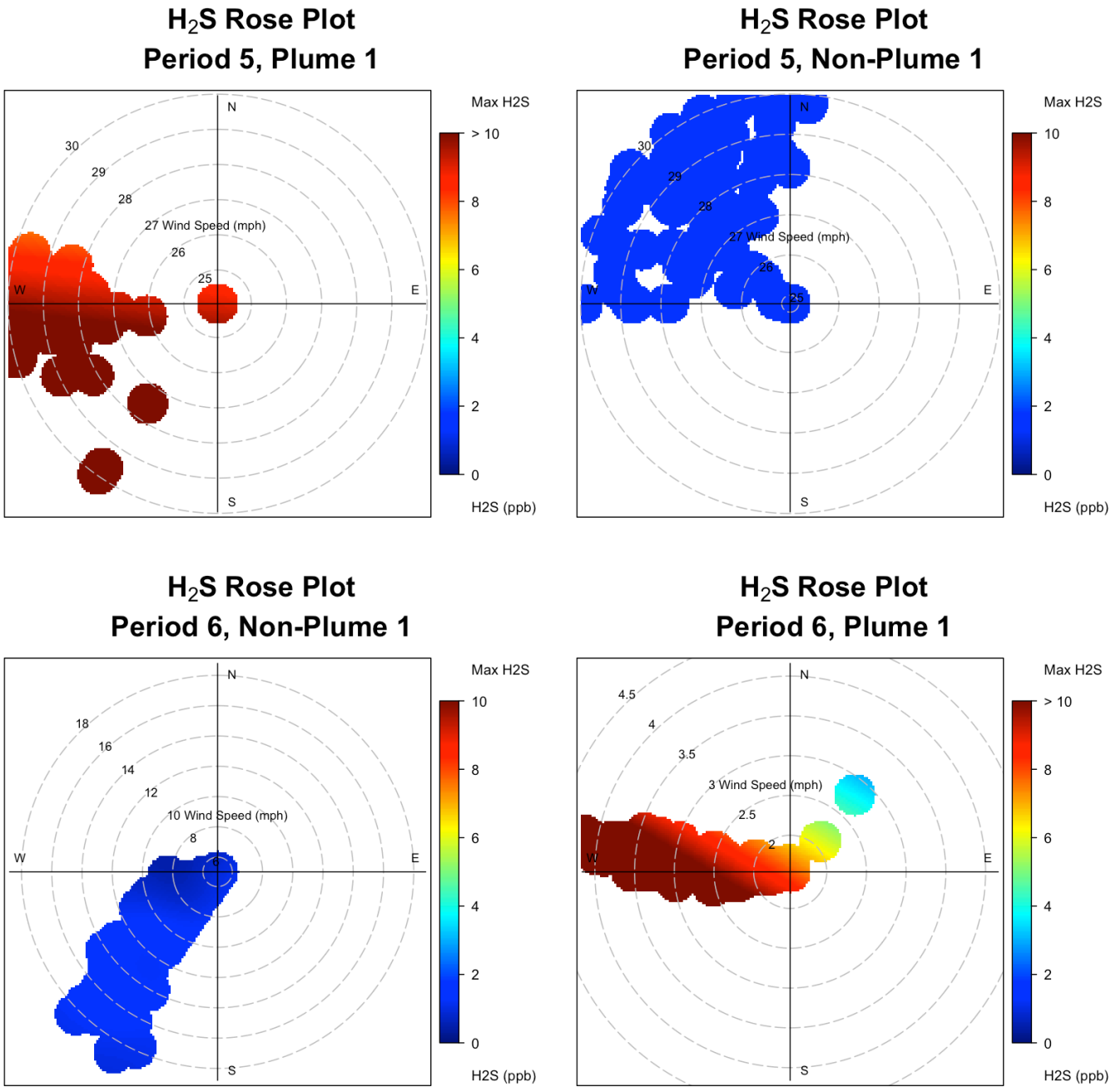

Figure 4-8. Hydrogen sulfide (H_2S) wind plots for periods 5 and 6. The top left plot represents period 5, plume 1; the top right plot represents period 5, nonplume 1; the bottom left plot represents period 6, plume 1; and the bottom right plot represents period 6, nonplume 1.

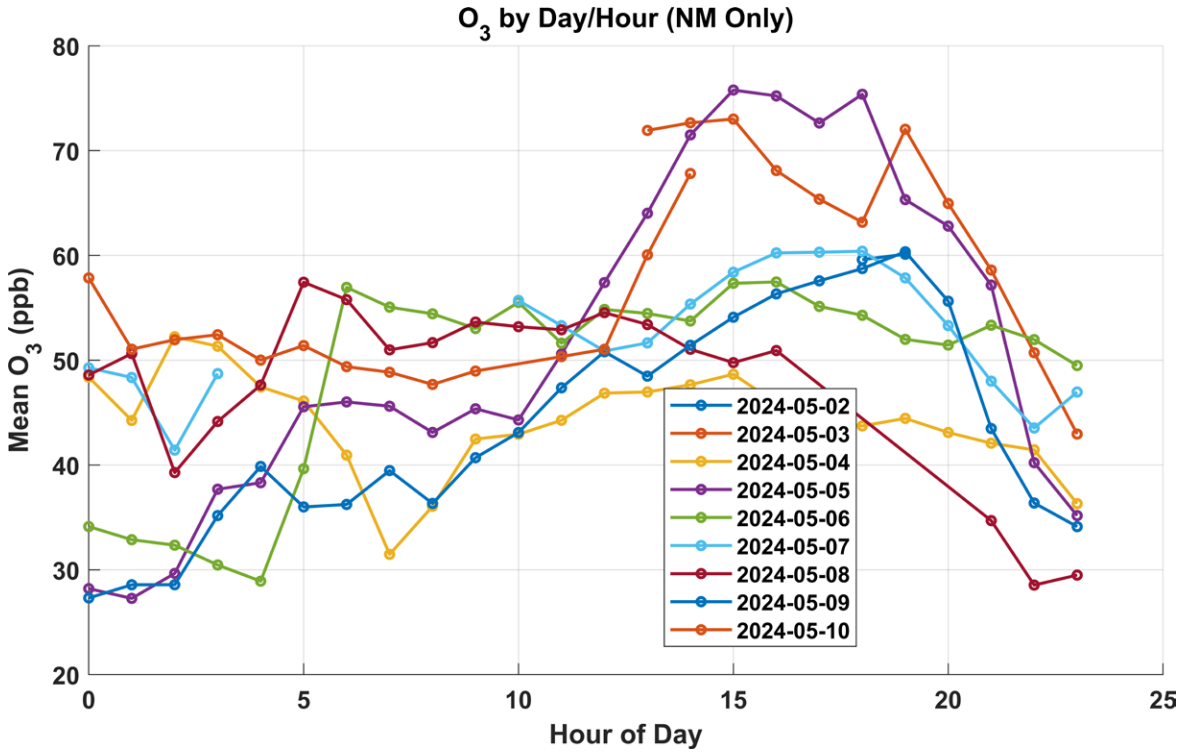

Figure 4-9. Hourly mean O_3 concentrations by day in New Mexico (one line represents 1 day – 9 days in total).

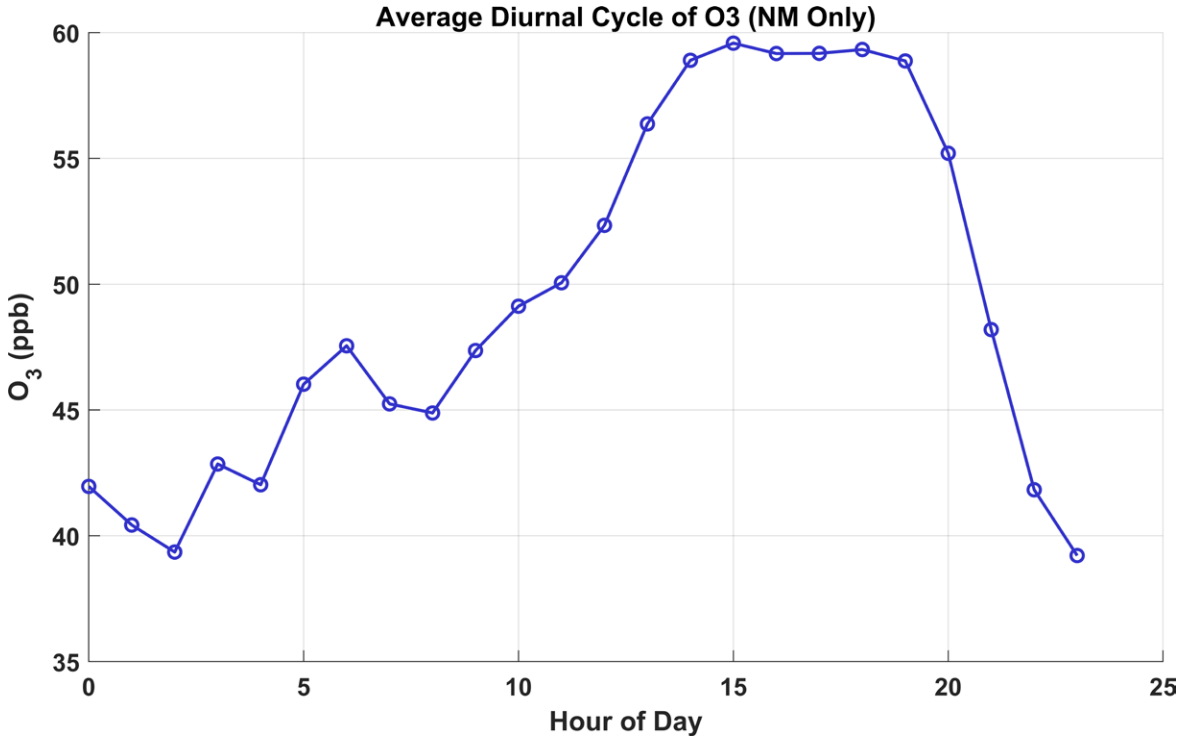

Figure 4-10. Average diurnal cycle of O_3 concentrations in New Mexico (averaged over 9 days).

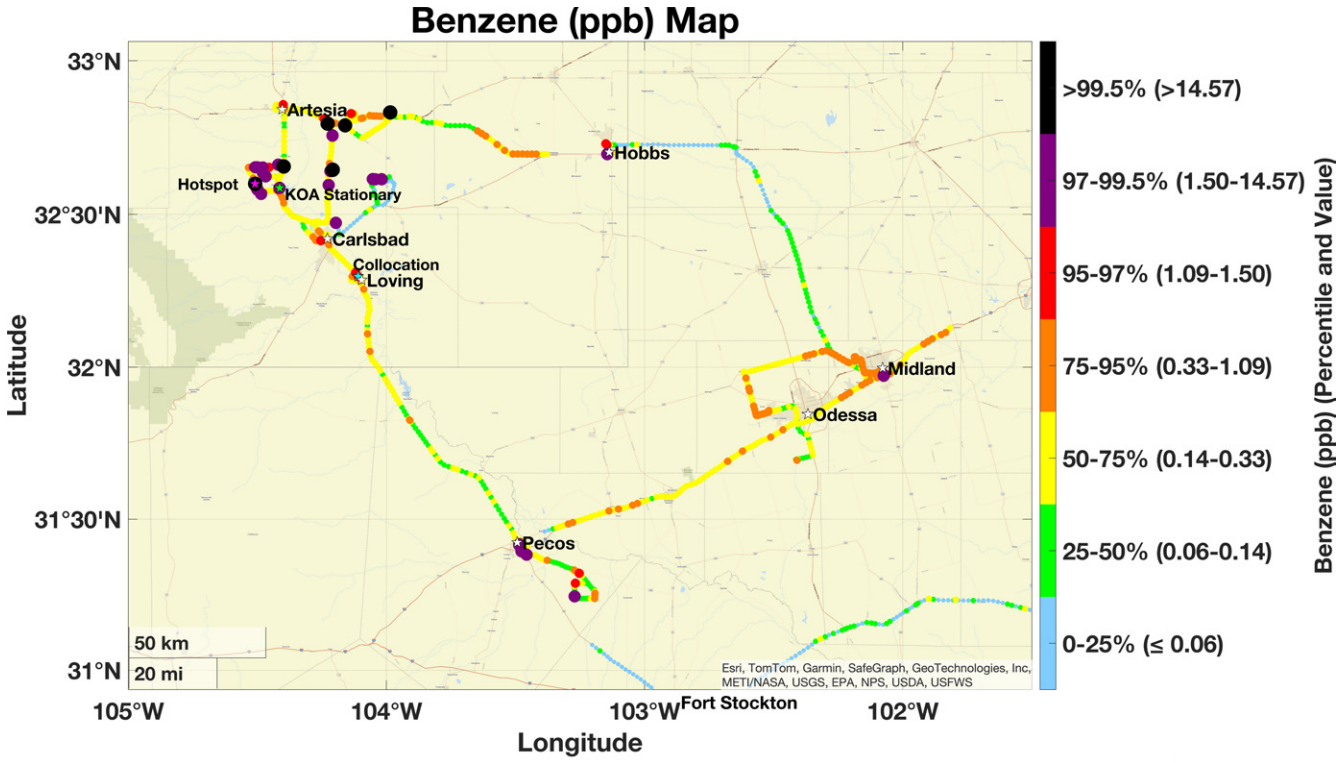

Figure 4-11. Spatial map of benzene concentrations.

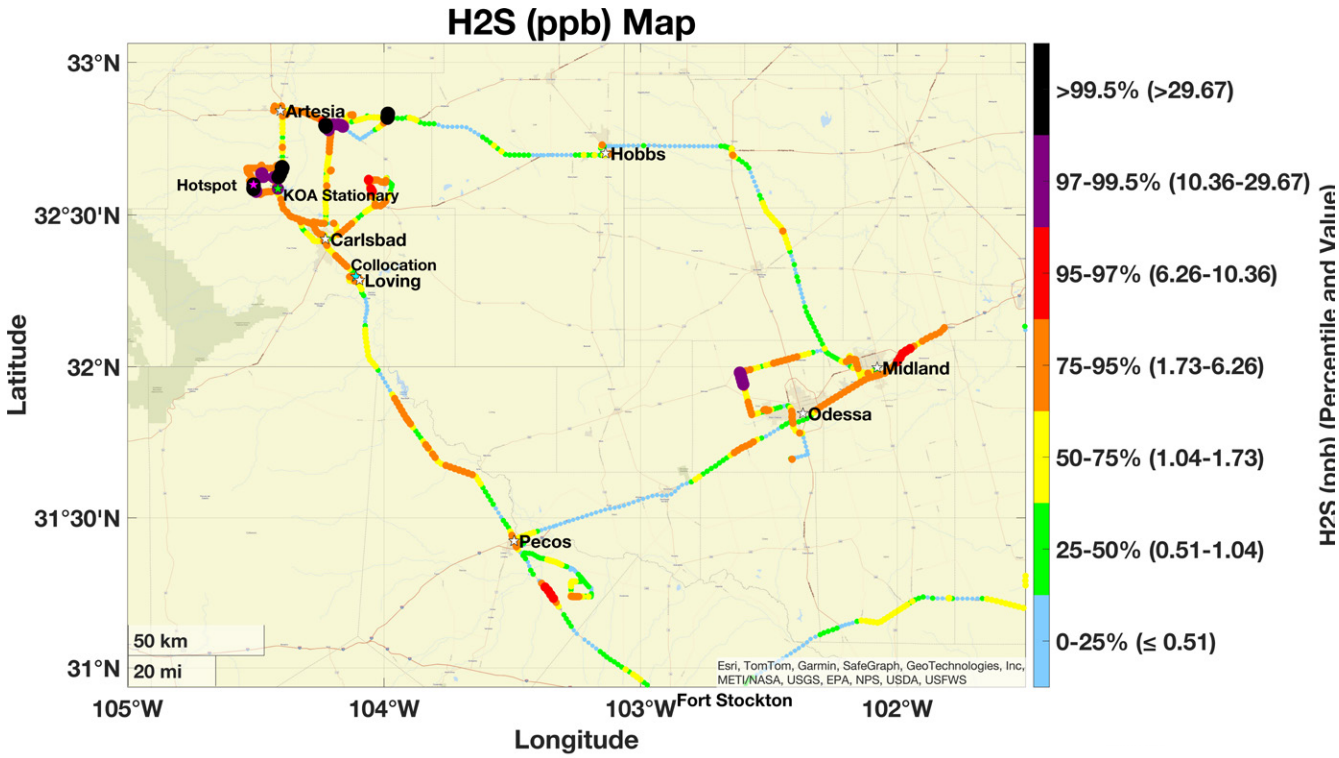

Figure 4-12. Spatial map of hydrogen sulfide (H_2S) concentrations.

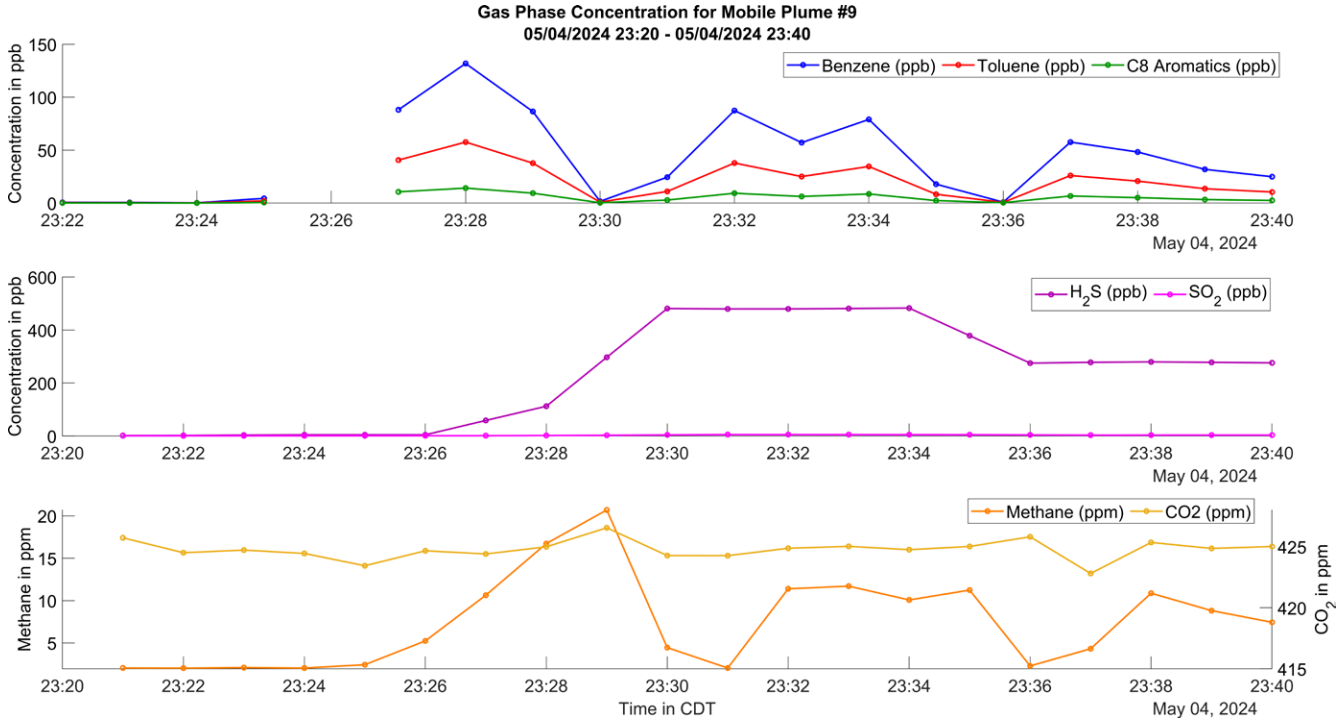

Figure 4-13. Time series plot of hydrogen sulfide (H_2S), sulfur dioxide (SO_2), methane, carbon dioxide (CO_2), benzene, toluene, and C8 aromatics concentrations as the van drives past mobile plume 9 (active flare).

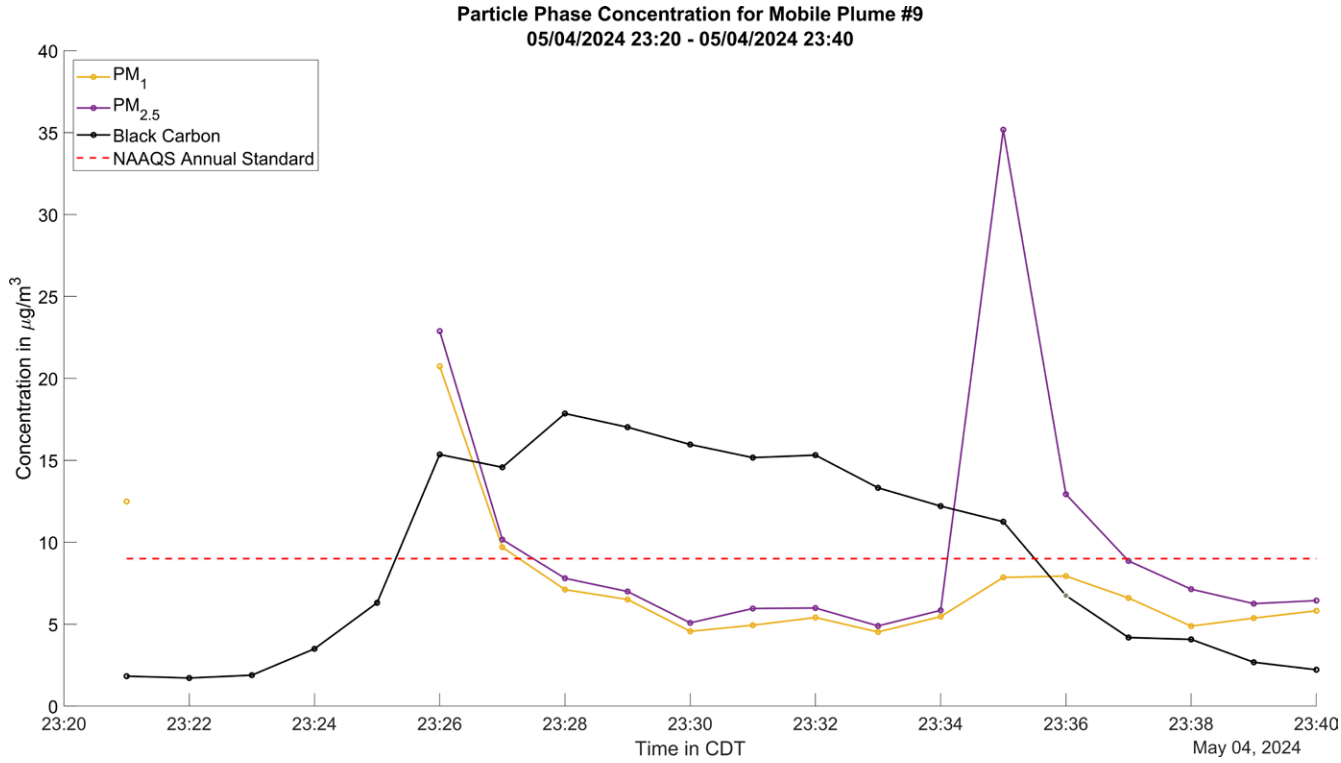

Figure 4-14. Time series plot of black carbon, PM_1, and $PM_{2.5}$ concentrations as the van drives past mobile plume 9 (active flare).

ures 4-16 and **4-17** show the time series of various gas-phase pollutant concentrations for mobile plume 6 (some storage tanks) as the van is driving by at different times of day.

As shown in the figures above, during the day (around 14:35), benzene, toluene, and C8 aromatics reached ~200 ppb, 100 ppb, and 50 ppb, respectively. The concentration of hydrogen sulfide also peaked at 300 ppb. Because of this substantial increase in pollutant concentrations during daylight hours, the mobile monitoring unit returned to the site at night for further measurements. Despite the lower planetary boundary layer at night, which typically results in reduced atmospheric mixing, no significant increase in gas-phase pollutants was observed. As depicted in Figure 4-16**,** while there was still a noticeable rise in the concentrations of benzene, toluene, and C8 aromatics (reaching ~25 ppb, 15 ppb, and 5 ppb, respectively), these levels were substantially lower than those observed during the day. Similarly, although the hydrogen sulfide concentration increased to ~6 ppb at night, it remained considerably lower than the daytime value. This observation is consistent with an episodic emissions source responsible for the observed increases in pollutants. Such variations have important implications for understanding regional air quality dynamics.

When the mobile monitoring van was positioned in proximity to emission sources (e.g., flares, storage tanks, or active well sites), concentrations of several air pollutants exceeded the minimal risk level for acute inhalation duration established by ATSDR. For instance, Figure 4-13 depicts the van near an active flare, while Figure 4-16 shows it downwind of storage tanks. In both scenarios, measured concentrations of benzene and hydrogen sulfide exceeded 100 ppb and 200 ppb, respectively — well above the ATSDR acute inhalation level of 9 ppb for benzene and 70 ppb for hydrogen sulfide.

Notably, during a return visit later that evening (Figure 4-17), benzene concentrations remained elevated, at approximately 30 ppb. Figure 4-14 presents particulate matter data near the flare, where $PM_{2.5}$ levels increased significantly to around 35 µg/m³ — the same level as the short-term $PM_{2.5}$ NAAQS and exceeding the annual NAAQS of 9 µg/m³. In fact, the concentration of black carbon alone at that location reached approximately 15 µg/m³, surpassing the annual $PM_{2.5}$ NAAQS on its own.

These mobile monitoring results indicate that pollutant concentrations can exceed the minimal risk level for acute inhalation duration from ATSDR when measurements are taken within 50 meters of the source. Such elevated levels pose potential health risks, particularly for on-site personnel exposed for extended durations, but as the concentrations decrease rapidly with the distance from wells, with significantly lower exposures in the neighborhood zones. It is worth

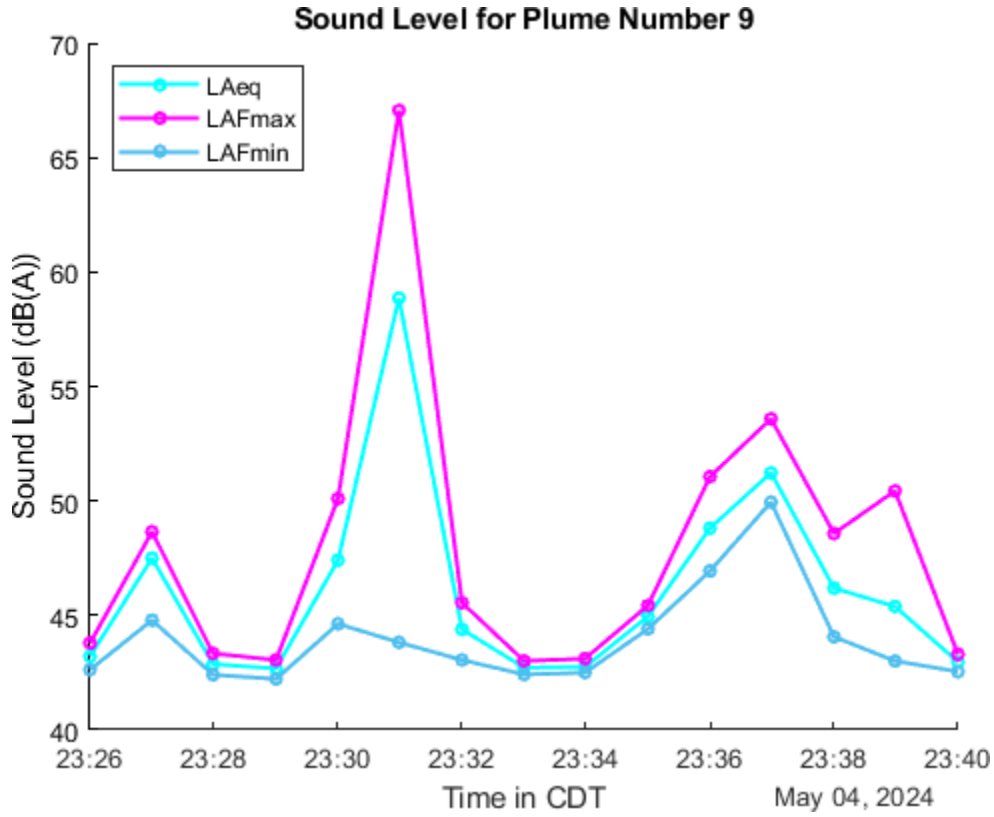

Figure 4-15. Time series plot of sound level as the van drives past mobile plume 9 (active flare).

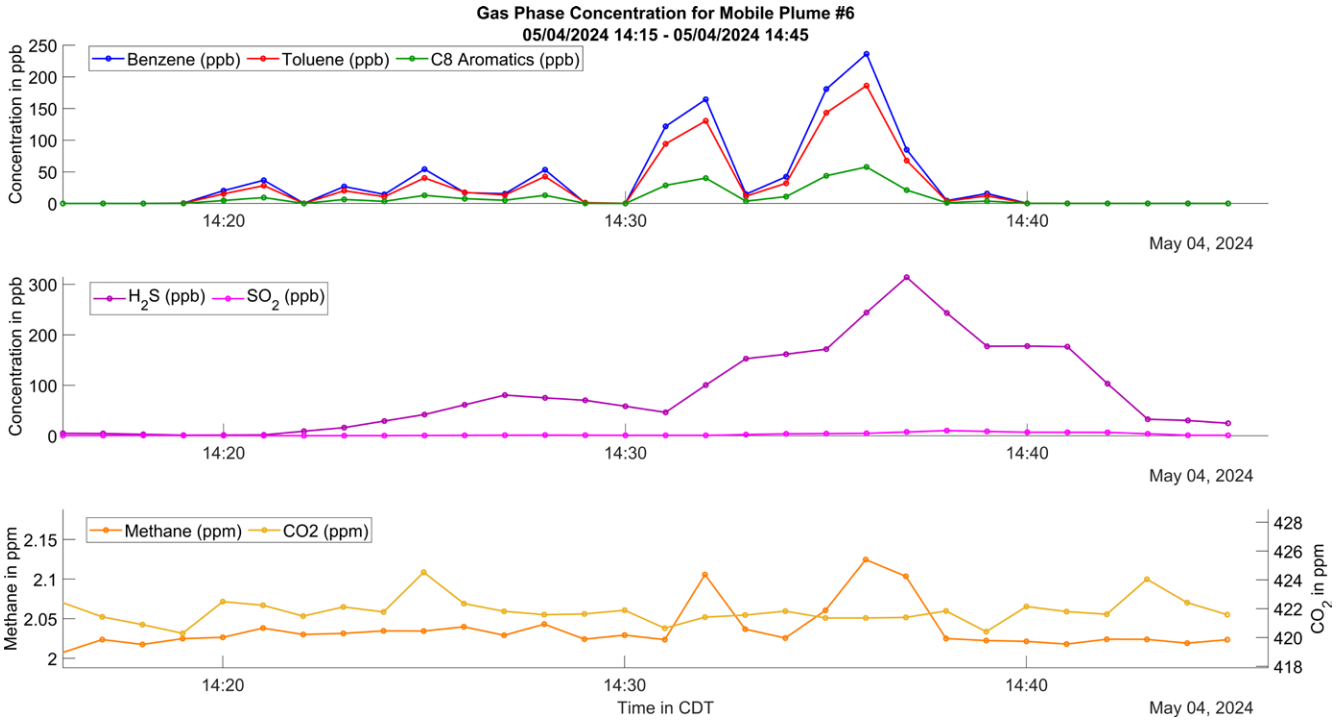

Figure 4-16. Time series plot of hydrogen sulfide (H_2S), sulfur dioxide (SO_2), methane, carbon dioxide (CO_2), benzene, toluene, and C8 aromatics concentrations as the van drives past mobile plume 6 during the day (storage tanks).

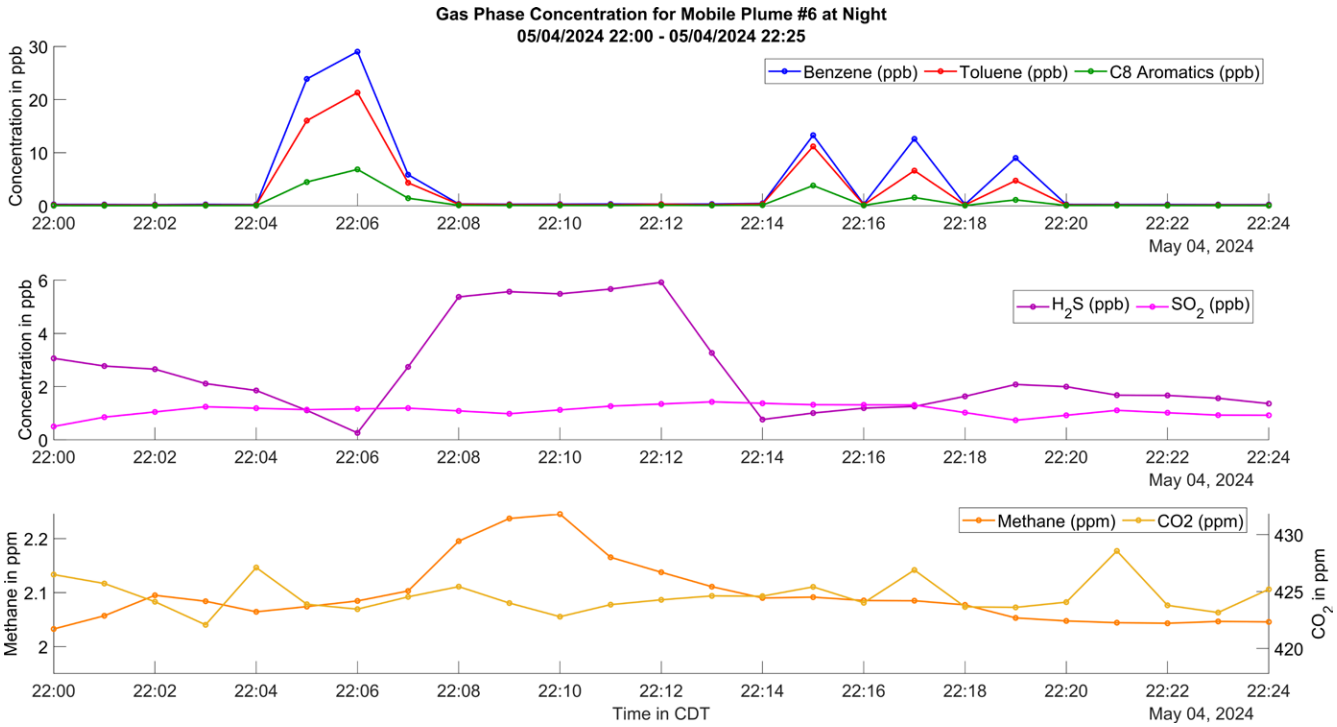

Figure 4-17. Time series plot of hydrogen sulfide (H_2S), sulfur dioxide (SO_2), methane, carbon dioxide (CO_2), benzene, toluene, and C8 aromatics concentrations as the van drives past mobile plume 6 at night (storage tanks).

noting, however, that the measurements and the short-term and long-term health standards or guidelines have different averaging times.

Moreover, **Figure 4-18** shows the electric van fingerprinting the plume detected at an identified "hotspot," capturing the unique chemical signature from this oil and gas extraction site, which was a high hydrogen-sulfide-emissions source. This hotspot is surrounded by oil and gas activity sites, including storage tanks and flares. The enhanced VOCs included aromatics expected from UOGD, along with sulfur-containing compounds and other oxygenated compounds such as $C_9H_{10}O_4H^+$ (likely an oxidation product of aromatics consistent with dimethoxybenzoic acid). The plume was characterized by the presence of a homologous series of aromatics from C6 to more than C15. During flaring, these aromatics are combusted to form multioxygen species that are difficult to detect by conventional methods, and their toxicity is unknown.

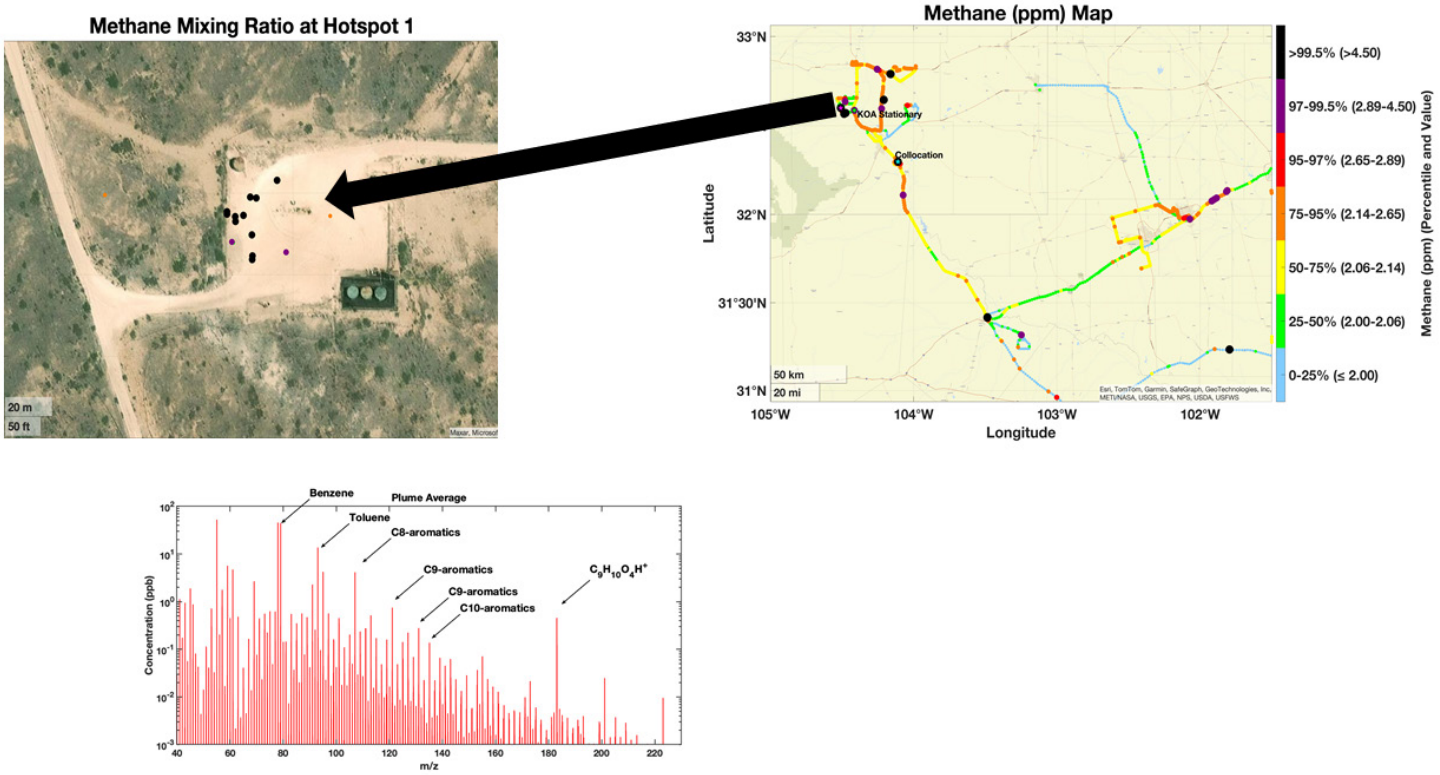

Figure 4-18. Enhanced VOCs from an identified "hotspot."

DISCUSSION AND CONCLUSIONS

Spatiotemporal observations conducted in the Permian region reveal notable contrasts compared with the Eagle Ford Shale. Air composition in the Permian exhibits a stronger "sulfuric" signature, with hydrogen sulfide concentrations in plumes reaching up to 482 ppb and methane concentrations peaking at 57.5 ppm. Hotspot locations associated with unconventional UOGD were fingerprinted alongside background concentrations.

In this campaign, the research team focused on wide spatiotemporal observations of oil and gas influence on air composition and fingerprinted both evaporative emissions and near and distant flaring contributions. Stationary measurements of benzene and toluene showed excellent agreement between the Vocus and GC instruments, with coefficients of determination (R^2) of 0.98 for both benzene and toluene. The Vocus instrument provided complementary data on highly oxygenated compounds associated with flaring, such as acetophenone, while GC measurements focused on light hydrocarbons. We plan for future analyses to compare individual signatures and source factor profiles to understand how distinct this region is relative to the Eagle Ford Shale. Additionally, to evaluate the potential influence of other sources, such as traffic, source apportionment analysis will be necessary to disentangle and quantify their contributions.

REFERENCES

Agency for Toxic Substances and Disease Registry (ATSDR). 2025. Minimal Risk Levels (MRLs) for Hazardous Substances. Available: *https://wwwn.cdc.gov/TSP/MRLS/mrlsListing.aspx* [accessed November 13, 2025].

Brodfuehrer SH, Blomdahl DC, Wahman DG, Speitel GE, Misztal PK, Katz LE. 2024. Simultaneous time-resolved inorganic haloamine measurements enable analysis of disinfectant degradation kinetics and by-product formation. Nature Water 2:434–442; *https://doi.org/10.1038/s44221-024-00227-4*.

Francoeur CB, McDonald BC, Gilman JB, Zarzana KJ, Dix B, Brown SS, et al. 2021. Quantifying methane and ozone precursor emissions from oil and gas production regions across the contiguous US. Environ Sci Technol 5513:9129–9139; *https://doi.org/10.1021/acs.est.0c07352*.

Pollack I B, Pan D, Marsavin A, Cope E J, Juncosa Calahorrano J, Naimie L, et al. 2023. Observations of ozone, acyl peroxy nitrates, and their precursors during summer 2019 at Carlsbad Caverns National Park, New Mexico. J Air Waste Manage Assoc 7312:951–968; *https://doi.org/10.1080/10962247.2023.2271436*.

Werner C, Meredith LK, Ladd SN, Ingrisch J, Kübert A, Van Haren J, et al, 2021. Ecosystem fluxes during drought and recovery in an experimental forest. Science 374:1514–1518; *https://doi.org/10.1126/science.abj6789*.

Zhang Y, Gautam R, Pandey S, Omara M, Maasakkers JD, Sadavarte P, et al. 2020. Quantifying methane emissions from the largest oil-producing basin in the United States from space. Sci Adv 6:eaaz5120; *https://doi.org/10.1126/sciadv.aaz5120*.

CHAPTER 5: ESTIMATING EMISSIONS FROM UNCONVENTIONAL OIL AND GAS DEVELOPMENT

INTRODUCTION

Emissions of criteria pollutants and air toxics from UOGD sources can have significant spatial and temporal variability. Currently available methods for estimating these emissions, such as the US EPA 2020 Nonpoint Oil and Gas Emission Estimation Tool Version 1.3 (US EPA oil and gas tool), provide annual average emissions rates and emissions aggregated at the county level. More detailed spatial and temporal information is needed to accurately estimate exposures to UOGD emissions. In addition, for hydrocarbons, there is limited data available on emission compositions, further limiting the information required to estimate exposures to UOGD emissions. Finally, for some source categories, new field measurements provide updated emission factors. This chapter provides an overview of the spatial and temporal allocation methods we developed in this work, the new emission factors we developed, and the emission composition data we assembled. We describe the TRACER model, which builds on and expands our previously developed Methane Emission Estimation Tool (MEET) (Allen et al. 2022). MEET is an open-source modeling tool that helps regulators, industry, and the research community more accurately track methane and other emissions in oil and gas production regions.

We then applied the methods to the estimation of emissions in the Marcellus oil and gas production region. Additional applications of these emission estimation tools are discussed in other chapters of this report.

STUDY DESIGN AND METHODS

Table 5-1 summarizes the source categories that were addressed in this work, which include upstream and midstream sources along the oil and gas supply chain, from preproduction and production to gas gathering, processing, and transmission. This chapter uses the Marcellus region as a case study, where sources such as well site compressors and dehydrators are negligible. These sources are excluded from the case study but are included in additional applications included in this report. In bold are the spatial and temporal allocations developed in this work that improve the methods used in existing inventories. **Table 5-2** summarizes the emission composition information used or developed in this work. Highlighted in bold is the emission composition information developed as part of this research that improves methods used in existing inventories. **Table 5-3** summarizes source categories for which new emission factor information was developed. Additional details on emission estimation methods are available in Chen and colleagues (2025), included as Additional Materials C for this report.

The spatial domain over which emissions were estimated in the Marcellus oil and gas production region is provided in **Figure 5-1**. The emissions were spatially aggregated using a 4 × 4 km grid and were estimated for the 2023 calendar year.

The emission estimation methods summarized in Tables 5-1 to 5-3 were applied to the Marcellus oil and gas production region, shown in Figure 5-1. The inventories were created at a variety of spatial and temporal scales to illustrate the complex spatial and temporal variability of the emissions. For example, emissions from compressor exhaust are assumed to be continuous and constant with no start time or duration. In contrast, other sources of emissions, such as drilling, hydraulic fracturing, and liquid unloading, are assumed to have defined starting and ending times, but when emissions occur, they are assumed to be emitted at a constant rate. Still other emission sources, such as completion flowbacks and tank flashing, may have emission rates that vary during the event. Some emissions, such as tank flashing, may be recurring, repeating on a random or defined schedule. Other defined duration emissions, such as drilling and hydraulic fracturing, may be one-time events for each well location. The spatial distribution, frequency, duration, and emission rate variability for each source are summarized in Table 5-1.

The emissions inventory tools developed in this work can create emissions inventories with temporal resolutions ranging from minutes to months. Emissions inventories with hourly resolution were created for the analyses presented in this chapter. This choice of temporal resolution was based on observational data. Observations of ambient concentrations of air pollutants in oil and gas production regions show strong diurnal variation, with peak concentrations in multiple regions occurring during late night and early morning hours. This diurnal variability is driven by a complex combination of temporal variability in meteorology and emissions as described in other chapters of this report; however, the observational evidence clearly suggests that an hourly temporal resolution will be required to assess patterns of ambient concentrations and exposures.

Emission of criteria air pollutants and individual molecular species were estimated based on combining either a volumetric flow rate of emissions or an activity factor (e.g., quantity of fuel combusted) with data on the composition of the emissions. The types of speciation profiles used for each source are summarized in Table 5-2. The specific compositions assumed for the Marcellus Shale are shown in **Table 5-4**.

DATA ANALYSIS

The development of new emission estimation methods as part of this work addressed the following topics:

Table 5-1. Source Types Included in the Emissions Inventory[a]

Source	Spatial Distribution	Frequency	Duration	Emission Rate Variability
		Well Site and Tank Batteries		
Drilling engines	**Well locations**	**One-time event for well**	**Variable**	None
Mud degassing	**Well locations**	**One-time event for well**	**Variable**	None
Hydraulic fracturing pumps	**Well locations**	**One-time event for well**	**Variable**	None
Completion flowbacks	**Well locations**	**One-time event for well**	**Variable**	**Variable**
Artificial lift engines	**Well locations**	Continuous	Continuous	None
Associated gas venting	**Well locations**	Continuous	Continuous	None
Condensate/crude tank venting	**Well locations**	**Based on production**	**Variable**	**Variable**
Produced water tank venting	**Well locations**	**Based on production**	**Variable**	**Variable**
Fugitives (leaks)	**Well locations**	**Based on leak probability**	**Variable**	**Variable**
Pneumatic pumps	**Well locations**	Continuous	Continuous	None
Pneumatic controllers	**Well locations**	**Based on malfunction rate**	**Variable**	**Variable**
Heaters	**Well locations**	Continuous	Continuous	None
Liquid unloading	**Well locations**	**Based on unloading frequency**	**Variable**	**Variable**
Flares	**Flare locations**	**Based on satellite observation**	**Variable**	**Variable**
		Gathering and Boosting Sites		
Compressor engines	**Well locations**	Continuous	Continuous	None
Dehydrators	**Well locations**	Continuous	Continuous	None
Acid gas removal	**Well locations**	Continuous	Continuous	None
Flares	**Flare locations**	**Based on satellite observation**	**Variable**	**Variable**
		Gas Processing Plants		
Site total emissions	**Plant locations**	Continuous	Continuous	None
Flares	**Flare locations**	**Based on satellite observation**	**Variable**	**Variable**
		Transmission Facilities		
Site total emissions	**Facility locations**	Continuous	Continuous	None

[a]Spatial and temporal allocations that improve existing inventories are in bold.

- UOGD emission sources have complex spatial and temporal distributions that can affect exposures.
- UOGD emission sources can have highly variable compositions that affect exposures.

As summarized in Tables 5-1 to 5-3, multiple improvements were made to existing emission estimation methods. The application of the emission estimation methods is described for the Marcellus oil and gas production region. Additional applications are described in subsequent chapters in which the emissions estimates are coupled with dispersion or chemical transport models.

RESULTS

A gridded emissions inventory for multiple pollutants was developed for the region shown in Figure 5-1. To illustrate key features of the inventories, results are reported for seven grid cells, listed in **Table 5-5**. Locations of these grid cells are shown in **Figure 5-2**. The grid cells were selected to have a variety of episodic and continuous emissions. Some grid cells had relatively large numbers of wells undergoing preproduction activities. Other grid cells had no new wells completed. Some grid cells had wells with liquid production. Other grid cells had wells with no liquid production.

Table 5-2. Speciation Profiles for Emission Sources[a]

Source	Speciation Profile
Well Site and Tank Batteries	
Drilling engines	US EPA oil and gas tool[b]
Mud degassing	Study-specific speciation profile
Hydraulic fracturing pumps	US EPA oil and gas tool[b]
Completion flowbacks	**Study-specific speciation profile by well type**
Artificial lift engines	US EPA oil and gas tool[b]
Associated gas venting	**Study-specific produced gas composition by well type**
Condensate/crude tank venting	**Study-specific oil tank vent composition by well type**
Produced water tank venting	**Study-specific vent tank vent composition by well type**
Fugitives (leaks)	**Study-specific produced gas composition by well type**
Pneumatic pumps	**Study-specific produced gas composition by well type**
Pneumatic controllers	**Study-specific produced gas composition by well type**
Heaters	US EPA oil and gas tool[b]
Liquid unloading	**Study-specific produced gas composition by well type**
Flares	**Study-specific speciation profile**
Gathering and Boosting Sites	
Compressor engines	**Study-specific throughput gas composition**
Dehydrators	**Study-specific produced gas composition**
Acid gas removal	**Study-specific produced gas composition**
Flares	**Study-specific throughput gas composition**
Gas Processing Plants	
Site total emissions	**Study-specific throughput gas composition**
Flares	**Study-specific throughput gas composition**
Transmission Facilities	
Site total emissions	**Study-specific throughput gas composition by grid cell**

[a]Emission composition assignments that improve existing inventories are in bold.

[b]US EPA *2020 Nonpoint Oil and Gas Emission Estimation Tool Version 1.3*.

Table 5-3. Emission Factors for Sources That Were Expanded or Improved in This Work

Source	Speciation Profile
Well Site and Tank Batteries	
Completion flowbacks	Emission factors based on data from field measurements (Allen et al. 2013)
Pneumatic pumps	Emission factors based on data from field measurements (Allen et al. 2013)
Pneumatic controllers	Emission factors based on data from field measurements (Allen et al. 2015a)
Liquid unloading	Emission factors based on data from field measurements (Allen et al. 2015b)
Flares	Emission factors based on data from field measurements (Chapter 3 and satellite observations [Earth Observation Group 2025])

A total of 266 wells are located in the seven selected grid cells. Wells that stopped production before 2023 or had no production information were eliminated, leaving a total of 220 wells in the simulations. The gas-to-oil ratios of all selected wells in the simulation were >10,000 SCF/BBL (standard cubic feet of gas per barrel of hydrocarbon liquid production), and gas-to-oil ratios calculated for production, aggregated over a grid cell, were >100,000 SCF/BBL for all of the grid cells in Table 5-5. The wells were characterized into three production types in the database as dry gas (0% to 1% wellhead liquids), wet gas (1% to 10% wellhead liquids), and liquids-rich gas (10% to 40% wellhead liquids). The well type distributions in each grid cell are listed in **Tables 5-6** and **5-7**.

Some emission sources listed in Table 5-1 were excluded from the inventory developed for the selected grid cells. Emission sources specific to oil wells, such as artificial gas lift engines and associated gas venting, were excluded because all wells in selected grid cells were gas wells. Flare operations and gas processing, as well as transmission operations, were not observed in the selected grid cells, but are present elsewhere in the domain. For the remaining sources, methane, ethane, and VOC emissions were simulated. Nitrogen oxides emissions were simulated for combustion sources only. Methods for estimating individual emission components are summarized in **Table 5-8.**

Preproduction emissions associated with well drilling and hydraulic fracturing were estimated with total emissions derived from the US EPA oil and gas tool. Emissions were spatially allocated to wells with preproduction activity, and emissions were temporally allocated based on the completion date. These emission estimation methods are described in more detail in Chapter 7 of this report. Hydraulic fracturing emissions were assigned in the 2 weeks before well completion. Drilling emissions were assigned in the 2 weeks before hydraulic fracturing.

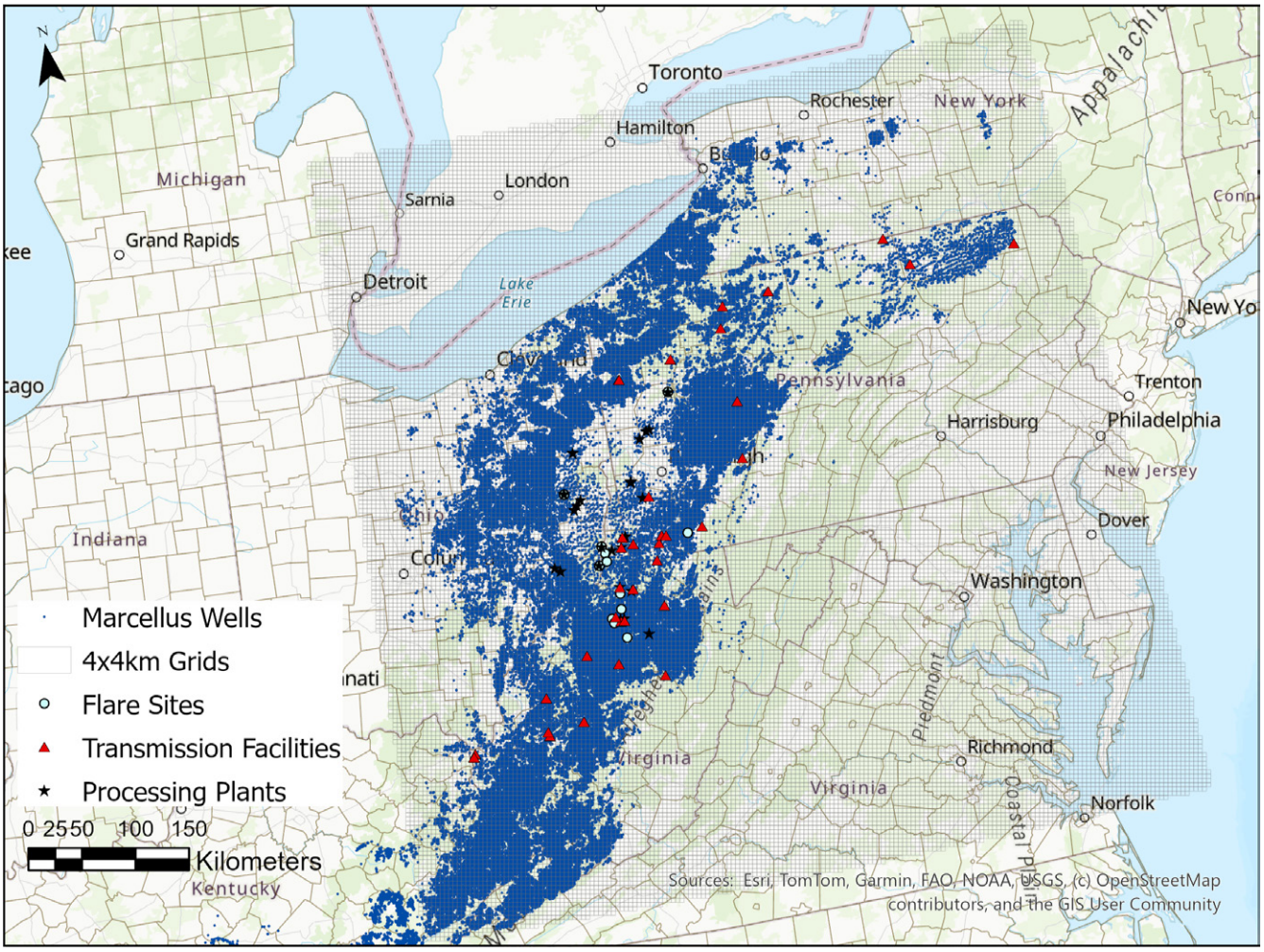

Figure 5-1. Spatial domain for Marcellus emissions inventory with well locations, midstream sites, and flare sites shown. Overlaid grid cells covered 98% active production wells in the Marcellus Shale. Only midstream and flare sites located in grid cells with wells are included in the simulation. Source: Adapted from Chen et al. 2025; Creative Commons license CC BY 4.0.

Table 5-4. Average Composition (in Percent) of Produced Gas in the Marcellus Shale[a]

Component	Wet Gas	Dry Gas
Ozone	0	0.00772
Helium	0	0.00372
Molecular Nitrogen	0.568	0.301
Carbon Dioxide	0.130	0.0518
Methane	76.8	97.4
Dimethylsulfide	14.9	2.11
Propane	4.94	0.0753
Isobutane	0.520	0.00297
Normal Butane	1.29	0.00530
Isopentane	0.268	0.000163
Normal Pentane	0.342	0.000278
Neopentane	0.00890	0
Hexane and All Heavier Hydrocarbons	0.217	0.000226

[a]Dry gas composition based on produced gas samples collected at 46 dry gas sites (no oil production); wet gas composition based on produced gas sample collected at one wet gas site (Allen et al. 2013).

continues next column

Table 5-5. Seven Grid Cells Selected for Detailed Reporting

Grid Cell	County	State	Marcellus Portion
1	Tyler	WV	Southwest
2	Greene	PA	Southwest
3	Lewis	WV	Southwest
4	Bradford	PA	Northeast
5[a]	Bradford	PA	Northeast
6	Bradford	PA	Northeast
7	Susquehanna	PA	Northeast

[a]The majority of grid cell 5 is located within Bradford County, PA, while a few wells in this grid are located in Sullivan County, Pennsylvania.

Hydrocarbon emissions time series from completion flowbacks, tank flash, leaks, pneumatic devices, and liquid unloading were simulated at hourly resolution. Both oil and water tank emissions are assumed to be controlled with vapor recovery units with 95% control efficiency on well sites with condensate production. Water tanks on sites without condensate production are not controlled. The emission factors and activity factors used in the simulations are summarized in **Table 5-9**. Activity factors were based on the basin-specific activity data from the Inventory of US Greenhouse Gas Emissions and Sinks (GHGI) in the year 2022 (US EPA 2024b), the most recent data available at the time of analysis.

Emissions from heaters were estimated with a constant emission rate calculated by combining county-specific emission factors available in the US EPA oil and gas tool and activity data from the GHGI. Site total methane, ethane, and VOC emissions from gathering and boosting sites were estimated

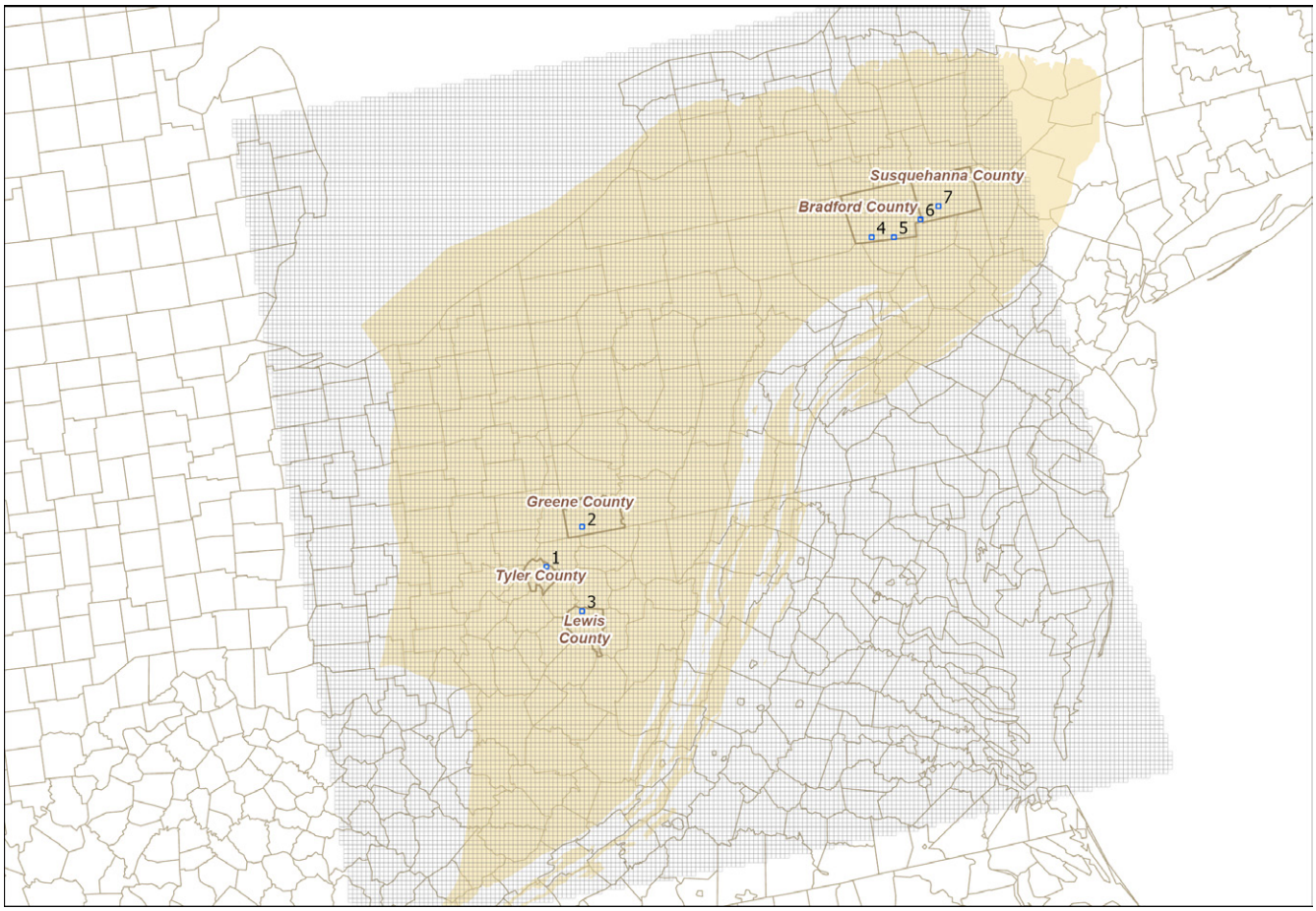

Figure 5-2. Locations of grid cells selected for detailed reporting.

Table 5-6. Well Types in Grid Cells Selected for Analysis

	Wells in Simulation							Wells Eliminated	
Grid Cell	Total	Horizontal/ Directional	Vertical	Dry Gas	Wet Gas	Liquid Rich Gas	Wells Completed in 2023	No Production in 2023	Missing Production Data
1	46	41	5	1	44	1	13	0	2
2	17	16	1	17	0	0	16	0	0
3	62	14	48	47	12	3	4	1	39
4	13	13	0	13	0	0	0	0	1
5	13	13	0	13	0	0	0	0	1
6	35	35	0	35	0	0	4	0	2
7	34	29	5	34	0	0	0	0	0

Table 5-7. Production in the Last 12 Months (Assumed to Represent Annual Production in 2023)

Grid Cells	County	Marcellus Portion	Gas (MCF)	Oil (BBL)	Water (BBL)	Gas-to-Oil Ratio (SCF/BBL)
1	Tyler, WV	Southwest	130,894,893	877,137	1,745,756	149,000
2	Greene, PA	Southwest	101,928,789	0	876,746	
3	Lewis, WV	Southwest	56,411,783	1,017	649,496	55,469,000
4	Bradford, PA	Northeast	22,202,653	0	62,021	
5	Bradford, PA	Northeast	54,76,523	0	2,848	
6	Bradford, PA	Northeast	46,326,381	0	65,172	
7	Susquehanna, PA	Northeast	15,169,203	0	9,275	

BBL = barrel; MCF = thousand cubic feet; SCF/BBL = standard cubic feet per barrel.

by combining the gas throughput normalized emission factor as reported by Zimmerle and colleagues (2020), gas throughput per grid cell, and throughput gas compositions at the level of grid cells. Throughput gas compositions at the level of grid cells were calculated using the produced gas compositions per well in the grid cell. Nitrogen oxides emissions are calculated based on methane emission rates due to combustion slip and the mass ratio of nitrogen oxide-to-methane emissions for four-stroke lean-burn (4SLB) engines with <90% load, as reported by US EPA AP-42 (US EPA 2025), assuming 38% of site total methane emissions are due to combustion slip (Zimmerle et al. 2020).

According to Vaughn and colleagues (2021), at gathering compressor stations in the Marcellus, >90% compressor engines are nonelectric, >80% nonelectric engines are 4SLB engines. The average load factor for 4SLB engines observed in the field is 85%. These assumptions affect nitrogen oxides emissions estimates.

Methane emissions from gas processing plants and transmission facilities were estimated based on facility-level data from the EPA Greenhouse Gas Program per site (US EPA 2024a). Ethane and VOCs emissions were estimated based on methane emissions and throughput gas compositions aggregated per grid cell. Nitrogen oxides emissions were estimated based on methane emissions due to compressor exhaust and EPA AP-42 emission factors (US EPA 2025). Engine types and load factors are assumed to be the same as those from gathering compressor stations due to a lack of data at processing and transmission sites. According to the EPA GHGI in the year 2022, methane emissions from compressor exhaust account for 66% site total methane emissions at processing plants, and 16% of total emissions at transmission facilities.

Annual hydrocarbon emissions from flare operations were estimated by combining the annual gas flare volume per flare site, a 98% flaring efficiency, and gas throughput compositions in grid cells in which the flare site is located. The annual

Table 5-8. Methods for Estimating Individual Emission Components for Developing Emissions Inventory in Selected Grid Cells

Source	Methane	Ethane	Volatile Organic Compounds	Nitrogen Oxides
Well Site and Tank Batteries				
Drilling engines	Total emissions based on county inventory; spatially and temporally allocated using methods described in Chapter 7	Assumed negligible	Total emissions based on county inventory; spatially and temporally allocated using methods described in Chapter 7	Total emissions based on county inventory; spatially and temporally allocated using methods described in Chapter 7
Hydraulic fracturing pumps	Total emissions based on county inventory; spatially and temporally allocated using methods described in Chapter 7	Ignored due to lack of data	Total emissions based on county inventory; spatially and temporally allocated using methods described in Chapter 7	Total emissions based on county inventory; spatially and temporally allocated using methods described in Chapter 7
Completion flowbacks	MEET	MEET	MEET	Not applicable
Artificial lift engines	Not applicable in gas regions			
Associated gas venting	Not applicable in gas regions			
Condensate/crude tank venting	MEET	MEET	MEET	Not applicable
Produced water tank venting	MEET	MEET	MEET	Not applicable
Fugitives (leaks)	MEET	MEET	MEET	Not applicable
Pneumatic pumps	MEET	MEET	MEET	Not applicable
Pneumatic controllers	MEET	MEET	MEET	Not applicable
Heaters	A constant rate calculated from emission and activity factors	Assumed negligible	A constant rate calculated from emission and activity factors	A constant rate calculated from emission and activity factors
Liquid unloading	MEET	MEET	MEET	Not applicable
Gathering and Boosting Sites				
Site total emissions	A constant rate calculated based on gas throughput	A constant rate calculated based on gas throughput	A constant rate calculated based on gas throughput	A constant rate calculated based on methane emissions and the nitrogen oxides-to-methane emission ratio
Gas Processing Plants				
Site total emissions	A constant rate calculated based on the Greenhouse Gas Reporting Program	Estimated based on methane emission rates and gas composition	Estimated based on methane emission rates and gas composition	A constant rate calculated based on methane emissions and the nitrogen oxides-to-methane emission ratio
Transmission Facilities				
Site total emissions	A constant rate calculated based on the Greenhouse Gas Reporting Program	Estimated based on methane emission rates and gas composition	Estimated based on methane emission rates and gas composition	A constant rate calculated based on methane emissions and the nitrogen oxides-to-methane emission ratio

MEET = Methane Emission Estimation Tool.

Table 5-9. Activity Factors and Emission Factors Used in Simulations[a]

Source	Activity Factor	Methane Emission Factor
Completion flowbacks	• Two-stage durations sampled from Allen et al. (2013) • Assigned to wells completed in 2023	Allen et al. (2013) distribution of measured emissions
Condensate/crude tank venting	One condensate tank per well with oil production	Determined by the thermodynamic tool of MEET based on separator conditions and produced gas compositions
Produced water tank venting	One water tank per well with water production	Determined by the thermodynamic tool of MEET based on separator conditions and produced gas compositions
Fugitives (leaks)	Leak equipment assigned to wells: • Tank: counts the same as above • Separator: 0/well if 1 phase of production; 1/well if 2 or 3 phases of production • Heater: 0.10/well (dry) or 0.06/well (wet), randomly assigned to wells • Meter/piping: 0.93/well, randomly assigned to wells • Acid gas removal unit: 0	Allen et al. (2013) distribution of measured emissions
Pneumatic pumps	Randomly assigned to wells based on average count: • For dry gas wells: 0.03 count/well • For wet gas wells: 0.01 count/well	Allen et al. (2013) distribution of measured emissions
Pneumatic controllers	Randomly assigned to wells based on average count: • For dry gas wells: 0.97 count/well (83% intermittent, 17% low bleed, 0.2% high bleed) • For wet gas wells: 0.63 count/well (77% intermittent, 23% low bleed, 0.1% high bleed)	• Allen et al. (2015a) distribution of measured emissions • Emissions transition between normal and abnormal operations
Liquid unloading	Assigned to the wells with the lowest gas-to-liquids production rates and completed before 2020, with randomly assigned unloading technology • 7% of wells: manual unloading without plunger lift • 4% of wells: manual unloading with plunger lift	Allen et al. (2015b) distribution of measured emissions

MEET = Methane Emission Estimation Tool.

[a]Emission factors were applied to methane emissions. Ethane and volatile organic compounds emissions were estimated from methane emissions and emission compositions.

gas flare volume per flare site identified in the study domain was reported by Earth Observation Group (2025) using VIIRS data. Total flare operating hours per year, calculated based on the flare detection frequency per site, were divided into flaring events up to 240 hours (10 days) per event. Flaring events were randomly assigned in the time series without overlapping in time. Hourly emission rates during flaring events were calculated as annual site total emissions normalized by total operating hours. Nitrogen oxides emissions were estimated based on methane emission rates and AP-42 emission factors (US EPA 2025).

Table 5-10 compares maximum and average emission rates for the seven grid cells. For methane, ethane, and VOC emissions, maximum hourly emission rates are typically several times the mean annual emission rate. Maximum hourly hydrocarbon emission rates can be up to several tens of times higher than average rates per grid cell, depending on the hydrocarbon type and grid location. In contrast, nitrogen oxides emissions (grid cell totals) vary less than hydrocarbon emissions do and are dominated by continuous emissions from gathering compressors during times without drilling activities. Note that this pattern would change if emissions were evaluated at individual sites rather than over the entire grid cell (see Chapter 7).

Time series for individual grid cells, disaggregated by source, are shown in **Figures 5-3** and **5-4**. The time series

Table 5-10. Maximum and Average Emission Rate (kg/hr) per Grid Cell

	Methane		Ethane		Volatile Organic Compounds		Nitrogen Oxides	
Grid cell	**Max**	**Mean**	**Max**	**Mean**	**Max**	**Mean**	**Max**	**Mean**
1	254.5	79.8	236.6	87.9	768.4	64.3	116.3	26.2
2	293.1	102.9	6.4	2.3	4.0	0.5	114.3	35.3
3	106.7	80.3	27.0	2.8	103.3	1.9	19.9	18.2
4	250.0	50.8	5.5	1.1	0.1	0.03	11.8	11.8
5	422.1	27.6	9.2	0.6	0.2	0.01	6.1	6.1
6	506.4	74.8	11.1	1.6	3.0	0.2	84.9	19.3
7	194.2	42.6	4.3	0.9	0.1	0.03	9.9	9.9

illustrates the importance of frequent, short-duration events, such as liquid unloading and well completions. Sources contributing to high hourly emission rates vary by pollutants. For hydrocarbon emissions, a high-rate liquid unloading event can temporarily lead to high regional hydrocarbon emissions. For nitrogen oxides emissions, high hourly emission rates in the time series are driven by clustered drilling activities.

If emissions are aggregated at a county-level scale, rather than a grid-level scale, the variability in emissions decreases. **Table 5-11** shows the effect of aggregating emissions at a county level, as opposed to a grid cell level, on ratios of maximum-to-average emission rates. In both Wetzel County, a wet gas production region in the southwestern Marcellus Shale, and in Bradford County, a dry gas production region in the northeast Marcellus, the ratio decreases significantly when emissions are aggregated at the county level for all emissions except nitrogen oxide, when compared with the mean of all the individual ratios of grid cells within the county. Differences between hydrocarbons (methane, ethane, and VOCs) are pronounced in the wet gas region but disappear in the dry gas region.

SENSITIVITY ANALYSES ON NITROGEN OXIDES EMISSIONS ESTIMATES

As shown in Figures 5-3 and 5-4, during times when there are no clustered drilling activities, nitrogen oxides emissions are primarily dominated by combustion emissions from compressor stations at gathering sites, as well as from processing and transmission facilities when they are present. Nitrogen oxides emissions from these sites were estimated based on methane emissions and EPA AP-42 emission factors (US EPA 2025) for natural gas-fired reciprocating engines, which depend largely on the type and load factor of the engines. **Table 5-12** shows the nitrogen oxides and methane emission factors per engine type and operating condition.

Because data were limited, analyses in the base scenario assumed all compressor engines at gathering, processing, and transmission facilities in the Marcellus Shale are 4SLB engines with <90% load, based on measurements (Vaughn et al. 2021) at gathering compressor stations. A nitrogen oxides-to-methane mass ratio of 0.68 (0.85 lb/MMBTU to 1.25 lb/MMBTU) for combustion sources is used in nitrogen oxides estimates. The engine population reported by Vaughn and colleagues represents the distribution of 49 engines from their study partners in the Marcellus and may be biased when extrapolating to the entire basin. In comparison, the US EPA oil and gas tool reported that 80% of compressors at gathering facilities were rich-burn compressors, with an average load factor of 98%. Using the US EPA-reported engine population, sensitivity analyses on nitrogen oxides emissions estimates were conducted by assuming all compressors at gathering, processing, and transmission facilities are 4SRB engines with >90% load, and a nitrogen oxides-to-methane mass ratio of 9.61 (2.27 lb/MMBTU to 0.23 lb/MMBTU) is used in calculations. However, this population might also be biased because of outdated data sources referred to in the EPA tool.

Figure 5-5 compares time series of nitrogen oxides emissions in Wetzel County with all 4SLB compressors and with all 4SRB compressors at gathering, processing, and transmission facilities. County total nitrogen oxides emissions are >10 times higher with rich-burn assumptions than with lean-burn assumptions. With rich-burn assumptions, total emissions are always dominated by constant combustion emissions from gathering and processing sites. In contrast, with lean-burn assumptions, nitrogen oxides emissions from clustered drilling activities — when they occur — are comparable with those from gathering and processing facilities, and lead to more

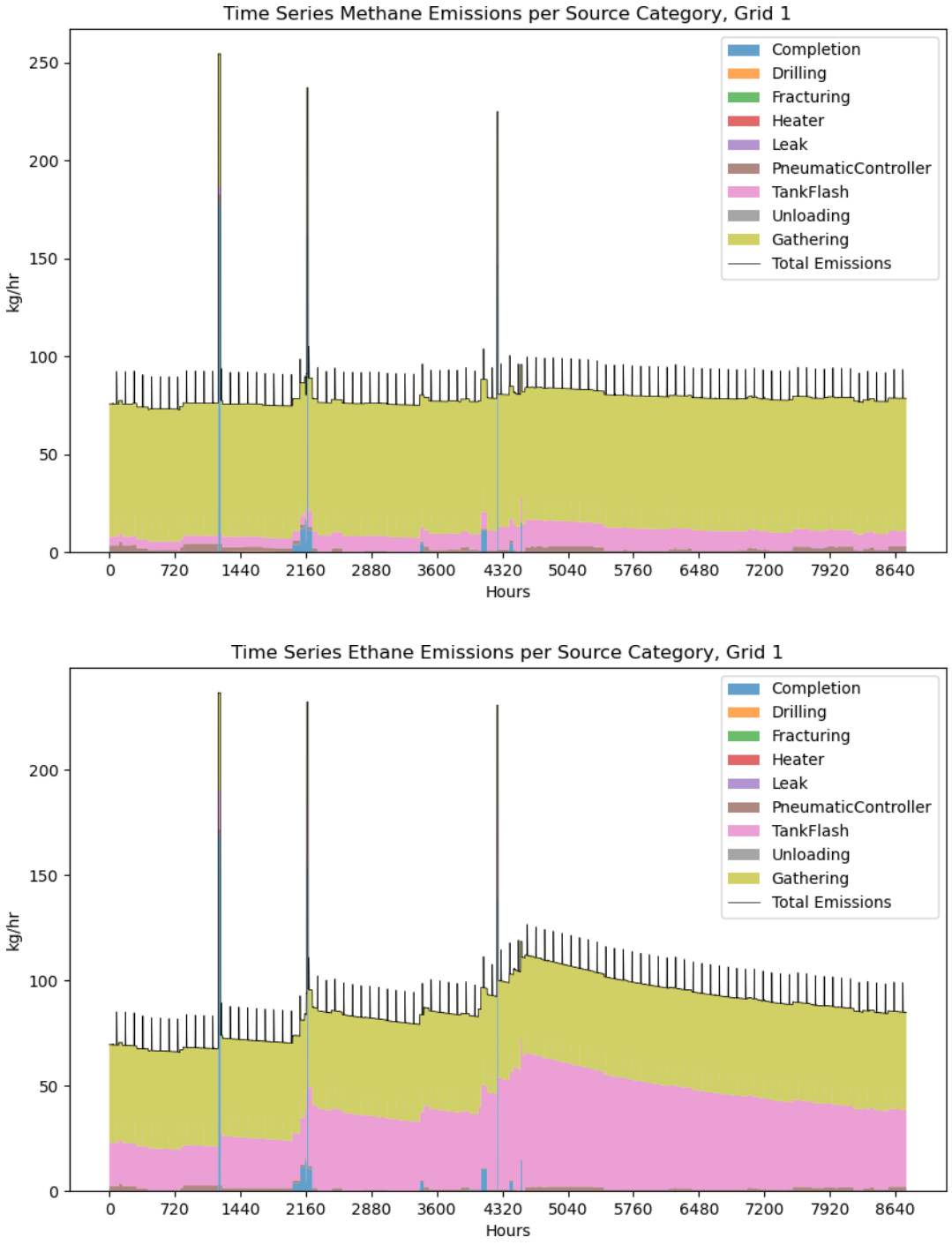

Figure 5-3. Time series of methane, ethane, volatile organic compounds, and nitrogen oxides emissions in grid cell 1, a wet gas region with ~30% producing wells in the region drilled and completed in 2023.

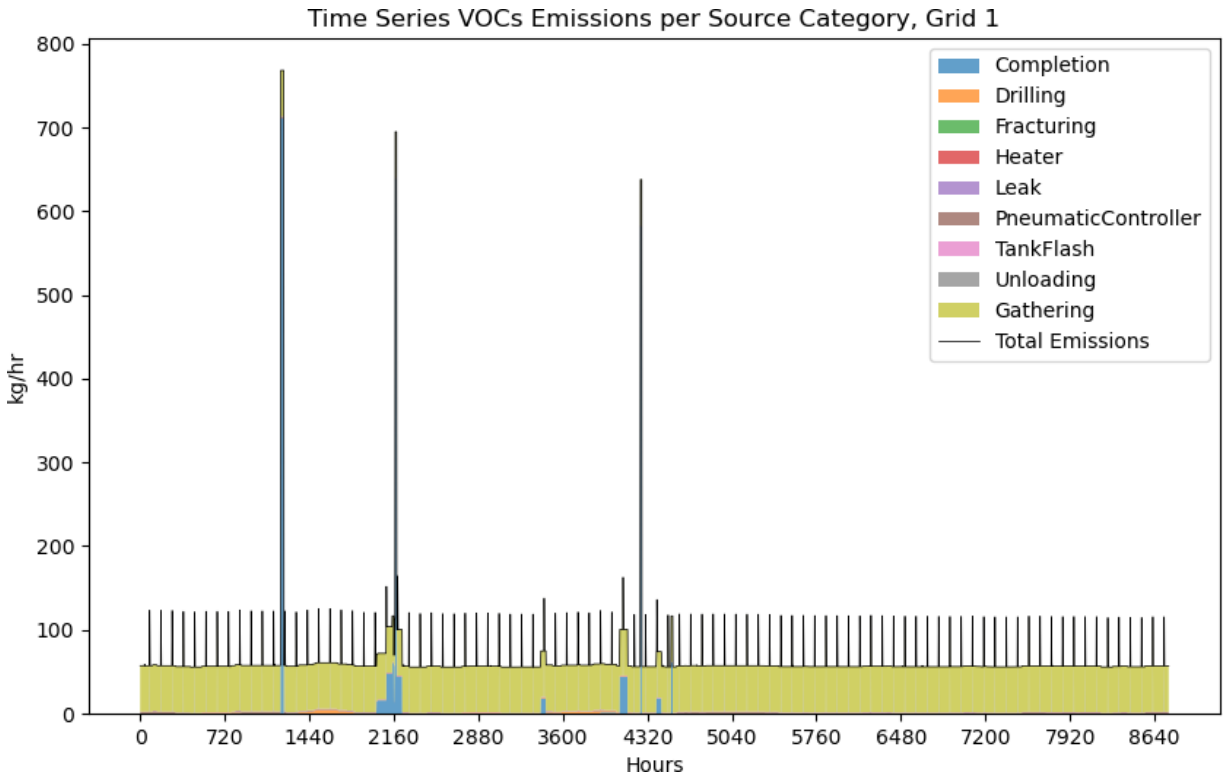

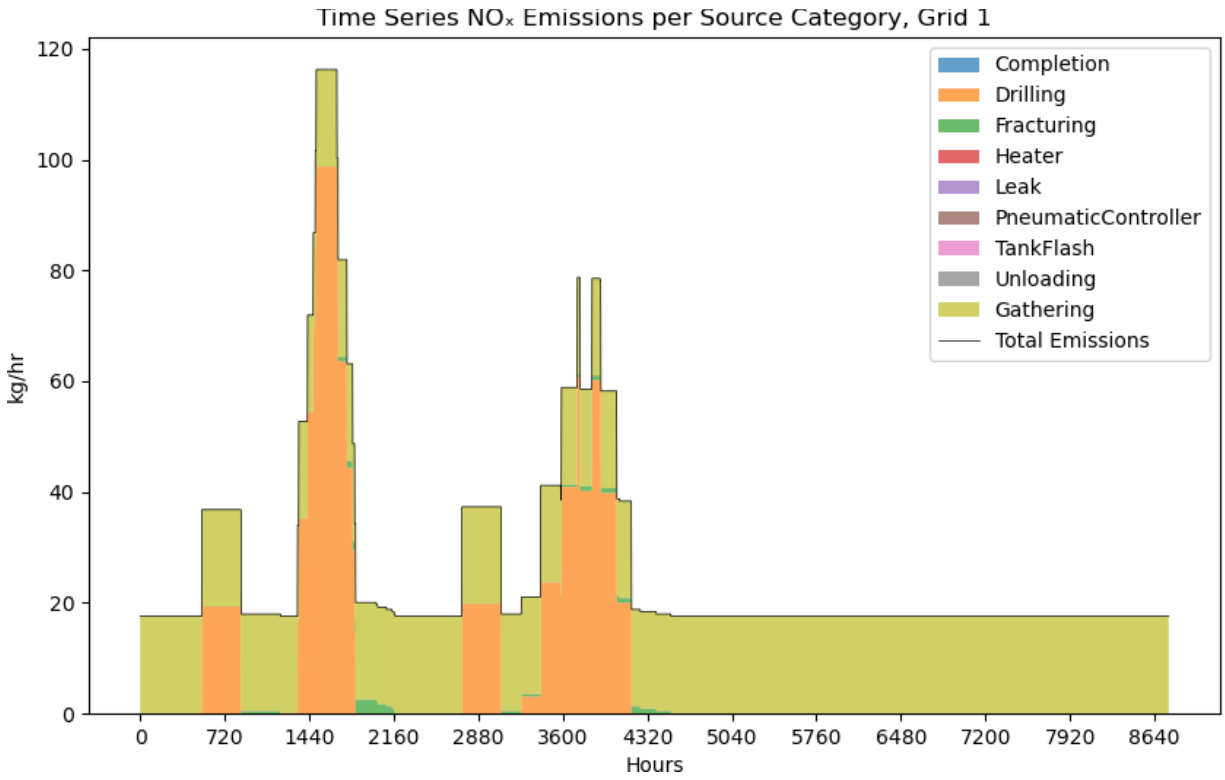

Figure 5-3. *(continued)*

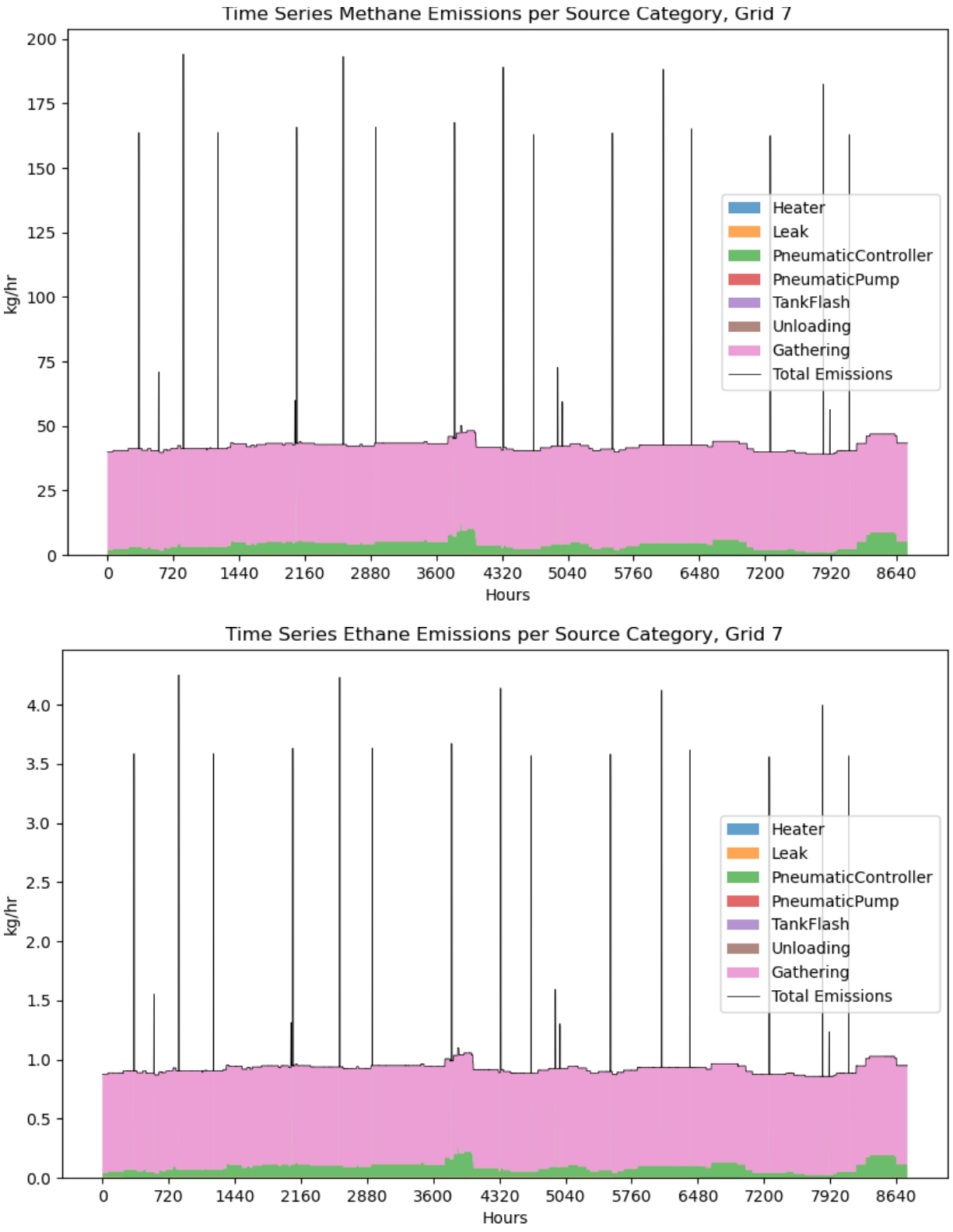

Figure 5-4. Time series of methane, ethane, volatile organic compounds, and nitrogen oxides emissions in grid cell 7, a dry gas region with no wells drilled and completed in 2023.

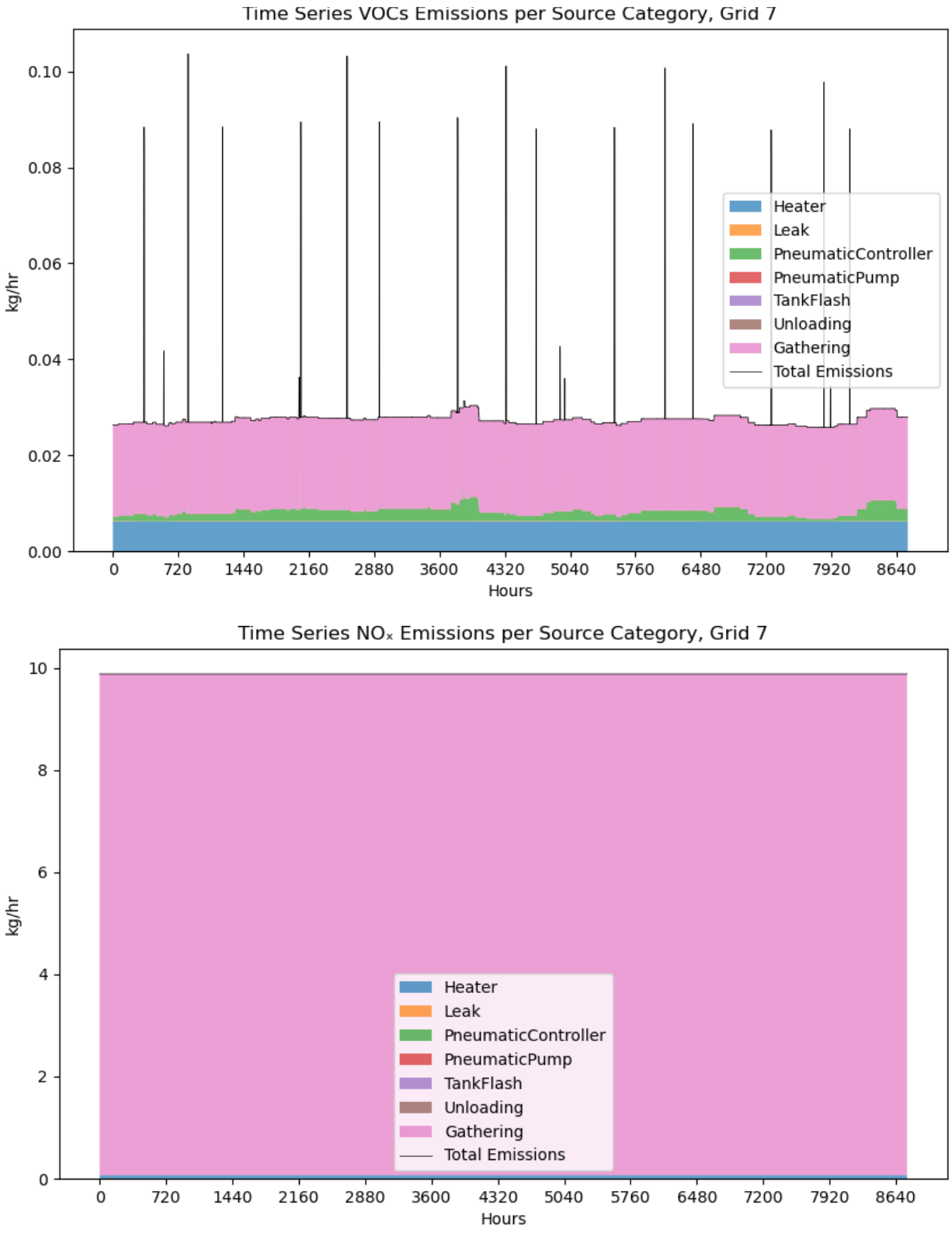

Figure 5-4. *(continued)*

Table 5-11. Ratios of Maximum-to-Average Hourly Emission Rates at a County Level and for Grid Cells Within Each County

	Methane	Ethane	Volatile Organic Compounds	Nitrogen Oxides
Wetzel County				
County aggregation	1.6	2.8	9.6	1.5
Grid cell: mean	5.0	7.3	30	2.1
Grid cell: median	2.0	3.6	19	1.0
Grid cell: max	42	51	243	11
Bradford County				
County aggregation	1.7	1.7	2.8	1.2
Grid cell: mean	7.2	7.2	8.0	1.4
Grid cell: median	1.2	1.2	1.2	1.0
Grid cell: max	103	103	103	5.8

Table 5-12. Nitrogen Oxides and Methane Emission Factors per Engine Type and Engine Operating Condition for Natural Gas-Fired Reciprocating Engines

	Engine Types		
	4SRB	4SLB	2SLB
Emission Factors per Gas (Lb/MMBTU Fuel Throughput)			
Nitrogen oxides (>90% load)	2.21	4.08	3.17
Nitrogen oxides (<90% load)	2.27	0.85	1.94
Methane	0.23	1.25	1.45
Nitrogen Oxides-to-Methane Ratio by Mass			
>90% load	9.61	3.26	2.19
<90% load	9.87	0.68	1.34

2SLB = two-stroke lean burn; 4SLB = four-stroke lean burn; 4SRB = four-stroke rich burn.

significant temporal variations in county total emissions. The ratio of maximum-to-mean hourly emission rate aggregated at the county level is 1.0 with rich-burn assumptions, compared with the ratio of maximum-to-mean hourly emission rate of 1.5 with lean-burn assumptions.

Nitrogen oxides emissions estimates are also sensitive to the assumptions of the fraction of methane emissions depending on combustion sources at gathering, processing, and transmission facilities, and scale linearly with the assumed fraction of combustion methane sources per facility. The reported estimates represent the best available information, given limited data availability.

DISCUSSION AND CONCLUSIONS

The application described in this chapter has demonstrated that UOGD emission sources have complex spatial and temporal distributions and that UOGD emission sources can have highly variable compositions. Additional applications, details of emission estimation methods, and additional discussions are available in Chen and colleagues (2025), included as Additional Materials C for this report.

REFERENCES

Allen DT, Cardoso-Saldaña FJ, Kimura Y, Chen Q, Xiang Z, Zimmerle D, et al. 2022. A Methane Emission Estimation Tool (MEET) for predictions of emissions from upstream oil and gas well sites with fine-scale temporal and spatial resolution: model structure and applications. Sci Total Environ 829:154277; *https://doi.org/10.1016/j.scitotenv.2022.154277*.

Allen DT, Pacsi A, Sullivan D, Zavala-Araiza D, Harrison M, Keen K. et al. 2015a. Methane emissions from process equipment at natural gas production sites in the United States: pneumatic controllers. Environ Sci Technol 49:633–640; *https://doi.org/10.1021/es5040156*.

Allen DT, Sullivan DW, Zavala-Araiza D, Pacsi AP, Harrison M, Keen K, et al. 2015b. Methane emissions from process equipment at natural gas production sites in the United States: Liquid unloadings. Environ Sci Technol 49:641–648; *https://doi.org/10.1021/es504016r*.

Allen DT, Torres VM, Thomas J, Sullivan D, Harrison M, Hendler A, et al. 2013. Measurements of methane emissions at natural gas production sites in the United States. Proc Nat Acad Sci 110:17768–17773; *https://doi.org/10.1073/pnas.1304880110*.

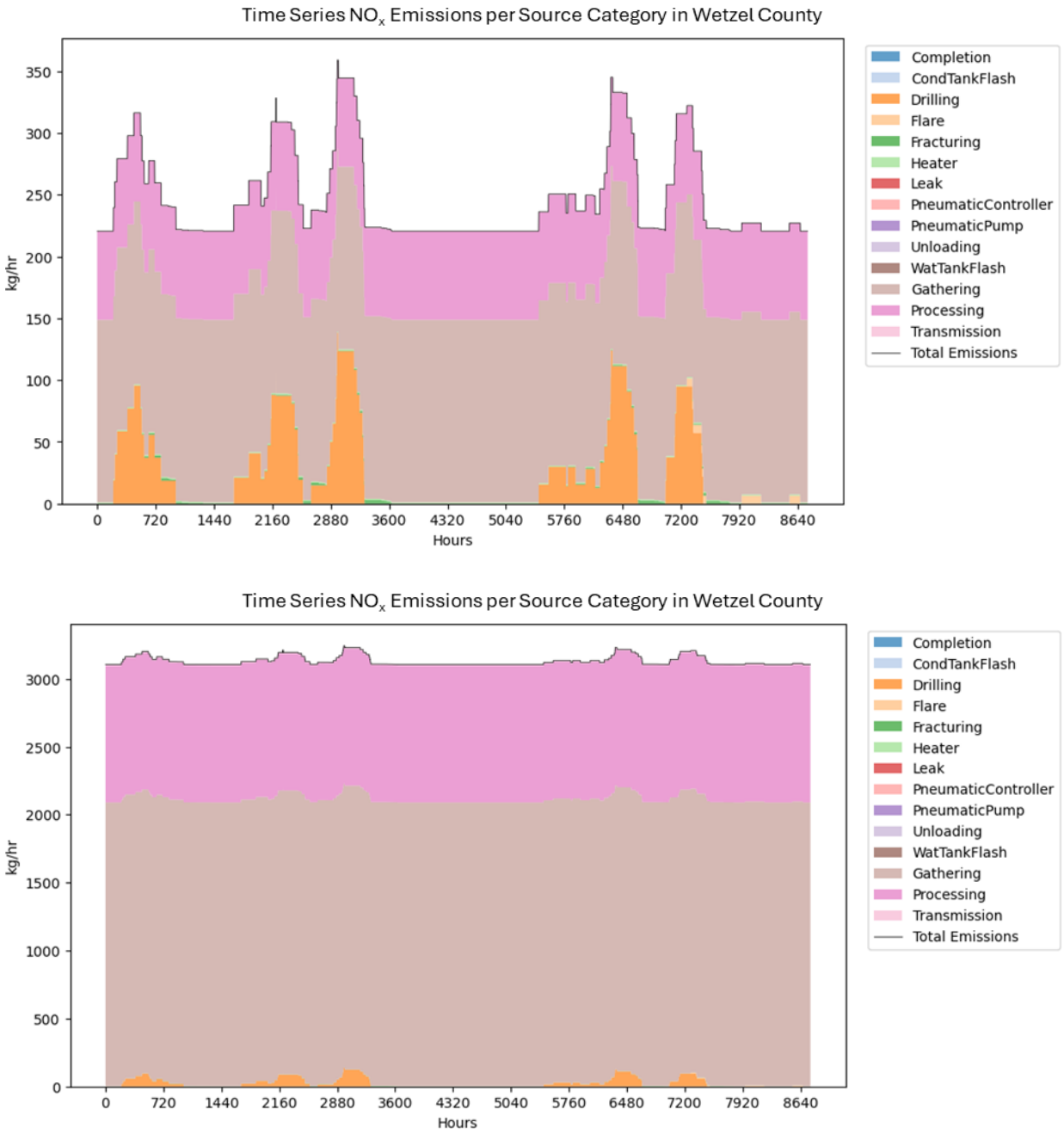

Figure 5-5. Time series of nitrogen oxides emissions in Wetzel County, assuming all compressors in gathering, processing, and transmission facilities are (A) 4SLB engines with >90% load, and (B) 4SRB engines with >90% load.

Chen Q, Raksi N, Niewenhous L, Almasalha SJ, Graves JD, Brown, et al. 2025. Spatial and temporal variability in atmospheric emissions from oil and gas sector sources in the Marcellus production region. Atmosphere 16:1048; *https://doi.org/10.3390/atmos16091048*.

Earth Observation Group. 2025. Global Gas Flaring Observed from Space. Available: *https://eogdata.mines.edu/products/vnf/global_gas_flare.html*

US Environmental Protection Agency (US EPA). 2022. 2020 Nonpoint Oil and Gas Emissions Estimation Tool V1.3. Available: *https://gaftp.epa.gov/Air/nei/2020/doc/supporting_data/nonpoint/oilgas/OIL_GAS_TOOL_v1.3/* [accessed 11 May 2025].

US Environmental Protection Agency (US EPA). 2024a. Facility Level Information on Greenhouse Gases Tool (FLIGHT) — 2023 Greenhouse Gas Emissions from Large Facilities. Available: *http://ghgdata.epa.gov/ghgp/main.do*.

US Environmental Protection Agency (US EPA). 2024b. Inventory of US Greenhouse Gas Emissions and Sinks: 1990–2022. EPA 430R-24004. Available *https://www.epa.gov/ghgemissions/inventory-us-greenhouse-gas-emissions-and-sinks-1990-2022*.

US Environmental Protection Agency (US EPA). 2025. Compilation of Air Pollutant Emission Factors from Stationary Sources (AP-42). Available: *https://www.epa.gov/air-emissions-factors-and-quantification/ap-42-compilation-air-emissions-factors-stationary-sources*.

Vaughn TL, Luck B, Williams L, Marchese AJ, Zimmerle D. 2021. Methane exhaust measurements at gathering compressor stations in the United States. Environ Sci Technol 55:1190–1196; *https://doi.org/10.1021/acs.est.0c05492*.

Zimmerle D, Vaughn T, Luck B, Lauderdale T, Keen K, Harrison M, et al. 2020. Methane emissions from gathering compressor stations in the US. Environ Sci Technol 54:7552–7561; *https://doi.org/10.1021/acs.est.0c00516*.

CHAPTER 6: COUPLING EMISSION ESTIMATION WITH DISPERSION MODELING

INTRODUCTION

As described in Chapter 5, the spatial and temporal patterns of emissions from UOGD sources are complex, and atmospheric dispersion is expected to further increase this complexity. This chapter describes the use of site-level emissions estimates from thousands of oil and gas sites, coupled with dispersion modeling, to estimate ambient concentrations of ethane at receptor sites. Emissions estimates and dispersion modeling for thousands of sites in the Eagle Ford oil and gas production region will be used to predict ambient concentrations at the TCEQ Karnes City site and will be compared with observations. The work described in this chapter has been published (Graves et al. 2025) and is included as Additional Materials D for this report.

STUDY DESIGN AND METHODS

MODELING DOMAIN

A 212 km × 208 km domain centered on the Karnes City sampling site was used, as shown in **Figure 6-1**. The domain includes three nested regions. In the 32 km × 32 km region closest to the TCEQ Karnes City site, 3,208 individual oil and gas well sites were identified using well locations from S&P Global US well and production data. Most well sites in the region contain very limited equipment, and most emissions are associated with liquid-handling equipment located at sites that manage the liquids from multiple wells (tank batteries). Therefore, emissions associated with oil, condensate, and produced water from each well were aggregated to 327 tank batteries in the 32 km × 32 km region, as identified visually with Google Earth imagery according to the proximity of tanks. All wells that had tanks on the same pad were routed to the tank(s) on-site. Each tank battery was assigned to an operator of the nearest well. Wells were then mapped to the tank batteries based on the operator and the nearest tank battery. Manual checks were conducted to minimize large discrepancies between the number of tanks and the number of wells mapped to them.

Sites located in the rectangular 48 km × 44 km domain centered on the TCEQ Karnes City site but outside the inner 32 km × 32 km domain were aggregated into point sources representing multiple sites. This part of the domain was divided into 1.33 km × 1.33 km grid cells, and all of the sources within each grid cell were aggregated and represented as a point source located at the centroid of the well sites within the grid cell. This region included a total of 1,782 well site locations aggregated into centroid locations in 319 grid cells.

Finally, sites located in a 212 km × 208 km rectangular domain centered on the TCEQ Karnes City site but outside the two inner domains were aggregated into point sources representing multiple sites in larger grid cells. The region was divided into 4 km × 4 km grid cells, and all of the sources within a grid cell were aggregated and represented as a point source located at the centroid of the sites within the grid cell. This region included a total of 15,516 well site locations aggregated into centroid locations in 974 grid cells.

The choice of nesting was based on a need to balance computation intensity and accuracy. Dispersion modeling showed that UOGD sources within 5 km of the TCEQ Karnes City site only contributed 38%, on average, to the mean concentrations predicted when all UOGD sources in the 200 km × 200 km domain were accounted for. UOGD sources within 10, 20, and 50 km of the Karnes site accounted for 67%, 88%, and 99% of average concentrations, respectively (see Chapter 6 Results section). This observation indicated that the large number of UOGD sites at significant distances from the central monitoring site could have a measurable effect on average concentrations. In contrast, as the distances between sources and the central monitoring site increased, the exact location of the individual sources became less important in predicting concentrations, and emissions from multiple nearby UOGD sites were aggregated into single point sources at the centroid of each grid cell.

EMISSION ESTIMATION

Routine emissions (i.e., emissions not associated with process upsets or equipment malfunctions) were modeled for upstream and major midstream sources in the oil and gas sector. Upstream (well site) emissions for all individual wells were estimated using the methods described in Chapter 5. Midstream emissions were estimated at the facility level using throughput-scaled methane emission factors (Mitchell et al. 2015; Zimmerle et al. 2020). Methane emissions estimates for upstream and midstream facilities were used to approximate ethane emissions according to facility-specific emission composition estimates. Additional details regarding the emission estimations are available in Chapter 5 and Additional Materials C.

DISPERSION MODELING

Dispersion modeling was performed using CALPUFF version 7.2. Meteorological modeling inputs were generated using the California Meteorological model (CALMET) version 6.5 with 4 km horizontal spatial resolution and 10 vertical layers at a 1-hour time resolution. The primary meteorological data for analysis in CALMET were regional surface observations of wind and temperature at 5-minute temporal resolution from the TCEQ Karnes City monitoring location. Surface-based meteorological observations from 21 National Weather Service stations (six Automated Surface Observing System 1-minute stations, 15 Integrated Surface Database hourly stations) were incorporated. Upper-air datasets of

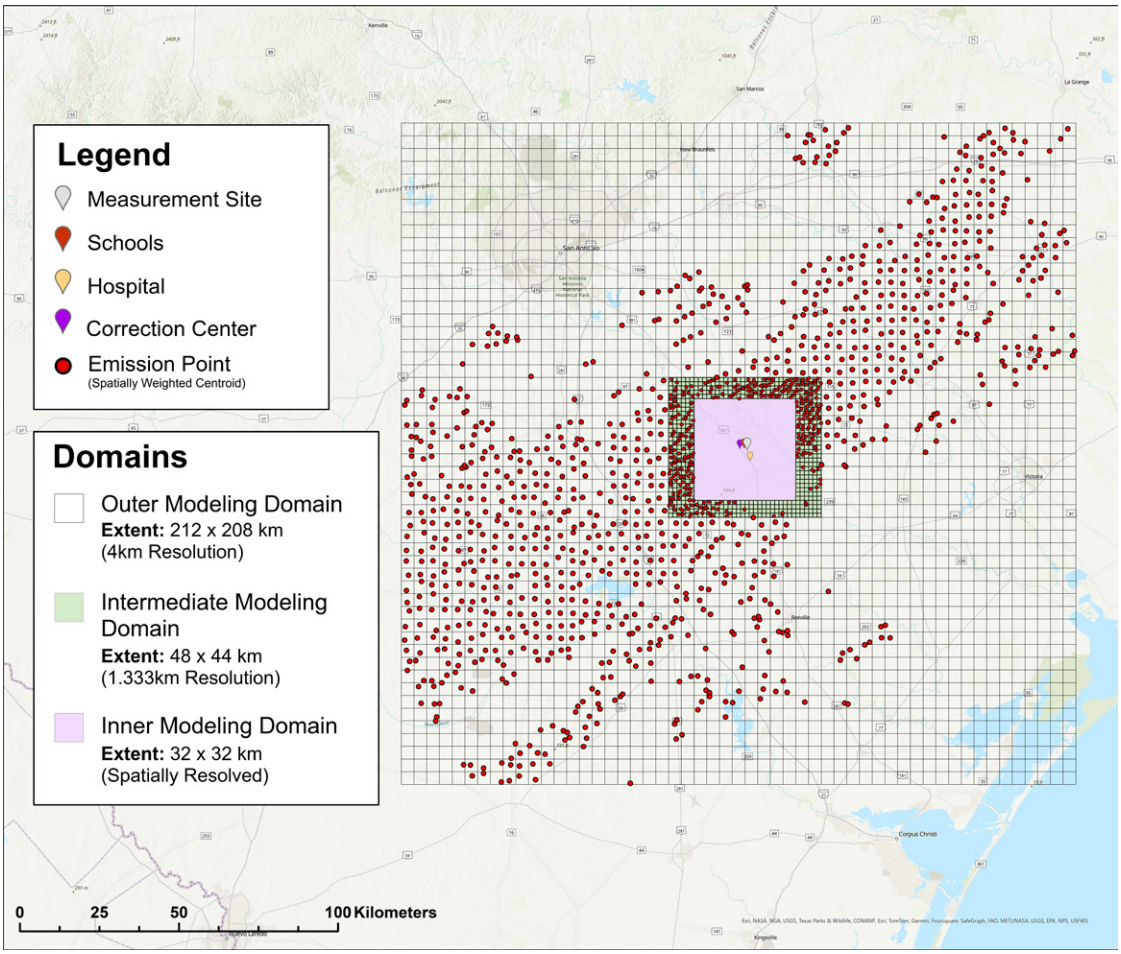

Figure 6-1. Nested modeling domain. Source: Reproduced from Graves et al. 2025; Creative Commons license CC-BY-ND 4.0.

hourly vertical profiles were extracted for eight horizontal grid cells of the high-resolution rapid refresh atmospheric model. The modeling period selected was March 5 to May 24, 2023, to correspond with the measurement campaign conducted in the Eagle Ford Shale. Additional details are available in Additional Materials D.

Some of the emissions were intermittent, with emission start times and durations unknown, and there is uncertainty in the equipment attributed to specific sites. Multiple simulations with different assumptions, including start and stop times of intermittent events and equipment assigned to specific sites, were simulated to account for these uncertainties. Ten Monte Carlo emission time series were conducted, and dispersion modeling was performed for each simulation. The results were used to generate distributions of estimated concentrations at the Karnes City measurement site associated with each source site at each hour. After all simulations were run, the mean concentration at each point in time from the 10 resulting concentration time series was used for analysis. Concentration enhancements at the receptor location were simulated with a 1-hour resolution.

Background concentrations are not included in the dispersion modeling. However, because contributors to the receptor site have been modeled up to 100 km away, the influence of background contributions from beyond that distance (where no additional oil and gas sites are present) is expected to be very small; we estimate less than 1 ppb of ethane.

HYDROCARBON CONCENTRATION DATA

Hydrocarbon concentrations used in the analyses were measured using an auto-GC located in Karnes City, operated by TCEQ in the Eagle Ford Shale oil and gas production region in south-central Texas, and surrounded by sites associated with oil and gas production. The auto-GC operates continuously with a 1-hour sampling cycle. Briefly, air collected at ~3 m above ground level is continuously drawn over a sorbent, which captures hydrocarbons, for 40 minutes. At the end of this sample collection period, the sorbent is rapidly heated, releasing the adsorbed hydrocarbons, which are then analyzed in a GC. The 20-minute analysis period allows for the quantification of ~40 different hydrocarbon species. These concentrations are reported on the TCEQ website.

DATA ANALYSIS

The analysis of predicted and observed concentrations at the Karnes City site addressed the following issues:

- Assess the extent to which ambient concentrations at receptor sites are impacted by relatively small numbers (hundreds) of UOGD sources that are within ~10 km of receptor sites and by large numbers (thousands) of UOGD sources that are tens of kilometers from receptor sites.
- Assess whether elevated concentrations observed at night are due to large, nonroutine emission events or routine emissions coupled with wind speeds and atmospheric stability conditions, which are conducive to producing elevated concentrations.
- Identify emission sources that lead to elevated ambient concentrations and the distance of these sources from the receptor site.

RESULTS

The analyses conducted in this work compare predicted and observed concentrations of hydrocarbons emitted by oil and gas operations. A variety of species could be considered in these analyses, but results for ethane are used to demonstrate the analysis methods. Ethane in this region is emitted primarily from oil and gas sources, with limited interference from other anthropogenic and biogenic sources. Ethane is also observed at relatively high concentrations compared with other hydrocarbons in the region.

Mean ethane concentrations predicted by the modeling of routine emissions are influenced by both near and distant UOGD sources. **Figure 6-2 (A)**shows a typical time series for hourly averaged ethane concentrations recorded by the TCEQ auto-GC monitoring station in Karnes City. The periods of very elevated concentrations are relatively short. As shown in **Figure 6-2 (B)**, peak concentrations, defined as the 99th percentile of observed concentrations, were almost exclusively recorded during the early morning hours.

Figure 6-3 shows the fraction of mean concentrations over all days of the simulation period that are accounted for by UOGD sources within 5, 10, 20, and 50 km of the receptor site, relative to all UOGD sources within 100 km of the receptor site. The values reported are the ratios, for each hour, of the average concentration predicted by sources within a specified distance to the average concentration predicted by all sources in the modeling domain, which extends to 100 km from the receptor site. Sources within 5 km contributed 38%, on average, to the mean concentrations predicted when all UOGD sources in the 200 km × 200 km domain were accounted for. There was a high degree of variability in this ratio, as shown in Figure 6-3, that depended on whether the nearest sources were upwind of the receptor site. Sources within 10, 20, and 50 km contributed 67%, 88%, and 99%, on average, of mean concentrations predicted when all UOGD sources in the 200 km × 200 km domain were accounted for. As the distance from the receptor increased, the variability in these ratios decreased.

Figure 6-4 shows 1 month of ethane concentrations at the Karnes City measurement location predicted by the coupled routine emissions and dispersion modeling. Observed ethane concentrations for the same time period are overlaid on the corresponding modeled values. **Figure 6-5** shows the distribution of predicted and observed ethane concentrations for the 3-month modeling period. Reproduction of the diurnal trend observed in the measurement data suggests that a majority of the largest ethane concentration enhancement episodes observed and predicted during this time period are the result of nighttime meteorological conditions coupled with routine emissions.

While many periods of elevated concentrations are accounted for by routine emissions, several are not predicted on the basis of routine emissions. **Figure 6-6** shows a 1-week period with observed concentration enhancements that are unmatched in the modeled data. These "unmatched" enhancement episodes are presumed to be driven by nonroutine emission events. To systematically identify elevated observed concentrations that were not predicted by the simulations, the 82-day modeling period was split into 72 daytime intervals (1-hour intervals starting at 9 a.m. through the interval that started at 5 p.m.; 9 hours) and 75 nighttime intervals (6 p.m.–8 a.m.; 15 hours). Periods of downtime were omitted from the analysis, resulting in 10 daytime periods and seven nighttime periods being removed. For each interval, the maximum concentration enhancement in the observed and modeled datasets was compared. If both enhancements were aligned in time and magnitude, the enhancement episode as considered matched. Alignment is defined as the observed and modeled maximum concentrations occurring within 1 hour of one another, with the ratio of their values (maximum modeled/maximum observed) being no greater than twice and no less than half.

To understand how predictions of daytime and nighttime enhancements might differ, matched and unmatched enhancement events were characterized for both daytime

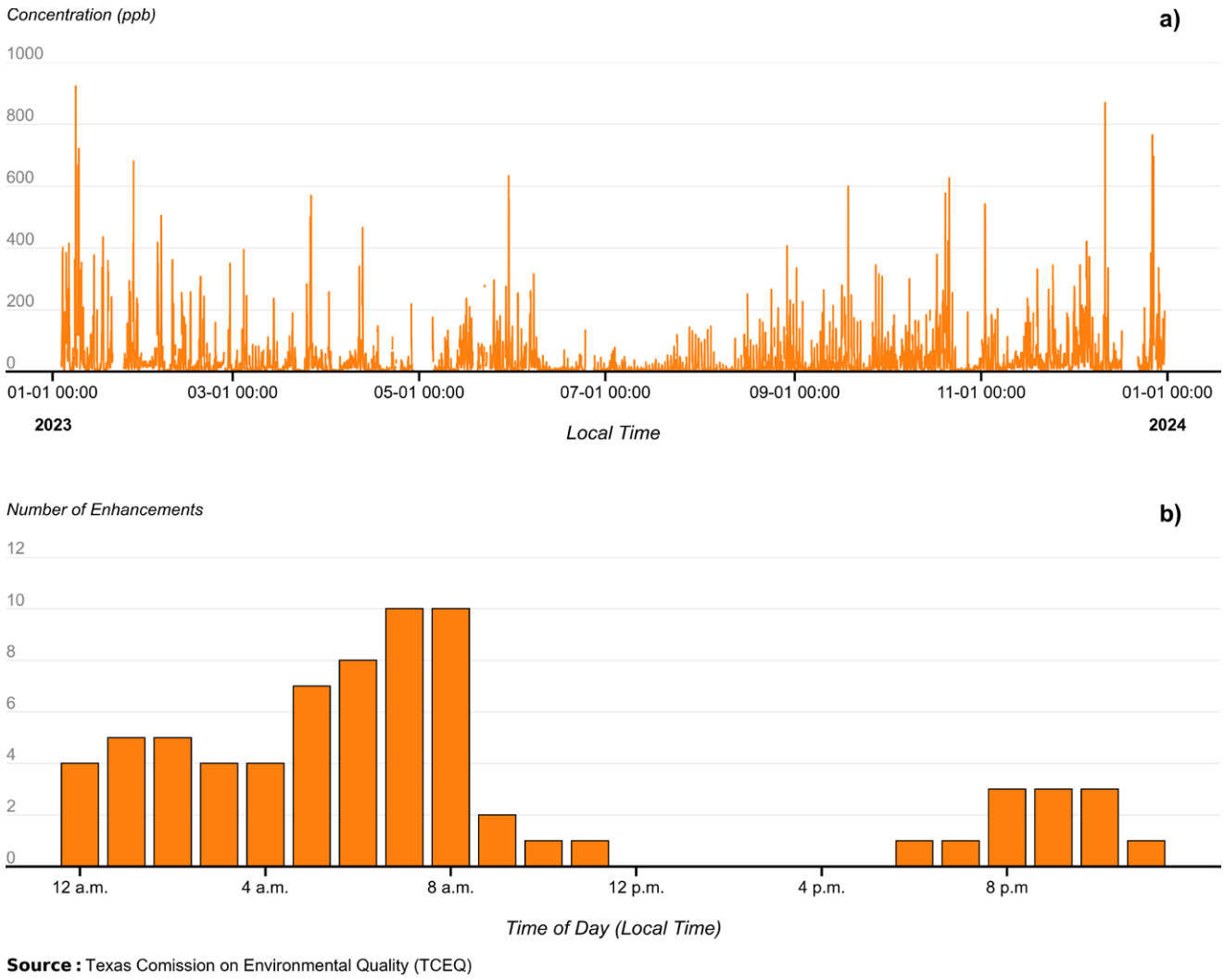

Figure 6-2. Yearlong time series for ethane at a ground site measuring hydrocarbons with hourly time resolution at the TCEQ auto-GC site in Karnes City (A); time-of-day distribution of the 99th percentile of hourly averaged concentrations (B). Source: Reproduced from Graves et al. 2025; Creative Commons license CC-BY-ND 4.0.

and nighttime periods. **Figure 6-7** classifies the number of matched and unmatched episodes, grouped by daytime and nighttime, using three different concentration enhancement thresholds to define enhancement episodes. In this approach, a 9-hour daytime or 15-hour nighttime period is considered to contain an enhancement episode if the peak observed concentration during that period exceeds a specified threshold (the 85th, 90th, or 95th percentile of all daytime or nighttime observations during the 72-day daytime or 75-day nighttime observed periods, respectively). The 85th, 90th, and 95th percentiles of observed concentrations are 22.7, 27.1, and 42.8 ppb, respectively, for daytime hours and 73.4, 90.1, and 145.3 ppb for nighttime hours. Using this approach, there were 33 daytime periods and 33 nighttime periods during which the maximum concentration enhancement was above the 85th percentile for all hours, 27 daytime periods and 25 nighttime periods above the 90th percentile, and 15 daytime periods and 17 nighttime periods above the 95th percentile. Daytime enhancement episodes at the 85th, 90th, and 95th percentile thresholds occurred slightly less frequently than nighttime enhancement episodes in the equivalent percentile. The fraction of episodes in the daytime and nighttime datasets not matched by the predictions associated with routine emissions began to diverge at higher peak concentrations. This observation suggests that many of the largest enhancements at night were driven by meteorology, while the largest events during the day were more likely driven by other phenomena. To understand what might be driving the largest daytime enhancements, an analysis of daytime periods with the highest maximum concentrations was conducted.

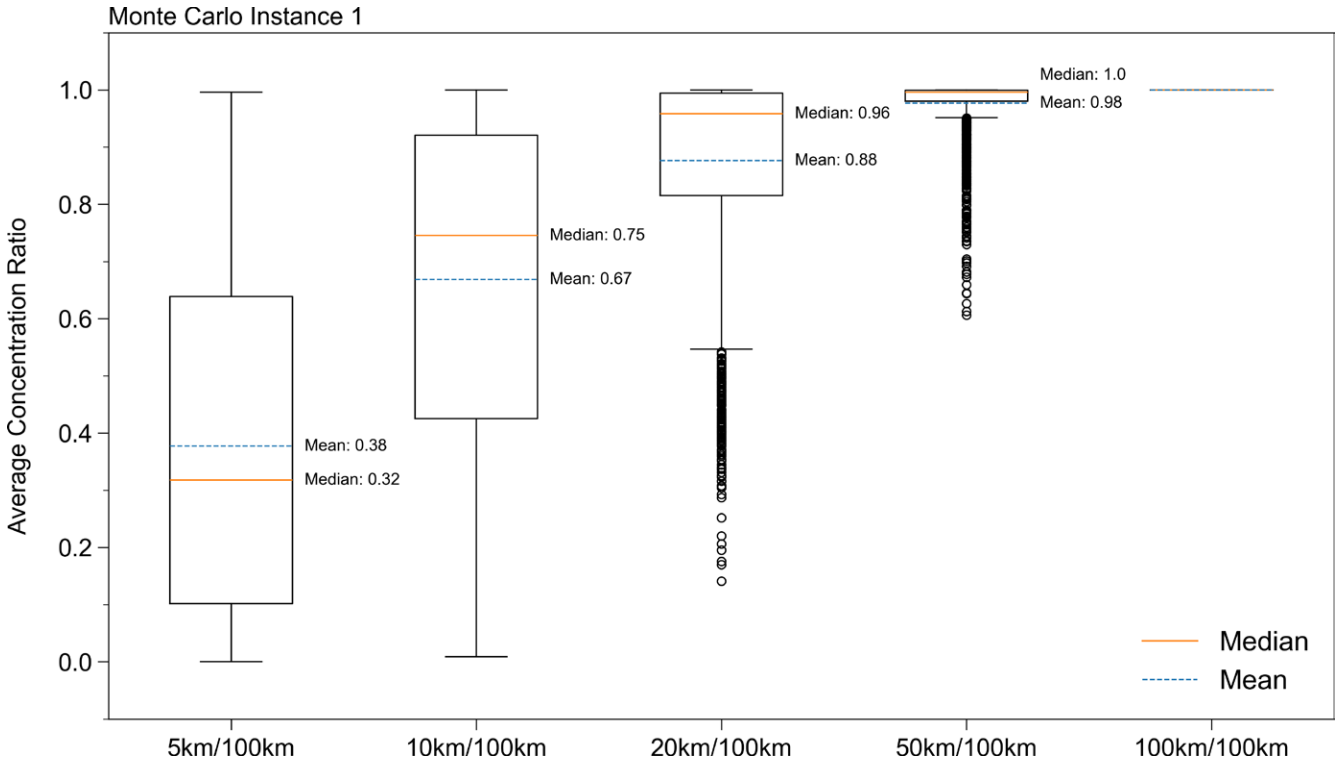

Figure 6-3. Hourly concentrations by contributions from different UOGD source distances. Each record in each of the box plots represents the concentration contribution from sources within × km from the receptor point, divided by the concentration contribution from UOGD sources within 100 km of the receptor point for each hour of the entire modeling period. Source: Reproduced from Graves et al. 2025; Creative Commons license CC-BY-ND 4.0.

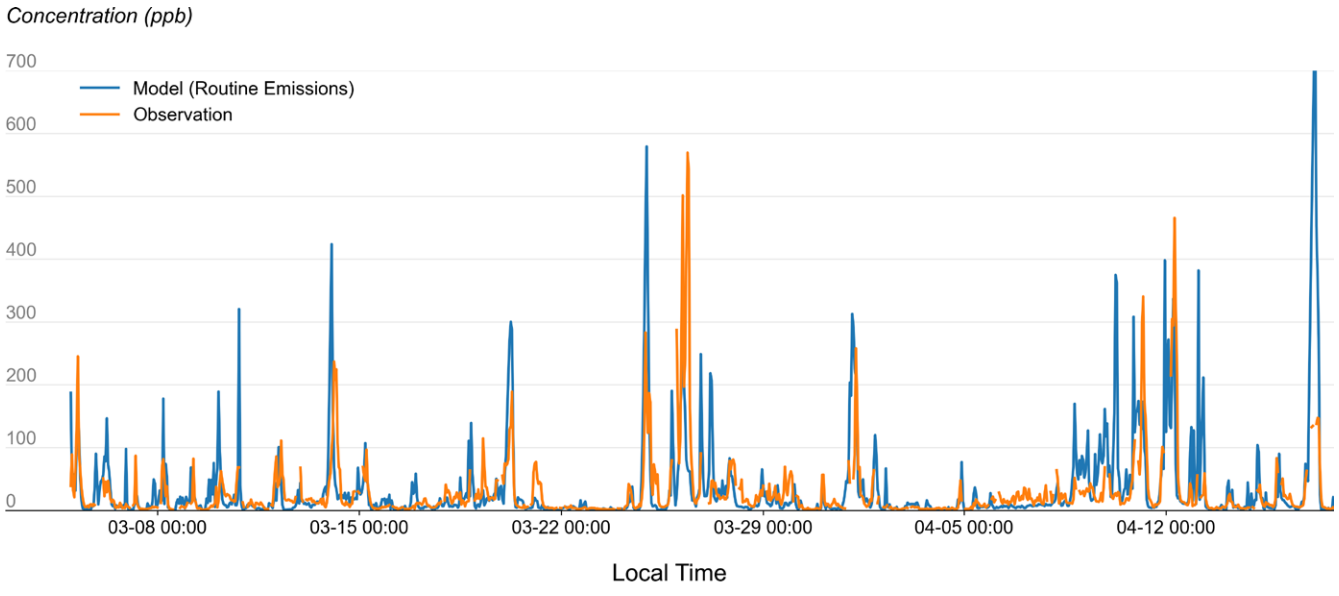

Source : Texas Comission on Environmental Quality (TCEQ)

Figure 6-4. Modeled and observed ethane time series. Source: Reproduced from Graves et al. 2025; Creative Commons license CC-BY-ND 4.0.

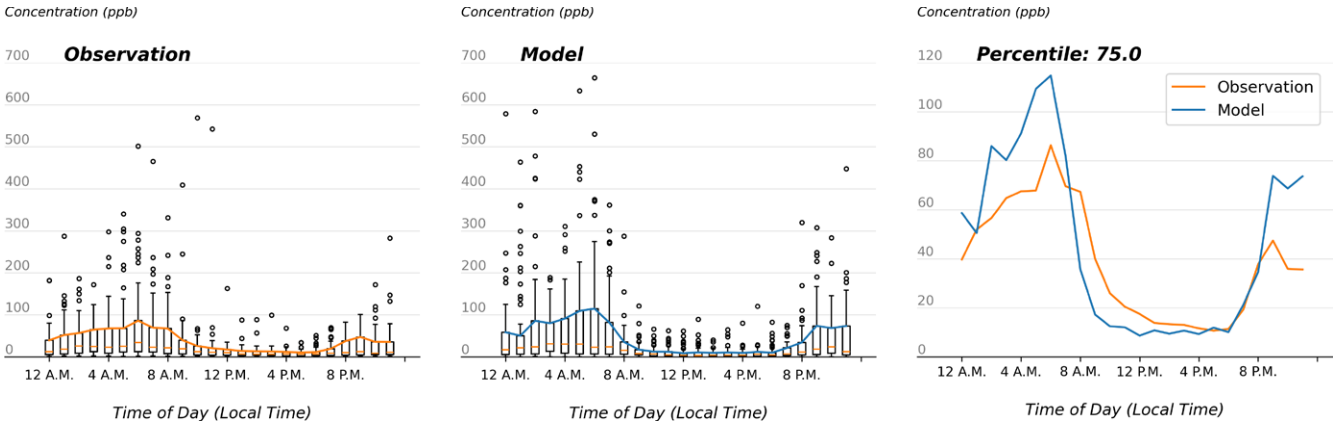

Figure 6-5. Time-of-day distributions for modeled and observed datasets. Source: Reproduced from Graves et al. 2025; Creative Commons license CC-BY-ND 4.0.

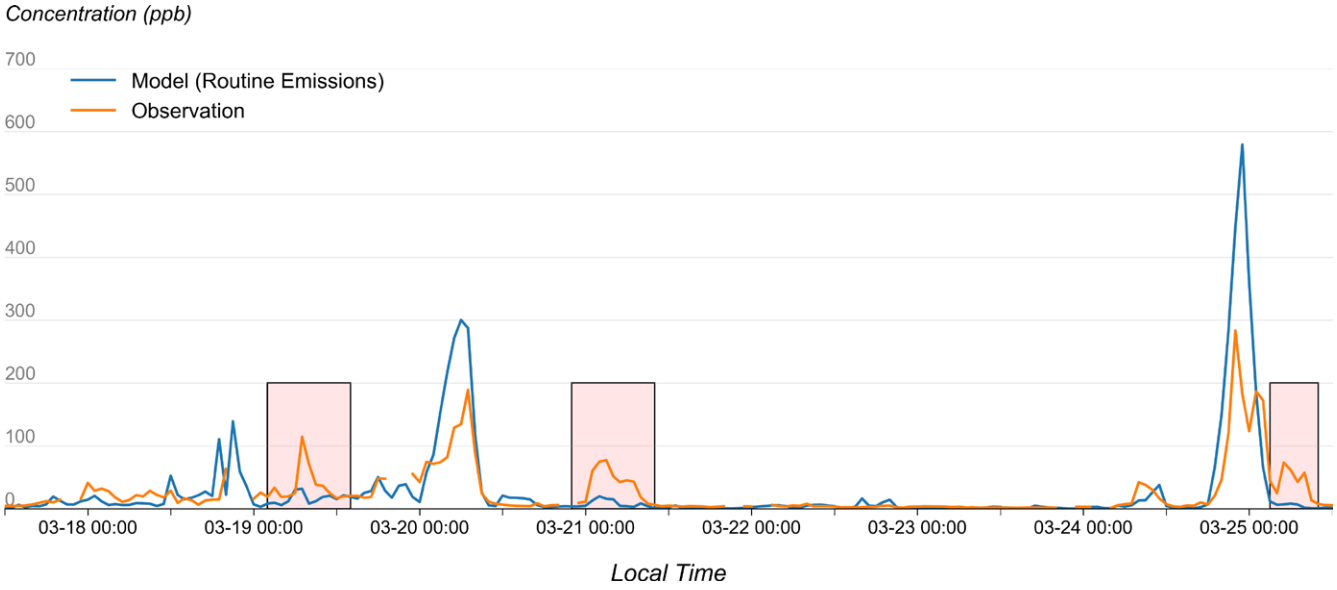

Figure 6-6. One-week modeling period with multiple unmatched observations. The orange line shows the observed data from the auto-GC, the blue line shows the model predictions using routine emissions, and the pink shaded boxes highlight "unmatched" concentration enhancements. Source: Reproduced from Graves et al. 2025; Creative Commons license CC-BY-ND 4.0.

Figure 6-8 shows the profiles of the daytime periods retained for analysis in the 95th percentile case. Many of the peaks occur at 9 a.m. during the nighttime-to-daytime transition. The coupled emissions and dispersion modeling generally predicts a much more rapid decrease in concentration after the nighttime peak, leading to many of the false negatives observed in the 95th percentile case. This projection may result from uncertainties in the dispersion model formulation (e.g., overestimation of the planetary boundary layer growth rate in the early morning), unaccounted-for sources that more frequently emit before noon, or both. Nonetheless, anomalous events can still be identified in the data (e.g., the very large enhancement at 10 a.m. in one of the clusters). Analyses were performed to identify the source locations that contributed to the highest predicted concentrations. Daytime and nighttime analyses were performed separately. **Figure 6-9** shows the UOGD source locations (within 5 km, 5 to 10 km, 10 to 20 km, and 20 to 50 km) that contributed to each of the top 20 peak predicted concentrations. When multiple top 20 events, day and night, occurred during consecutive hours, they were grouped into enhancement clusters. The analyses show that distant sources of routine emissions can contribute significantly to the highest observed concentrations.

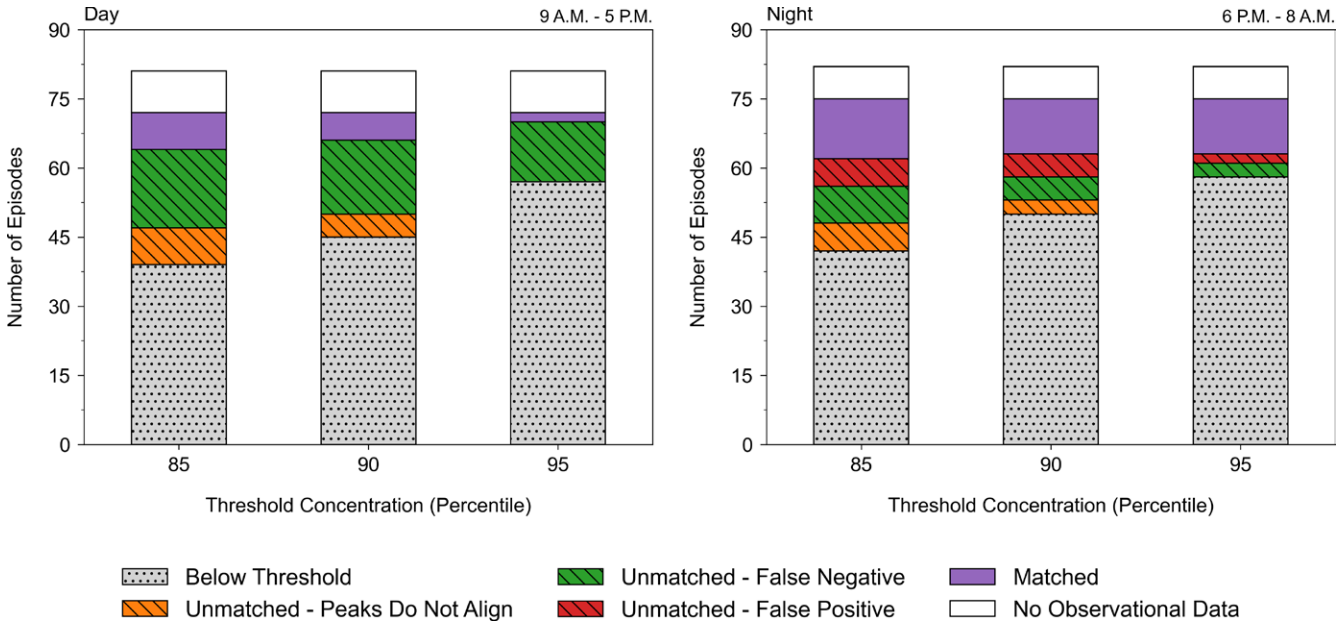

Figure 6-7. Categorizations of daily maxima daytime and nighttime ethane concentrations. Counts in gray are periods when the maximum daytime and nighttime ethane concentrations were below the 85th, 90th, and 95th percentiles of the concentrations observed over the entire study period (day: 22.7, 27.1, and 42.8 ppb; night: 73.4, 90.1, and 145.3 ppb, respectively). Counts in purple are days when the ratio of predicted-to-observed concentrations was between 0.5 and 2. Day counts in green (false negative) and red (false positive) indicate days when the ratios were <0.5 and >2.0, respectively. Day counts in orange indicate peaks that are not aligned in time.

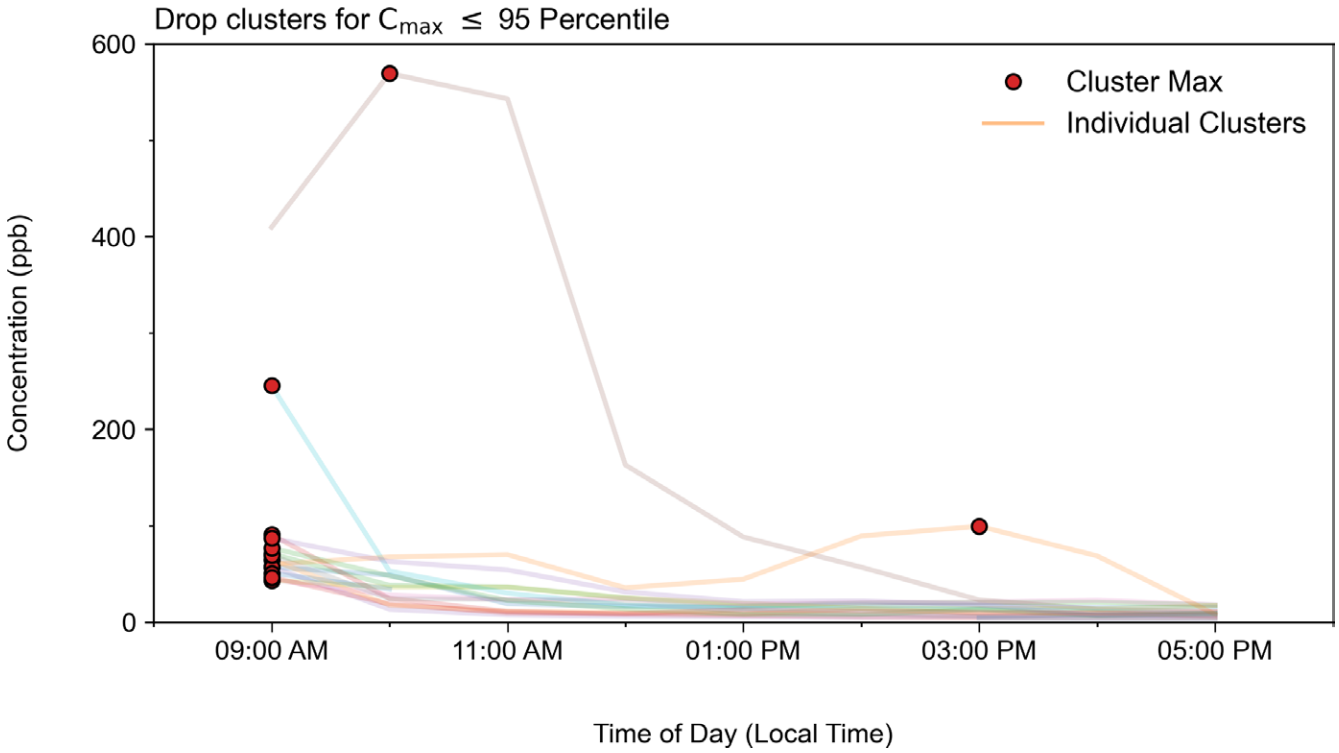

Figure 6-8. Hourly and maximum observed concentrations for daytime periods during which the maximum concentration during the period is greater than the 95th percentile of all daytime concentrations (i.e., the daytime 95th percentile threshold).

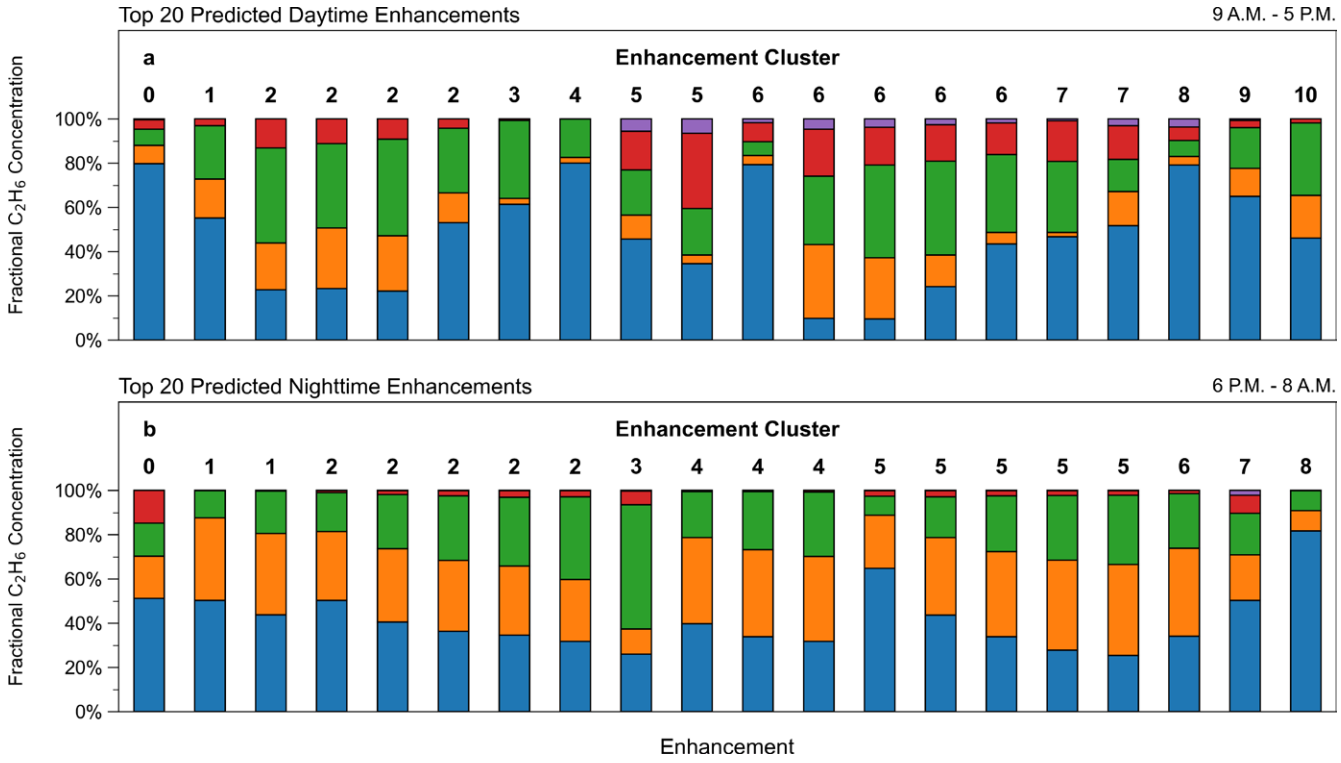

Figure 6-9. UOGD source locations (within 5 km, 5 to 10 km, 10 to 20 km, and 20 to 50 km) that contributed to each of the top 20 peak predicted concentrations at night (A) and during the day (B). When multiple top 20 events, day and night, occurred during consecutive hours, they were grouped into enhancement clusters. Source: Reproduced from Graves et al. 2025; Creative Commons license CC-BY-ND 4.0.

DISCUSSION AND CONCLUSIONS

Overall, the analyses discussed in this chapter show that ambient concentrations at receptor sites are affected by both relatively small numbers (hundreds) of UOGD sources that are within ~10 km of receptor sites and by large numbers (thousands) of UOGD sources that are tens of kilometers from receptor sites. Because ambient concentrations at receptor sites, and therefore exposure at those sites, are influenced by UOGD sources that are tens of kilometers away, setback distances between UOGD sites and specific land uses are not a universal solution to reducing exposure. Elevated concentrations observed at night can be due to both large nonroutine emission events and routine emissions, coupled with wind speeds and atmospheric stability conditions that are conducive to producing elevated concentrations. Identifying emission sources that lead to elevated ambient concentrations requires coupled emission and dispersion modeling applied over modeling domains that extend over tens of kilometers and account for complex meteorology. Overall, these analyses show that emissions modeling, when integrated with dispersion modeling, can be a powerful tool for characterizing exposures, although it remains both data- and computationally intensive.

REFERENCES

Graves J, Kimura Y, Modi M, Stokes S, Meyer M, Hildebrandt Ruiz L, et al. 2025. Source attribution of elevated ethane concentrations detected by regional monitors in oil and gas production regions. ACS ES&T Air 2:2038–2046; *https://doi. org/10.1021/acsestair.5c00235*

Mitchell AL, Tkacik DS, Roscioli JR, Herndon SC, Yacovitch TI, Martinez DM, et al. 2015. Measurements of methane emissions from natural gas gathering facilities and processing plants: measurement results. Environ Sci Technol 49:3219–3227; *https://doi.org/10.1021/es5052809*.

Zimmerle D, Vaughn T, Luck B, Lauderdale T, Keen K, Harrison M, et al. 2020. Methane emissions from gathering compressor stations in the US. Environ Sci Technol 54:7552–7561; *https://doi.org/10.1021/acs.est.0c00516*.

CHAPTER 7: COUPLING EMISSIONS INVENTORIES WITH CHEMICAL TRANSPORT MODELS*

INTRODUCTION

The availability of emissions inventories with advanced features, such as detailed spatial and temporal allocations, can improve predictions of the formation and accumulation of photochemical air pollutants such as ozone. To demonstrate the potential importance of detailed emissions inventories in air quality management for photochemical air pollutants, the effect of detailed spatial and temporal allocation of UOGD nitrogen oxides emissions on predicted ozone formation was examined using hydraulic fracturing emissions in the Eagle Ford Shale region of Texas as a case study. We couple the emissions model with chemical transport modeling to evaluate the impacts of nitrogen oxides emissions from UOGD on regional concentrations of ozone. The emissions model for the Marcellus Shale is described in Chapter 5; the emissions model for the Eagle Ford Shale used here is described in Additional Materials E, which is a published manuscript describing results from this work (Modi et al. 2025). In most photochemical modeling, emissions from hydraulic fracturing are allocated at the county level and distributed uniformly as an area source across all grid cells in a county. The emissions are typically allocated to all hours during a year. The actual emissions only occur at well sites that are fractured and during a period of a few days to a few weeks at each well. More accurate spatiotemporal allocation of hydraulic emissions can cause increases of up to three orders of magnitude in instantaneous emission rates at specific sites compared with countywide distributions that are annual averages. The impacts of these spatial and temporal allocations of emissions on predicted ozone levels in San Antonio, the seventh largest city in the country and an ozone nonattainment area, were assessed using the CAMx.

STUDY DESIGN AND METHODS

The base case emissions used in this work are derived from the 2019 Base Case Emission Inventory, V1, developed by the TCEQ. The 2019 base case is a part of the modeling platform developed by TCEQ to support revisions in the state implementation plan for ozone for Bexar County, Dallas-Fort Worth, and Houston-Brazoria Galveston (TCEQ 2023). In this work, nitrogen oxides (nitric oxide and nitrogen dioxide) emissions from oil and gas sources for the 27 Eagle Ford Shale counties were removed from the 2019 base case and substituted with spatially and temporally resolved nitrogen oxides emissions. Four scenarios (Cases 1–4) for spatial and temporal allocation of hydraulic fracturing nitrogen oxides emissions were developed. In one scenario (Case 1), nitrogen oxides emissions were evenly distributed to all active wells in the Eagle Ford region, assuming continuous emissions throughout the year. In other scenarios (Cases 2–4), nitrogen oxides emissions from hydraulic fracturing engines in Karnes County were allocated only to fractured wells, with durations ranging from 2 days to 2 weeks. The CAMx (version 7.10) was utilized to simulate ozone impacts from the emission scenarios. The CAMx modeling grid and the meteorological episode used in this work have been used by the TCEQ to evaluate ozone state implementation plans. Methods are described in more detail in Additional Materials E, which is a published manuscript (Modi et al. 2025).

DATA ANALYSIS

This work evaluates the impacts of accurate accounting for the spatial and temporal allocation of oil and gas emissions on predicted ozone formation and accumulation.

RESULTS

Case 1 distributed the TCEQ total nitrogen oxides emissions evenly in each of the Eagle Ford Shale counties, such that, within a county, each well emitted the same amount of nitrogen oxides emissions, with constant emissions throughout the year. Cases 2–4 performed adjustments in Karnes County and distributed nitrogen oxides emissions from hydraulic fracturing in Karnes County only to fractured wells in the county. All other nitrogen oxides emissions within Karnes County, as well as the TCEQ total nitrogen oxides emissions in all other counties, were kept the same as Case 1.

In Case 1, for which nitrogen oxides emissions from hydraulic fracturing in Karnes County were distributed evenly among all 4,185 oil and gas wells in Karnes County, the hydraulic fracturing emissions per well were 0.47 tons for the year. These emissions per well were further reduced to 0.001 tons/day when allocated evenly throughout the year (**Table 7-1**). For Cases 2–4, nitrogen oxides emissions from hydraulic fracturing were spatially allocated only to 436 fractured wells, significantly increasing the emissions per well to 4.44 tons. The temporal allocation in Cases 2–4 reduced the emission duration and made nitrogen oxides emissions from a fractured well more concentrated. As a result, nitrogen oxides emission rate from hydraulic fracturing (in tons/day) for a well in Case 1 was approximately 300 times lower than Case 2, 600 times lower than Case 3, and 2,200 times lower than Case 4, for which emissions were localized and episodic, allocated only to fractured wells for a period of 2 days–2 weeks.

At any given time, only a small percentage of the total wells have fracturing emissions, which last from 2 days to 2 weeks. As a result, the spatial and temporal distribution

*Chapter 7 is a summary of Additional Materials E, Modi et al. 2025, Creative Commons license CC-BY-NC-ND 4.0.

Table 7-1. Allocation and Estimation of TCEQ Total Nitrogen Oxides Emissions from Hydraulic Fracturing in Karnes County per Well (in Tons per Day) for Cases 1–4

Cases	Nature of Nitrogen Oxides Emissions from Hydraulic Fracturing	Nitrogen Oxides Emissions from Hydraulic Fracturing Allocated in Karnes County[a,b] (Tons/Year)	No. of Wells with Allocated Emissions[a,b]	Nitrogen Oxides Emissions per Well (Tons/Event)	Emission Duration (Days)	Emissions per Well (Tons/Day)
Case 1	Continuous and annual	1,958[a]	4,185[a]	0.47	365	0.001
Case 2	Continuous for 2 weeks	1,936[b]	436[b]	4.44	14	0.3
Case 3	Continuous for 1 week	1,948[b]		4.47	7	0.6
Case 4	Continuous for 2 days	1,958[b]		4.49	2	2.20

[a]For Case 1, total nitrogen oxides emissions were allocated to all active wells within the 27 Eagle Ford Shale counties. Within Case 1, nitrogen oxides emissions from hydraulic fracturing were allocated to all wells in Karnes County.

[b]For Cases 2–4, nitrogen oxides emissions from hydraulic fracturing were allocated only to wells fractured in Karnes County in the year 2019, while keeping all other nitrogen oxides emissions in all counties the same as Case 1. There are slight differences in total nitrogen oxides emissions between Cases 1 and 4. These differences arise because the completion dates of some of the fractured wells were close to the year start date (January 1, 2019). Consequently, their fracturing emission events did not fall entirely within 2019, leading to slightly differing total emissions, depending on the assumed duration of the fracturing.

of nitrogen oxides emissions from hydraulic fracturing can vary significantly, with emission rates for specific wells at specific times differing by up to three orders of magnitude. This variability may require a detailed spatial and temporal allocation of fracturing emissions to accurately predict the spatial distribution and magnitude of ozone formation.

To assess the impacts of spatially and temporally allocated nitrogen oxides emissions on regional ozone, the daily maximum of 8-hour average ozone concentrations (MDA8 ozone) were calculated for each grid cell within the domain on every episode day for Cases 1–4. Using Case 1 as the baseline scenario, the differences in MDA8 ozone were computed for three spatially paired scenarios: Case 2–Case 1, Case 3–Case 1, and Case 4–Case 1. This computation was done for each grid cell and each episode day. The maximum and minimum differences in MDA8 ozone concentrations were then identified across the domain for each of the three paired scenarios for each episode day, resulting in two values per day. These values were used to identify "high-impact periods" — the days or months when the most significant positive and negative impacts on MDA8 ozone concentrations occurred relative to Case 1, driven by differences in nitrogen oxides allocation.

As the emission duration decreased from Cases 1 to 4 (Table 7-1), significant changes were estimated in the domain-wide MDA8 ozone concentrations throughout the entire episode. One of the high-impact periods was the month of August (**Figure 7-1**), during which the domain-wide maximum MDA8 ozone concentrations were consistently 6, 8, and 10 ppb higher than the annual distribution (Case 1) for the 2-week, 1-week, and 2-day emission periods, respectively. Similar results were also reported during most of July and September. Moreover, there were at least 2 days in every month from June to August when MDA8 ozone concentrations were 9, 12, and 16 ppb higher than the annual distribution for the 2-week, 1-week, and 2-day emission periods, respectively.

When hydraulic fracturing emissions were concentrated in time and space (Cases 2–4), regions with high nitrogen oxides emissions experienced prompt reactions between nitric oxide and ozone, forming nitrogen dioxide and thus reducing local ozone concentrations. This observation explains the decreasing MDA8 ozone concentrations and increasing negative differences in MDA8 ozone concentrations from Case 4 to Case 2 (Figure 7-1). With regional transport, nitrogen dioxide can travel downwind and further react in the atmosphere, contributing to more ozone formation away from the emission sources. This process leads to higher ozone concentrations in downwind areas, explaining why higher MDA8 ozone concentrations were estimated in Cases 2–4 compared with Case 1. Results are described in more detail in Additional Materials E.

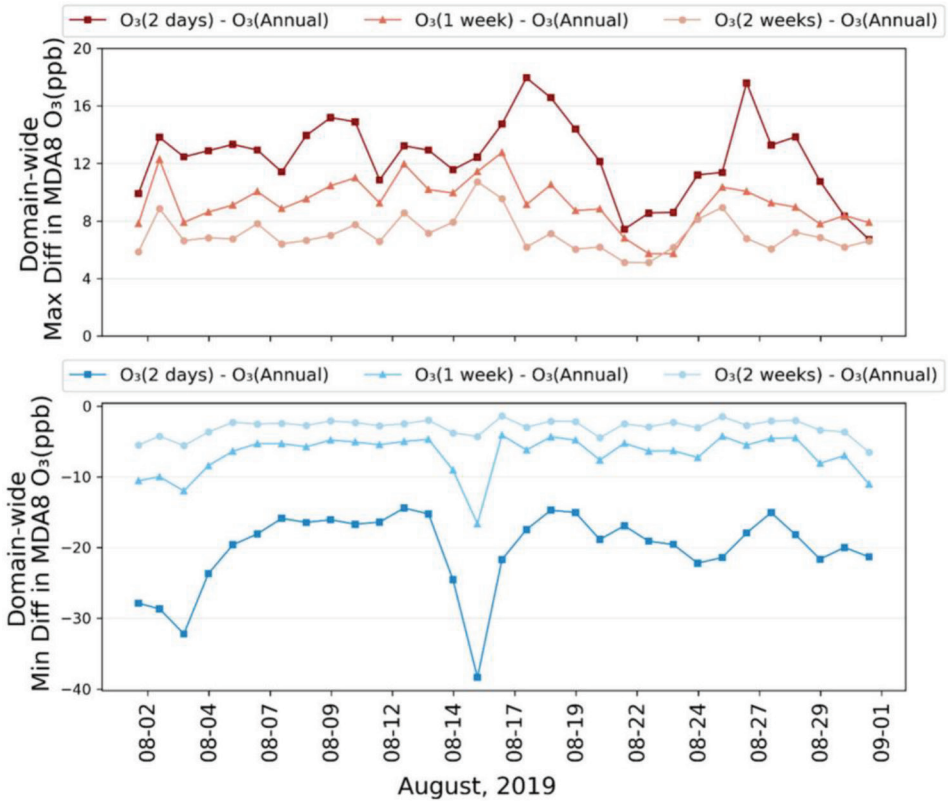

Figure 7-1. Maximum and minimum differences in domain-wide MDA8 ozone (O_3) between the 2-day to 2-week emission periods (Cases 2 to 4) and the annual distribution (Case 1) for August 2019.

DISCUSSION AND CONCLUSIONS

In October 2022, the US EPA reclassified San Antonio, Bexar County, from a "marginal" to a "moderate" level of nonattainment for the Ozone NAAQS. The results presented in this work demonstrate that different allocation methods of nitrogen oxides emissions from hydraulic fracturing, ranging from annual distribution to more episodic and local distribution, result in nitrogen oxides emission rates from hydraulic fracturing at individual sites that vary by two to three orders of magnitude. UOGD activities like hydraulic fracturing contribute ~10% of total nitrogen oxides emissions in the Eagle Ford Shale, but occur only at selected well sites and last for only 1–2 weeks before production. Accurate spatial and temporal allocation of nitrogen oxides emissions can lead to increased localized ozone formation in a nitrogen oxides-limited region like the Eagle Ford Shale. These results highlight the need for allocating nitrogen oxides emissions from UOGD according to the nature and contribution of the source, especially in nitrogen oxides-limited oil and gas production regions. If the assessment of hydraulic fracturing activities in similar regions does not account for the nature of emissions (i.e., spatial allocation and duration), then it might become difficult to identify mitigation strategies to reduce ozone concentrations below NAAQS and maintain attainment. Similar results might be expected for drilling activity.

REFERENCES

Modi M, Kimura Y, Hildebrandt Ruiz L, Allen D. 2025. Fine-scale spatial and temporal allocation of nitrogen oxides emissions from unconventional oil and gas development can result in increased predicted regional ozone formation. ACS ES&T Air 2:130–140; *https://doi.org/10.1021/acsestair.4c00077*.

Texas Commission on Environmental Quality (TCEQ). Texas Air Quality Modeling (2019 Platform). Available: *https://www.tceq.texas.gov/airquality/airmod/data/tx2019*.

CHAPTER 8: ASSESSING THE PERFORMANCE OF DISPERSION MODELS

INTRODUCTION

The TRACER tools developed in this work apply dispersion models to estimate local concentrations of pollutants. Multiple dispersion models, employing different calculation approaches and different assumptions, are available for use. The performance of dispersion models in predicting ambient concentrations at the fixed ground monitor, as described in Chapter 6, was evaluated. The work described in this chapter has been submitted to Environmental Au for review and is available as a preprint at ChemRxiv (10.26434/chemrxiv-2025-xkhh9) (Graves et al. 2026).

STUDY DESIGN AND METHODS

The performance of the following four dispersion model formulations in predicting the structure of plumes from oil and gas facilities was assessed:

1. The AERMOD suite of tools maintained by the EPA
2. The CALPUFF dispersion model using similarity theory to predict dispersion parameters
3. The CALPUFF dispersion model using stability classification to predict dispersion parameters
4. A single-equation formulation of a Gaussian plume with time-invariant parameters and dispersion parameters estimated based on stability classifications

These four dispersion model formulations can lead to distinctly different plume structures. To evaluate the performance of the models, a series of analyses comparing spatial and temporal concentration distributions predicted by AERMOD, CALPUFF, and a single-equation Gaussian model was conducted in the Eagle Ford oil and gas production region described in Chapter 6. Time-varying estimates of routine hydrocarbon emission from 10,000+ sources in the Eagle Ford Shale were input to the dispersion models, and concentrations were predicted at a centralized measurement location, at which ground-level hydrocarbon measurements are also available.

CALPUFF

The modeling configuration was identical to the simulations from Chapter 6. Briefly, dispersion modeling was performed using CALPUFF version 7.2. Hourly gridded meteorological inputs with 10 vertical layers and a spatial resolution of 4 km were generated using CALMET version 6.5. Observations from National Weather Service stations (Integrated Surface Database; Automated Surface Observing Systems) and on-site measurements from a CAMS operated by TCEQ were incorporated as surface-based meteorological inputs to CALMET. Prognostic upper-air inputs were incorporated from hourly vertical profiles extracted from individual grid cells of the high-resolution rapid refresh model. Observational soundings were omitted because the nearest rawinsonde observations were more than 150 km from the modeling site. Land use and 1-degree terrain data were obtained from the United States Geological Survey National Land Cover Database and United States Geological Survey National Elevation Dataset, respectively. Using stability classification to predict dispersion parameters, CALPUFF simulations were performed at a 1-hour temporal resolution for the 3-month modeling period (March 5, 2023–May 24, 2023).

AERMOD

Dispersion modeling was performed using AERMOD version 22112. Meteorological inputs for AERMOD were prepared using AERMET version 22112. The AERMOD modeling suite prepares profiles of wind, temperature, and turbulence that are assumed to be constant over the entire modeling domain. It requires only a single source of surface and upper-air meteorological measurements as observational inputs, but can accommodate multiple data sources to supplement missing or imprecise (e.g., calm wind conditions) entries in the surface measurements. In practice, if multiple surface data sources, including on-site data, are incorporated, a single surface site is usually identified as the "primary" site, and a selection of supplemental "secondary" sites can be provided. There is currently no method for automatically substituting missing values in the upper-air data. AERMET can also incorporate prognostic inputs prepared with the Mesoscale Model Interface Program as a substitute for either surface or upper-air measurements. Hourly measurements of wind speed, direction, and temperature from the TCEQ CAMS site were used as the primary surface dataset. Hourly measurements from the nearest integrated surface database station were included as a secondary data source to supplement missing and calm hours in the on-site measurements. Observational soundings were incorporated as upper-air inputs from the rawinsonde station in Corpus Christi, Texas. Land use and 1-degree terrain data were obtained from the United States Geological Survey National Land Cover Database and the United States Geological Survey National Elevation Dataset, respectively. Dispersion modeling was simulated at a 1-hour temporal resolution for the 3-month modeling period (March 5, 2023–May 24, 2023).

SINGLE-EQUATION GAUSSIAN

Dispersion modeling was performed using a single-equation Gaussian implementation that accounts for plume reflections (**Equation 8-1**).

$$C = \frac{Q}{2\pi u \sigma_y \sigma_z} \exp\left(-\frac{1}{2}\frac{y^2}{\sigma_y^2}\right) \left[\exp\left(-\frac{1}{2}\frac{(z-h)^2}{\sigma_z^2}\right) + \exp\left(-\frac{1}{2}\frac{(z+h)^2}{\sigma_z^2}\right) \right] \quad \textbf{(8-1)}$$

Meteorological inputs for the single-equation Gaussian model were identical to those used in the CALPUFF simulations. Gridded inputs cannot be used in the single-equation Gaussian formulation, so surface meteorological variables for the CALPUFF grid cell closest to the emission point were used as inputs for all timesteps. The dispersion parameters $(\sigma_y \cdot \sigma_z)$ were estimated using the industrial source complex parameterizations for rural terrain that were based on Pasquill-Gifford stability classes. Dispersion modeling was simulated at a 1-hour temporal resolution for the 3-month modeling period (March 5, 2023 – May 24, 2023).

The modeling domain for the simulations is shown in **Figure 8-1.** The domain is broadly representative of the unconventional oil and gas production regions in the United States, and the central receptor site is typical of potential exposure locations. Additional details of the modeling domain and the emissions used in the simulations are provided in Chapter 6.

DATA ANALYSIS

Analyses were performed to assess the performance of the different air pollution dispersion models used in the TRACER model in simulating plume structures and observed concentrations. Qualitative and statistical performance metrics based on literature approaches (Chang and Hanna 2004) and regulatory frameworks (US EPA 1992) were evaluated. Model performance may vary in different applications and across different demands, so multiple model uses were considered. For example, 8-hour averaged ambient concentrations of primary pollutants used for NAAQS attainment assessments may be relatively insensitive to the matching of spatial and temporal patterns of model predictions at 1-hour resolution. In contrast, hourly estimates of acute exposure to air toxics may have much more rigorous demands on spatial and temporal precision in model predictions.

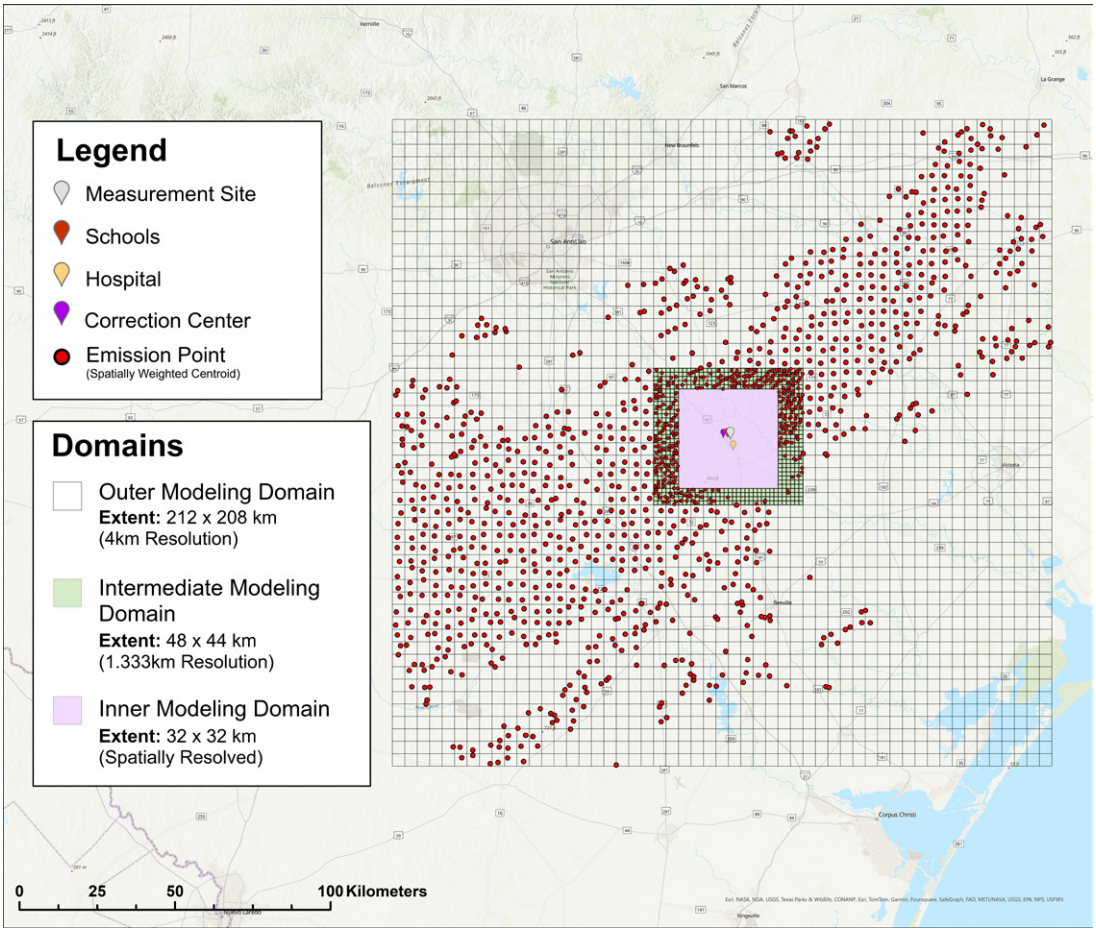

Figure 8-1. Nested modeling domain used in assessing the performance of dispersion models.
Source: From Graves et al. 2026; Creative Commons license CC-BY-ND 4.0.

Hourly resolution predictions of ambient ethane concentrations from each model were evaluated. In the first step, exploratory data analysis is conducted to investigate qualitative performance indicators (e.g., consistent model underprediction of high observed concentrations). Exploratory analysis included absolute and rank-ordered parity plots between predicted and observed concentrations and quantile-quantile plots. These analyses can provide insight into the relationship between the observed concentrations and the model predictions over a range of conditions that complements the information from individual statistical measures.

The second step involves first evaluating each model using a screening test to determine whether it meets the minimum standards for operational performance outlined in the US EPA's Protocol for Determining the Best Performing Model. The test is based on measures of fractional bias (**Equation 8-2**) for the mean and standard deviation of the 25 highest observed and predicted values.

$$FB_i = 2 \cdot \frac{OB_i - PR_i}{OB_i + PR_i} \qquad \textbf{(8-2)}$$

OB_i = Mean or standard deviation of the top 25 observed enhancements

PR_i = Mean or standard deviation of the top 25 predicted enhancements

FB_i = Fractional bias of distribution statistic i (standard deviation or mean)

The fractional bias is a measure of whether a model tends to over- or underestimate observations on average. It is symmetrical around 0 and bounded by the range [−2, 2]. Evaluating the fractional bias for the mean and standard deviation of the top 25 modeled and observed enhancements is a means of estimating how well the model reproduces the highest observed enhancements with reasonable confidence. The screening analysis considers a model to have met the minimum standards for operational performance if the absolute value of both metrics is less than 0.67 (i.e., over- or underprediction by a factor of 2). However, the computed values are typically plotted against one another, and a bounding box with dimensions x = ±0.67 and y = ±0.67 is overlaid on the figure to visually identify which models are within the threshold (**Figure 8-2**). Plotting the data this way allows for the directionality of each metric to be evaluated. Positive values of fractional bias correspond to model underpredictions, whereas negative values correspond to model overpredictions.

The screening test has been included as a reference metric for comparing model performance using commonly applied regulatory benchmarks. In the EPA protocol, more comprehensive statistical analyses are applied to models that meet the minimum standard for operational performance. However, these analyses are intended to evaluate model performance in the context of regulatory applications with emphasis on analyses of the highest predicted concentrations at networks

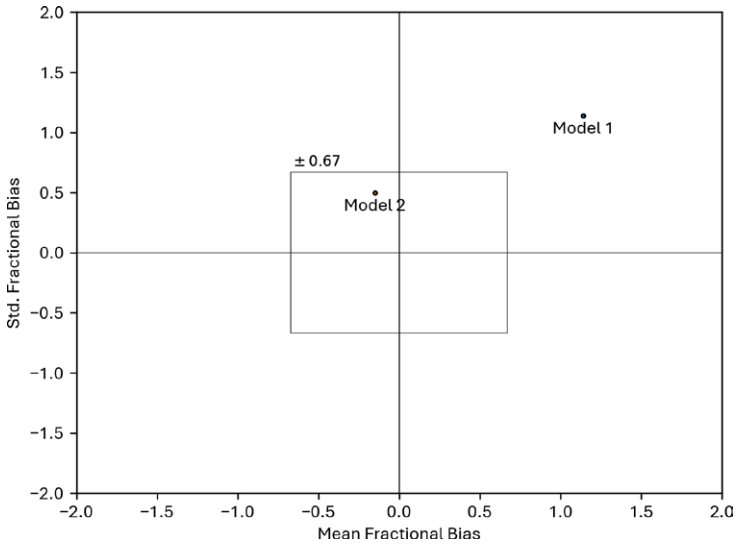

Figure 8-2. Plotting convention for evaluating the fractional bias of the mean and standard deviation of the top 25 predicted enhancements as outlined in the US EPA Protocol for Determining the Best Performing Model. Example data are used for illustrative purposes. Fractional biases for each model are paired and plotted as scatter points. Models with biases falling within the ± 0.67 bounding box are considered to have met the minimum standard for operational performance. Source: From Graves et al. 2026; Creative Commons license CC-BY-ND 4.0.

of measurement sites. In this work, metrics are designed more to evaluate performance in estimating exposure and in identifying emission events. Thus, for the models that pass the screening test, several bivariate analyses are applied as additional performance metrics instead.

Pearson correlation coefficient (**Equation 8-3**) and Spearman's rank correlation (**Equation 8-4**) were derived for each model using observed and modeled concentrations as the analysis variables.

$$r = \frac{\Sigma(x_i - \overline{x})(y_i - \overline{y})}{\sqrt{\Sigma(x_i - \overline{x})^2 (y_i - \overline{y})^2}} \qquad \textit{(8-3)}$$

r = correlation coefficient
x_i = values of the x-variable in the sample
$\overline{x}$ = mean of the values of the x-variable
y_i = values of the y-variable in the sample
$\overline{y}$ = mean of the values of the y-variable

$$\rho = \frac{\Sigma(x_{i,r} - \overline{x}_r)(y_{i,r} - \overline{y}_r)}{\sqrt{\Sigma(x_{i,r} - \overline{x}_r)^2 (y_{i_r} - \overline{y}_r)^2}} \qquad \textit{(8-4)}$$

ρ = Spearman's rank correlation coefficient
$x_{i,r}$ = ranked values of the x-variable in the sample
$\overline{x}_r$ = mean of the ranked values of the x-variable
$y_{i,r}$ = ranked values of the y-variable in the sample
$\overline{y}_r$ = mean of the ranked values of the y-variable

In each case, records from the observed and modeled time series are paired in time, and the strength of their covariance is evaluated. With the Pearson correlation, the observed and modeled concentration values are compared directly. With the Spearman rank correlation, each reported concentration in the observed and modeled time series is first ranked relative to the other records in that time series (e.g., observed records are only compared with other observed records), and, while maintaining the original time pairing, the covariance of these ranks is compared. The Spearman rank correlation evaluates monotonic relationships between two variables, which need not be linear. It is also less sensitive to the influence of a handful of extreme values because the rank ordering removes large variations in the data. Here, the Pearson correlation is used as a measure of how well each model reproduces the absolute concentrations measured at the ground-truth receptor at each point in time, and to evaluate conditions where the model may be more or less representative of the observations (e.g., day or night). The Spearman rank correlation is used here as a measure of how well the models predict the ranking of the enhancements (e.g., are the highest predicted concentrations associated with the highest observed concentrations), regardless of the magnitude of the enhancement. This gives an indication of whether the model is reproducing more general trends in the data, regardless of its tendency to over- or underestimate these enhancements. Bivariate analysis was conducted for the entire time series, as well as daytime and nighttime periods individually, to evaluate whether diurnal effects may strongly influence the association between model predictions and observations.

Fractional bias (**Equation 8-5)** is computed for the average of the entire observed and modeled datasets, providing a more comprehensive estimate of model bias over the range of estimated values when compared with the screening analysis. A geometric mean bias (**Equation 8-6**) is also calculated using the entire dataset. The geometric mean is like the arithmetic mean, but it uses logarithmic versions of the differences between observed and modeled concentrations and is useful for datasets that span several orders of magnitude, especially when ratios of predicted and observed concentrations display a large range (e.g., $1 \cdot 10^{-2} - 1 \cdot 10^{2}$) of values.

$$FB = \frac{(\overline{C_o} - \overline{C_p})}{0.5(\overline{C_o} + \overline{C_p})} \qquad \textit{(8-5)}$$

$$MG = \exp(\overline{\ln C_o} - \overline{\ln C_p}) \qquad \textit{(8-6)}$$

FB = fractional bias
MG = geometric mean bias

Normalized mean square error (**Equation 8-7**) and normalized absolute error (**Equation 8-8**) are calculated as error metrics. Both measures provide information about the spread of the residuals between predicted and observed concentrations, and they are commonly used metrics for evaluating model performance. The squared error indicates how closely a model predicts an individual observation. The mean of the squared error for every pair of predictions and observations in a test dataset indicates how well, on average, the model predicts the range of test data. The absolute error is a similar metric but is less sensitive to outliers. Both metrics are normalized by representations of the means of the observed and modeled values to facilitate more straightforward cross-model comparisons.

$$NMSE = \frac{\overline{(C_o - C_p)^2}}{\overline{C_o}\,\overline{C_p}} \qquad \textit{(8-7)}$$

$$NAE = \frac{\overline{|C_o - C_p|}}{0.5(\overline{C_o} + \overline{C_p})} \qquad \textit{(8-8)}$$

NMSE = normalized mean squared error.
NAE = normalized absolute error.

The fraction of data within a factor of two of observations (**Equation 8-9**) is also evaluated.

FAC2 = fraction of data that satisfies:

$$0.5 \le \frac{C_p}{C_o} \le 2.0 \qquad \textit{(8-9)}$$

In each metric:

C_p denotes predicted concentrations

C_o denotes observed concentrations

$\overline{overline}$ denotes an average

The ideal model would have a geometric mean bias and a fraction of predictions within a factor of two of observations equal to 1, and a fractional bias and normalized mean square error of 0. Models are compared based on how close to ideal each of these metrics is.

RESULTS

A 6-week time series of hourly ethane concentrations at the centralized receptor site predicted by CALPUFF (stability classification), AERMOD, and the single-equation Gaussian model (referred to as SEGAUSS in figures) is shown in **Figure 8-3**. Observations are overlaid onto each time series. Each model generally predicts the timing of elevated enhancement events with reasonable precision, but the magnitude of the enhancements is inconsistent. AERMOD generally predicts the lowest concentrations of the three models, as illustrated in the parity plots in **Figure 8-4,** and, for several hours, it predicts null concentrations. These null concentrations occur under calm wind conditions, during which the default configuration of AERMOD does not calculate dispersion. These calm wind conditions most frequently occur at night (**Figure 8-5**) and often when observed concentrations, as predicted by the single-equation Gaussian model, are relatively elevated (**Figure 8-6**). AERMOD can be instructed to lower the wind speed associated with calm hours (the "calms" threshold) from the default of 0.5 m/sec, but it is not recommended unless the user is certain the wind speed data were collected using an instrument with high sensitivity (e.g., a sonic anemometer). The wind measurements at the TCEQ CAMS site were collected using a cup anemometer, which has much lower precision when wind speeds are below 0.5 m/sec, so no additional sensitivity analyses reducing the calm threshold were conducted. The magnitude of many of the enhancements predicted by the single-equation Gaussian model is more consistent with CALPUFF predictions than with AERMOD predictions (**Figure 8-7**). However, several of the highest concentrations predicted by the single-equation Gaussian are significantly enhanced compared with the other models and the observations. These enhancements are

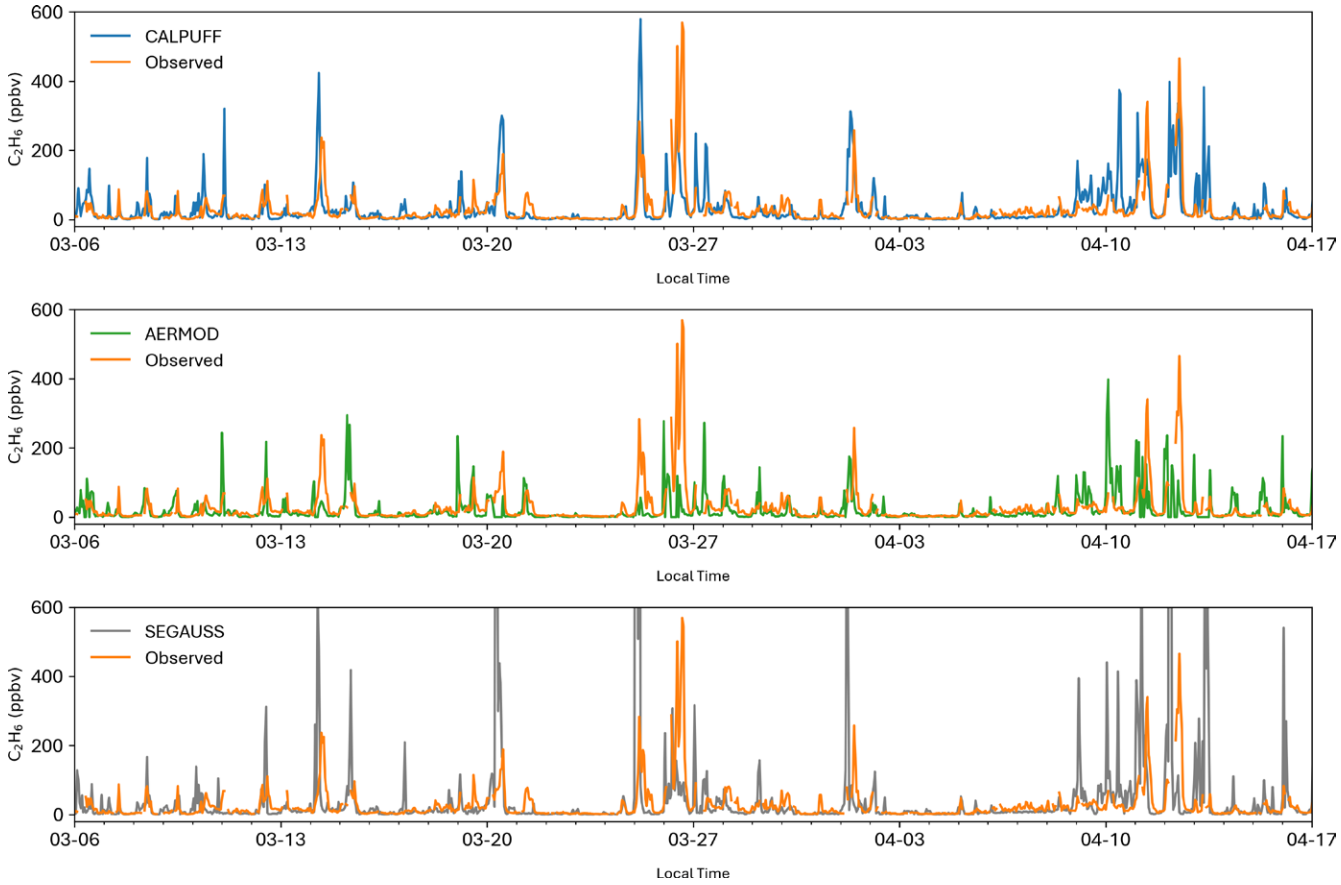

Figure 8-3. Time series of ethane concentrations at the receptor site predicted by CALPUFF (stability classification), AERMOD, and the single-equation Gaussian (SEGAUSS) models. Source: From Graves et al. 2026; Creative Commons license CC-BY-ND 4.0.

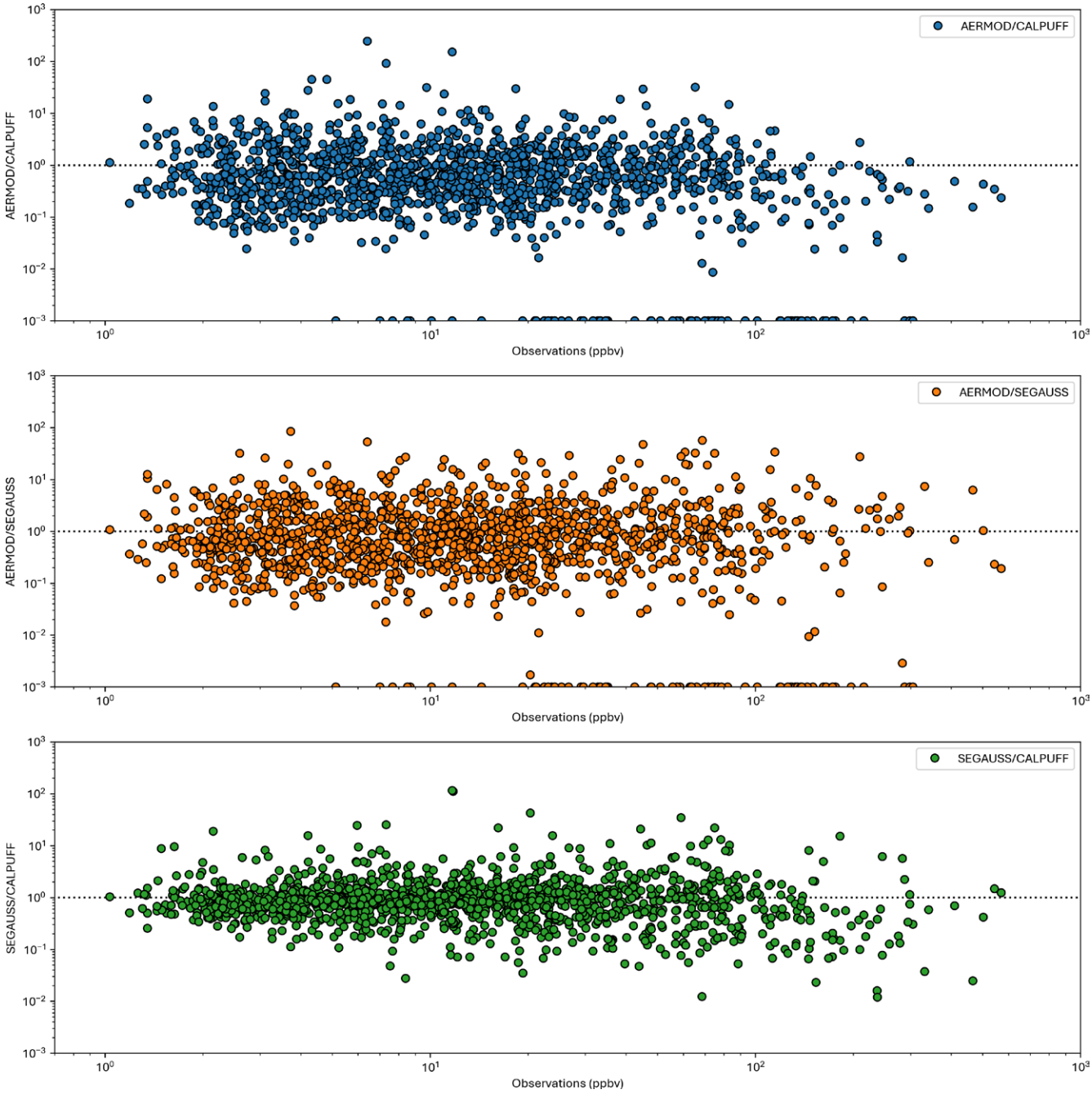

Figure 8-4. Log-log parity plots showing time-paired model prediction ratios for each measured ethane concentration in the observed time series. Null ratios have been replaced with 1×10^{-3} for plotting on the log scale.

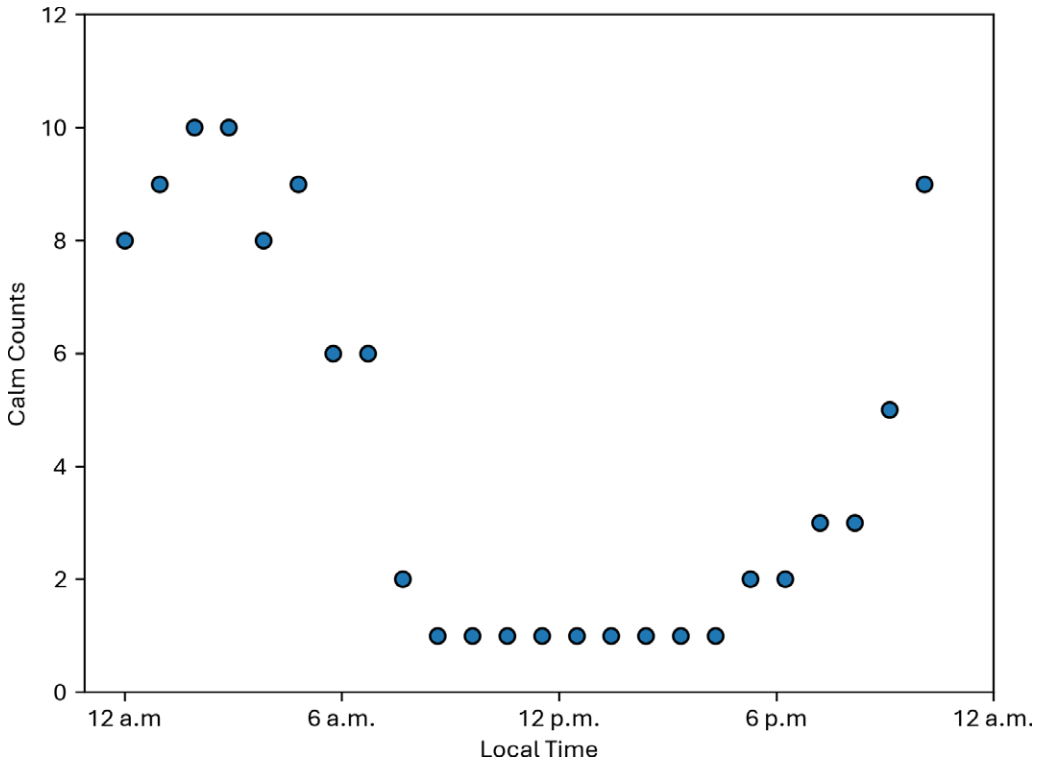

Figure 8-5. Number of calm hours in AERMOD by hour of day in the 3-month modeling period. Source: From Graves et al. 2026; Creative Commons license CC-BY-ND 4.0.

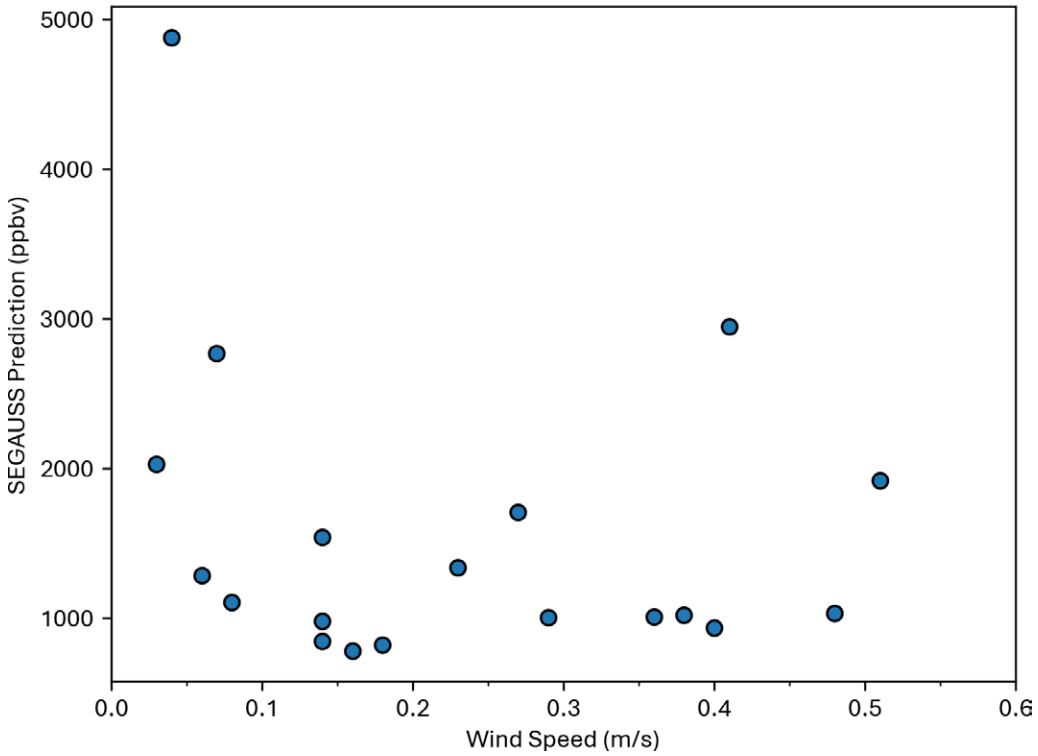

Figure 8-6. Wind speeds for the 20 highest predicted enhancements of ethane from the single-equation Gaussian model (SEGAUSS).

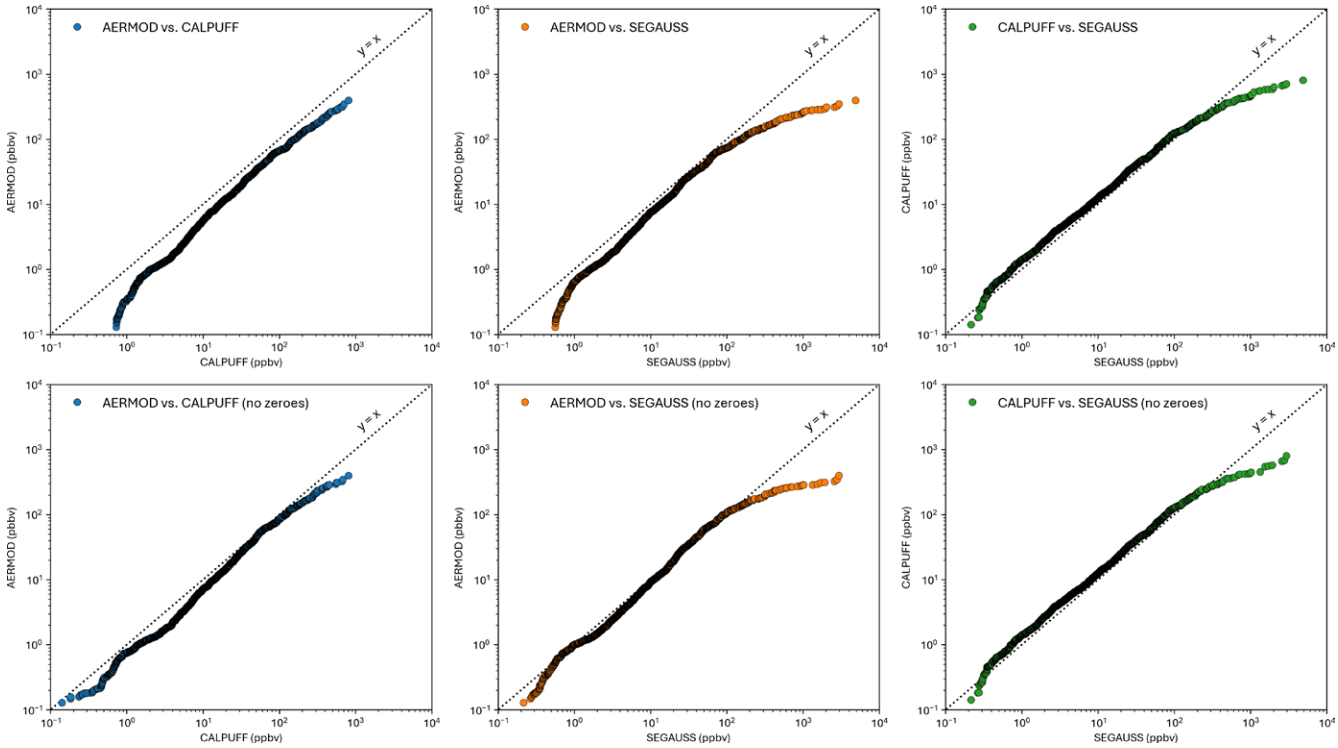

Figure 8-7. Quantile-quantile plots for CALPUFF, AERMOD, and the single-equation Gaussian (SEGAUSS) models. Ethane concentration enhancements are presorted in each time series and then plotted against one another. Timestamps with no predicted concentration in the AERMOD dataset have been removed.

typically associated with very low wind speeds and can likely be explained by extremely low rates of dispersion predicted under these conditions. In every model, the dispersion calculations are likely most uncertain during calm wind speed conditions. CALPUFF, however, appears best suited to predict these periods.

Time-of-day distributions are shown in **Figures 8-8** and **8-9**. AERMOD, CALPUFF, and the single-equation Gaussian model regularly predict nighttime periods of high concentrations consistent with observations. However, each model generally struggles to accurately predict the timing and magnitude of the day-to-night transition. The magnitude of enhancements also varies considerably between the models. CALPUFF and the single-equation Gaussian model consistently predict higher ground-level concentrations than AERMOD at all times of the day **(**Figure 8-7 and Figure 8-9**)**. However, the distribution of predicted concentrations from AERMOD and CALPUFF more precisely matches the distribution of observed enhancements, particularly among the highest quantiles **(Figure 8-10**). In the quantile-quantile plots in Figure 8-10, model predictions and observed concentrations are presorted by magnitude such that the nth quantile of the model predictions is paired with the nth quantile of observations. The quantile pairs are plotted as scatter points. These figures illustrate whether the models make reasonable predictions under the range of observed conditions, regardless of how well the predicted and observed time series match. For example, the single equation Gaussian formulation predicts several extreme concentrations that are much higher than the largest observed concentrations and largest predicted concentrations from AERMOD and CALPUFF, implying that, under certain conditions, the model may make unrealistic predictions. The lowest concentrations predicted by each of the three models are considerably lower than the observations, but no regional background correction has been applied to the observations (Figure 8-10). AERMOD and CALPUFF tend to predict similar distributions in the middle- and high-concentration ranges (Figure 8-10). The single-equation Gaussian model generally shows poor performance for predicting both the highest and lowest range of observed enhancements (Figure 8-10). These differences, particularly at the extremes of each distribution, may be explained by variations in the complexity of each model when calculating dispersion.

Dispersion estimates will generally be most imprecise under extreme meteorological conditions, typically coinciding with times when, in the absence of extreme emission events, observed concentrations are at their extremes, and meteorological data may be most imprecise. In this case, each of the models may predict the general trends in the timing and ranking of observed enhancements, but their

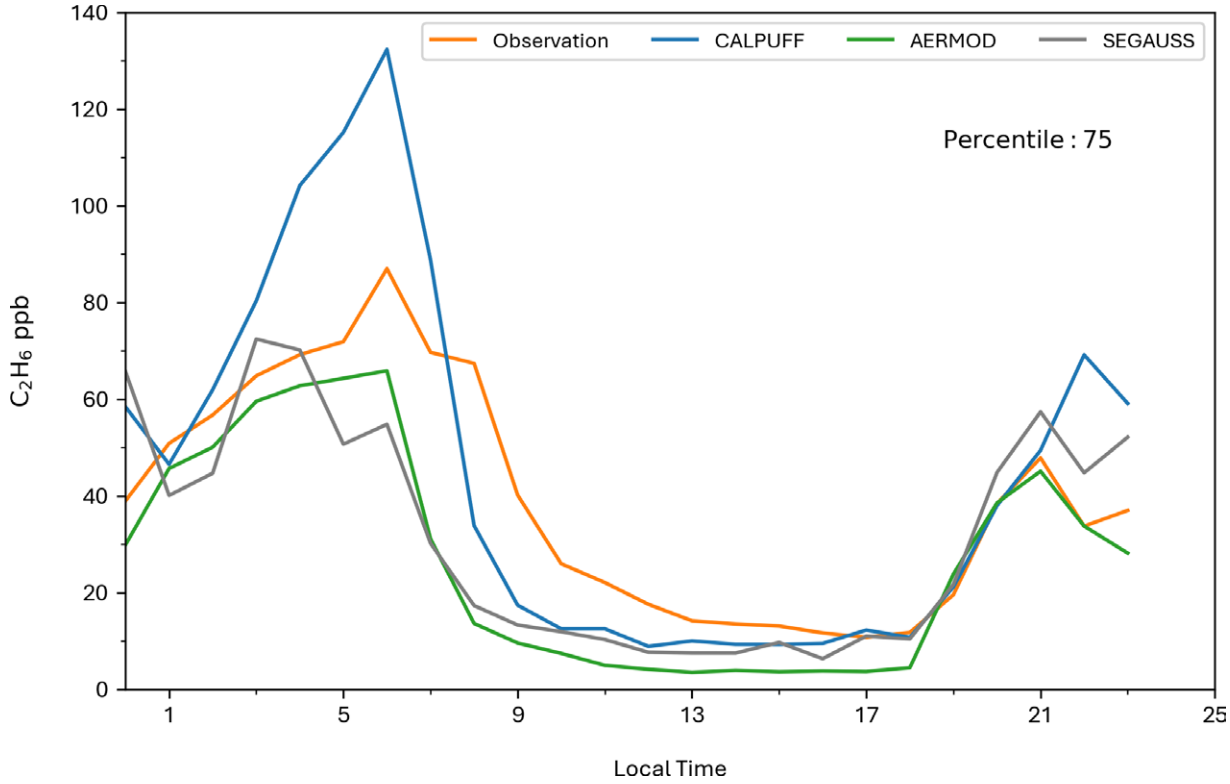

Figure 8-8. Time-of-day distributions of the 75th percentile of observed and CALPUFF, AERMOD, and SEGAUSS predicted concentrations of ethane.

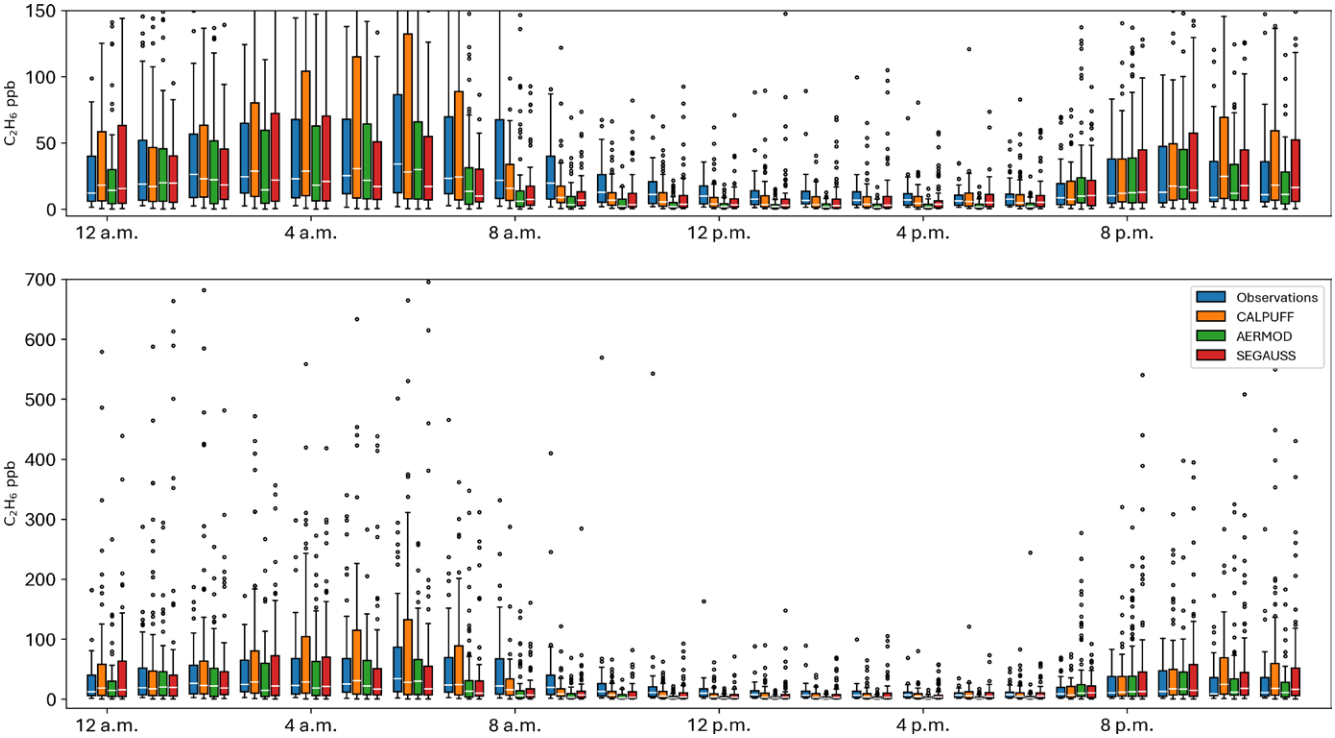

Figure 8-9. Hourly ethane concentration distributions for observations and model predictions. The lower figure shows most of the range of all values (some extreme values limit the interpretability of the figure when included). The upper figure shows the same data plotted over a smaller range for easier viewing of interquartile ranges. White lines are medians. Source: From Graves et al. 2026; Creative Commons license CC-BY-ND 4.0.

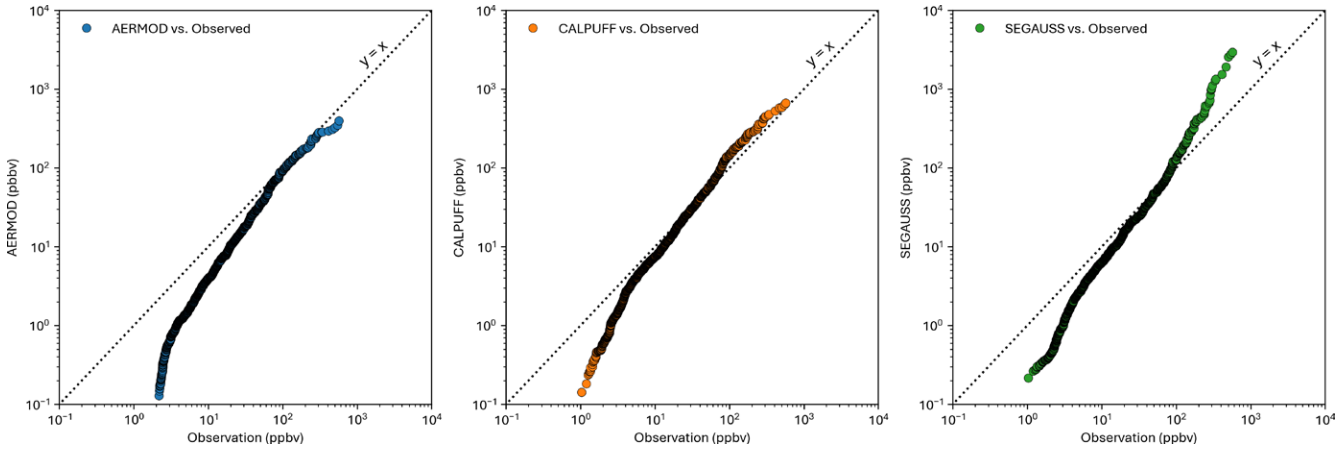

Figure 8-10 Quantile-quantile plots for observed and modeled ethane enhancements over the entire modeling period. Ethane concentration enhancements are presorted by magnitude in each time series such that the n^{th} quantile of the model predictions is paired with the n^{th} quantile of observations. The quantile pairs are then plotted. Source: From Graves et al. 2026; Creative Commons license CC-BY-ND 4.0.

quantification of the magnitude of these enhancements may be relatively imprecise. The degree of imprecision in these quantifications will be influenced by how rigorously the models treat the atmospheric processes driving dispersion. For example, Gaussian plume models assume the rate of advection is always much greater than the rate of dispersion in the along-plume direction, so their predictions are usually uncertain under calm wind conditions when this assumption becomes invalid. AERMOD was developed to avoid unrealistic predictions under these conditions by skipping dispersion calculations for timesteps when wind speeds are below a specific threshold (here 0.5 m/s). Similar precautions are absent in the single equation Gaussian formulation, leading to predictions that are significantly enhanced over the other models under low wind speed conditions (Figure 8-6).

Parity plots (**Figures 8-10** and **8-11**) indicate that CALPUFF has even rates of over- and underprediction when paired in time with observed concentrations, across the range of observed values between around 2 ppb and 100 ppb. For very low observed concentrations, CALPUFF tends toward slight underprediction (again noting no background correction on observations), and on the very high end, it tends toward slight overprediction. AERMOD displays a much more variable behavior across the range of observed concentrations, but generally tends to underpredict most observed enhancements when paired in time. The single-equation Gaussian has tighter clustering around the factor of 2 lines on the lower end of the observed enhancements, but beginning in the middle range of observations, it begins to display much greater variance in its predictions. Of the largest enhancements that the single-equation Gaussian does predict correctly, it generally tends to significantly overpredict the concentration. Each of the log-log parity plots shows a relatively linear relationship with varying degrees of correlation between the observations and model predictions, suggesting a monotonic log-linear relationship exists; this association appears stronger in CALPUFF than in AERMOD and the single-equation Gaussian. Comparing bivariate correlation coefficients between the models supports this observation (**Figure 8-12**). Each of the models has weaker linear associations (Pearson correlation) than monotonic associations (Spearman correlation), suggesting that the models are performing reasonably well at identifying the timing and ranking of peaks, but the degree of over- and underprediction of the magnitudes of each peak has a nonlinear dependence on observed concentration. Each model appears to predict the timing of the highest and lowest observed concentrations with reasonable precision. CALPUFF demonstrates the highest precision in these ranges, but notable uncertainty is still observed.

Each of the models was subjected to the screening procedure to confirm model performance above the minimum acceptable level for use in regulatory applications. Separate analyses were conducted for all modeling hours, daytime hours, and nighttime hours individually. CALPUFF and AERMOD meet the acceptable performance metrics of ±0.67 for the fractional bias of the mean and standard deviation of the top 25 enhancements (Equation 8-2) during the nighttime and all-hours categories, but do not meet the performance threshold during the daytime (**Figure 8-13**). The single-equation Gaussian does not meet the performance threshold at any time. The spatial distribution of the biases is generally consistent in each of the time-of-day categories: AERMOD is the most positively biased model in both metrics (Equation 8-2), and the single-equation Gaussian is the most negatively biased of the three models.

Table 8-1 shows statistical metrics calculated for each of the models for multiple time-of-day categories. For each comparison, every metric was compared with its ideal value,

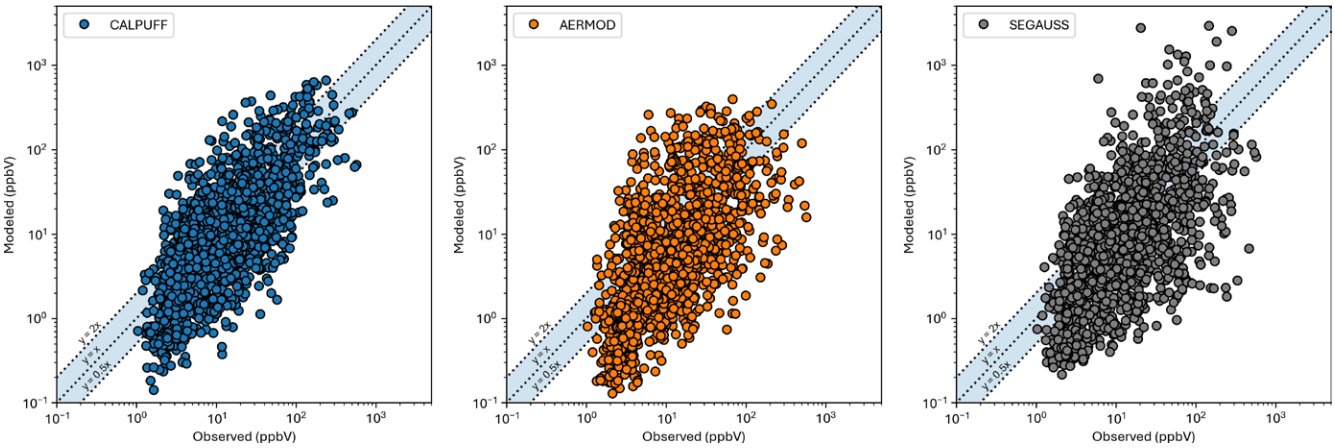

Figure 8-11. Parity plots for observed and modeled enhancement of ethane values directly. Enhancement values are paired in time and plotted. Null records have been converted to a value of 0.1 for plotting on the log scale. Source: From Graves et al. 2026; Creative Commons license CC-BY-ND 4.0.

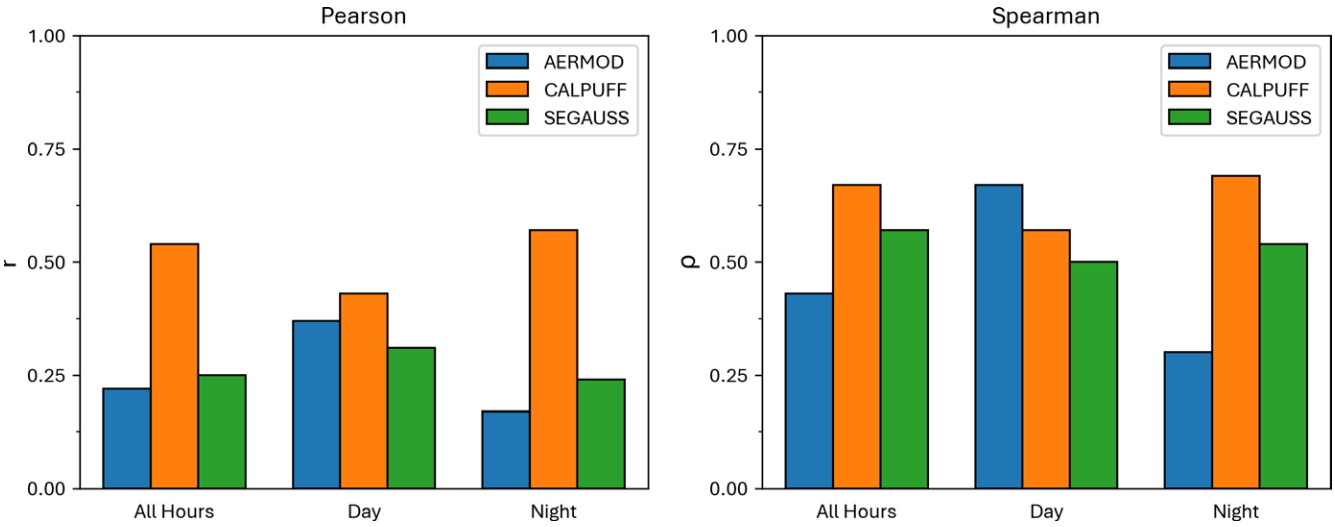

Figure 8-12. Pearson and Spearman correlation coefficients between ethane observations and each of the three models for all hours, nighttime, and daytime hours individually.

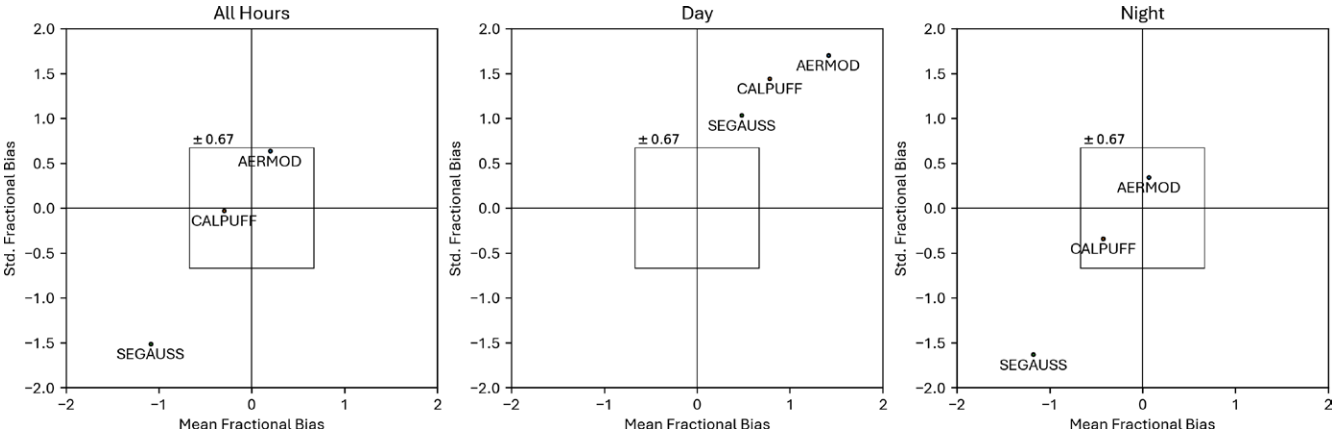

Figure 8-13. Fractional biases of the top 25 predicted ethane enhancements from AERMOD, CALPUFF, and the single-equation Gaussian (SEGAUSS) against the top 25 observations for all hours and daytime and nighttime hours only. Models with biases outside the bounding region ± 0.67) are considered to perform below an acceptable level for use in regulatory applications. Source: From Graves et al. 2026; Creative Commons license CC-BY-ND 4.0.

Table 8-1. Statistical Metrics for Each Dispersion Model Nominally Ranked by Performance[a]

Model	Time of Day	Fraction of Predictions within a Factor of Two of Observations	Normalized Mean Square Error	Normalized Absolute Error	Geometric Mean Bias	Fractional Bias
CALPUFF	Night	0.4	2.71	0.82	1.06	−0.29
CALPUFF	All hours	0.41	3.69	0.83	1.31	−0.16
AERMOD	Night	0.37	3.88	1.08	2.54	0.14
AERMOD	All hours	0.29	5.76	1.11	3.29	0.32
CALPUFF	Day	0.41	8.62	0.91	1.79	0.51
SEGAUSS	Day	0.38	9.45	1.03	2.2	0.48
SEGAUSS	Night	0.36	18.5	1.21	1.26	−0.53
SEGAUSS	All hours	0.37	22.42	1.18	1.58	−0.39
AERMOD	Day	0.17	26.63	1.29	4.82	1.25

[a]Ranking is determined by attempting to minimize the distance between the ideal and reported values for each metric simultaneously. The ideal value for the fraction of predictions within a factor of two of observations and the geometric mean bias is 1. For all other metrics, the ideal value is 0.

Source: From Graves et al. 2026; Creative Commons license CC-BY-ND 4.0.

and models were nominally ordered by the distance each of their metrics was from ideal. The ideal value for the fraction of predictions within a factor of two observations and the geometric mean bias is 1. For all other metrics, the ideal value is 0. The nominal rankings suggest that CALPUFF would be the best-performing model at a 1-hour time resolution under the night and all-hours categories.

Many approaches for evaluating air quality model performance exist. Here, the distance-from-ideal performance analysis presents a generalized approach for identifying models that produce the most balanced predictions derived from multiple statistical metrics when measurements are only available at a single location. In practice, performance metrics and analysis methods will typically be fit-for-purpose. In this case, weights might be assigned to each metric, or different metrics might be used entirely. For example, regulatory applications might prefer conservative models, especially when environmental conditions are conducive to ambient concentration enhancements (e.g., nighttime). In this case, model predictions with negative fractional biases may be preferred. Alternatively, acute exposure analyses may prefer model predictions with a more ideal fraction of predictions within a factor of two of observations, a lower normalized absolute error, and a higher correlation coefficient to estimate temporal exposure patterns more accurately.

Figure 8-14 compares model exposure predictions in a longer-term scenario, showing the fraction of total observed concentrations in each time-of-day category predicted by each model over the entire 3-month modeling period. In this case, CALPUFF still demonstrates the best performance in the all-hours category, and its long-term average agreement with observation is much better than may be suggested by looking at the hourly performance metrics alone.

DISCUSSION AND CONCLUSIONS

Analysis of three commonly used dispersion models (AERMOD, CALPUFF, and a single-equation Gaussian model), used in the TRACER model, with distinctly different model formulations for predicting transport of pollutants over multiple kilometers in simple terrain, yields qualitatively similar, but quantitatively different, concentration profiles. These differences are expected to be amplified in cases with more complex terrain where uncertainties in meteorological inputs are more significant, and the simplifying assumptions used in the less rigorous models are less likely to be applicable. Statistical analyses of model predictions can be a useful tool for evaluating the performance of different models. However, several metrics should be used. Consideration should also be given to the features and limitations of different models. For example, AERMOD may not predict enhancements during low wind speed conditions. These conditions can be associated with high observed concentrations, which can limit the performance of AERMOD, especially for acute exposure analyses. In contrast, the capabilities of CALPUFF to model non-steady-state behavior and consider spatial and temporal variations in gridded meteorological fields may make it uniquely capable of handling longer-range transport in complex terrain.

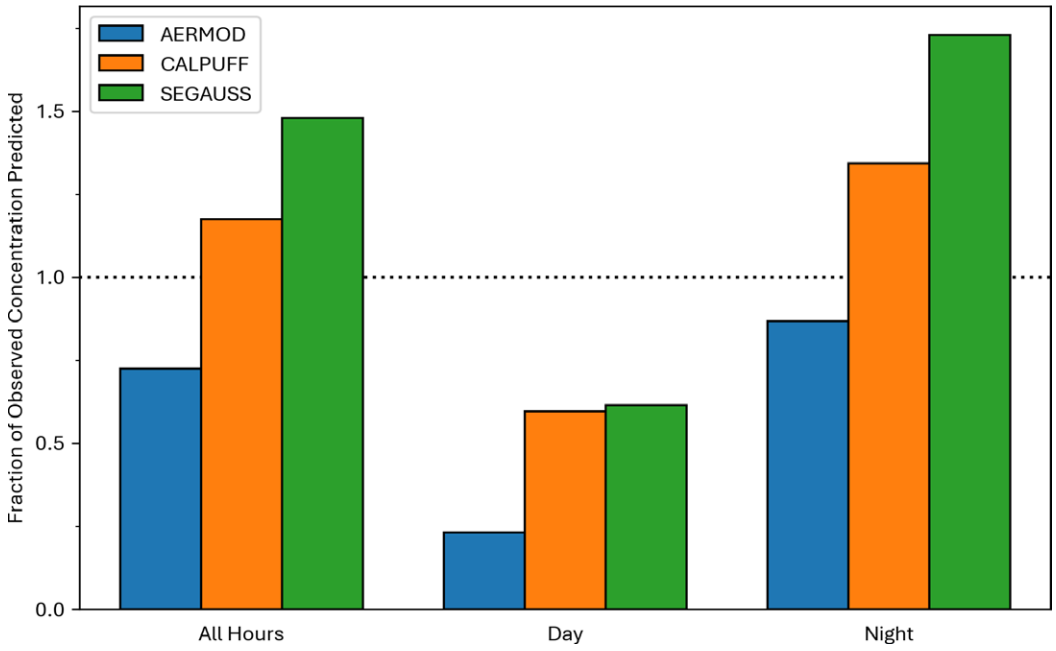

Figure 8-14. Fraction of total observed concentrations by each model for each time-of-day category over the course of the entire modeling period.

REFERENCES

Chang JC, Hanna SR 2004. Air quality model performance evaluation. Meteorol Atmos Phys 87:167–196; *https://doi.org/10.1007/s00703-003-0070-7*.

Graves J, Kimura Y, Modi M, Stokes S, Meyer N, Hildebrandt Ruiz L, et al. 2026. Performance of dispersion models in predicting ambient ethane concentrations at a regional air quality monitor in an oil and gas producing region. ACS Environ Au [preprint]; *https://chemrxiv.org/doi/full/10.26434/chemrxiv-2025-xkhh9*.

US Environmental Protection Agency (US EPA). 1992. Protocol for Determining the Best Performing Model; *https://www.epa.gov/sites/default/files/2020-10/documents/model_eval_protocol.pdf* [accessed 10 May 2025].

CHAPTER 9: UOGD EXPOSURE ANALYSIS AND IMPLICATIONS FOR FUTURE HEALTH STUDIES

INTRODUCTION

Ambient concentration measurements, emissions estimates, and models discussed in the previous chapters can advance exposure assessments for future health studies by reducing uncertainties in exposure model inputs. In this chapter, we use these TRACER tools to estimate spatial-temporal variability in concentrations from all sources and from individual UOGD processes surrounding Karnes City. Whereas the previous chapters developed exposure model inputs and compared models' abilities to assess temporal concentration variability at a central monitor, this chapter focuses more on comparisons between models, with a particular eye toward applicability for assessing spatial-temporal exposure variability. We compare the more advanced modeling systems, such as CALPUFF, with relatively simple distance-based models historically used in some epidemiological analyses. Additionally, we compare the relative contributions of individual UOGD processes to concentrations across Karnes County. Finally, we develop recommendations for appropriate model choice.

Using source- and process-specific emissions developed for the Eagle Ford Shale region described in previous chapters, we quantified VOC exposures using multiple methods of varying complexity to inform future epidemiological health analyses and risk assessments. We have identified spatial variability of modeled pollutant concentrations throughout Karnes County at multiple time-average scales (i.e., daily average, average across 3 months, and day-night differences). Additionally, we quantified the influence of factors including the UOGD process, emission location, and meteorological variability on VOC concentrations. Using the modeled concentration contributions from UOGD wells, we calculated population-weighted exposures by racial, ethnic, and income group in Karnes County at the census block group level. This analysis highlights the extent to which methane and air toxic concentrations vary in time and space; these results will inform the ability of future epidemiological studies to separate the effects of these pollutants on acute and chronic health outcomes.

METHODS

Informed by previous exposure assessments of UOGD activity air emissions (Cushing et al. 2021; Gonzalez et al. 2023), we applied multiple methods to quantify temporal and spatial variability in methane, ethane, propane, n-hexane, benzene, and toluene exposure. Using the models, we assessed the factors that drive modeled exposure variability. Finally, we quantified population-weighted exposure variability among racial or ethnic and income population groups in Karnes County at the census block level.

DATA

MODELED UOGD EMISSIONS

We incorporated emissions from UOGD activity across an area encompassing Karnes County, near the center of the Eagle Ford Shale region (Additional Materials F, Table F-1; Figure F-1). To spatially apportion emissions, we used the emissions site groupings described in Chapter 8 (Figure 8-1). Each of the tank battery, emissions weighted centroids, and grid locations used in the modeling represents a varying number of source-process locations (Appendix F, Table F-1). Estimation of process-specific exposure fields is an important innovation of this work, and it may enable epidemiologists to uncover differences in health responses to UOGD processes, which each have different spatial, temporal, and chemical signatures (Allen et al. 2022). More information on the emissions modeling is provided in Chapters 5 and 6 and their Additional Materials.

CONCENTRATION OBSERVATIONS AND METEOROLOGY DATA

Meteorological data, recorded at 5-minute intervals (later averaged to hourly intervals), were obtained from the TCEQ's ground observation site (CAMS 1070) located in Karnes. The data include wind speed (in miles per hour) and wind direction (in degrees from north). Wind speed was rounded to the nearest 0.5 mph, and wind direction was rounded to the nearest integer degree. To ensure compatibility between meteorological and spatial datasets, spatial data were transformed into a uniform Lambert conformal conic projection. Methane concentration observations were from the methane instrument colocated with the TCEQ site during the study period. For other pollutants (ethane, propane, toluene, n-hexane, and benzene), concentration data were obtained from the TCEQ via the TAMIS Web Interface (TCEQ 2025). Additional information on instrumentation and measurement procedures is provided in Chapter 3.

POPULATION DATA

We obtained census block group demographic data from the 5-year American Community Survey for the Eagle Ford Shale area in 2022 (US Census Bureau 2022). The demographic information for this study included population by race or ethnicity and median household income. Variables of interest included total population, non-Hispanic White alone, non-Hispanic Black alone, non-Hispanic Asian alone, non-Hispanic Native alone, non-Hispanic Native Hawaiian and Other Pacific Islander alone, Hispanic, and median household income. To assess exposure differences in populations by income, we divided the Eagle Ford Shale income

dataset into quantiles, roughly aligning with the 25th and 75th percentiles. We defined high income as above $75,000 per year, low income as below $45,000, and middle income between these values.

EXPOSURE ASSESSMENT APPROACHES

We applied four approaches for assessing spatial-temporal concentrations of UOGD-associated air pollutants. The purpose of these comparisons was to test the extent to which the simplifying assumptions used in these methods limit the ability to quantify the spatial-temporal variability that would drive health studies of UOGD activity. Interest among researchers and policymakers (Baker et al. 2020; Gilmore et al. 2019) in reduced-complexity exposure models additionally motivated the inclusion of such models. All approaches assume nonreactivity, which is reasonable on the hourly time scales explored here, but CAMx modeling presented in Chapter 7 shows evidence that the assumption may not apply in all cases, for example, in the case of nitrogen oxides' influence on ozone formation (Modi et al. 2025).

Full descriptions of each model are provided here — including for models applied in previous chapters — to explain in detail the models' application in the spatial-temporal exposure assessment.

INVERSE DISTANCE WEIGHTING

The simplest approach we used was inverse distance weighting (IDW). In this model, the concentration of a pollutant at any given location is inversely related to the distance from the emission source. This approach assumes that pollutants disperse from the source in all directions, with concentrations decreasing as the distance from the source increases. We defined the IDW exposure at location *i* from source *j* for pollutant *p* as

$$IDW_{i,j,p} = \frac{1}{D_{i,j}} \times E_{i,j,p} \quad \textbf{(9-1)}$$

where $E_{i,j,p}$ is emissions of pollutant *p* from source *j*; $D_{i,j}$ is the distance of source *j* to the centroid of each receptor grid cell *i*.

Following chemical transport modeling used in other portions of this study and the analysis below relating grid resolution to various census geography sizes, we used a 1.33 × 1.33 km grid receptor cell covering Karnes County. To apply IDW, we established a 5 km buffer surrounding each emissions location. Geodesic methods were used to calculate the distance between each source and its surrounding receptors (grid cells). To prevent excessively high weights for receptors located very close to the source, a minimum distance threshold of 50 m was applied. The calculation involved calculating the distance between each source and each receptor cell, a total of at most 44 calculations within each 5 km buffer. The inverse distance between each source-receptor pair was then weighted by hourly emissions to calculate $IDW_{i,j,p}$ in each period.

IDW exposure estimates are not calculated in exposure units (e.g., ppb or μg/m^3) and are instead reported as relative exposure indices. This limits their comparability with observed concentrations or air quality standards; however, they can still be used to assess spatial-temporal exposure variability (Shan et al. 2024).

INVERSE DISTANCE WEIGHTING WITH WIND SPEED AND DIRECTION

Another limitation of the IDW model is that it does not consider wind direction or wind speed. To incorporate the influence of meteorology while maintaining IDW's computational nimbleness, we added parameterizations of wind speed and wind direction into the IDW model to create the IDWmet model:

$$IDWmet_{i,j,p} = \frac{1}{D_{i,j}} \times E_{i,j,p} \times \cos(\text{atan 2}\,(\sin(\theta_2 - \theta_1), \cos(\theta_2 - \theta_1)) \times \frac{1}{u} \quad \textbf{(9-2)}$$

where θ_1 is the angle (degree) between source and receptor, and θ_2 is wind direction (degree) at receptor grid cell, *u* is wind speed in m/sec. This model normalized IDW concentrations in the direction of wind to 1 and opposite the wind direction to zero. Inverse wind speed is included as a corollary to the Gaussian plume model described below. This model uses the same source-receptor distance matrix as the *IDW* model.

We applied IDWmet for all sources to estimate exposure on the same 1.33 × 1.33 km grid receptor cells used in the IDW model. Similar to the IDW model, IDWmet produces concentrations as a relative index. Because the IDWmet approach is in different units than the original IDW model, exposure indices from the two approaches are not directly comparable, but we present approaches to compare them below.

GAUSSIAN PLUME MODEL

The Gaussian plume model is a widely used mathematical framework for predicting the steady-state dispersion of pollutants emitted from a point source, such as a smokestack, into the atmosphere (Brusca et al. 2016). Because of its simplicity and adaptability, the Gaussian plume model and its derivatives are commonly applied in air quality assessments and regulatory compliance studies to estimate concentrations of pollutants near industrial sources and to assess potential human exposure (Scott et al. 2003). However, it is more prone to errors in complex terrains and under nonconstant meteorological conditions (Environmental Emergency Response Section 2025). The Gaussian plume model defines concentrations downwind from a source as

$$C(x,y) = \frac{Q}{2\pi\sigma_z\sigma_y u} \times e^{\left(-\frac{y^2}{2\sigma_y^2}\right)} \times \left\{ e^{\left(-\frac{(z-h)^2}{2\sigma_z^2}\right)} + e^{\left(-\frac{(z+h)^2}{2\sigma_z^2}\right)} \right\} \quad \textbf{(9-3)}$$

To efficiently apply the Gaussian plume model to each UOGD source and consider hourly meteorology and emissions variability, we applied the model to the set of observed meteorological conditions for a single-source location and then used those results as a lookup table to apply to each source at each time period. We first defined a generic grid with resolution 25 × 25 m spanning from −1,500 m to +1,500 m in the *y* direction and 0 (i.e., the source location) to 10,000 m in the *x* direction (i.e., the direction the wind is blowing). We applied Equation 9-3 to this grid for each wind speed between 0.5 and 22 mph with an interval of 0.5 mph, source heights of 0.2, 2, and 5.5 m, and each Pasquill stability class A through F (Seinfeld and Pandis 2006). In this stage, we assumed $Q = 1 g/s$. This resulted in a total of 38,428,632 calculations (1 source × 792 [stability class, wind speed, and source height] combinations × 48,521 grid cells) for a single-source representative of the range of meteorological conditions and source height observed in Karnes County. These calculations had to be done just once.

For each hour and each emissions source, we selected the gridded concentration map that corresponded to the actual meteorological conditions. We rotated the map to match the actual wind direction and multiplied the concentrations by the actual emissions (Q) in that period. Next, we aggregated the concentrations at the fine points to the same 1.33 × 1.33 km grid used in the IDW modeling using area weighting. This approach yielded concentration fields associated with each source in each time period, which were further summed by source and averaged over time to create the concentration fields reported below.

AERMOD

The American Meteorological Society/Environmental Protection Agency Regulatory Model Improvement Committee was established to integrate advanced modeling techniques into the US EPA's air quality models. This initiative led to the development of the AERMOD modeling system, which incorporates air dispersion modeling based on planetary boundary layer turbulence structure and scaling concepts, similar to the Gaussian model discussed earlier. AERMOD is designed to handle emissions from both surface and elevated sources and applies to both simple and complex terrain. The AERMOD system includes two input data preprocessors, AERMET, a meteorological data preprocessor, and AERMAP, a terrain data preprocessor. We applied the AERMOD modeling system using the same meteorology and emissions data as noted above, but we modeled daily average, daytime, and nighttime explicitly as single time steps, instead of using the hourly time steps used in Chapter 8. This choice was made to facilitate spatial exposure modeling on the fine-scale grid.

CALPUFF

CALPUFF is a non-steady-state Lagrangian air quality modeling system. CALPUFF considers spatially varying wind flow fields and other boundary layer meteorological effects, such as dispersion in stagnant conditions and dry deposition. Because the model is set up to run on a three-dimensional gridded domain, the computational demand of CALPUFF is substantially larger than that of AERMOD and the other models. The results presented here are derived using stability classes, similar to those used in previous chapters of this report.

POPULATION EXPOSURE METRICS

We estimated population-weighted exposure for different demographic populations. Population-weighted exposure for each group d is calculated as

$$Population-weighted\ exposure_d = \frac{\sum_{b=1}^{B} C_b \times P_{d,b}}{\sum_{b=1}^{B} P_{d,b}} \qquad \textbf{(9-4)}$$

where C_b is the mean concentration of pollutants at the location b (for location $b = 1 \ldots B$), and $P_{d,b}$ is the population of the demographic group d at location b. PWE_d is calculated separately for each demographic group (d)'s population spatial distribution, and it represents the average population-weighted exposure for each group.

Gridded exposure estimates were apportioned to census geographical units (census block groups) using area weighting. For example, if 50% of a census block group intersects with one grid cell and 50% intersects with a second grid cell, the census block group is assigned the average concentration of the two grid cells.

RESULTS

In this section, we first describe the emissions and assess groups of sources and source type influence on the central monitor in Karnes City. Next, we compare the influence of meteorological and emissions variability on concentrations at the central monitor. After that, we describe the spatial concentration variability. Lastly, we quantify the extent to which exposure to UOGD emissions in Karnes County is distributed heterogeneously across demographic groups.

COMPUTATIONAL DEMAND AND SPATIAL PATTERNS FROM THE EXPOSURE MODELS

AERMOD requires a calculation for each source-receptor pair in the domain, a total of 4,142,950 calculations (1,691 source locations × 2,450 grid cells) in each modeled period (e.g., hour). While the two IDW models required calculating the distance between each source-receptor pair (i.e., the same number of calculations as AERMOD), these distances only needed to be computed once; weighting by emissions and meteorology (in the case of IDWmet) was trivial relative to the distance measures. The Gaussian model approach required 38,428,632 Gaussian plume calculations, with each calculation rotated to each degree between 0° and 359°

Table 9-1. Exposure Assessment Methods, Ordered from Least to Most Complex

Name	Assumptions	% of AERMOD Calculations for 100 Periods
Inverse distance weighting (IDW)	Concentration decreases as the inverse of the distance from a source.	1%
Inverse distance weighting + wind speed and direction (IDWmet)	Concentration decreases as the inverse of distance from a source in the primary wind speed and direction.	1%
Gaussian plume model	Pollutants disperse following a Gaussian pattern in the direction of the wind.	9%
AERMOD	AERMOD assumes steady-state conditions to calculate concentration.	100%
CALPUFF	Pollutants are transported as puffs that consider variable meteorological conditions throughout a three-dimensional grid.	–

AERMOD calculations assumed for 100 periods.

(**Table 9-1**). Again, these only needed to be performed once, and the remaining steps of exposure calculation required only multiplying the exposure fields by emissions. Because CALPUFF is run on a three-dimensional grid and tracks how emissions influence all locations, we did not estimate the relative number of calculations for CALPUFF. In general, CALPUFF's run time is several orders of magnitude longer than the dispersion models.

Single-source exposures for a given period have very different spatial patterns depending on the assessment method (**Figure 9-1**). With longer temporal averaging (results discussed below for the 3-month study period), the spatial distributions from the three methods become more similar as the narrower plume from the Gaussian model averages out to look similar to IDWmet. Values plotted in Figure 9-1 show an additional limitation of the IDW methods: results are in nonintuitive relative units. To aid interpretation, we scale these methods using a linear regression with Gaussian results.

UOGD ACTIVITY CONTRIBUTIONS CONCENTRATIONS AT THE MEASUREMENT SITE

UOGD process emission rates of ethane in Eagle Ford Shale are dominated by liquid unloading, tank flashing, and pneumatic controllers (**Table 9-2**). Tank battery sources, within the 15 km inner domain, contribute about 50% of the total emissions in the Eagle Ford Shale. Hourly emissions of all pollutants are correlated across the Eagle Ford Shale, with Pearson correlations typically above 0.7 except for n-hexane (Additional Materials F, Figure F-2).

We quantified contributions to concentrations at the Karnes City measurement site, UOGD locations, and processes from March 20 to May 14, 2023. We focused comparisons with observations on ethane because UOGD sites were expected to be the primary ethane sources in the county (Ku et al. 2024) (**Figures 9-2** and **9-3)**; other pollutant plots are shown in Additional Materials F, Figure F-3 through Figure F-7. Because of initial results showing nighttime concentration enhancements and to align with periods with differing human activity patterns, we compared concentrations relative to observations averaged at three temporal scales: daily (24-hour), nighttime (6 p.m.–6 a.m.), and daytime (6 a.m.–6 p.m.) average.

Relative to ethane observations, all models are correlated, with Pearson correlations at 0.50 or above, except for the IDW model (Figure 9-3). IDWmet is the most correlated with observations, with a Pearson correlation of 0.76. CALPUFF and the Gaussian model have a similar correlation (0.57) with observations. CALPUFF is much less biased than the other models, with a mean bias of 2 ppb (normalized mean bias = 7.6%). The next best model by bias is AERMOD, with a mean bias of −9 ppb (normalized mean bias = −33%); the other models are substantially more biased. This suggests that, while the simpler models are sufficient for capturing daily observed concentration variance, the more sophisticated CALPUFF model can substantially reduce bias in estimating absolute daily concentrations, likely because it is better at capturing the influence of distant sources. The Gaussian model performs poorly in the daytime hours (negative correlation compared with observations; Additional Materials F, Figure F-8), likely because it does not consider exposures beyond 10 km. At night (Additional Materials F, Figure F-9), the Gaussian model has a similar correlation with observations as AERMOD, potentially due to slower wind speeds increasing the relative importance of nearby sources.

Bias in the IDW and IDWmet is reliant on the linear regression approach, transforming the raw unitless exposure to concentrations originally derived by the Gaussian model. To align with updated emissions data, we scaled the concentration outputs of the Gaussian and IDW-based models using the ratio of emissions, assuming 95% control on tank battery emissions to the original emissions that assumed 98% control. This correction allowed us to update concentration magnitudes without re-running the models. The Gaussian model has much more negative mean bias than AERMOD, and hence, so do the IDW models. The models tend to be well-correlated with each other in time except for IDW (Additional Materials F, Figure F-10 through Figure F-15).

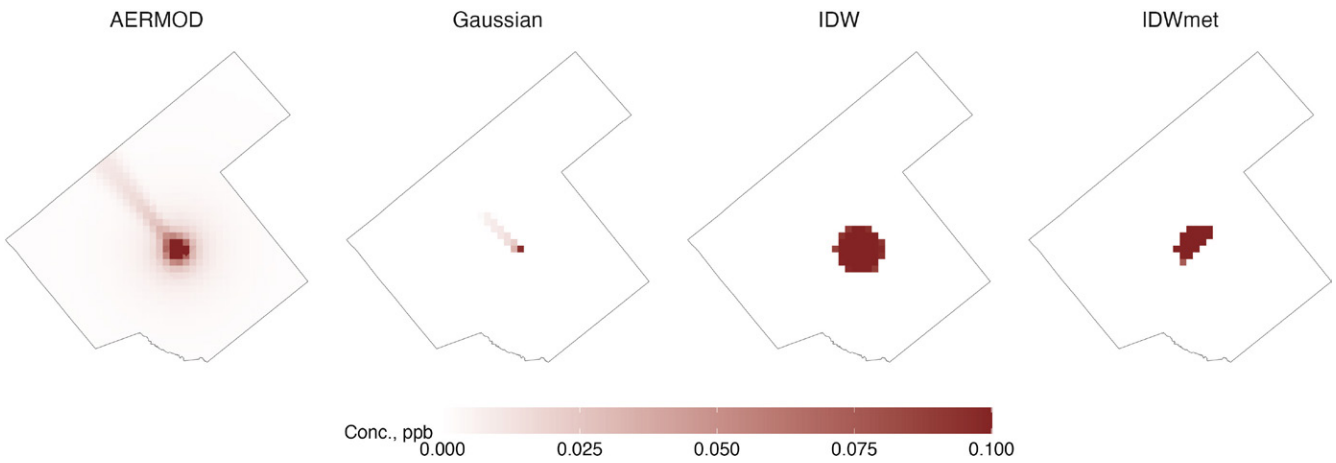

Figure 9-1. Spatial distribution of emissions from an oil and gas extraction site in Karnes County, Texas, modeled using various exposure assessment approaches. The analysis compares AERMOD, a Gaussian plume dispersion model; an inverse distance weighting (IDW) approach without incorporating wind speed and direction [unitless]; and an IDW approach incorporating wind speed and direction [unitless]. For the wind-augmented models, a constant wind speed of 2 m/sec, stability class "D," and a wind direction of 135° from true north were assumed.

Table 9-2. Emissions Rates and Relative Concentrations to Observations at the Measurement Site by Source Location (All Types), Source Type (All Locations), and Exposure Assessment Method[a]

Location or Source Type	Total Emissions (kg/hr)	Contribution to Concentration at Measurement Site (%) (AERMOD)	Contribution to Concentration at Measurement Site (%) (CALPUFF)
Tank battery	1,051	85	94
Emissions-weighted centroids (1.33 × 1.33 km)	425	8	2
Emissions grid centroids (4 × 4 km)	1,476	6	4
Leak	43	<1	–
Ground leak	29	<1	–
Pneumatic controllers	792	33	–
Tank flashing	998	44	–
Liquid unloading	1,026	20	–
Flares	21	<1	–

[a]Results are from AERMOD and CALPUFF for March 20, 2023 (results available only by location for CALPUFF).

DAY-NIGHT CONCENTRATION VARIABILITY

Enhanced nighttime concentrations of ethane relative to daytime levels were observed during the study period (**Figure 9-4**). On average, observed daytime ethane concentrations were 0.62 times the nighttime concentrations, with a standard deviation of 0.41 and a range of 0.15–2.2. The modeled outputs from IDWmet and the Gaussian approaches were closely aligned with these observations. Specifically, the IDWmet model yielded a mean day-to-night ratio of 0.67 (standard deviation: 0.28, range: 0.10–1.4), while the Gaussian model produced a mean ratio of 0.59 (standard deviation: 0.32, range: 0.09–1.3). Compared with observations, the CALPUFF model demonstrated a slightly lower mean day-to-night ratio of 0.5, with a wider variability (standard deviation: 0.5, range: 0.01–2.8).

Modeled day:night ratios are primarily dictated by meteorological variability because the emissions estimated by

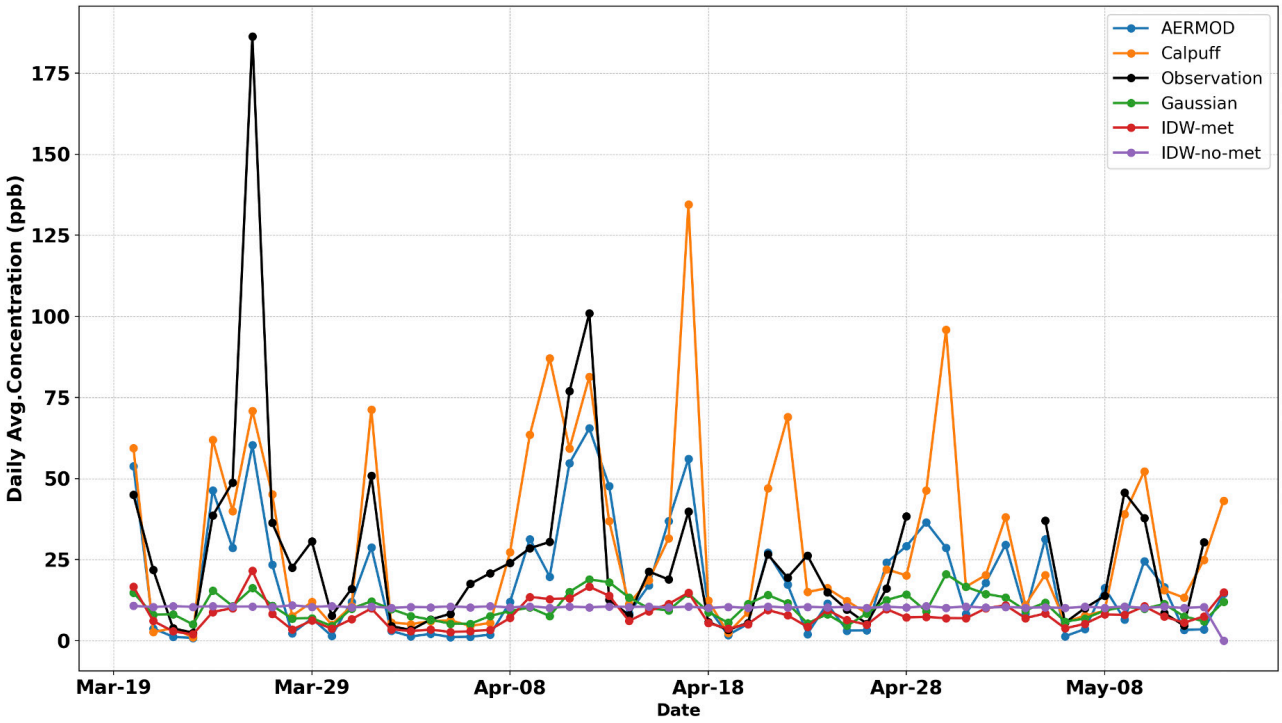

Figure 9-2. Daily average ethane concentrations from each of the models and observations at the Karnes City measurement site.

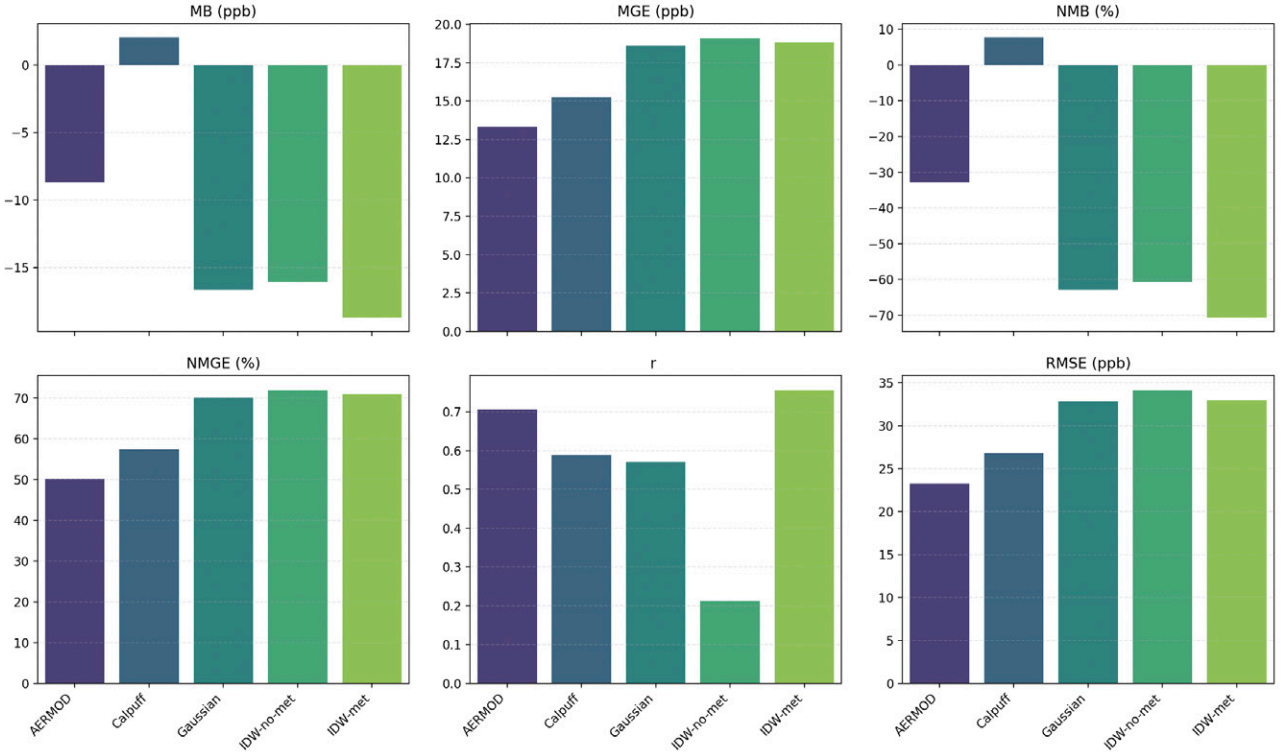

Figure 9-3. Evaluation statistics for the models for daily average ethane concentrations observed at Karnes City, March 20–May 14, 2023. MB = mean bias; (N)MB = (normalized) mean bias; (N)MGE = (normalized) mean gross error; RMSE = root mean squared error; r = Pearson correlation coefficient.

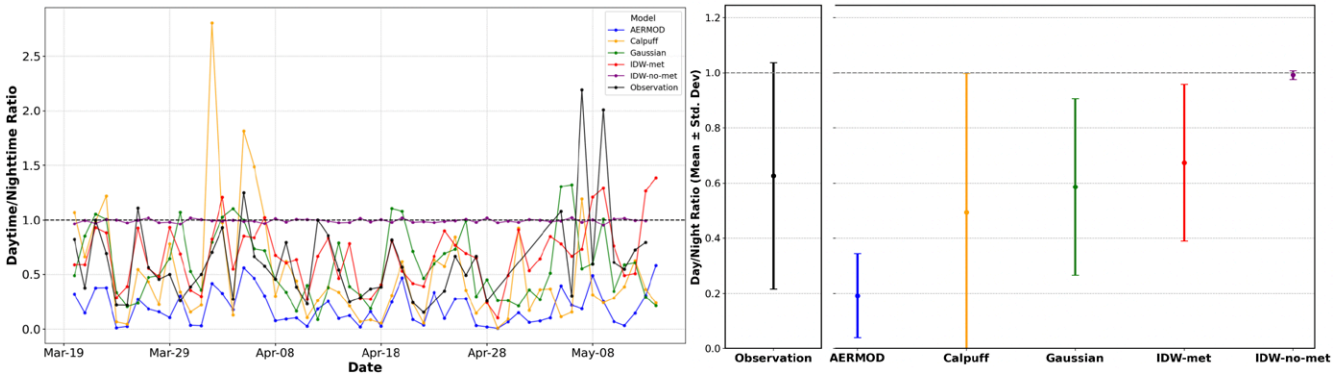

Figure 9-4. Temporal day:night ethane concentration ratios assessed using each of the exposure assessment approaches. Left: time series; right: mean and standard deviation of each time series.

the TRACER model are relatively constant between day and night. Overall, the Gaussian and IDWmet models capture observed variability in day:night ratio. There are exceptions, such as May 7–9, which are potentially tied to larger daytime emissions events not captured in the emissions model. CALPUFF yields greater variability and much higher day:night ratios than observations and the other models, with most days greater than 1. The simple IDW model — average day-to-night ratio of 1 (standard deviation: 0.01, range: 0.95–1.0) — shows almost no variability in the day:night ratio (all variation is emissions-driven in IDW) (Figure 9-4).

In Additional Materials F, Figure F-16 through Figure F-19 and in accompanying text, we applied AERMOD to explore the influence of factors including wind speed and direction, emissions variability, and terrain variability in determining modeled concentrations at the central monitor.

SPATIAL CONCENTRATION VARIABILITY

Spatial concentration contributions modeled by AERMOD from all UOGD operations follow similar patterns for all pollutants (**Figure 9-5** and Additional Materials F, Figure F-20). Concentrations are elevated in the central part of the county in a band running from southwest to northeast. Low levels of UOGD activity in the southeastern part of the county, combined with the predominant weather pattern (typical winds are from the southeast), lead to low UOGD concentration contributions in the southeastern part of the county. Day-night concentration differences are mostly due to meteorological differences (spatial concentration variations follow similar patterns in the daytime and nighttime).

Spatially, nearby sources (tank batteries) dominate the ethane concentration contributions in Karnes County (Additional Materials F, Figure F-21), although farther UOGD sources also contributed to concentrations in areas far from the center of the county. Each process type contributes to observed concentrations at unique spatial patterns (Additional Materials F, Figure F-22). This finding highlights the added utility of models that consider distant sources.

POPULATION EXPOSURE IN KARNES COUNTY

We selected the 1.33 × 1.33 km grid resolution as a balanced choice in terms of spatial resolution and computational efficiency. Ninety percent of block groups in Eagle Ford Shale are larger than 1.33 × 1.33 km, suggesting sufficient ability of our selected grid to capture between-block group variability (additional data and discussion presented in Additional Materials F, Figure F-23 through Figure F-28 and related text). Future health studies may select a different spatial resolution depending on the resolution of their population or health data. Of the models we assessed that were computationally lightweight enough to run for all receptor locations (thus excluding CALPUFF), AERMOD performs the best; therefore, we used that model to assess population-weighted exposure and exposure inequalities.

POPULATION EXPOSURE ACROSS RACIAL OR ETHNIC GROUPS

The American Community Survey reports populations in Karnes County of 4,849 for the White group, 931 for the Black group, and 8,318 for the Hispanic (all races) group. The summed total of all other population groups (including Native, Asian, and Hawaiian and Pacific Islander) was 190 (1% of the total population); therefore, we present only results for the White, Black, and Hispanic groups. Population-weighted exposure to UOGD in Karnes County shows differences across racial or ethnic groups and income levels (**Figures 9-6** and **9-7**). Population-weighted exposure to UOGD was higher in the Hispanic (all races) and White populations than in the Black population. For example, the median exposure to ethane among the Hispanic populations is 1.9 ppb during the day and 20.0 ppb at night (note that AERMOD is biased low in its day:night ratio; Figure 9-4). The White population was exposed to about 10% less ethane than the Hispanic population during the day and nighttime, and the Black population was exposed to about 40% less ethane than the Hispanic population. The results are generally consistent across pollutants and day/night, although the White

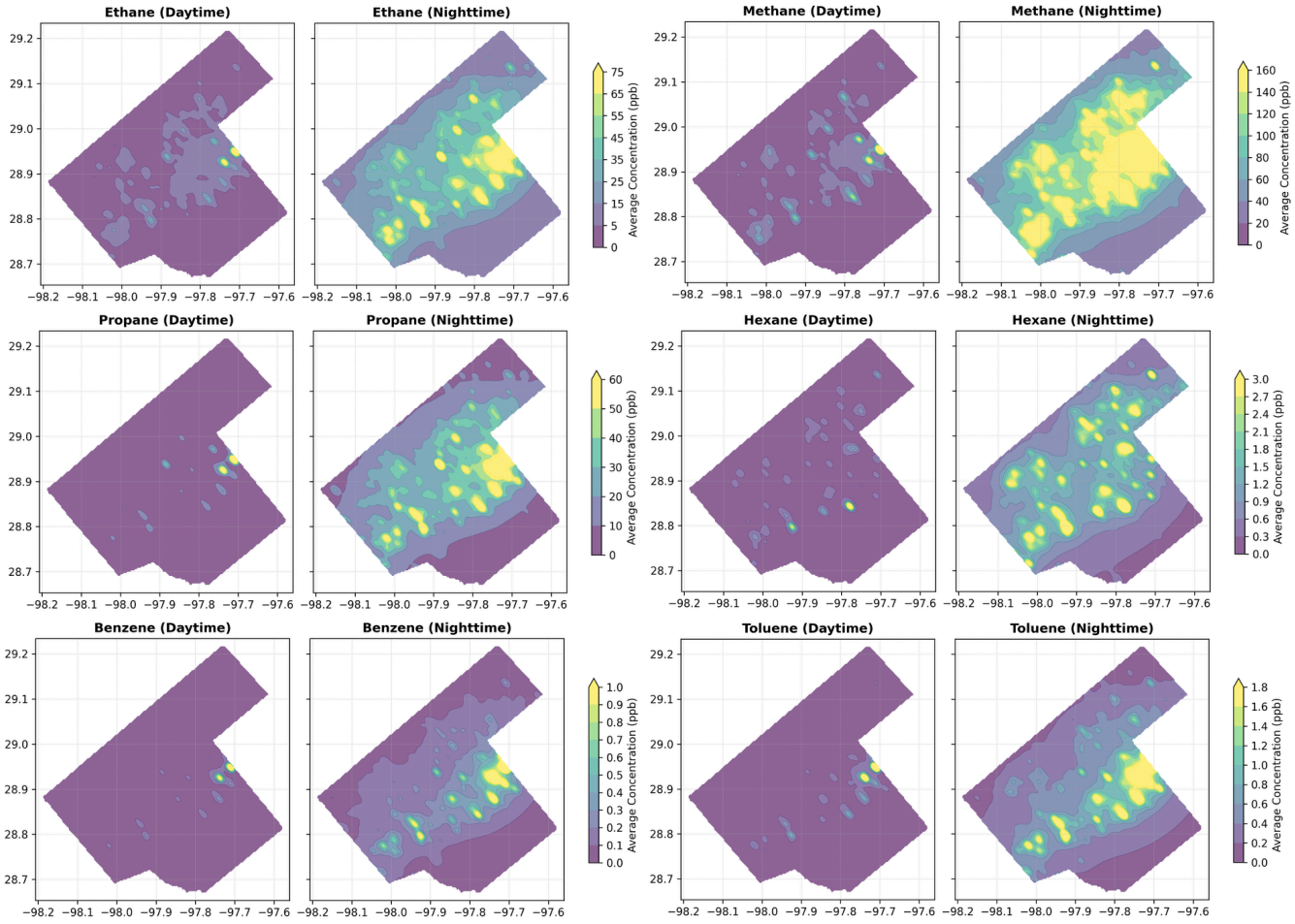

Figure 9-5. Day and nighttime concentrations of methane, ethane, propane, n-hexane, benzene, and toluene from UOGD modeled by AERMOD.

population has the highest median exposure to hexane. These findings highlight a racial or ethnic disparity in which the Hispanic population faces higher pollutant exposure to UOGD activity in Karnes County than the Black population included in this study.

Across pollutants, the middle-income group was exposed to higher levels than the other groups, with a 20% difference between the middle-income group and the high-income group, which had the lowest exposure (Figure 9-7). For example, the median nighttime population-weighted exposure to ethane for the low-income, middle-income, and high-income groups was 21.3, 22.9, and 19.4 ppb, respectively. During the day, ethane exposure showed a similar pattern, with median values of 2.0 ppb for low-income, 2.2 ppb for middle-income, and 1.8 ppb for high-income groups. These concentrations (and all others throughout this chapter) represent ethane enhancements from UOGD activity and do not consider background concentrations. Similar trends were observed for the other pollutants. These results are from the AERMOD model, and population-weighted concentrations from UOGD are expected to be higher than those from CALPUFF, given its performance.

The exposure differences across racial or ethnic and income groups reflect differential spatial distributions of housing relative to UOGD activities, as higher and lower income groups may both reside closer to these sources because of factors like property costs or historical land use practices. These findings underscore the importance of considering both racial or ethnic and socioeconomic disparities in exposure assessments related to oil and gas extraction activities. The population-level exposure disparities presented here apply to Karnes County. The entire Eagle Ford Shale or other areas of UOGD activity may yield differing relative exposures among the racial or ethnic and income groups.

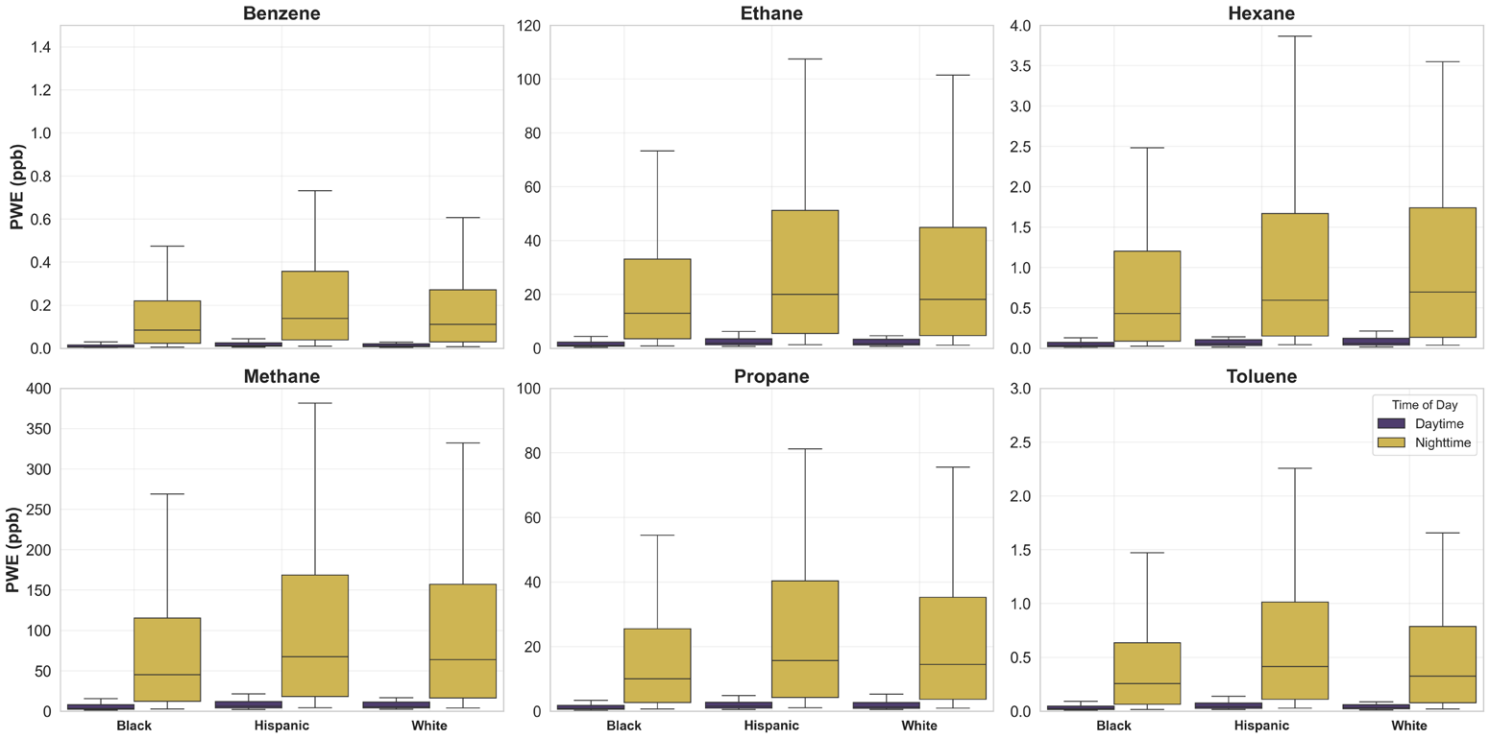

Figure 9-6. Population-weighted exposure from UOGD for Karnes County demographic groups for multiple pollutants. Results are from the AERMOD model, and distributions describe daily variability. PWE = population-weighted exposure.

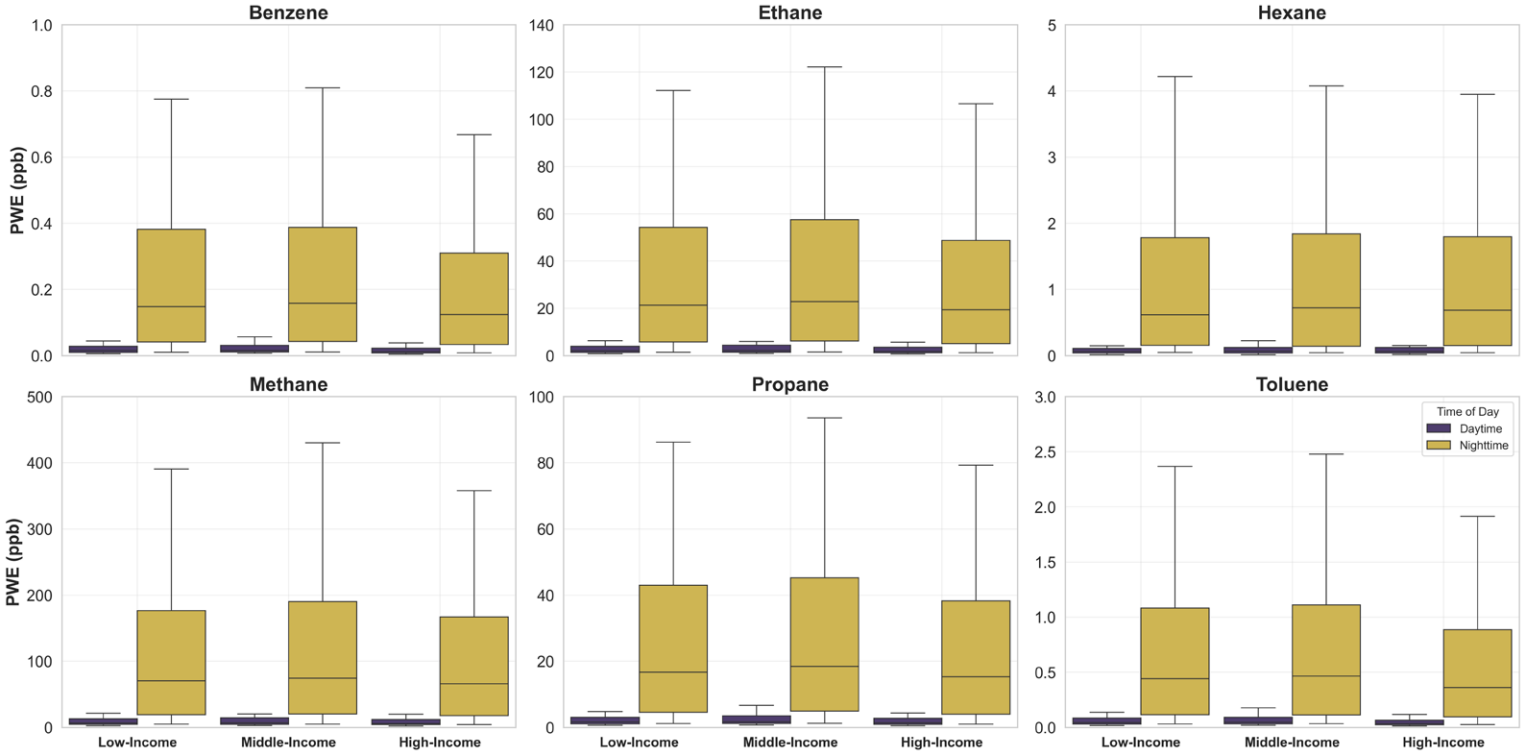

Figure 9-7. Income-based population-weighted exposure for different pollutants from UOGD in Karnes County, Texas. Results are from the AERMOD model, and distributions describe daily variability. PWE = population-weighted exposure.

Table 9-3. Previous Studies Assessing Exposure to UOGD Activity and Their Approaches to Quantify Processes That Dictate Exposure

Citation	Exposure Description	Pollutants	Emission Location	Activity	Emission Magnitude	Atmospheric Transport	Atmospheric Chemistry
AirTox-Screen	Combination of AERMOD and CMAQ	Criteria pollutants, air toxics	County level		National Emissions Inventory and Toxic Release Inventory		CMAQ
Gonzalez et al. 2022	Assessed observed concentration variability with upwind oil and gas activity in California		Well specific	Monthly preproduction activity and oil/gas volume produced	NA	Upwind, 1 km buffers to 10 km	NA
Kanayankottupoyil and John 2025	Assessed concentrations at TCEQ monitors using ambient observation data, linked with oil and gas activities by VOC ratios	Multiple nonmethane organic compounds	Number of wells within monitor radius	Annual oil and gas produced	NA	1, 3, and 5 mi buffer	NA
Archer et al. 2024	Assessed exposure using annual average oil and gas production volume from active wells within 1 km	NA	Well specific	Annual average oil and gas produced	NA	1 km buffer	NA
Hoang et al. 2024	Assessed exposure as to whether a cancer case lived within 1 km of a well	NA	Well specific	NA	NA	1 km buffer	NA
Koehler et al. 2018	Assessed exposure to specific processes—compressor engines, impoundments, and flaring—and well development phases using spatial principal component analysis decomposition on a 5 km^2 grid	NA	Well specific	Operation dates	NA	Various distance and inverse distance metrics, including metrics derived from spatial principal component analysis	NA
Cushing et al. 2021	Assessed nightly exposure to flares based on the population living within a certain distance	NA	Flare specific	Nighttime flaring from the VIIRS satellite	NA	NA	NA
Li et al. 2020	Assessed the influence of oil and gas wells on particle radioactivity using upwind wells within 20 km	Radioactivity	Well specific	NA	NA	Upwind, 20 km buffer	NA

NA = not applicable.

PUBLIC HEALTH IMPLICATIONS

Interest in UOGD air pollution impacts on public health has grown with increasing UOGD activity in the United States. Researchers have conducted exposure assessments using multiple methods that account to varying degrees for the processes that influence ambient concentrations from UOGD activity (**Table 9-3**). These processes include the emission location, activity (e.g., volume of gas extracted), emission magnitude, atmospheric transport, and atmospheric chemistry.

Some studies have used UOGD infrastructure datasets from third-party intermediates to identify specific wells, such as Enverus (Gonzalez et al. 2022; Li et al. 2020) or state agencies such as the Texas Railroad Commission (Cardoso-Saldaña et al. 2021; Kanayankottupoyil and John 2025) or California Geologic Energy Management Division (Archer et al. 2024). These sources do include information on well location, dates of operation, and activity measures such as the volume of gas produced. However, they do not include air pollution emissions, so previous studies have relied on proxy metrics to approximate emissions variability. Cushing and colleagues used satellite observations of flares in Texas to assess flaring emissions exposure. Oil and gas operation emissions are estimated by the US EPA in the National Emissions Inventory for US counties (Cushing et al. 2021).

Public health researchers often use simpler alternatives to atmospheric modeling to assess atmospheric transport and chemistry. Popular tools for assessing atmospheric transport include distance-based metrics, such as inverse distance weighted activity or counting the number of sources within geopolitical bounds (e.g., census tracts or counties). Some studies (e.g., Gonzalez et al. 2022) have used only upwind sources to approximate exposure, with downwind sources serving as the control. Most existing studies have focused on long-term (e.g., annual) exposure assessment.

VOCs and other emissions (e.g., nitrogen oxides) participate in chemical reactions that influence exposure. Such reactions are best assessed with chemical transport models; however, these models are limited by relatively coarse grid resolution and longer run times compared with dispersion models (precluding the ability to assess influence from individual sources or source groups). Nevertheless, a population-level assessment of exposure to specific UOGD well sources would benefit from the broader application of chemical transport models.

The US EPA's AirToxScreen combines output from the Community Multiscale Air Quality Modeling System (CMAQ) for criteria air pollutants and AERMOD for air toxics. AirToxScreen uses the National Emissions Inventory, which is at the county spatial resolution, for criteria air pollutants (US EPA 2024). For non-CMAQ chemicals, AirToxScreen uses information from the Toxic Release Inventory. The US EPA uses AERMOD to assess exposure to oil and gas sources, and the US EPA has made annual average source group-specific exposure available at the census block group level.

Our exposure assessments have several benefits over previous UOGD exposure assessment efforts, with innovations in the temporal scale, the type of pollutants included, emissions quantification, and atmospheric transport. We quantified daily and subdaily exposure to six specific VOCs: benzene, ethane, propane, n-hexane, methane, and toluene. Importantly, we identified enhancements in nighttime concentrations and found that AERMOD and distance-based methods that incorporate wind speed can approximate observed day:night ratios.

Our assessment of well-specific emissions using TRACER tools enabled the identification of hotspots within Karnes County (mostly in the eastern middle part of the county). Using well-specific exposure assessment tools, we quantified the influence of specific UOGD development processes and well locations. The spatial resolution of our models had important implications for group-specific exposure: the Hispanic (all races) population had about 10% higher exposure than some other groups across most pollutants, with the Black population (which mostly lives upwind of UOGD sources) having the lowest UOGD exposure.

DISCUSSION AND CONCLUSIONS

This chapter uses TRACER tools leveraging UOGD process-specific emissions and exposure models described in previous chapters to advance the ability to model spatial-temporal UOGD exposure variability. The VOCs (methane, ethane, propane, n-hexane, benzene, and toluene) are commonly found in natural gas and are typically released together during extraction, processing, and handling operations, including leaks, flaring, and venting. This co-emission pattern reflects the composition of natural gas and the operational practices in oil and gas fields where equipment handling, storage, and transport contribute to simultaneous releases of various hydrocarbons. Spatially and temporally correlated emissions of multiple species from a consistent set of sources that are nonreactive (or do not react quickly) foreshadow potential difficulty in differentiating the health impacts of these pollutants using population-level exposures from air quality models and typical epidemiological methods.

We have shown the strengths and limitations of multiple methods to assess UOGD source-specific concentration enhancements and spatial-temporal exposure patterns. Reduced-complexity approaches benefit from relatively less computational demand and can capture salient features (e.g., spatial-temporal variability) found in observations and more complex models. However, reduced-complexity approaches (including AERMOD) produce biased concentration contribution metrics relative to the more sophisticated CALPUFF model.

All models recreated observed day:night ratios in observed VOC concentrations except the simple IDW model. Adding a correction for wind speed and direction to IDW improved performance substantially. Day-night differences have implications for exposure, epidemiological, and risk assessments. For example, while concentrations are higher at night, humans may be more active during the day, so it is not clear from these results alone when the greater contribution to total exposure would be.

Modeled VOC concentration contributions from UOGD are highly variable across Karnes County. Combined with spatial differences among population group residences, spatial variability in UOGD emissions leads to large differences in exposure between racial or ethnic and income groups. The spatial resolution of our models had important implications for group-specific exposure: the Hispanic (all races) populations had about 10% higher exposure than some other groups across most pollutants, with the Black population (which mostly lives upwind of UOGD sources) having the lowest UOGD exposure.

REFERENCES

Allen DT, Cardoso-Saldaña FJ, Kimura Y, Chen Q, Xiang Z, Zimmerle D, et al. 2022. Methane Emission Estimation Tool MEET for predictions of emissions from upstream oil and gas well sites with fine-scale temporal and spatial resolution: model structure and applications. Sci Total Environ 829:154277; *https://doi.org/10.1016/jscitotenv2022154277*.

Archer H, González DJX, Walsh J, English P, Reynolds P, Boscardin WJ, et al. 2024. Upstream oil and gas production and community COVID-19 case and mortality rates in California, USA. GeoHealth 8:e2024GH001070; *https://doi.org/10.1029/2024GH001070*.

Baker KR, Amend M, Penn S, Bankert J, Simon H, Chan E, et al. 2020. Database for evaluating the InMAP, APEEP, and EASIUR reduced complexity air-quality modeling tools. Data Brief 28:104886; *https://doi.org/10.1016/j.dib.2019.104886*.

Brusca S, Famoso F, Lanzafame R, Mauro S, Garrano AMC, Monforte P. 2016. Theoretical and experimental study of Gaussian plume model in small scale system energy. Procedia 101:58–65; *https://doi.org/10.1016/j.egypro.2016.11.008*.

Cardoso-Saldaña FJ, Pierce K, Chen Q, Kimura Y, Allen DTA. 2021. Searchable database for prediction of emission compositions from upstream oil and gas sources. Environ Sci Technol 55:3210–3218; *https://doi.org/10.1021/acs.est.0c05925*.

Cushing LJ, Chau K, Franklin M, Johnston JE. 2021. Up in smoke: characterizing the population exposed to flaring from unconventional oil and gas development in the contiguous US. Environ Res Lett 16:034032; *https://doi.org/10.1088/1748-9326/abd3d4*

Environmental Emergency Response Section. Training on Atmospheric Dispersion in Urban Environments. Available: *https://eer.cmc.ec.gc.ca/projets/CUDM/urbanDispersion_page3.html* [accessed 18 January 2025].

Gilmore EA, Heo J, Muller NZ, Tessum CW, Hill JD, Marshall JD, et al. 2019. An inter-comparison of the social costs of air quality from reduced-complexity models. Environ Res Lett 14:074016; *https://doi.org/10.1088/1748-9326/ab1ab5*.

Gonzalez DJX, Francis CK, Shaw GM, Cullen MR, Baiocchi M, Burke M. 2022. Upstream oil and gas production and ambient air pollution in California. Sci Total Environ 806:150298; *https://doi.org/10.1016/j.scitotenv.2021.150298*.

Gonzalez DJX, Nardone A, Nguyen, AV, Morello-Frosch R, Casey JA. 2023. Historic redlining and the siting of oil and gas wells in the United States. J Expo Sci Environ Epidemiol 33:76–83; *https://doi.org/10.1038/s41370-022-00434-9*.

Hoang TT, Rathod RA, Rosales O, Castellanos MI, Schraw JM, Burgess E, et al. 2024. Residential proximity to oil and gas developments and childhood cancer survival. Cancer 130: 3724–3733, *https://doi.org/10.1002/cncr.35449*.

Kanayankottupoyil J, John K. 2025. Assessing the impact of oil and gas activities on ambient hydrocarbon concentrations in north Texas: a retrospective analysis from 2000 to 2022. Atmos Environ 340:120907; *https://doi.org/10.1016/j.atmosenv.2024.120907*.

Koehler K, Ellis JH, Casey JA, Manthos D, Bandeen-Roche K, Platt R, et al. 2018. Exposure assessment using secondary data sources in unconventional natural gas development and health studies. Environ Sci Technol 52:6061–6069; *https://doi.org/10.1021/acs.est.8b00507*.

Ku I-T, Zhou Y, Hecobian A, Benedict K, Buck B, Lachenmayer E, et al. 2024. Air quality impacts from the development of unconventional oil and gas well pads: air toxics and other volatile organic compounds. Atmos Environ 317:120187; *https://doi.org/10.1016/j.atmosenv.2023.120187*.

Li L, Blomberg AJ, Spengler JD, Coull BA, Schwartz JD, Koutrakis P. 2020. Unconventional oil and gas development and ambient particle radioactivity. Nat Commun 11:5002; *https://doi.org/10.1038/s41467-020-18226-w*.

Modi M, Kimura Y, Hildebrandt-Ruiz L, Allen DT. 2025. Fine-scale spatial and temporal allocation of nitrogen oxides emissions from unconventional oil and gas development can result in increased predicted regional ozone formation. ACS ES&T Air 2:130–140; *https://doi.org/10.1021/acsestair.4c00077*.

Scott HM, Soskolne CL, Wayne-Martin S, Ellehoj EA, Coppock RW, Guidotti TL, et al. 2003. Comparison of two atmospheric-dispersion models to assess farm-site exposure to sour-gas processing-plant emissions. Prev Vet Med 57:15–34; *https://doi.org/10.1016/S0167-5877(02)00207-6*.

Seinfeld JH, Pandis SN. 2006. Atmospheric chemistry and physics. In: Air Pollution to Climate Change. Hoboken, NJ: Wiley.

Shan X, Casey JA, Shearston JA, Henneman LRF. 2024. Methods for quantifying source-specific air pollution exposure to serve epidemiology, risk assessment, and environmental justice. GeoHealth 8:e2024GH001188; *https://doi.org/10.1029/2024GH001188*.

Texas Commission on Environmental Quality (TCEQ). Texas Commission on Environmental Quality Air Monitoring. Available: *https://www.tceq.texas.gov/airquality* [accessed 27 January 2025].

United States Census Bureau. Measuring America's People and Economy. Available: *https://www.census.gov/en.html* [accessed 6 October 2022].

US Environmental Protection Agency (US EPA). 2024. Technical Support Document. EPA's Air Toxics Screening Assessment 2020 AirToxScreen TSD. Available: *https://www.epa.gov/system/files/documents/2024-05/airtoxscreen_2020-tsd.pdf* [accessed 16 January 2025].

CHAPTER 10: SUMMARY OF PROJECT FINDINGS AND IMPLICATIONS (SYNTHESIS)

In this project, we developed the TRACER model to assess exposures to air pollutants from UOGD and to inform future health studies. The model combines detailed emissions modeling with dispersion modeling to predict concentrations for various pollutants at receptor sites (**Figure 10-1**).

The project's main focus was on the Eagle Ford Shale in south-central Texas, a large oil and gas production region that includes the production of dry gas, wet gas, and oil. This heterogeneity of production types makes the Eagle Ford Shale a microcosm of UOGD sites across the United States. The project was later expanded to also include mobile measurements in the Permian Basin and modeling in the Marcellus Shale oil and gas production region.

The emissions model we developed can also be coupled with chemical transport models to evaluate impacts of UOGD emissions more regionally, and to account for impacts of chemical transformation on air quality and human exposure. In this work, we coupled the emissions model to the chemical transport model CAMx to evaluate the impacts of UOGD emissions on ozone, a secondary pollutant.

We also conducted targeted stationary and mobile measurements in the Eagle Ford Shale to evaluate emissions from flaring, which were then included as inputs to the model, and to provide a comprehensive dataset for model evaluation. We conducted measurements as well in the Permian Basin near the HEI-funded stationary monitoring site located in Loving, New Mexico. Although the measurements in the Permian Basin provided insights into the spatial variability of measurements in the region, the opportunity to colocate with the stationary monitoring site, and the opportunity to compare measurements with those in the Eagle Ford Shale, we did not conduct any modeling in the Permian Basin because modeling in that region was outside the scope of the current report. We are currently conducting modeling work in the Permian Basin, with results to be published later in 2026.

SUMMARY OF KEY FINDINGS

We found that destruction efficiencies and emission ratios from flares are highly variable, which led us to use median values in emissions modeling (Chapter 3). Ambient concentrations at receptor sites, and therefore population exposures, have high diurnal variability, with the highest concentrations and exposures observed at night. Elevated concentrations observed at night can be due to both large nonroutine emissions events and routine emissions, coupled with wind

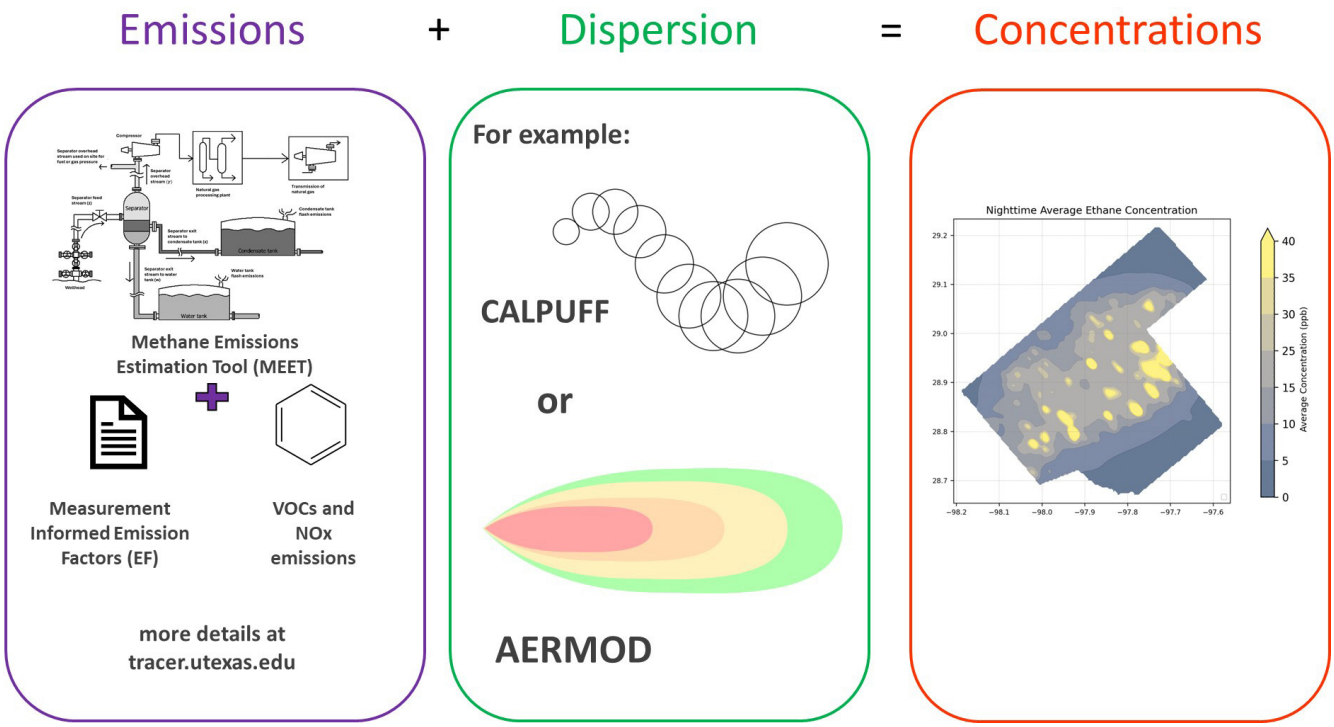

Figure 10-1. Schematic of the TRACER model, combining emissions and dispersion modeling to predict concentrations for various pollutants at receptor sites. The TRACER model was expanded and improved from an existing model for methane emissions.

speeds and atmospheric stability conditions that are conducive to producing high concentrations. In the Permian Basin, we observed much higher concentrations of hydrogen sulfide than in the Eagle Ford Shale, suggestive of differences in oil and gas composition (Chapter 4). We also observed high concentrations of ozone in the Permian, consistent with measurements made at the stationary monitoring site.

Our modeling analyses show that thousands of UOGD sites contribute to concentrations observed at one particular receptor site and, therefore, to population exposures. For example, in the Eagle Ford Shale, UOGD sources within 5, 10, 20, and 50 km of a receptor site accounted for 38%, 67%, 88%, and 99% of average concentrations, respectively (Chapter 6). Furthermore, our emissions modeling demonstrates that UOGD emission sources have complex spatial and temporal distributions and that UOGD emission sources can have highly variable compositions (Chapter 5). Thus, modeling to predict population exposures to UOGD emissions needs to account for myriad sources and spatial and temporal distribution of emissions, as well as the chemical complexity, and is therefore computationally quite expensive. The TRACER model we have developed makes these complex predictions possible.

Different approaches can be used to model the dispersion of pollutants after they are emitted. In this work, we evaluated three commonly used dispersion models (CALPUFF, AERMOD, and Gaussian plume) for their performance in estimating observed concentrations at a single receptor site (Chapter 8). We also evaluated two additional, lower-complexity models for their performance in estimating concentrations across Karnes County (Chapter 9). These lower-complexity models included IDW and IDWmet. in the predominant wind direction. As demonstrated by several performance metrics, CALPUFF generally performs best and is also the most computationally expensive model. In the reduced-complexity modeling, accounting for wind speed and direction substantially improves the ability to capture spatial-temporal variability at a central measurement site, but doing so generally does not reduce bias in modeled concentrations.

Our exposure analyses in Karnes County in the Eagle Ford Shale revealed that all populations experience higher exposure from UOGD at night than during the day (Chapter 9). In Karnes County, particularly the Hispanic and the middle-income population (defined as between the 25th and 75th percentiles) experience higher exposure.

RECOMMENDATIONS FOR FUTURE WORK

We recommend that future mobile measurements in UOGD regions include those for ethane and light hydrocarbons (e.g., propane, butane) for enhanced source apportionment of UOGD sources. Attaining these measurements will require installing a gas chromatograph on a mobile measurement platform, which has not been done before, to our knowledge, but should be possible on a larger mobile measurement platform. Ethane can be measured with a dedicated instrument purchased for this purpose. Future measurements are needed to evaluate emissions from particular sources on the well sites, ideally with operator cooperation, knowledge of activities at the well site, and access to the site so that measurements can be taken closer to the sources.

These proposed future measurements, as well as measurements conducted as part of the work described in this report, are not designed to assess exposure directly. Instead, exposures are assessed using models (emissions models coupled with dispersion or chemical transport models), and measurements are used to provide input to models and to provide a comprehensive dataset for model performance evaluation.

This project conducted modeling most comprehensively for the Eagle Ford Shale region. As additional future work, we suggest modeling in other UOGD regions in the United States. While the model development conducted as part of this project has laid the groundwork for model implementation in other regions, differences in equipment used, industry practices, oil and gas composition, topology, and meteorology, among others, suggest that implementation of this model in other regions will still require substantial effort. Measurements of source emission factors suggested above can be used to improve modeling in the Eagle Ford Shale and elsewhere; therefore, updated modeling in the Eagle Ford Shale (after implementation of additional emission factors and emission composition) would also be valuable. Because our work focused on evaluating community exposures, we did not concentrate on modeling the dispersion of pollutants from a single well site. However, the model could be used to model dispersion of emissions from a well site, and the results of such modeling activities could be used to evaluate the impacts of setback distances. However, as we have pointed out in this report, exposure at a particular receptor point might be affected by UOGD sources up to 50 km away. As such, implementation of setback distances may not be sufficient to protect communities from exposure to UOGD emissions.

Our project focused on exposure analysis in Karnes County, Texas — the county with both the highest well density and the highest population density in the Eagle Ford Shale — where we also conducted the most detailed emissions and dispersion modeling. Future work could focus on evaluating exposures in other Eagle Ford Shale counties or elsewhere in the United States, following completion of the corresponding emissions modeling.

MAIN STRENGTHS AND LIMITATIONS OF THE WORK

We have developed a powerful model to evaluate community exposures to pollutants of concern to human health emitted from UOGD. The geographical scope of our exposure

analysis was limited given resource and time constraints. A limitation of our emissions modeling is the paucity of data on emission composition from different UOGD sources. Our measurements were also limited by not having the capability of measuring ethane and small alkanes on our mobile platform. As suggested above, these limitations can be addressed in future work.

Despite these limitations, the measurements we conducted provided unprecedented insights into the composition of emissions from unassisted flares in UOGD regions, and the dataset we collected at the stationary location allowed detailed model performance evaluation. The modeling tools we have developed, and the modeling we have conducted, enable detailed evaluation of community exposures to UOGD emissions. The TRACER model can be used by decision-makers to inform policies aimed at reducing human exposure to pollutants from UOGD.

DATA AVAILABILITY STATEMENT

Data described in this report are available *here* or via request to the principal investigator (Lea Hildebrandt Ruiz, *lhr@che.utexas.edu*). Available data include time series of measurements and spatial and temporal pollutant concentrations in the Eagle Ford Shale.

Additional data and details on the topics discussed in Chapters 5, 6, 7, 8, and 9 are also available via the corresponding published manuscripts. Manuscripts describing results from Chapters 3 and 4 are in preparation.

- **Chapter 5**
  Chen Q, Raksi N, Niewenhous L, Almasalha SJ, Graves JD, Brown V, et al. 2025. Spatial and temporal variability in atmospheric emissions from oil and gas sector sources in the Marcellus production region. Atmosphere 16:1048; *https://doi.org/10.3390/atmos16091048*.
- **Chapter 6**
  Graves J, Kimura Y, Modi M, Stokes S, Meyer M, Hildebrandt Ruiz L, et al. 2025. Source attribution of elevated ethane concentrations detected by regional monitors in oil and gas production regions. ACS ES&T Air 2:2038–2046; *https://doi.org/10.1021/acsestair.5c00235*.
- **Chapter 7**
  Modi M, Kimura Y, Hildebrandt Ruiz L, Allen DT. 2025. Fine-scale spatial and temporal allocation of nitrogen oxides emissions from unconventional oil and gas development can result in increased predicted regional ozone formation. ACS ES&T Air 2:130–140; *https://doi.org/10.1021/acsestair.4c00077*.
- **Chapter 8**
  Graves J, Kimura Y, Modi M, Stokes S, Meyer N, Hildebrandt Ruiz L, et al. [In review]. Performance of dispersion models in predicting ambient ethane concentrations at a regional air quality monitor in an oil and gas producing region. ACS Environ Au.
- **Chapter 9**
  Bohloul M, Rasel M, Hildebrandt Ruiz L, Allen DT, Kimura Y, Graves J, et al. [In review]. Spatiotemporal exposure assessment of air pollution from unconventional oil and gas development in the Eagle Ford Shale, Texas, using multiple dispersion models. ACS ES&T Air.

ACKNOWLEDGMENTS

We thank the city of Karnes City for its hospitality in allowing us to take measurements on its property. We are grateful to several individuals for logistical support, especially Fernando Rios and Kirby Haertner. We thank Dr. Nirvan Bhattacharyya for assistance during the Spring 2023 measurements. We thank the TCEQ for allowing us to locate our instrumentation adjacent to their site as well as for publicly sharing data collected at their monitoring stations. We also thank the Center for Energy and Environmental Resources at The University of Texas at Austin for administrative support.

HEI QUALITY ASSURANCE STATEMENT

The conduct of this study was subjected to independent audits by RTI International staff members Dr. David Wilson, Dr. Charbel Harb, and Mr. Ryan Chartier. These staff members are experienced in quality assurance (QA) oversight for air quality monitoring, modeling, and exposure assessment, and statistical modeling.

The QA oversight program consisted of a remote audit of the draft final report and the data processing steps. Key details of the dates of the audit and the reviews performed are listed below.

Audit: Final Remote Audit

Date: March 2025 – April 2025

Remarks: The final remote audit consisted of two parts: (1) review of the draft final project report and (2) audit of data processing steps. The review of the draft final report focused on ensuring that the methods are well documented and the report is easy to understand. The review also examined whether the report highlighted key study findings and whether the limitations were supported by the data presented. The data audit included a review of the datasets and codes for data reduction, processing, and analysis, and comparison of the data outputs with reported data. This portion of the audit was restricted to the key components of the study and associated findings. Selected codes for air quality data reduction and modeling were sent to RTI for review.

The codes were reviewed at RTI to verify, to the extent feasible, linkages between the various scripts; confirmation of the models and model variables reported; and verification of

key tables, figures, and data outputs. The codes appear to be largely consistent with the models described in the report and follow the overall model development procedure described. The values themselves were verified by RTI using the data and scripts provided by the investigators.

Except for very few minor discrepancies, most of which were superficial in nature, no major quality-related issues were identified from the review of the codes, data, and the report. Recommendations were made to address noted discrepancies and typographical errors, and included general edits for improved clarity. Those recommendations were addressed in the final report.

A written report was provided to HEI. The QA oversight audit demonstrated that the study was conducted according to the study protocol. The final report appears to be representative of the study conducted.

David Wilson, PhD, Statistician, Quality Assurance Auditor

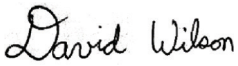

Charbel Harb, PhD, Environmental Scientist, Quality Assurance Auditor

Ryan Chartier, MS, Air Quality and Exposure Scientist, Lead Quality Assurance Auditor

Date: October 1, 2025

ADDITIONAL MATERIALS ON THE HEI WEBSITE

Additional Materials A through F contain material not included in the main report. They are available on the HEI website at *www.healtheffects.org/publications.*

Additional Materials A: Chapter 3

Additional Materials B: Chapter 4

Additional Materials C: Chapter 5

Additional Materials D: Chapter 6

Additional Materials E: Chapter 7

Additional Materials F: Chapter 9

ABOUT THE AUTHORS

Lea Hildebrandt Ruiz is an associate professor in the McKetta Department of Chemical Engineering at The University of Texas at Austin (UT Austin). She received her PhD in chemical engineering and engineering & public policy from Carnegie Mellon University in 2011. Her research expertise includes atmospheric chemistry and anthropogenic influences on air quality and human exposure in indoor and outdoor environments. Her team's measurements use advanced mass spectrometry methods on mobile and stationary measurement platforms and laboratory chamber experiments. Lea has been the lead investigator for multiple air quality studies in indoor and outdoor environments, including studies on air quality impacts of UOGD, wildfires, cooking, and disinfection. The quality of her research has been recognized by awards from the American Chemical Society, the American Institute of Chemical Engineers, and the US National Science Foundation. She is the author of over 70 papers and has served on the Science Advisory Board of the US EPA, on the Board of Directors of the American Association for Aerosol Research, and as graduate advisor and chair of the graduate studies committee at UT Austin.

David Allen is the Norbert Dittrich-Welch Chair Professor in the McKetta Department of Chemical Engineering at UT Austin, and codirector of the Energy Emissions Modeling and Data Lab, where he leads a team of over 40 researchers and staff. He is also the co-director of UT Austin's Center for Energy Environmental Systems Analysis. He received his MS and PhD in chemical engineering from the California Institute of Technology. David is the author of seven books and over 250 papers, primarily in the areas of urban air quality, the engineering of sustainable systems, and the development of materials for environmental and engineering education. He has been a lead investigator for multiple air quality measurement studies, which have had a substantial impact on the direction of air quality policies. He directs the Air Quality Research Program for the State of Texas, and he is the founding editor-in-chief of the American Chemical Society's journal *ACS Sustainable Chemistry & Engineering.* He has developed environmental educational materials for engineering curricula and for the university's core curriculum, as well as engineering education materials for high school students. He led the development of a yearlong high school engineering course, Engineer Your World, which is used in hundreds of high schools nationwide.

Pawel Misztal is an assistant professor in the Maseeh Department of Civil, Architectural, and Environmental Engineering at UT Austin. Misztal received his MSc in analytical chemistry from Maria Curie-Sklodowska University in Poland and his PhD in chemistry from the University of Edinburgh. His

research integrates atmospheric chemistry, air quality engineering, and human exposure science using high-resolution mobile and stationary platforms. He specializes in real-time measurements of volatile organic compounds and other trace gases, particulate matter, and ozone precursors across diverse environments, outdoors and indoors. Pawel has led research funded by the A.P. Sloan Foundation, the US National Science Foundation, the US Department of Energy, and the US Department of Homeland Security, and has conducted major field campaigns in collaboration with the California Air Resources Board, TCEQ, and other agencies. He has authored over 60 peer-reviewed publications, serves as associate editor for Frontiers, and reviews proposals for the US EPA and other organizations.

Elizabeth Matsui is a professor of population health and pediatrics, associate dean for faculty academic affairs, and director of the Center for Health and Environment: Education and Research at Dell Medical School at UT Austin. She received her MD from Vanderbilt University and completed her residency in pediatrics at the University of California at San Francisco in 1996. She joined the faculty at Johns Hopkins in 2003 and was promoted to professor in 2015 before joining the faculty at Dell Medical School at UT Austin in 2018. Elizabeth is a pediatric allergist–immunologist and epidemiologist, and a leading international expert on environmental exposures and their effects on asthma and other allergic conditions.

Roger Peng is a professor of statistics and data sciences at UT Austin and has published extensively in the area of indoor and outdoor air pollution and health, both in the substantive and the methodological literature. He received his MS and PhD in statistics from the University of California, Los Angeles. He has developed novel approaches to integrating complex national databases for assessing population health effects of environmental exposures and is the author of over a dozen software packages implementing statistical methods for environmental studies, methods for reproducible research, and data distribution tools. Roger's work is highly interdisciplinary and has resulted in contributions to both the scientific and statistical methods literature. He has been a principal investigator on grants from the National Institutes of Health and the US EPA to develop important evidence about the health effects of PM and oxidant gases. His current work also focuses on the development of novel concepts for characterizing data analytic processes and for building theoretical frameworks for data analysis.

Yosuke Kimura is a research associate at the Center for Energy and Environmental Systems Analysis at UT Austin. He received his MS in sanitary engineering from Kyoto University and his PhD in civil engineering from UT Austin. His research experience includes air quality modeling-related activities, such as photochemical modeling and emissions modeling. Yosuke has been participating in various emissions modeling framework development, such as the MEET and the Fire Inventory from the National Center for Atmospheric Research.

David Sullivan is a research associate in the Center for Energy and Environmental Resources at UT Austin. He received his MS in operations research and industrial engineering and his PhD in management science and information systems from UT Austin. He specializes in ambient monitoring projects measuring speciated hydrocarbons, speciated particulate matter, and other pollutants around the State of Texas, as well as statistical analysis of ambient pollution and meteorological data. In an earlier career, David was a team leader and section manager at the TCEQ. He is a member of the American Statistical Association and the Air & Waste Management Association.

Shannon Stokes joined the Center for Energy and Environmental Resources at UT Austin in 2019 and the Energy Emissions Modeling and Data Lab in 2024. She received her PhD in environmental engineering from UT Austin. She has contributed to and managed projects involving multiple universities, oil and gas operators, and consulting companies; has worked on projects with state and federal funding; and has extensive experience proposing and planning measurement campaigns, incorporating insights into the measurement technology capabilities and the methane and VOC emission sources from oil and gas and nonoil and gas sources. Shannon has experience exploring a variety of data sources, including public databases (Greenhouse Gas Program reporting websites, gridded inventories, and state and federal permitting sites) and published data from independent research (emissions observed in past campaigns) to obtain information to inform current projects. She also has experience estimating emissions using a variety of tools — from simple production-based estimates to time series predictions using MEET — and using these emissions estimates to interpret data from measurement campaigns and other sources.

Elena McDonald-Buller is a senior research engineer (retired) at the Center for Energy and Environmental Systems Analysis at UT Austin with more than 25 years of experience. Her research interests include air quality modeling of gas-phase and particulate air pollution; analysis of air quality and meteorological measurements from surface, aircraft, and satellite platforms; emissions inventory assessment and development; domestic and international energy system transitions and policy impacts; and the influences of land use/land cover change and extreme weather events on air quality. Elena has served as lead or co-lead investigator on numerous projects for the US EPA, US National Science Foundation, US Department of Energy, TCEQ, and local governments in Texas. She has served as a project manager for the Texas Air Quality Research Program for more than a decade.

Leif Jahn is a physical scientist at the US EPA. He received his PhD in chemistry at Carnegie Mellon University, studying the chemical and physical aging of biomass burning aerosol and how these changes impact reactivity and ice nucleation ability. He specializes in using on- and offline techniques, particularly mass spectrometry, to characterize volatile organic compounds and particles in the atmosphere. Before joining the US EPA, Leif worked as a research scientist and postdoctoral research associate in the groups of principal investigators Lea Hildebrandt Ruiz and Pawel Misztal, contributing to numerous projects with a research focus on characterizing VOC emissions from varied sources, VOC oxidation processes, and secondary organic aerosol formation.

Mrinali Modi is a postdoctoral fellow in the McKetta Department of Chemical Engineering at UT Austin, where she works on characterizing emissions from carbon capture systems utilizing amine scrubbing. She received her PhD in chemical engineering at UT Austin, where her research focused on assessing the impacts of spatially and temporally resolved emissions from UOGD on air quality and community exposures. Mrinali's research experience spans greenhouse gas emissions estimation, atmospheric modeling, and geospatial and statistical analysis, supporting environmental challenges related to air quality, climate, and public health across diverse geographic regions. She has contributed to global methane emissions assessments, uncertainty quantification, and reconciliation efforts through the United Nations Environment Programme's Oil and Gas Methane Partnership 2.0.

Joel Graves is a doctoral candidate advised by David Allen in the McKetta Department of Chemical Engineering at UT Austin. His research uses emissions and dispersion modeling to characterize ambient air quality in oil and gas production regions. Joel has experience with several dispersion models, including CALPUFF and AERMOD, and their associated preprocessors. He has served as the outreach chair and president of the Graduate Leadership Council in the McKetta Department of Chemical Engineering at UT Austin.

Kat Konon is a doctoral candidate in Lea Hildebrandt Ruiz's research group. Before attending UT Austin, she completed her undergraduate degree in chemical engineering at the University of Connecticut and then worked for a year at an environmental consulting company. Her research focuses on anthropogenic air quality impacts in outdoor and indoor environments. Kat has conducted gas and particle-phase measurements in UOGD regions, coastal communities, and areas affected by wildfires. In the lab, she studies the impacts of chlorine chemistry on the formation of secondary pollutants using an environmental chamber and has presented her work at annual conferences hosted by HEI, the American Association for Aerosol Research, and the American Geophysical Union.

Lea El Khoury is a doctoral candidate in Lea Hildebrandt Ruiz's research group. She received her BS in chemical engineering from the Holy Spirit University of Kaslik, Lebanon. Her research involves studying the effects of air pollutants and their reactions in the atmosphere on air quality and environmental justice. Her thesis contributes to the understanding of anthropogenic influences on air quality, from personal and industrial emissions. Lea has hands-on experience with fieldwork, laboratory techniques, instrumentation, and data analysis to quantify the impact of aerosol and gas pollutants and has presented her work at the HEI and American Association for Aerosol Research annual conferences.

Pearl Abue received her PhD in chemical engineering from UT Austin in 2024. During her doctoral studies, she worked with Lea Hildebrandt Ruiz's research group on evaluating indoor and outdoor air quality using advanced mass spectrometry in lab environmental chamber experiments and stationary field measurements. She also co-investigated research involving indoor disinfection and unconventional oil and gas drilling emissions measurements. With a strong research background, Pearl has coauthored several publications. Currently, she does most of her work in McKinsey & Company's Global Energy & Materials Practice, where they apply their expertise to address complex challenges in the energy and materials sectors.

Shihao Zhai is a doctoral candidate in Lea Hildebrandt Ruiz's research group. Before attending UT Austin, he earned his bachelor's degree in chemical engineering from the University of Connecticut. His research focuses on quantifying anthropogenic emissions and their effects on regional and local air quality. He has conducted field measurements of gas- and particle-phase pollutants in regions with UOGD, as well as in coastal, urban, and wildfire-affected areas. In the lab, Shihao studies how different volatile organic compounds, in combination with chlorine and other atmospheric oxidants, can contribute to particle formation. He also serves as the Enrichment Chair of the Graduate Leadership Council in the McKetta Department of Chemical Engineering at UT Austin.

Austin Turner is a current master's student working as a graduate assistant in the Farquhar Lab at the University of Maryland, College Park. He previously worked as a research assistant in the Hildebrandt Ruiz research group at UT Austin, where he received his BS in geology and chemistry. Austin conducted field research for three separate campaigns in both the Eagle Ford and Permian Basin oil fields, assessing the air quality impacts of conventional and UOGD. As part of these projects, he assisted with data analysis, instrument maintenance, and both stationary and mobile field measurements of primary and secondary pollutants.

Sewar Almasalha is a PhD student in David Allen's group at UT Austin. She received her BS in chemical engineering from Texas A&M University. Her research explores methods for the quantification of emission events from oil and natural gas systems, as well as describing their spatial and temporal patterns and impacts on local and regional air pollutant formation. Sewar is interested in developing accessible analytical frameworks for measurement-informed emission estimation and has presented her work at the annual HEI and American Geophysical Union conferences.

Chou-Hsien "Sam" Lin is a third-year PhD student and graduate research assistant in Pawel Misztal's research group at UT Austin. He received his BS in architectural engineering from UT Austin and now focuses on the intersection between air quality and human health in his graduate work. Sam has conducted field measurements in regions associated with wildfires, UOGDs, and heavy industrial emissions and has presented his work at the conferences of the HEI, the American Geophysical Union, and the International Society of Indoor Air Quality and Climate.

Evelyn Deveraux is a PhD student advised by Pawel Misztal in the Maseeh Department of Civil, Architectural, and Environmental Engineering at UT Austin. She received her BS in environmental engineering at UT Austin in 2021. She has contributed to field measurement campaigns investigating emissions of volatile organic compounds and other trace gases from oil and gas infrastructure, wildfires, and battery fires. Evelyn has performed experiments investigating optimization methods for the mass spectrometry instrument she operates during field campaigns. She has also contributed to research characterizing emissions from humans in indoor environments and emissions associated with chemosensory communication in animal models.

Daniel Blomdahl is a postdoctoral fellow working with Professor Peter DeCarlo in the Environmental Health and Engineering Department at Johns Hopkins University. He received his PhD in civil engineering from UT Austin in 2024. His research expertise is characterizing volatile trace gases in various environments, including urban, rural, and indoor regimes and near emission sources such as oil and gas extraction and petrochemical refineries. Daniel uses mass spectrometry instruments on both mobile and stationary platforms, and his measurements of air toxics in fence-line communities are used in health risk models and assessments.

Daniel Sung is an MS student working with Pawel Misztal at UT Austin, where he earned his BS in environmental engineering. His primary research focuses on the spatiotemporal analysis of ambient air quality. He has participated in multiple field campaigns across the Permian Basin region, San Diego, El Paso, Los Angeles, and Beaumont. In addition to outdoor air quality, Daniel is also interested in indoor air quality driven by human activity and has presented his work at the American Geophysical Union Conference.

Qining Chen is a research engineering scientist at the Center for Energy and Environmental Systems Analysis and the Energy Emissions Modeling Data Lab at UT Austin. She earned her PhD in chemical engineering from UT Austin in 2021. Her research focuses on the measurement, modeling, and assessment of greenhouse gas emissions, particularly methane from oil and gas supply chains and chemical production systems. She has experience in developing high-resolution spatial and temporal greenhouse gas emissions inventories and advancing methodologies for life-cycle assessment of greenhouse gas emissions across the oil and gas supply chains. Qining has also contributed to detecting and analyzing methane emission events using continuous monitoring systems in oil and gas production fields. Her work includes the design and optimization of sensor networks deployed in the Permian Basin in Texas, and the development of algorithms for sensor data processing and emission event analytics.

Lucas Henneman is an assistant professor of environmental engineering at George Mason University in Fairfax, Virginia. He completed his postdoctoral research at Harvard School of Public Health (2017–2020) and earned his PhD at Georgia Tech (2017). He studies relationships between air pollution emissions sources, air quality, human exposure (including inequities), and human health. His recent work involves developing and applying models that enable exposure studies of large numbers of individual air pollution sources. Lucas is the primary investigator on a HEI Rosenblith Award quantifying source contributions to $PM_{2.5}$ across the United States.

Munshi Md Rasel is a process engineer at the Norman M. Cole Jr. Water Recycling Facility in Fairfax County, Virginia. He earned his PhD in environmental engineering from George Mason University in December 2024, where his research integrated atmospheric modeling with exposure disparity analysis. His expertise lies at the intersection of air pollution modeling, human exposure assessment, and environmental health. His work focuses on understanding how emissions from industrial and energy-related sources contribute to ambient air pollution and disparities in population exposure. In his current role, Munshi applies data-driven process optimization and regulatory compliance strategies to enhance wastewater treatment performance and sustainability.

Mohammadreza Bohloul is a PhD student in environmental engineering at George Mason University, working under the supervision of Lucas Henneman. His research focuses on air pollution modeling and exposure assessment. He integrates atmospheric dispersion modeling with population-weighted exposure analysis to evaluate the health implications of air pollution across diverse spatial and temporal scales. Before beginning his doctoral studies, he served as a researcher and lecturer in chemical engineering and worked as a process engineer. He is the author of seven papers and has presented his work at the Community Modeling and Analysis System International Conference. In addition to his research

contributions, he has served as a peer reviewer for three international journals and major conferences, including the 2025 International Society of Exposure Science and the International Society for Environmental Epidemiology Annual Conference. Mohammadreza is a coauthor of two technical books on air pollution dispersion modeling and adsorption process simulation and a member of the American Academy of Environmental Engineers and Scientists.

OTHER PUBLICATIONS RESULTING FROM THIS RESEARCH

Bohloul M, Rasel M, Hildebrandt Ruiz L, Allen DT, Kimura Y, Graves J, et al. [In review]. Spatiotemporal exposure assessment of air pollution from unconventional oil and gas development in the Eagle Ford Shale, Texas, using multiple dispersion models. ACS ES&T Air.

Chen Q, Raksi N, Niewenhous L, Almasalha SJ, Graves JD, Brown V, et al. 2025. Spatial and temporal variability in atmospheric emissions from oil and gas sector sources in the Marcellus production region. Atmosphere 16:1048; *https://doi.org/10.3390/atmos16091048*.

Graves J, Kimura Y, Modi M, Stokes S, Meyer M, Hildebrandt Ruiz L, et al. 2025. Source attribution of elevated ethane concentrations detected by regional monitors in oil and gas production regions. ACS ES&T Air 2:2038–2046, *https://doi.org/10.1021/acsestair.5c00235*.

Graves J, Kimura Y, Modi M, Stokes S, Meyer N, Hildebrandt Ruiz L, et al. 2026. Performance of dispersion models in predicting ambient ethane concentrations at a regional air quality monitor in an oil and gas producing region. ACS Environ Au [preprint]; *https://chemrxiv.org/doi/full/10.26434/chemrxiv-2025-xkhh9*.

Modi M, Kimura Y, Hildebrandt Ruiz L, Allen DT. 2025. Fine-scale spatial and temporal allocation of nitrogen oxides emissions from unconventional oil and gas development can result in increased predicted regional ozone formation. ACS ES&T Air 2:130–140; *https://doi.org/10.1021/acsestair.4c00077*.

Research Report 240, *Predictive, Source-Oriented Modeling and Measurements to Evaluate Community Exposures to Air Pollutants and Noise from Unconventional Oil and Gas Development,* by L. Hildebrandt Ruiz et al.

INTRODUCTION

The scale and rate of onshore oil and natural gas development in the United States since the early 2000s differ markedly from earlier periods, driven by technological changes involving increased use of hydraulic fracturing and horizontal drilling. Although hydraulic fracturing has captured much public attention, the process itself is not new, nor are horizontal drilling or the extraction of oil and gas from unconventional formations, such as tight (i.e., low permeability) sandstone and shale. What is new is the use of high-volume (millions of gallons of water per well) multistage hydraulic fracturing combined with horizontal drilling (thousands of feet in length).

Unconventional oil and natural gas development (UOGD*) has been associated with a wide range of potential exposures to chemical agents (e.g., radioactive material, those found in wastewater, and odorous compounds) and nonchemical agents (e.g., noise, light, and vibration). The rapid expansion of this development has caused concerns about its potential effects on human health and has created knowledge gaps about exposures that must be addressed to better understand potential health effects on communities.

In August 2020, HEI Energy issued *Request for Applications E20-1*: Community Exposures Associated with Unconventional Oil and Natural Gas Development. HEI sought to fund studies that would apply a combination of approaches to quantify the spatial and temporal variability in population exposures to UOGD-generated outdoor air pollutants and noise (see Preface).

Dr. Hildebrandt Ruiz was one of three investigators funded under this RFA. Hildebrandt Ruiz and colleagues at The University of Texas at Austin proposed to develop a model to assess exposures to air pollution from UOGD and to inform future health studies. The study included extensive monitoring and modeling of various air pollutants and focused originally on the Eagle Ford Shale in Texas, a large oil and gas production region. The study was later extended to two other UOGD regions, in close collaboration with the other two studies funded under this RFA.

The HEI Energy Research Committee recommended the study for funding because it had several strong features. In particular, the Research Committee was enthusiastic about the proposed model and the detailed monitoring using state-of-the-art instruments. The Committee also thought that Hildebrandt Ruiz had assembled a strong team with demonstrated air quality monitoring and modeling expertise.

This Commentary provides the HEI Energy Review Committee's independent evaluation of the study. It is intended to aid the sponsors of HEI and the public by highlighting both the strengths and limitations of the study and by placing the results presented in the Investigators' Report into a broader scientific and regulatory context.

SCIENTIFIC AND REGULATORY BACKGROUND

UOGD OVERVIEW

UOGD processes occur on and off the well pad and include the following:

Field development: Exploration, pad preparation, vertical and horizontal drilling, and well completion (casing and cementing, perforating, acidizing, hydraulic fracturing, flowback, and well testing) in preparation for production and management of wastes.

Production operations: Extraction, gathering, processing, and field compression of gas; extraction and processing of oil and natural gas condensates; management of wastes and produced water that is naturally present in underground water formations in the soil and brought to the surface during oil and gas extraction; and construction and operation of field production facilities.

Post-production: Well closure and land reclamation.

Some UOGD operations are regulated at the federal level under the Clean Air Act, the Clean Water Act, and the Safe Drinking Water Act, whereas state authorities play a major role in governing UOGD more generally. UOGD-related rules vary among states, with some defining minimum setback

Dr. Lea Hildebrandt Ruiz's 2-year study, "Predictive, Source-Oriented Modeling and Measurements to Evaluate Community Exposures to Air Pollutants and Noise from Unconventional Oil and Gas Development," began in January 2022. Total expenditures were $3,419,798. The draft Investigators' Report from Hildebrandt Ruiz and colleagues was received for review in January 2025. A revised report was received in June 2025. A second revised report, received in July 2025, was accepted by the HEI Energy Review Committee in August 2025.

During the review process, the HEI Energy Review Committee and the investigators had the opportunity to exchange comments and clarify issues in both the Investigators' Report and the Review Committee's Commentary. This Commentary has not been reviewed by public or private party institutions, including those that support HEI Energy, and may not reflect the views of these parties; thus, no endorsements by them should be inferred.

* A list of abbreviations and other terms appears at the end of this report.

distances between UOGD sites and specific land uses such as residences and schools to protect local populations.

UOGD PROCESSES

Different UOGD processes release air pollution, noise, and other chemical and nonchemical agents into the environment (e.g., outdoor air, soil, surface water, and groundwater) that are complex and highly variable. These releases and resulting human exposures are caused by numerous UOGD process-related factors, including variation in operator practices and regulatory requirements. Releases can also happen because of accidental spills and leaks. The level of UOGD activity can vary widely between and across regions and over time in response to fluctuating market conditions.

The well-pad preparation phase involves land clearing and other activities similar to many types of construction. Various chemicals are used to drill, develop, and complete the well. The completion step often includes the process of hydraulic fracturing. Following hydraulic fracturing, pressure is released, and the injected fluids, along with natural brines in the source rock, flow back to the surface during a period referred to as flow or flowback (Guarnone et al. 2012). Once a well is completed, it enters the production phase during which fluids continue to flow back to the surface. Over time, the composition of the fluids becomes increasingly dominated by natural brines. This fluid is commonly referred to as produced water and must be managed properly along with flowback, drilling muds, and other wastes.

While developing a well or during production, exposures can be associated with vehicle exhaust and emissions from various types of equipment (e.g., compressors and pneumatic devices). Pneumatic controllers are used to operate valves that control liquid level, pressure, and other process variables, whereas pneumatic pumps use gas pressure to drive a fluid by raising or reducing the pressure of the fluid.

UOGD EMISSIONS AND TRANSPORT PATHWAYS

UOGD processes can release methane, volatile organic compounds (VOCs), and other pollutants of concern to human health. UOGD emissions to air can occur on or off well pads and originate from equipment and other sources, or releases (e.g., leaks, venting from storage tanks, or volatilization from surface spills). The unloading of liquids can be an important source of emissions; this process involves clearing liquids (i.e., water and liquid hydrocarbons) that have accumulated in mature gas wells and that can slow or even halt gas production. Flaring of natural gas is a major source of emissions in some oil-producing regions where gas is produced along with oil, but insufficient infrastructure is available to transport and sell the gas. For this reason and others (e.g., safety), natural gas is sometimes burned on-site (i.e., flared).

Chemicals that have been released into the environment then disperse and can react in the atmosphere, leading to widely varying concentrations and potential exposures at local and regional scales (Allen 2014; Bell et al. 2017; Mitchell et al. 2015; Vaughn et al. 2018; Zavala-Araiza et al. 2015). A few studies have used air quality monitoring data or modeling to address regulatory needs, such as assessing setback distances between UOGD and residences (Banan and Gernand 2018; Garcia-Gonzales et al. 2019; Haley et al. 2016; McCawley 2013).

UOGD EXPOSURE

A growing body of scientific literature addresses potential human exposures to a range of chemical and nonchemical agents that can be associated with UOGD (Deziel et al. 2022; HEI Energy Research Committee 2019; HEI Energy Research Committee 2020). Although many of these studies provide valuable information for understanding population exposures, only a small group has been conducted with the direct aim of estimating potential air pollution and noise exposures from UOGD (Allshouse et al. 2019; Maskrey et al. 2016; Paulik et al. 2018; Pennsylvania Department of Environmental Protection 2018). Knowledge gaps remain, however, about how these exposures potentially affect human health.

STUDY OBJECTIVES

The overarching goal of Hildebrandt Ruiz's study was to develop the TRAcking Community Exposures and Releases (TRACER) model to assess exposures to air pollutants from UOGD and to inform future health studies. The investigators specified the following seven study aims:

1. Conduct field measurements in the Eagle Ford Shale in Texas.
2. Conduct field measurements in the Permian Basin in New Mexico.
3. Estimate emissions from UOGD, including an application of the TRACER model to the Marcellus Shale in the Northeastern United States.
4. Couple the emissions estimates with dispersion models for primary pollutants.
5. Couple the emissions estimates with chemical transport models for secondary pollutants.
6. Assess the performance of various dispersion models.
7. Analyze exposure from UOGD and consider implications for future health studies.

The study team conducted detailed mobile and fixed-site monitoring campaigns over 3 months in the Eagle Ford Shale in 2023 and over 2 weeks in the Permian Basin. They conducted extensive modeling in the Eagle Ford Shale and the Marcellus Shale regions, including the development of improved UOGD emissions estimates, dispersion modeling for primary pollutants, and chemical transport modeling for secondary pollutants.

SUMMARY OF APPROACH AND METHODS

Hildebrandt Ruiz and colleagues used a combination of measurement and modeling approaches at various study sites to assess the quality of the TRACER model, which they advanced and refined from an existing model for methane emissions. The TRACER model combined emissions modeling with dispersion modeling to assess exposure to various air pollutants from UOGD. The capabilities of the preexisting model were expanded from modeling the emission and dispersion of methane from single UOGD well pads to assessing population exposures from multiple well pads. The expanded model included additional sources of emissions, regional-scale modeling, a broad suite of pollutants of concern to human health, including secondary pollutants, and evaluation of the model for the purpose of exposure assessment in future health studies (**Commentary Table 1**).

The original scope of work focused on the Eagle Ford Shale region in Texas. The project was later expanded to also include monitoring in the Permian Basin in New Mexico and modeling in the Marcellus Shale region in Ohio, Pennsylvania, and West Virginia.

AIR POLLUTION AND NOISE MONITORING

Eagle Ford Shale

The investigators conducted detailed outdoor air pollution and noise monitoring in Karnes City, Texas, and neighboring towns located in the center of the Eagle Ford Shale.

Real-time mobile and fixed-site measurements were collected during 8 weeks in the spring and 4 weeks in the fall of 2023. The mobile measurements were conducted using an electric van that drove routes on public roads to characterize the areas close to UOGD flaring locations. The van was equipped with state-of-the-art instrumentation, such as a Vocus 2R proton transfer reaction time-of-flight mass spectrometer. The Vocus provided high-resolution data, including real-time VOCs. A suite of air pollutants was examined, including particulate matter (PM), nitrogen oxides (NO_x), and numerous air toxics (see Commentary Table 1). When plumes (high or peak concentrations) were observed, the investigators parked the van downwind from the emission sources to better characterize the composition of the plumes. Thirty-five active UOGD locations were characterized in the sampling area. The investigators also conducted noise measurements at the same time. Eleven drives were conducted during the spring campaign, and eight drives were conducted during the fall campaign, amounting to about 2,300 km and 5,600 minutes of measurements.

The van was parked at an ambient "background" US Environmental Protection Agency (US EPA) monitoring station run by the Texas Commission on Environmental Quality (TCEQ) in Karnes City to conduct fixed-site measurements for about 3 weeks during the spring campaign. The site is surrounded by UOGD activity. PM_1 (particulate matter with an aerodynamic diameter of less than 1 µm) mass and composition were measured at this fixed site. Moreover, the investigators leveraged hourly measurements of various nonmethane VOCs collected by TCEQ using an automated gas chromatograph. In the Commentary, this fixed site is referred to as the Karnes City monitoring site.

Monitoring data were checked, preprocessed, and calibrated using standardized methods. Measurements from the mobile monitoring campaign were averaged over 10-second intervals, whereas fixed-site measurements were averaged over 1 hour. The investigators produced time-series plots for various pollutants and noise levels and reported averages and distributions. In addition, the investigators identified 17 plumes for more detailed analysis using observations of flares at individual wells. They used these data to estimate the emission ratios of 12 individual VOCs. Emission ratios were calculated per plume as the ΔVOC to ΔCO_2 ratio for each VOC and expressed per ppt/ppm CO_2. The emission data were integrated into the TRACER model, as described below. The Eagle Ford Shale monitoring results are described in Chapter 3 of the report.

Permian Basin

The investigators conducted a similar mobile monitoring campaign in Carlsbad, New Mexico, and neighboring towns located in the Permian Basin, one of the most productive UOGD regions in the United States. Mobile measurements were collected over 2 weeks in spring 2024. In addition, for several nights over 1 week, the van was parked to conduct fixed-site measurements at the Carlsbad KOA campground. A validation study was conducted over 2 days at a fixed site in Loving, New Mexico, to investigate whether different instruments measuring VOCs (benzene and toluene) produced consistent results.

The mobile measurements followed a similar design to the Eagle Ford Shale campaigns and included over 2,900 km of data and 18,700 minutes of measurements. Note that these mobile measurements were averaged over 1-minute intervals (compared with the 10-second intervals described in the other study area). Similar pollutants were measured as those in the Eagle Ford Shale, except that $PM_{2.5}$ and PM_{10} (particulate matter with an aerodynamic diameter of less than 2.5 and 10 µm, respectively) measurements were added. Results were presented as time-series plots for various pollutants and noise and spatial maps to visualize pollutant concentrations across the study region. From the fixed-site data, the investigators generated wind plots to examine whether high concentrations of hydrogen sulfide were associated with specific wind conditions during the night. The Permian Basin monitoring results are described in Chapter 4 of the report.

AIR POLLUTION EMISSION MODELING

The investigators describe the Methane Emission Estimation Tool (MEET) (Allen et al. 2022), which they developed further to create the TRACER model. *MEET* is an open-source

Commentary Table 1. Summary of Data and Approach

UOGD Region	Pollutants	Period	Monitoring or Modeling Approach	Aim	Chapter
Eagle Ford Shale	Methane, ethane, benzene, and many other volatile organic compounds. Carbon dioxide, nitrogen oxides, ozone, hydrogen sulfide, and sulfur dioxide. PM1 mass and composition, black carbon, and noise	March 28 to May 14, 2023, and October 20 to November 15, 2023	Mobile monitoring: on-road and while parked Collocated fixed-site monitoring at one background site from TCEQ	1	3
Permian Basin	Same as above, except addition of $PM_{2.5}$ and PM_{10}, and omission of PM composition	April 29 to May 12, 2024	Mobile monitoring: on-road and while parked Fixed-site monitoring at one site at night	2	4
Marcellus Shale	Four air pollutants: methane, ethane, total volatile organic compounds, and nitrogen oxides	2023	Emissions modeling	3	5
Eagle Ford Shale	Nitrogen oxides and ozone	2019	Chemical transport model, Comprehensive Air Quality Model with Extensions (CAMx)	5	7
Eagle Ford Shale	Ethane	March 5 to May 24, 2023	Air pollution dispersion model (CALPUFF)	4	6
Eagle Ford Shale	Ethane	March 5 to May 24, 2023	Various air pollution dispersion models (CALPUFF, AERMOD, Gaussian model)	6	8
Eagle Ford Shale	Six volatile organic compounds: methane, ethane, propane, n-hexane, benzene, and toluene	March 20 to May 14, 2023	Various exposure assessment approaches with increasing levels of complexity (e.g., CALPUFF and AERMOD)	7	9

PM = particulate matter with an aerodynamic diameter of less than 1, 2.5, or 10 μm; TCEQ = Texas Commission on Environmental Quality.

modeling tool to help regulators, industry, and the research community more accurately track methane and other emissions in oil and gas production regions. Currently available methods for estimating these emissions, such as the US EPA oil and gas tool (US EPA 2022), provide annual average emission rates and emissions aggregated at the county level, but emissions exhibit variability over much smaller temporal and spatial scales.

MEET estimates emission rates for each UOGD source by multiplying activity data by emission factors, selected from a library of measurements or user-defined data. Activity data describe the number of sources or events within a certain spatial extent or equipment category, and emission factors describe the corresponding emission rates associated with each of these sources or activities. See **Commentary Figure 1** for the basic structure of MEET.

Chapter 5 of the report provides an overview of how the investigators expanded the MEET model to form the TRACER model. The expanded model includes updated emissions from additional UOGD sources from the measurement campaigns, improves the spatial and temporal resolution of UOGD emissions, and broadens to a suite of nonmethane pollutants of concern for human health. Of note is that the investigators improved or expanded emission factors of five UOGD sources: completion flowbacks, pneumatic pumps, pneumatic controllers, liquid unloading, and flares. The TRACER model can create emissions inventories with temporal resolutions ranging from minutes to months, and with spatial resolutions ranging from exact well locations to county-level or even coarser levels.

The investigators provided detailed descriptions of emission estimation methods only for the application to the

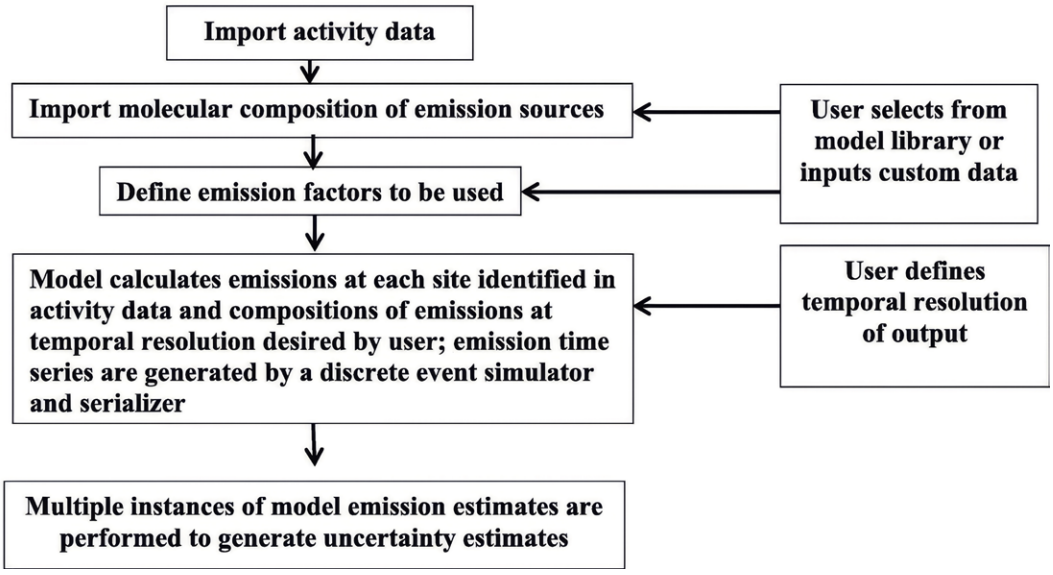

Commentary Figure 1. Basic structure of MEET, which was expanded and improved to create the TRACER model. Source: Reproduced from Allen et al. 2022; Creative Commons license *CC BY 4.0*.

Marcellus Shale region because the data required for the modeling — rather than the calculation procedures — vary by location.

Application of the TRACER Model to the Marcellus Shale

The investigators describe an application of the TRACER model to the Marcellus Shale region. The investigators used the TRACER model to estimate emissions for different UOGD sources for four air pollutants (methane, ethane, total VOCs, and NO_x). For this application, they created emissions inventories with hourly resolutions for 2023 with data spatially aggregated using 4 km × 4 km grids. NO_x emissions were estimated for combustion of UOGD sources only (e.g., drilling and hydraulic fracturing, compressors). Emissions from drilling and hydraulic fracturing were allocated only to fractured wells during the 2 weeks preceding production, consistent with the chemical transport modeling described later in this Commentary.

To illustrate key features of the inventories, the investigators reported results for seven grids in five different counties and also provided county-level summaries for two counties. They reported maximum and average hourly emissions rates for all modeled UOGD sources combined and reported separately for each of the grid cells and counties. The emission modeling and the application to the Marcellus Shale region are described in Chapter 5, with further details in the additional materials (Chen et al. 2025).

AIR POLLUTION DISPERSION MODELING IN EAGLE FORD SHALE

Chemical Transport Modeling

The investigators examined the importance of detailed spatial and temporal allocation of NO_x emissions from hydraulic fracturing on predicted ozone formation in the Eagle Ford Shale in 2019 — a region with abundant VOCs. They used this case study to develop parts of the TRACER model.

Base case NO_x emissions were derived from the 2019 emissions inventory developed by TCEQ. The TCEQ emissions inventory provided season-specific NO_x emissions for each of the 27 Eagle Ford Shale counties for 47 UOGD sources. In the case study, these NO_x emissions from oil and gas sources for the Eagle Ford Shale counties were removed from the base case and substituted with spatially and temporally resolved NO_x emissions to create four scenarios. In the first scenario, the county-level NO_x emissions for all UOGD sources were distributed evenly to all active oil and gas wells in the Eagle Ford region (42,038 in total), with assumed continuous emissions throughout the year. In the other three scenarios, NO_x emissions from hydraulic fracturing engines in Karnes County specifically were allocated only to fractured wells, with different durations (2 days, 1 week, or 2 weeks) of emissions for fracturing operations at individual wells. Of 4,185 wells in Karnes County, 436 were fractured in 2019.

The study team used the Comprehensive Air Quality Model with Extensions (CAMx) to simulate ozone impacts from the base case and the four scenarios. CAMx is a chemical transport model with different spatial resolutions depending on the modeling domain (36 and 12 km^2 grids for the contiguous United States and 4 km^2 grids for central and eastern Texas). The modeling period was from June to September 2019, and the temporal resolution of the model was 1 hour.

The investigators calculated the daily maximum of 8-hour average ozone concentrations for all scenarios and maximal and minimum differences across scenarios. The chemical transport modeling results are described in Chapter 7, with further details in the additional materials (Modi et al. 2025).

Air Pollution Dispersion Modeling

The investigators applied the TRACER model to estimate emissions from individual wells and coupled the emissions with an air pollution dispersion model (CALPUFF) to estimate air pollution concentrations at receptor sites in the Eagle Ford Shale. Unlike the chemical transport model described above, the air pollution dispersion model does not account for chemical transformations in the atmosphere.

They used a diagnostic three-dimensional meteorological model (CALMET), with meteorological input data from the Karnes City monitoring site. The investigators note that a variety of compounds could be considered in these analyses, but that they focused on ethane, which, in the Eagle Ford Shale region, is emitted almost entirely by oil and gas operations. The modeling period selected was March 5 to May 24, 2023, to correspond with the Eagle Ford Shale monitoring campaign described earlier in this Commentary.

Emissions were estimated using the TRACER model for individual wells or tank batteries for various UOGD sources. Tank batteries may be located on or off well pads and consist of a group of tanks and other liquid-handling equipment that is connected to receive crude oil and produced water from a well. Emissions were also estimated at the facility level (thus aggregated over multiple wells) using throughput-scaled methane emission factors and facility-specific emission composition estimates derived from earlier studies (e.g., Allen et al. 2013; 2015a; 2015b; Mitchell et al. 2015; Zimmerle et al. 2020).

For the air pollution dispersion modeling, the team selected a domain of approximately 200 km × 200 km centered on the Karnes City monitoring site using data on more than 20,000 oil and gas wells. The domain included three nested regions (inner, intermediate, and outer modeling domain) (**Commentary Figure 2**). Individual wells (3,208 in total) were spatially resolved in a 32 km × 32 km region of the Karnes City monitoring site (inner modeling domain). For computational reasons, wells outside the inner modeling domain were aggregated (up to 4 km × 4 km) into point sources representing multiple wells. The temporal resolution of the model was 1 hour.

They analyzed the contribution of different source distances (5, 10, 20, and 50 km) to the average and peak concentrations predicted when all UOGD sources in the modeling domain were accounted for. The air pollution dispersion modeling results are described in Chapter 6, with further details in the additional materials (Graves et al. 2025).

To assess the performance of CALPUFF and two other air pollution dispersion models (AERMOD and a Gaussian model), the study team compared predicted and observed hourly concentrations of ethane at the Karnes City monitoring site. While all models use the same modeling domain and spatial and temporal resolutions as CALPUFF, they use different meteorological input data and formulations of how the pollutants would disperse in the ambient atmosphere. The investigators assessed model performance using multiple measures, including a "screening" test for regulatory applications, correlations, root-mean square errors, and bias. The screening test is passed when the model's under- or overprediction is less than a factor of 2. The evaluation of the various air pollution dispersion models is described in Chapter 8.

Exposure Modeling

The investigators described various approaches to estimate exposure to six VOCs (methane, ethane, propane, n-hexane, benzene, and toluene) from UOGD in Karnes County with increasing levels of complexity, including various air pollution dispersion models.

The investigators obtained meteorological data and emissions data for subsequent exposure modeling. They obtained meteorological data from the Karnes City monitoring site. The investigators used the TRACER model to estimate emissions for different UOGD sources. They estimated emissions from individual tank batteries, where most emissions occur, rather than from individual wells. Individual tank batteries (402 in total) were spatially resolved in a 15 km × 15 km region of the Karnes City monitoring site (inner modeling domain). For computational reasons, tank battery locations outside the inner modeling domain were aggregated (up to 4 km × 4 km) into point sources representing sometimes multiple locations.

Next, the investigators applied various approaches with increasing levels of complexity to quantify temporal and spatial variability in the exposure of six VOCs. The modeling period selected was March 20 to May 14, 2023, to correspond with the earlier-described Eagle Ford Shale monitoring campaign. The temporal and spatial resolution of the exposure models was 1 hour and 1.3 km × 1.3 km grid cells, respectively.

Multiple methods were used to estimate exposure. First, inverse distance weighting was used, in which the pollutant concentration at a given location is inversely related to the distance from the emission source. The investigators applied this inverse distance weighting approach with and without meteorological data (wind speed and direction). They established a 5 km buffer surrounding each emissions source

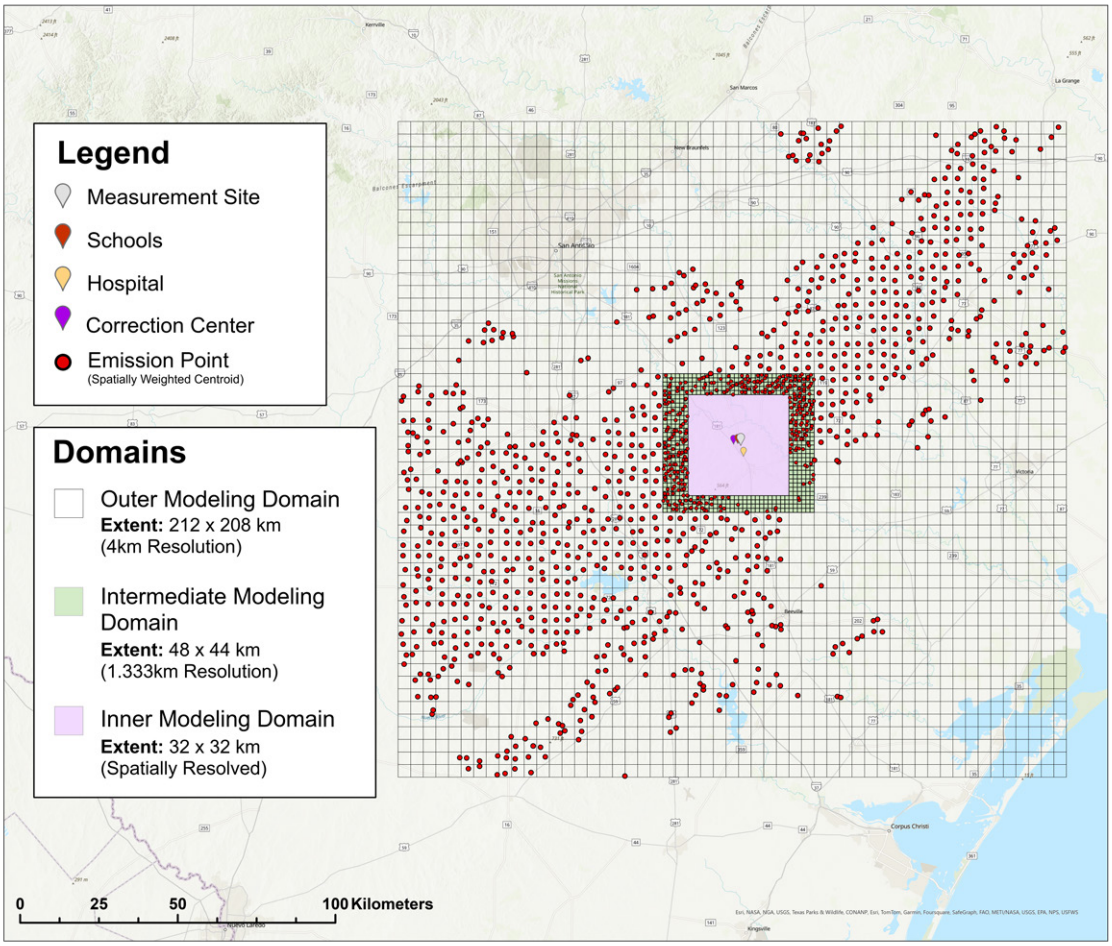

Commentary Figure 2. Nested air pollution dispersion modeling domain in the Eagle Ford Shale. Source: Investigators' Report Figure 6-1.

location and calculated the distance between each source and its surrounding grid cells.

Next, a Gaussian plume model was used. This model disperses the pollutants in the shape of a normal (Gaussian) distribution in both horizontal and vertical directions as they move downwind from the source. The Gaussian model does not consider the influence from a source farther than 10 km from the emission point. Lastly, two increasingly complex air pollution dispersion models were applied with a much larger modeling domain, AERMOD and CALPUFF, with different formulations of how the pollutants would disperse in the ambient atmosphere.

The investigators reported emission rates by various UOGD sources for ethane and calculated Pearson correlations between emissions from all sources and the six VOCs. They assessed model performance by comparing model predictions with observations from the Karnes City monitoring site, with a focus on ethane. The investigators conducted additional analyses with AERMOD. For example, AERMOD was used to estimate population-weighted exposure from UOGD across racial and ethnic groups and income levels obtained from census data in Karnes County. The exposure modeling results are described in Chapter 9 of the report.

SUMMARY OF RESULTS

AIR POLLUTION AND NOISE MONITORING

Observations of ambient concentrations of air pollutants in UOGD regions showed strong diurnal variation, with (short-term) peak concentrations occurring during late night and early morning hours. Mean concentrations for various air pollutants and noise from the entire UOGD measurement campaigns in Eagle Ford Shale and Permian Basin were generally relatively low and did not exceed the National Ambient Air Quality Standards concentrations and other health-related guidelines (**Commentary Table 2**). Caution is warranted because the measurements and the short-term health standards and guidelines have different averaging times. Measurements were conducted for a total of 3 months in Eagle Ford Shale in 2023, and for 2 weeks in Permian Basin in 2024.

Commentary Table 2. Mean Concentrations of Various Air Pollutants and Noise from UOGD Measurement Campaigns in Eagle Ford Shale and Permian Basin Regions, together with Short-term Health Standards and Guidelines

	Mean in Eagle Ford Shale	Mean in Permian Basin	
Type of Campaign	Fixed-Site Monitoring[a]	Mobile Monitoring[b]	Short-Term Health Standards and Guidelines
Methane	2.2 ppm	2.2 ppm	
Ethane	35 ppb	NR	–
Benzene	0.1 ppb	0.5 ppb	9 ppb (acute-duration inhalation from ATSDR)
Toluene	0.2 ppb	0.4 ppb	2,000 ppb (acute-duration inhalation from ATSDR)
Formaldehyde	1.0 ppb	1.0 ppb	40 ppb (acute-duration inhalation from ATSDR)
C8 aromatic compounds	0.01 ppb	0.2 ppb	–
Nitrogen oxides	2 ppb	NR	100 ppb (NAAQS for NO_2 – Annual 98th percentile of 1-hour daily maximum concentrations, averaged over 3 years)
Ozone	36 ppb	48 ppb	70 ppb (NAAQS – Annual fourth-highest daily maximum 8-hour concentration, averaged over 3 years)
Hydrogen sulfide	1.7 ppb	2.3 ppb	70 ppb (acute-duration inhalation from ATSDR)
Sulfur dioxide	0.4 ppb	1.0 ppb	75 ppb (NAAQS – Annual 99th percentile of 1-hour daily maximum concentrations, averaged over 3 years)
PM_1	6.7 µg/m^3	5.8 µg/m^3	–
$PM_{2.5}$	NR	8.8 µg/m^3	35 µg/m^3 (NAAQS – 98th percentile of 24-hour concentration, averaged over 3 years)
Black carbon	NR	0.6 µg/m^3	–
Noise (LAeq)	50 dB	NR	70 dB (LAeq US EPA guideline averaged over 24 hours)

NR = not reported; ATSDR = Agency for Toxic Substances and Disease Registry; LAeq = A-weighted, equivalent continuous sound pressure level; NAAQS = National Ambient Air Quality Standards; PM_1 = particulate matter with an aerodynamic diameter of less than 1 µm; US EPA = United States Environmental Protection Agency.

[a] Observations obtained from fixed-site measurement data at the Karnes City monitoring site and averaged over 1-hour intervals from a 3-month sampling campaign in 2023. Data were averaged over the spring and fall campaigns, if available. Note that an automated gas chromatograph operated by TCEQ was used for the various VOCs, if available.

[b] Observations obtained from mobile measurement data and averaged over 1-minute intervals from a 2-week sampling campaign in spring 2024. Note that the Vocus data were for the various VOCs.

Air Pollution Emissions Observations

Hildebrandt Ruiz and colleagues used mobile measurements in the Eagle Ford Shale region to identify 17 plumes and estimate emission ratios derived from observations of flares at individual wells. The largest emission ratios were reported for benzene (average 89 ppt/ppm CO_2), followed by C8 aromatic compounds and acetaldehyde (both 64 ppt/ppm CO_2), and then toluene (44 ppt/ppm CO_2). The emission ratios of all other measured VOCs were small (all <4.8 ppt/ppm CO_2). The investigators found high variability in emission ratios of VOCs across the flaring sites.

AIR POLLUTION EMISSION MODELING IN MARCELLUS SHALE

For methane, ethane, and VOC emissions, maximum hourly emission rates for all UOGD sources were typically several times the mean annual emission rate (**Commentary Table 3**). In contrast, maximum NO_x emissions from UOGD combustion sources varied less than hydrocarbon emissions. The variability in emissions decreased when aggregated at a county-level scale compared with a grid-level scale. Note that the emission rates were averaged over 4 km × 4 km.

AIR POLLUTION DISPERSION MODELING IN EAGLE FORD SHALE

Chemical Transport Modeling

Hydraulic fracturing appeared to be an important contributor of NO_x emissions from UOGD in the Eagle Ford Shale, accounting for approximately 10% of total NO_x emissions from UOGD in 2019.

The study team reported spatial and temporal variability in NO_x emission rates from hydraulic fracturing that ranged over two to three orders of magnitude across the scenarios. This variability occurs because, at a given time, only a small percentage of the total wells have fracturing emissions, which last for 2 days to 2 weeks before production begins.

The improved emissions estimates might have led to increased estimated ozone formation in the Eagle Ford Shale region — a region with abundant biogenic VOCs and a region that is generally upwind of the San Antonio ozone nonattainment region. For several days in August 2019, for example, estimated ozone concentrations were consistently 6 to 10 ppb higher in the areas north of the Eagle Ford Shale (such as San Antonio) for the 2-day to 2-week emission periods compared with the annual county-level distribution.

Air Pollution Dispersion Modeling

The study team reported that mean and peak ethane concentrations at the Karnes City monitoring site are influenced by both near and distant UOGD sources in the Eagle Ford region. Mean concentrations were affected by UOGD emission sources up to 50 km away from the Karnes City monitoring site. In contrast, peak concentrations at night were primarily due to sources within 20 km of the site. On average, sources within 5 km of the Karnes City monitoring site contributed 38% to the mean ethane concentrations predicted when all sources in the 200 km × 200 km domain were accounted for. Sources within 10, 20, and 50 km contributed on average 67%, 88%, and 99%, respectively, to the mean ethane concentrations.

Commentary Table 3. Maximum and Hourly Emission Rates of Methane and Nitrogen Oxides for the Seven Grid Cells (4 km × 4 km) in the Marcellus Shale Region

			Methane (All UOGD Sources)		Nitrogen Oxides (Combustion Sources)	
Grid Cell	County	Marcellus portion	Average (kg/hr)	Factor Difference[a]	Average (kg/hr)	Factor Difference[a]
1	Tyler, WV	Southwest	79.8	3.2	26.2	4.4
2	Greene, PA	Southwest	102.9	2.8	35.3	3.2
3	Lewis, WV	Southwest	80.3	1.3	18.2	1.1
4	Bradford, PA	Northeast	50.8	4.9	11.8	1.0
5	Bradford, PA	Northeast	27.6	15.3	6.1	1.0
6	Bradford, PA	Northeast	74.8	6.8	19.3	4.4
7	Susquehanna, PA	Northeast	42.6	4.6	9.9	1.0

[a] Factor difference between the maximum and hourly emission rate.

There was a high degree of variability in those percentages from hour to hour, depending on whether the nearest UOGD sources were upwind from the site and whether stable atmospheric conditions with low wind speed occurred, which may facilitate peak concentrations.

The air pollution dispersion models (CALPUFF, AERMOD, and the Gaussian model) predicted the timing and ranking of the plumes with reasonable precision, but the actual magnitude of the plumes varied considerably. The best-performing model depends on which performance measure is important and for which application. For example, both CALPUFF and AERMOD passed a "screening test" for regulatory applications, and the Gaussian model did not. AERMOD generally underpredicts across the observed range of ethane concentrations, CALPUFF underpredicts only at low observed concentrations, and the Gaussian model overpredicts at high observed levels. CALPUFF seemed to perform better when looking at correlations with ethane observations compared with the other two models.

Further examination of AERMOD showed that UOGD emissions and meteorology, primarily wind speed and direction, were the most influential factors on modeled ethane concentrations at the Karnes City monitoring site.

Exposure Modeling

Ethane emission rates from three specific UOGD sources were estimated to be the largest in the Eagle Ford Shale: emissions from liquid unloading (1,026 kg/hr), tank flashing (998 kg/hr), and pneumatic controllers (792 kg/hr). Emissions from unloading are typically very short in duration, whereas tank flashing and pneumatic emissions, expressed as hourly averages, are relatively constant. Emission rates were typically highly correlated across pollutants (correlation >0.7).

Similarly high correlations (>0.7) were reported across the different exposure models for ethane and the other VOCs, except for the inverse weighting models without meteorological data. The latter model did not correlate with the other models.

Daily estimates from the exposure models were moderately to highly correlated (0.6–0.8) with ethane observations at the Karnes City monitoring site, except for the inverse weighting model (0.2) (**Commentary Table 4**). A negative bias was reported for all models except CALPUFF, with models underestimating ethane measurements by up to 20 ppb (70%). CALPUFF appeared to be the best-performing model in reducing bias. However, it is also the most computationally intensive model. The next best model in reducing bias was AERMOD, a less computationally demanding model.

Using the AERMOD model, population-weighted exposure estimates of six VOCs across racial and ethnic groups and income levels from UOGD in Karnes County were generally low.

HEI ENERGY REVIEW COMMITTEE 'S EVALUATION

In its independent review of the study, the HEI Energy Review Committee found that the study presented a comprehensive approach to evaluating air pollution from UOGD. The Committee thought the study findings and the TRACER model would be of broad interest and value to a wide audience, such as resource managers, state and federal policymakers, UOGD industry practitioners, research scientists, and local communities.

STRENGTHS OF THE STUDY

The Review Committee noted several strengths of the research. First, the Committee was impressed by the detailed mobile and fixed-site monitoring campaigns and use of state-of-the-art instrumentation that provided high-resolution data. The investigators collected 3 months of data in the Eagle Ford Shale in Texas and used advanced instrumentation, such as mass spectrometry, to measure real-time VOCs. A suite of air pollutants was examined, including PM and its composition, NO_x, and numerous air toxics. The Committee also appreciated the 2-week measurement campaign in the Permian Basin in New Mexico.

Commentary Table 4. Performance Measures of the Different Exposure Models for Daily Mean Ethane Concentrations at the Karnes City Monitoring Site

Exposure Model	Correlation	Root-Mean Square Error (ppb)	Mean Bias (ppb)	Normalized Mean Bias (%)
Inverse distance weighting without meteorology	0.21	34	−16	−61
Inverse distance weighting with meteorology	0.76	33	−19	−71
Gaussian plume model	0.57	33	−17	−63
AERMOD	0.70	23	−9	−33
CALPUFF	0.59	27	2	7.6

Second, the extensive modeling efforts were notable, including the development of improved UOGD emissions estimates, dispersion modeling, and chemical transport modeling. The development of the TRACER model could provide a useful tool for future exposure and health studies of UOGD in the United States. The TRACER model could also be a useful tool to track UOGD exposure over time, given that UOGD industry practices and governance might change.

Third, the Committee appreciated the broad scope of the study with extensive monitoring and modeling across three key UOGD regions: Eagle Ford Shale, Permian Basin, and Marcellus Shale. Such a broad and ambitious scope makes the results relevant and widely applicable across geographical boundaries.

Fourth, the Committee found the many methodological contributions valuable, including a detailed evaluation of various air pollution dispersion models in predicting the structure of plumes from oil and gas facilities, exploration of influencing factors of the models, and a comparison of various exposure approaches with increasing levels of complexity.

Although the Committee broadly agreed with the investigators' conclusions, the report had some weaknesses and limitations that should be considered when interpreting the results.

LIMITATIONS

Need for More Discussion, Integration, and Synthesis

Although the investigators have conducted an impressive amount of work, the report reads as a standalone, sometimes overly technical, project that is not well integrated across the chapters. Moreover, some chapters, such as the introductory chapters, were not well developed. The lack of integration might stem partly from the study's history because the mobile monitoring in the Permian Basin and modeling in the Marcellus Shale began after other aspects of the research had already started. Hence, it is unsurprising that some of the results, such as the monitoring data, are not fully integrated in later chapters.

The Review Committee noted that many important details were lacking regarding the emissions inventory used in the current study. Details lacking include what data sources were used and during which years, what the spatial and temporal resolution was, and, importantly, how the emissions estimates from UOGD were improved. It is unclear whether and how the monitoring data were used in the emissions estimates and subsequent modeling in later chapters.

The Committee noted the lack of discussion in some chapters and a very short overarching synthesis chapter, which limited the discussion of the findings and their implications. Whereas some discussions have been added in response to earlier feedback from the Committee, further exploration of the following topics could increase the utility of the report:

1. A discussion of what would be the best exposure model given the uncertainties in emissions and other sources of uncertainty, how to best evaluate model performance, and the practical feasibility of the models for different applications and user groups.
2. An expanded discussion on the applicability of the TRACER model to other UOGD regions and potential future UOGD practices.
3. Further discussion of the generalizability of the study results to different industry practices within and across basins.
4. Elaboration on the public health implications, particularly because the mean air pollution levels from UOGD were generally low, albeit with short-term peak concentrations, particularly at night.

The Committee thought the lack of thorough discussion, integration, and synthesis across the many parts of the study was a missed opportunity to maximize the study's impact and limited the generalizability of the findings.

RECOMMENDATIONS FOR AREAS OF FUTURE WORK

The Review Committee identified three specific areas of future work that would be valuable and of interest. First, it would be important to apply the TRACER model in the Permian Basin, one of the most productive UOGD regions in the United States. Such an application would demonstrate the usefulness and broad applicability of the model in different types of regions with different industry practices within and across basins. It is encouraging that the study team is planning to complete this work in 2026.

Second, the Committee strongly encourages a more thorough evaluation of the TRACER model with measurements for multiple pollutants and for additional sites. In the current study, the investigators only used measurements obtained at a single site (the Karnes City monitoring site) and mainly for one pollutant (ethane).

Third, the Committee recommends exploration of a range of potential exposures to chemical agents (e.g., radioactive material, those found in wastewater, and volatile compounds) and nonchemical agents (e.g., noise, light, and vibration) that can be associated with UOGD in addition to air pollution (Deziel et al. 2022; HEI Energy Research Committee 2019; HEI Energy Research Committee 2020). The current study addressed air pollution only, and, to a limited extent, noise. Hence, more work is needed to assess the wide range of different types of exposures from UOGD and to inform future health studies.

CONCLUSIONS

The study by Hildebrandt Ruiz and colleagues used a combination of measurement and modeling approaches at various study sites to assess the quality of the TRACER model, which they advanced and refined from an existing model for methane

emissions. The TRACER model combined emissions modeling with dispersion modeling to assess exposure to various air pollutants from UOGD. The expanded model included additional sources of emissions, regional-scale modeling, a broad suite of pollutants, and evaluation of the model for the purpose of exposure assessment in future health studies. The original scope of work focused on the Eagle Ford Shale region in Texas. The project was later expanded to also include monitoring in the Permian Basin in New Mexico and modeling in the Marcellus Shale region in Ohio, Pennsylvania, and West Virginia.

The broad scope of the study, detailed monitoring campaigns, and use of state-of-the-art instrumentation that provided high-resolution data were the strengths of the study. Other strengths were the extensive modeling efforts, including the development of improved UOGD emissions estimates, dispersion modeling, and chemical transport modeling.

Among the main findings was that the investigators found that ethane concentrations were affected by UOGD emission sources up to 50 km away. The study reported typically high correlations between ethane and other VOCs from different exposure models and with direct observations. CALPUFF appeared to be the best-performing model in reducing bias for ethane.

While comprehensive, the HEI Energy Review Committee thought the lack of discussion, integration, and synthesis in the report limited the generalizability of the findings. The lack of integration might stem partly from the study's history because mobile monitoring in the Permian Basin and modeling in the Marcellus Shale region began after other aspects of the research had already started. The Committee recommends three areas of future work: application of the TRACER model in the Permian Basin, one of the most productive UOGD regions in the United States; a more thorough evaluation of the TRACER model beyond mainly ethane; and expansion of research efforts to other potential chemical and nonchemical exposures related to UOGD, in addition to air pollution.

Overall, the Committee thought the study findings and the TRACER model would be of broad interest and value to a wide audience, such as resource managers, state and federal policymakers, UOGD industry practitioners, research scientists, and local communities.

ACKNOWLEDGMENTS

The HEI Energy Review Committee thanks the ad hoc reviewers for their help in evaluating the scientific merit of the Investigators' Report. The Committee is also grateful to Donna Vorhees for oversight of the study, to Hanna Boogaard for assistance with review of the Investigators' Report and preparation of its Commentary, to Tara Hamilton for editing the Investigators' Report and its Commentary, and to Kristin Eckles and Hope Green for their roles in preparing this HEI Research Report for publication.

REFERENCES

Allen DT, Cardoso-Saldaña FJ, Kimura Y, Chen Q, Xiang Z, Zimmerle D, et al. 2022. A Methane Emission Estimation Tool (MEET) for predictions of emissions from upstream oil and gas well sites with fine-scale temporal and spatial resolution: Model structure and applications. Sci Total Environ 829:154277; *https://doi.org/10.1016/j.scitotenv.2022.154277*.

Allen DT, Cardoso-Saldaña FJ, Kimura Y. 2017. Variability in spatially and temporally resolved Emissions and hydrocarbon source fingerprints for oil and gas sources in shale gas production regions. Environ Sci Technol 51:12016–12026; *https://doi.org/10.1021/acs.est.7b02202*.

Allen DT, Pacsi AP, Sullivan DW, Zavala-Araiza D, Harrison M, Keen K, et al. 2015a. Methane emissions from process equipment at natural gas production sites in the United States: pneumatic controllers. Environ Sci Technol 49:633–640; *https://doi.org/10.1021/es5040156*.

Allen DT, Sullivan DW, Zavala-Araiza D, Pacsi AP, Harrison M, Keen K, et al. 2015b. Methane emissions from process equipment at natural gas production sites in the United States: liquid unloadings. Environ Sci Technol 49:641–648; *https://doi.org/10.1021/es504016r*.

Allen DT. 2014. Atmospheric emissions and air quality impacts from natural gas production and use. Annu Rev Chem Biomol Eng 5:55–75; *https://doi.org/10.1146/annurev-chembioeng-060713-035938*.

Allen DT, Torres VM, Thomas J, Sullivan DW, Harrison M, Hendler A, et al. 2013. Measurements of methane emissions at natural gas production sites in the United States. Proc Natl Acad Sci USA 110:17768–17773; *https://doi.org/10.1073/pnas.1304880110*.

Allshouse WB, McKenzie LM, Barton K, Brindley S, Adgate JL. 2019. Community noise and air pollution exposure during the development of a multi-well oil and gas pad. Env Sci Technol 53:7126–7135; *https://doi.org/10.1021/acs.est.9b00052*.

Banan Z, Gernand JM. 2018. Evaluation of gas well setback policy in the Marcellus Shale region of Pennsylvania in relation to emissions of fine particulate matter. J Air Waste Manag Assoc 68:988–1000; *https://doi.org/10.1080/10962247.2018.1462866*.

Bell C, Vaughn T, Zimmerle D, Herndon S, Yacovitch T, Heath G, et al. 2017. Comparison of methane emission estimates from multiple measurement techniques at natural gas production pads. Elem Sci Anth 5:79; *https://doi.org/10.1525/elementa.266*.

Chen Q, Raksi N, Niewenhous L, Almasalha SJ, Graves JD, Brown V, et al. 2025. Spatial and temporal variability in atmospheric emissions from oil and gas sector sources in the Marcellus production region. Atmosphere 16:1048; *https://doi.org/10.3390/atmos16091048*.

Deziel NC, Clark CJ, Casey JA, Bell ML, Plata DL, Saiers JE. 2022. Assessing exposure to unconventional oil and gas development: Strengths, challenges, and implications for epidemio-

logic research. Curr Environ Health Rep 9:436–450; *https://doi.org/10.1007/s40572-022-00358-4*.

Garcia-Gonzales DA, Shonkoff SBC, Hays J, Jerrett M. 2019. Hazardous air pollutants associated with upstream oil and natural gas development: a critical synthesis of current peer-reviewed literature. Annu Rev Public Health 40:283–304; *https://doi.org/10.1146/annurev-publhealth-040218-043715*.

Graves JD, Kimura Y, Modi M, Stokes S, Meyer M, Hildebrandt Ruiz L, et al. 2025. Source attribution of elevated ethane concentrations detected by regional monitors in oil and gas production regions. ACS ES&T Air. 2:2038-2046; *https://doi.org/10.1021/acsestair.5c00235*.

Guarnone M, Rossi F, Negri E, Grassi C, Genazzi D, Zennaro R. 2012. An unconventional mindset for shale gas surface facilities. J Nat Gas Sci Eng 6:14–23; *https://doi.org/10.1016/j.jngse.2012.01.002*.

Haley M, McCawley M, Epstein AC, Arrington B, Bjerke EF. 2016. Adequacy of current state setbacks for directional high-volume hydraulic fracturing in the Marcellus, Barnett, and Niobrara Shale plays. Environ Health Perspect 124:1323–1333; *https://doi.org/10.1289/ehp.1510547*.

HEI Energy Research Committee. 2019. Potential Human Health Effects Associated with Unconventional Oil and Gas Development: A Systematic Review of the Epidemiology Literature. Special Report 1. Boston, MA: Health Effects Institute.

HEI Energy Research Committee. 2020. Human Exposure to Unconventional Oil and Gas Development: A Literature Survey for Research Planning. Communication 1. Boston, MA: Health Effects Institute.

Maskrey JR, Insley AL, Hynds ES, Panko JM. 2016. Air monitoring of volatile organic compounds at relevant receptors during hydraulic fracturing operations in Washington County, Pennsylvania. Environ Monit Assess 188:1–12; *https://doi.org/10.1007/s10661-016-5410-4*.

McCawley M. 2013. Air, Noise, and Light Monitoring Results. Available: *https://www.cdc.gov/niosh/nioshtic-2/20049534.html*.

Mitchell AL, Tkacik DS, Roscioli JR, Herndon SC, Yacovitch TI, Martinez DM, et al. 2015. Measurements of methane emissions from natural gas gathering facilities and processing plants: measurement results. Environ Sci Technol 49:3219–27; *https://doi.org/10.1021/es5052809*.

Modi M, Kimura Y, Hildebrandt Ruiz L, Allen DT. 2025. Fine-scale spatial and temporal allocation of NO_x emissions from unconventional oil and gas development can result in increased predicted regional ozone formation. ACS EST Air 2:130–140; *https://doi.org/10.1021/acsestair.4c00077*.

Paulik LB, Hobbie KA, Rohlman D, Smith BW, Scott RP, Kincl L, et al. 2018. Environmental and individual PAH exposures near rural natural gas extraction. Environ Pollut 241:397–405; *https://doi.org/10.1016/j.envpol.2018.05.010*.

Pennsylvania Department of Environmental Protection. 2018. Long-term ambient air monitoring project: Marcellus Shale gas facilities.

US EPA (United States Environmental Protection Agency). 2022. 2020 Nonpoint Oil and Gas Estimation Tool Version 1.3.

US EPA (United States Environmental Protection Agency). 2016. Hydraulic Fracturing for Oil and Gas: Impacts from the Hydraulic Fracturing Water Cycle on Drinking Water Resources in the United States. (Final Report). EPA/600/R-16/236F, 2016. Washington, DC: US EPA.

Vaughn TL, Bell CS, Pickering CK, Schwietzke S, Heath GA, Pétron G, et al. 2018. Temporal variability largely explains top-down/bottom-up difference in methane emission estimates from a natural gas production region. Proc Natl Acad Sci USA 115:11712–11717; *https://doi.org/10.1073/pnas.1805687115*..

Zavala-Araiza D, Allen DT, Harrison M, George FC, Jersey GR. 2015. Allocating methane emissions to natural gas and oil production from shale formations. ACS Sustain Chem Eng 3:492–498; *https://doi.org/10.1021/sc500730x*.

Zimmerle D, Vaughn T, Luck B, Lauderdale T, Keen K, Harrison M, et al. 2020. Methane emissions from gathering compressor stations in the US. Environ Sci Technol 54:7552–7561; *https://doi.org/10.1021/acs.est.0c00516*.

ABBREVIATIONS AND OTHER TERMS

ACSM	Aerosol Chemical Speciation Monitor
AERMET	A meteorological data preprocessor
AERMOD	An atmospheric dispersion modeling system
ATSDR	Agency for Toxic Substances and Disease Registry
CALMET	California Meteorological model
CALPUFF	An atmospheric dispersion modeling system
CAMS	continuous ambient monitoring station
CIMS	chemical ionization mass spectrometer operated in iodide mode
CMAQ	Community Multiscale Air Quality Modeling System
GC	gas chromatography
GHGI	Inventory of US Greenhouse Gas Emissions and Sinks
IDW	inverse distance weighting
IDWmet	inverse distance weighting, plus wind speed and direction
LAeq	A-weighted, equivalent continuous sound pressure level
LBeq	B-weighted, equivalent continuous sound pressure level
MDA8	daily maximum of 8-hour average
MEET	Methane Emission Estimation Tool
NAAQS	National Ambient Air Quality Standards
PM	particulate matter
$PM_{2.5}$	particulate matter ≤2.5 µm in aerodynamic diameter
PM_{1}	particulate matter <1 µm in aerodynamic diameter
PM_{10}	particulate matter <10 µm in aerodynamic diameter
SEGAUSS	single-equation Gaussian implementation
SEMS	Scanning Electrical Mobility Spectrometer
TAMIS	Texas Air Monitoring Information System
TCEQ	Texas Commission on Environmental Quality
TRACER	TRAcking Community Exposures and Releases (model)
UOGD	unconventional oil and gas development
US EPA	United States Environmental Protection Agency
VIIRS	Visible Infrared Imaging Radiometer Suite
VOC	volatile organic compound

HEI BOARD, ENERGY COMMITTEES, and STAFF

BOARD OF DIRECTORS

Richard A. Meserve, Chair *Senior of Counsel, Covington & Burling LLP; President Emeritus, Carnegie Institution for Science; former Chair, US Nuclear Regulatory Commission*

Stephen Corman *President, Corman Enterprises*

Martha J. Crawford *Operating Partner, Macquarie Asset Management*

Ana V. Diez Roux *Dana and David Dornsife Dean and Distinguished University Professor of Epidemiology, Dornsife School of Public Health, Drexel University; Director, Drexel Urban Health Collaborative*

Michael J. Klag *Dean Emeritus and Second Century Distinguished Professor, Johns Hopkins Bloomberg School of Public Health*

Alan I. Leshner *CEO Emeritus, American Association for the Advancement of Science*

Catherine L. Ross *Regents' Professor Emerita, City and Regional Planning and Civil and Environmental Engineering, Georgia Institute of Technology; Chairman of the Board of Directors of the Auto Club Group, American Automobile Association*

Martha E. Rudolph *Environmental Attorney, Former Director of Environmental Programs, Colorado Department of Public Health and Environment*

Karen C. Seto *Frederick C. Hixon Professor of Geography and Urbanization Science, Yale School of the Environment, Yale University*

Jared L. Cohon *President Emeritus and Professor, Civil and Environmental Engineering and Engineering and Public Policy, Carnegie Mellon University, In Memoriam 1947–2024*

ENERGY COMMITTEE OF THE HEI BOARD OF DIRECTORS

Martha E. Rudolph, Chair *Colorado Department of Public Health and Environment*

Michael J. Klag *Dean Emeritus and Second Century Distinguished Professor Emeritus, Johns Hopkins Bloomberg School of Public Health*

Richard A. Meserve *Senior of Counsel, Covington & Burling LLP; President Emeritus, Carnegie Institution for Science; former Chair, US Nuclear Regulatory Commission*

Jared L. Cohon *President Emeritus and Professor, Civil and Environmental Engineering and Engineering and Public Policy, Carnegie Mellon University, In Memoriam 1947–2024*

HEI ENERGY RESEARCH COMMITTEE

George Hornberger, Chair *Distinguished Professor Emeritus, Vanderbilt University*

Shari Dunn-Norman* *Associate Professor, Department of Geological Sciences and Engineering, Missouri University of Science and Technology*

Stefanie Ebelt Sarnat* *Associate Professor, Department of Environmental Health, Rollins School of Public Health, Emory University*

Alfred Eustes *Associate Professor Emeritus, Petroleum Engineering Department, Colorado School of Mines*

Julia Haggerty *Associate Professor of Geography, Department of Earth Sciences, Montana State University*

Howard Hu* *Professor and Flora L. Thornton Chair, Department of Preventive Medicine, Keck School of Medicine, University of Southern California, Los Angeles*

Kirsten Koehler *Professor, Department of Environmental Health and Engineering, Bloomberg School of Public Health, Johns Hopkins University*

Judy S. LaKind* *Adjunct Associate Professor, Department of Epidemiology and Public Health, University of Maryland School of Medicine*

Christopher Paciorek *Adjunct Professor and Research Computing Consultant, Department of Statistics, University of California, Berkeley*

*Shari Dunn-Norman, Stefanie Ebelt Sarnat, Howard Hu, and Judy S. LaKind rotated off the Research Committee before this report's publication.

Continues next page

HEI BOARD, ENERGY COMMITTEES, and STAFF

HEI ENERGY REVIEW COMMITTEE

STAFF AND CONSULTING SCIENTISTS

*Elizabeth Mannshardt rotated off the Review Committee before this report's publication.

Continues next page

HEI BOARD, ENERGY COMMITTEES, and STAFF

(*Staff and Consulting Scientists, continued*)

Samantha Miller *Research Assistant*

Victor Nthusi *Consulting Research Fellow*

Pallavi Pant *Head of Global Initiatives*

Allison P. Patton *Senior Scientist*

Yasmin Romitti *Staff Scientist*

Anna Rosofsky *Senior Scientist and Community Health and Environmental Research Initiatives Lead*

Abinaya Sekar *Consulting Research Fellow*

Robert Shavers *Operations Manager*

Eva Tanner *Staff Scientist*

Alexis Vaskas *Digital Communications Manager*

RESEARCH REPORT

NUMBER 240
MARCH 2026

Health Effects Institute
One Beacon Street
Suite 21300
Boston, Massachusetts 02108, USA
+1-617-488-2300

www.healtheffects.org
www.HEIenergy.org